DISS. ETH NO. 24067

Production of heterologous metabolites in mammalian synthetic biology

A thesis submitted to attain the degree of

DOCTOR OF SCIENCES of ETH ZURICH

(Dr. sc. ETH Zurich)

presented by

Marius MÜLLER

Diplom Biotechnologe, École supérieure de Strasbourg (M.Sc.)

born on 25.11.1984

citizen of

Germany

accepted on the recommendation of

Prof. Dr. Martin Fussenegger / Examiner
Prof. Dr. Yaakov Benenson / Co-Examiner

2017

Introduction

General Introduction

The discipline of synthetic biology is an engineering approach to biology with standardization, modularization and rational design of (artificial) biological systems by the use and assembly of single "parts". Mammalian synthetic biology in particular emphasizes the improvement of biologics production, drug screening or direct biomedical applications. Engineered designer cells that calculate and respond to a set of compounds, encapsulated into alginate and implanted into a patient's body can early diagnose and counteract disease states.

This work fosters the progress of mammalian synthetic biology at various levels by implementing the production of heterologous compounds in order to improve common approaches or establish new applications:

In a first project, we established a blue light-responsive gene regulation system and applied this as a mammalian cell-based screening platform for sunscreen efficacy. We capitalized on a UV-A and blue light-dependent heterodimerization system from *Arabidopsis thaliana*, combined with a site-specific protease and conditional translocation of a transcription factor.

Further we broadened the scope of possible effector molecules. As the production of secondary metabolites such as nonribosomal peptides are restricted to bacteria and fungi, we sought to transfer the synthesis via nonribosomal peptide synthases (NRPS) to mammalian cells for the direct capitalization of its benefits. As a pioneering example for a nonribosomal peptide we chose the production of the blue pigment indigoidine. Its characteristic coloration could further be used as a universal reporter system in bacteria as well as in mammalian cells.

In order to process biological input signals, synthetic biology creates synthetic circuits inspired by electronic engineering, that perform arithmetics, calculations and biocomputation. We established the missing link between digital electronic devices and analog nature. Inspired by the human olfaction, where an analog gaseous signal is converted into a binary perception in the brain, we created a multipopulation

consortium, where a distinct cell population converts fragrances into common compounds (the essential amino acid tryptophan and the incretin GLP-1), which are sensed by a processing population that performs digital AND-, OR-, NOR-arithmetics.

A cell-communication based human tissue pacemaker orthologous to the circadian clock could lay the basis for patient-defined rhythmic administration of drugs. For the first time, we show a tissue oscillator coupled to a joint metabolite, consisting of multiple populations that oscillate around the production and degradation of joint L-tryptophan.

We believe that the findings of this work will advance designs and applications of mammalian synthetic biology.

Zusammenfassung

Die Fachrichtung der Synthetische Biologie stellt einen Ingenieursansatz zur Biologie mit der Standardisierung, Modularisierung und dem rationellen Entwurf von Systemen unter der Benutzung und dem Zusammenbau von einzelnen biologischen "Teilen" dar.

Ziele der synthetischen Biologie von Säugerzellen im Speziellen sind eine Verbesserung der Biopharmazeutikaproduktion, die Suche nach spezifischen Wirkstoffen oder direkte biomedizinische Anwendungen. Die Zellen werden dabei so entwickelt, dass sie computerähnliche Berechnungen durchführen und auf eine Reihe von Stoffen und Substanzen reagieren können. Wenn diese Designerzellen in Alginat verkapselt und in den Körper eines Patienten implantiert werden, diagnostizieren solche Zellimplantate frühzeitig Krankheiten und wirken diesen entgegen.

Durch das Konzept der Produktion von artfremden Stoffen schafft es diese Arbeit den Fortschritt der Synthetischen Biologie von Säugerzellen in verschiedenen Bereichen voran zu bringen, gängige Ansätze zu verbessern und neue Anwendungen zu etablieren:

Im ersten Projekt wurde ein blaulichtsensitives Genregulationssystem konstruiert und die so veränderten Säugerzellen als Screening-Plattform verwendet um die Effizienz von Sonnencremes zu testen. Dafür wurde ein UV-A und Blaulicht-abhängiges Heterodimerisierungssystem aus *Arabidopsis thaliana* angewandt und mit einer sequenzspezifischen Protease und bedingter Translokation eines Transkriptionsfaktors kombiniert.

Zudem, wurde der Anwendungsbereich verfügbarer Effektor Molekülen erweitert. Da die Produktion von Sekundärmetaboliten - wie beispielsweise nichtribosomale Peptide- bislang beschränkt auf Bakterien und Pilze ist, wurde eine Möglichkeit gesucht die Synthese von Sekundärmetaboliten auf Säugerzellen zu übertragen um diese direkt nutzbar zu machen.

Als wegweisendes Beispiel für ein nichtribosomales Peptid entschieden wir uns für die Produktion des blauen Pigments Indigoidin. Seine charakteristische Färbung konnte des

Weitern als universelles Reportersystem in Bakterien wie auch in Säugerzellen etabliert werden.

Inspiriert durch das Elektroingenieurswesen, kreiert die Synthetische Biologie künstliche Schaltkreise, die Arithmetik und (Bio-)Berechnungen durchführen um biologische Eingangssignale zu prozessieren.

Wir haben das fehlende Glied zwischen digitalen elektronischen Geräten und analoger Natur implementiert. Inspiriert vom menschlichen Geruchsinn der analoge Gassignale in eine binäre Wahrnehmung im Gehirn konvertiert, wurde ein Konsortium aus verschiedenen Zellpopulationen kreiert. Eine bestimmte Zellpopulation wandelt dabei einen Duft in gemeinsame Stoffe um (die essentielle Aminosäure Tryptophan und inkretines GLP-1), die daraufhin von einer weiteren Prozesszellpopulation detektiert werden und schließlich digitale AND-, OR- und NOR-Arithmetik ausführt.

Ein gekoppelter künstlicher Zeitgeber, basierend auf menschlichen Zellen und der parallel zur inneren Uhr tickt, könnte die Grundlage für eine auf den Patienten abgestimmte rhythmische Medikamentendarreichung bilden. Zum ersten Mal wurde hier ein Gewebeoszillator der aus verschiedenen Populationen besteht und analog zur Produktion und Degradation des gemeinsamen Metaboliten L-Tryptophan oszilliert gezeigt.

Wir glauben, dass die Forschungsergebnisse dieser Arbeit kommende Prinzipien und Anwendungen der synthetischen Biologie von Säugerzellen voranbringen wird.

Synthetic Biology

There have only been few scientific disciplines that have emerged so rapidly and successfully as synthetic biology. First pioneering works in 2000 included a genetic "toggle switch" (Gardner et al. 2000) and a ring oscillator named "repressilator" (Elowitz et al. 2000), which demonstrated the principle of gene switches and their potential applications when interconnected. Another important feature was the use of orthogonal, system-independent genetic parts or biologic building blocks to form gene networks or circuits. Apparent also is the influence of several scientific disciplines especially engineering sciences, as standardization (and reliability) of these single parts, predictability and the rational design of circuits are key poles of synthetic biology. Therefore synthetic biology relies on synergies with multidisciplinary fields such as computational systems biology that guides this rational design and the engineering of sophisticated gene circuits and furthermore helps in providing a profound understanding of the systems (Smolke et al. 2011). Sharing similar techniques with standard molecular biology, synthetic biology however raised quickly due to strong advances in the field of decoding and synthesis of genetic codes and cheap DNA synthesis for the construction of orthologous building blocks. Further tools for the creation of synthetic biology systems include complete synthetic and orthologous systems such as synthetic XNAs (Pinheiro et al. 2012), synthetic tRNAs (Des Soye et al. 2015) or even complete artificial organisms (Hutchison et al. 2016) and in combination with the novel CRISPR/Cas9 gene editing technology and analogs (Argonaut (Gao et al. 2016), Cpf1 (Zetsche et al. 2015)) enabled a new upwind to the field (Dominguez et al. 2016).

Starting with systems analogous to electrical engineering such as genetic switches, memory devices to pulse generators, oscillators, logic gates, filters or biocomputation systems (Khalil et al. 2010), over time the applications became more diverse and clinically relevant: biomedical approaches featured diagnostic devices for the detection of diseases such as viral infections (Pardee et al. 2016), cancer (Danino et al. 2015) or profiling of allergy states (Auslander et al. 2014b, Slomovic et al. 2015).

Also synthetic gene circuits were applied for drug discovery (Benam et al. 2016, Braff et al. 2016), biologics production (Tastanova et al. 2016), biocomputational

devices (Rubens et al. 2016) and therapeutic strategies (Heng et al. 2015, Kojima et al. 2015, Morsut et al. 2016, Roybal et al. 2016) including stem cell differentiation (Saxena et al. 2016b).

Metabolic engineering in synthetic biology

Metabolic engineering as a discipline emerged in the 1990s, dealing with the engineering and adaptation of metabolic pathways in respect to the synthesis of a desired (natural) product (Bailey 1991). Borders between metabolic engineering and synthetic biology are fluent, as synthetic constructs and resulting networks and circuits -common building blocks of synthetic biology- are often used to engineer new metabolic pathways or improve its performances (Stephanopoulos 2012, Awan et al. 2016). Prominent examples of this synergy include the production of the antimalarial drug precursor artemisinic acid (Ro et al. 2006), where researcher transferred the pathway from the natural production host (slow growing plant) to the fast-growing and inexpensive yeast as heterologous production host. Another recent example established the production of opioids in yeast by the transfer and functional expression of up to 23 heterologous enzymes (Galanie et al. 2015). Also bioremediation approaches, such as the degradation of heavy metal contaminants (Haferburg et al. 2010) apply the principles of metabolic engineering and synthetic biology (Brune et al. 2012). On an industrial scale, transfer of entire pathways to easy-to-handle hosts such as bacteria or yeast is used for the production of food additives (such as vanillin) or fragrances (Hayden 2014). In respect to biopharmaceutical compounds, natural products and its derivatives make up a major part of marketed drugs (Newman et al. 2007, Bade et al. 2010, Awan et al. 2016). Key players in these secondary metabolite pathways are often megaenzymes, which catalyze multiple synthesis steps, such as polyketide synthases (PKS) or nonribosomal peptide synthases (NRPS). The later consist of several modules, each sequentially catalyzing a conversion step –analogous to modern industrial assembly lines. As the name suggests, these synthesis routes are independent of the ribosome and mRNA, still having amino acids as educts (Reimer et al. 2016). The resulting nonribosomal peptides, secondary metabolites, have broad biological activities, ranging from siderophores (such as

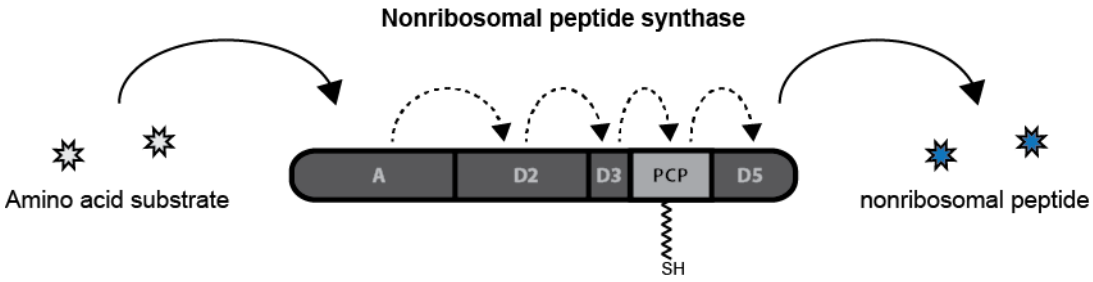

Figure 1. Principle of nonribosomal peptide synthases (NRPS).

NRPS constitute of multiple catalytic domains (D). The synthesis is initiated by the binding of an amino acid substrate to the adenylation domain (A). The position-dependent sequential catalytic cascade results in the production of the mRNA-independent nonribosomal peptide. The peptidyl carrier protein domain (PCP) stands out in this process, as the enzyme's phosphopantetheinyl cofactor needs to be transferred to the NRPS by a second enzyme (PPTase) to render it active.

enterobactin), toxins, pigments (such as indigoidine) to immunosuppressants (such as cyclosporine), antibiotics and antiviral- and anticancer compounds (such as echinomycin (Watanabe et al. 2006)). In recent years the heterologous production of these valuable natural compounds came into focus of synthetic biology (Meyer et al. 2016, Zebec et al. 2016, Zhao et al. 2016), and resulted in pioneering examples such as the synthesis of the antibiotic feglymycin (Gonsior et al. 2015) or the anticancer drug echinomycin (Watanabe et al. 2006). A fruitful synergy between metabolic engineering and synthetic biology could pave the way for the production of new pharmaceutically relevant compounds as well as ease the access, production and costs for existing drugs.

From gene switches to complex gene circuits in mammalian cells

One of the key aspects of synthetic biology is the in-depth characterization of standard building blocks and the subsequent engineering of regulatory networks to complex biological circuits. These circuits are commonly based on gene switches, which perform an (genetic) output in the presence of a defined input. Prominent examples of these switches are transcription factors from heterologous or homologous hosts. The most extensively studied system is the tetracycline antibiotics-resistance mechanism in

bacteria (Berens et al. 2003). Herein the resistance gene for tetracycline is regulated by the tetracycline repressor protein TetR (Cuthbertson et al. 2013). TetR binds to its cognate operator sequence tetO, a 15 base pair palindromic sequence on the DNA, thereby preventing binding of the RNA Polymerase II and transcription of downstream genes. Binding of tetracycline to the binding pocket of tetR induces a conformational switch and prevents the repressor protein from binding to the DNA, hence allows transcription of the resistance gene. The feature of conditional DNA-binding and DNA-dissociation in presence or absence of a ligand has been widened to a broad range of other transcription factor families in order to respond to an extensive panoply of inducer/repressor molecules. Transfer of these systems to a mammalian background additionally requires the fusion of an activation/-repression domain to the DNA-binding protein, such as for example the VP16 activation domain from the Herpes Simplex Virus to the tetR resulting in the tetracycline-responsive transactivator (tTA)(Gossen et al. 1992). In combination with the cognate promoter this enables turning on or off of the desired output gene –analogous to example (electronic) light switches.

Another example exclusive to eukaryotes are G-Protein coupled receptors (GPCRs), which are heptahelical membrane-bound molecule-sensing actuators. In the presence of a cognate extracellular ligand, an intracellular signal transduction, that relies on a conformational change of the GPCR and activation of the associated G protein, leads to a cellular response. The two principal signal cascades involved are the cAMP signal pathway and the phosphatidylinositol signal pathway. Rewiring of these pathways to a desired output can be achieved by tapping into the pathways at certain steps. For example, does the $G\alpha_S$-protein-dependent signaling cascade increase internal cAMP after receptor activation, which in a final step of the signal cascade, leads to the phosphorylation of the CREB-1 protein that translocates to the nucleus and binds to its cognate Promoter and drives gene expression. Replacing endogenous genes with the desired output enables synthetic input-output cascades.

Further trigger switches include other receptor systems (such as notch signaling (Themeli et al. 2016), or interleukin-signaling (Schukur et al. 2015), input-sensitive cyclases (Kim et al. 2015a, Kim et al. 2015b), aptazymes (Auslander et al. 2011) and engineered proteins, which can be rewired in a similar fashion with a desired (heterologous) gene/protein output (such as an inducer-responsive dCas9 (Oakes et al. 2016)).

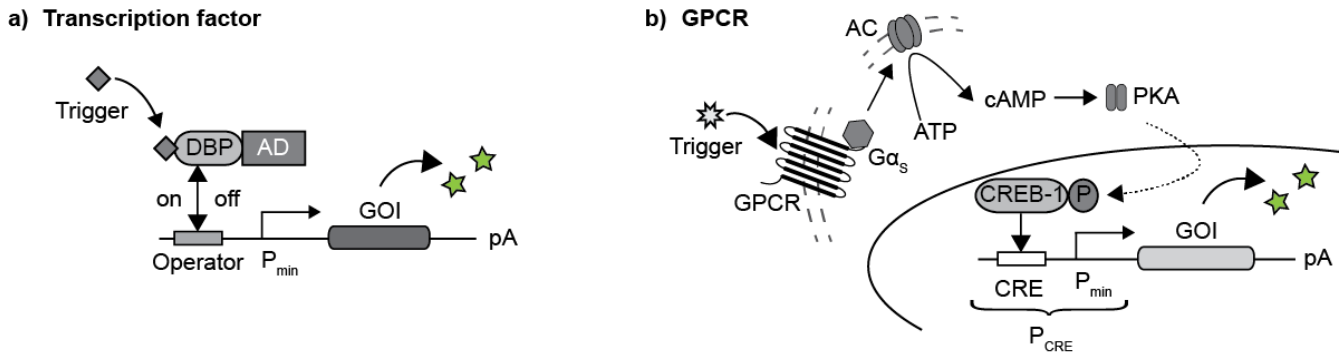

Figure 2 Principle of trigger-inducible gene switches.

a) Transcription factor gene switches. External trigger-inducible protein switches consist of a heterologous transcription factor (such as tetR) with its DNA-binding protein (DBP) that is fused to a mammalian activation domain (AD)(such as VP16). Addition of the respective trigger molecule (e.g. tetracycline) results in a conformational change of the DBP and enables (ON-Type Systems) or disables (OFF-Type Systems) its binding to the cognate DNA-Operator sequence. When bound to the DNA, the fused AD recruits RNA Polymerase II to the minimal Promoter (P_{min}) resulting in expression of the gene of interest (GOI).

b) Rerouting of endogenous signaling pathways (GPCR). Upon binding of a ligand to the respective membrane-bound G protein-coupled receptor (GPCR) that is linked to a stimulatory G_s protein, the Gα subunit is released from the GPCR and activates adenylyl cyclase (AC). AC converts ATP to the second messenger cyclic AMP (cAMP), which binds to the regulatory subunits of protein kinase A (PKA). These subunits then translocate to the nucleus and phosphorylate the cAMP-responsive element binding protein 1 (CREB-1), which enables its binding to the cognate operator site, the cAMP-responsive element (CRE), with an adjacent minimal Promoter (P_{min}) and promotes (target) gene expression (GOI).

These molecular switches have become standard tools in synthetic biology, leading to basic operations such as logic gates (Gaber et al. 2014) or bistable switches (Kramer et al. 2005) similar to the beginning of electronic engineering. These systems can

respond to input triggers such as environmental influences including pH (Auslander et al. 2014a), electromagnetic (Stanley et al. 2012) and brain waves (Folcher et al. 2014), temperature (Boorsma et al. 2000, Weber et al. 2003) and light (Ye et al. 2011) as well as physiologic compounds such as cosmetics (Gitzinger et al. 2009), food additives (Gitzinger et al. 2012), vitamins (Weber et al. 2007).

Gene switches can be combined with "processing units" or actuators, which enable a processing of the external signal, essential for synthetic biological circuit designs. These actuators range from recombinases, such as CRE, Flp or B3 recombinases, processing genetic information on the DNA level (pre-transcriptional), to combinations of transcription factors such as seen for the tetracycline-responsive transactivator (transcriptional), to RNA-binding proteins, such as L7Ae or MS2 protein, to regulate translation (pre-translational), to proteases such as the TEV protease, which process proteins (posttranslational). Due to advances in these components combined with engineering principles, complexity and processing capacity of synthetic circuits have dramatically increased in recent years which lead to first "biocomputational" approaches: amongst those were genetic memory devices (Yang et al. 2014), arithmetic operations (Benenson 2012), calculations reminiscent to computers (Auslander et al. 2012a, Purcell et al. 2014), dynamic systems (Prochazka et al. 2014) with complex synthetic oscillatory systems (Tigges et al. 2009, Danino et al. 2010, Tigges et al. 2010). These circuits are strongly inspired by the concepts of electric engineering, where single components (e.g. transistors as switches) are interconnected to complex electronic systems. The fundamental setup of synthetic biology circuits of sensing external input signals, with subsequent integration, processing and conversion to a final output, builds the basis for complex real-world applications.

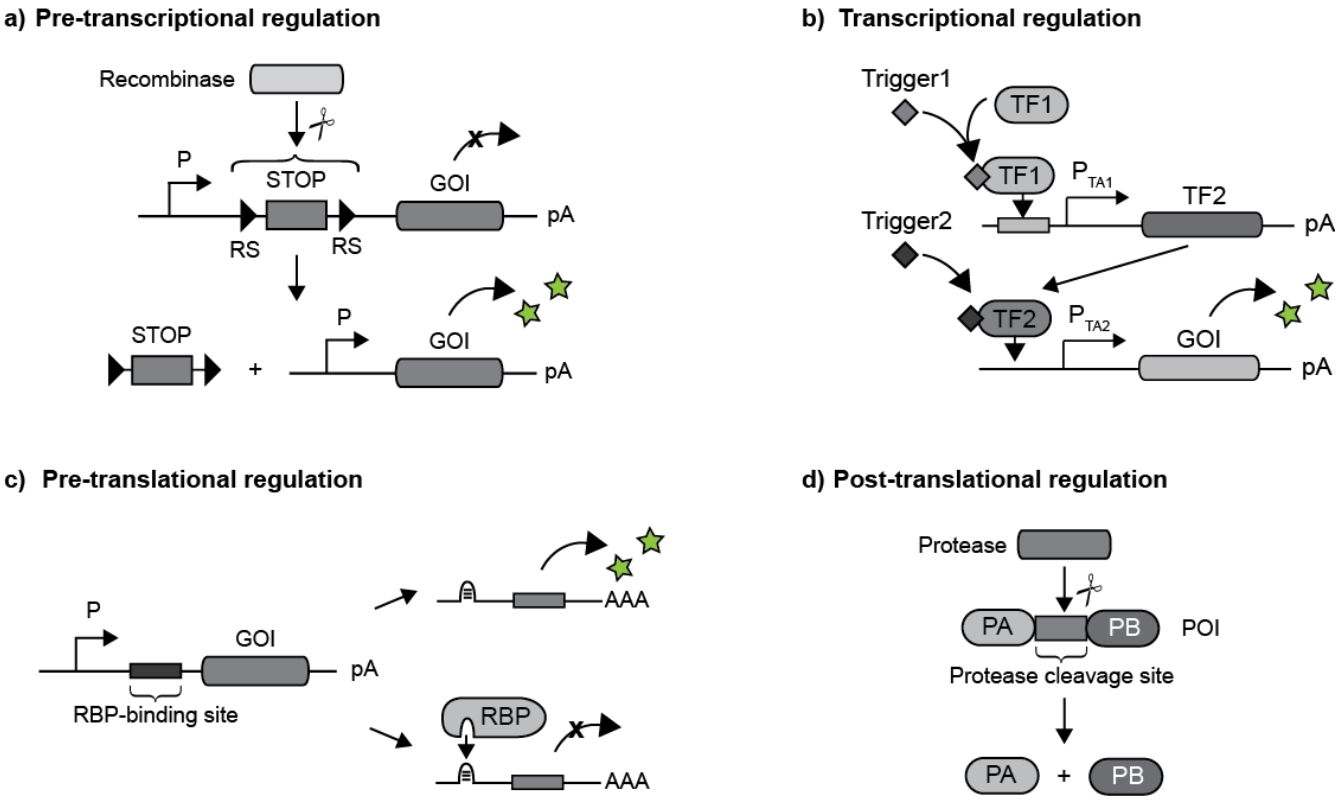

Figure 3 Principles of intracellular actuators

a) Regulation on a pre-transcriptional level. Recombinases as "molecular DNA scissors" cut DNA at specific recognition sites (RS). Regulation can be achieved by the removal of a transcriptional STOP-cassette (STOP), which prevents transcription by a promoter (P) of a gene of interest (GOI). In presence of the recombinase, the STOP-cassette is removed and enables transcription. **b)** Regulation on a transcriptional level. Multiple transcription factors (TF) can be interconnected such as transcription factor 1 binds to its cognate promoter (P_{TF1}) and induces the expression of a second transcription factor (TF2), which selectively binds to its promoter (P_{TF2}) and drives the expression of the gene of interest (GOI). Such regulation circuits can for example serve to amplify signals or to regulate a system with multiple inputs (trigger). **c)** Regulation on a pre-translational level. Introducing an RNA-binding protein (RBP)-binding site in the 5'- untranslated region of a transcript allows regulation by an RNA-binding protein (such as L7Ae). Only in the absence of the RBP translation takes place, while in the presence of the RBP it binds to its cognate loop structure of the mRNA inhibiting translation. **d)** Regulation on a post-translational level. Site-specific proteases cleave engineered proteins of interest (POI) at a cognate amino acid cleavage site. In presence of such a protease two fusion proteins (PA+PB) are cleaved.

Mammalian designer cells and applications

Although some of the biologic parts work in prokaryotes as well as eukaryotes, unarguably, mammalian cells bear a higher complexity in genetics, systematics (e.g. compartmentalization) and interconnected signaling pathways which renders the design and construction of synthetic circuits more complicated. First approaches to the field featured characterization of (orthologous) trigger-inducible and fine-tunable gene switches, mainly for the production of biopharmaceutical proteins such as the aforementioned tetracycline-inducible system (Gossen et al. 1992) or pristinamycin (Fussenegger et al. 2000). These switches could be applied for mammalian-cell-based drug discovery (Weber et al. 2005), scoring valuable compounds and cytotoxicity at the same time (Weber et al. 2009, Slomovic et al. 2015). Another mammalian cell-based approach could also profile patient's allergy in their blood (Auslander et al. 2014b) or classify cancer via a synthetic circuit (Xie et al. 2011).

First mammalian input-based logics were constructed of single switches for basic arithmetics such as AND, OR, NOR, NAND gates (Kramer et al. 2004a, Kramer et al. 2004b, Kramer et al. 2005) as a response to three independent input molecules. This analogy to electronic circuits was continued by the first construction of a "biocomputer" –able to perform calculations (Auslander et al. 2012a). With this level of sophistication synthetic gene networks have the potential to early diagnose pathologic situations with therapeutic intervention in a closed-loop manner. Such "smart implants" are the result of engineering mammalian cells and encapsulation and subsequent implantation into the patient's body (Auslander et al. 2012b). For example, designer-cell implants with embedded therapeutic gene networks have been successfully used to diagnose, prevent and cure experimental gouty arthritis (Kemmer et al. 2010), obesity (Rossger et al. 2013), Grave's disease (Saxena et al. 2016a) and psoriasis (Schukur et al. 2015).

Not limited to human applications, these "prosthetic networks" were also applied for sperm release during ovulation in cows (Kemmer et al. 2011). Herein designer cells could sense an ovulation trigger, upon which encapsulated bull sperms were released and lead to insemination of the host animal.

Further progress in the field such as increased spatio-temporal resolution, with for example oscillating gene expressions in these smart implants could allow to periodically administer therapeutics in a temporal-defined manner.

Contribution of this work

The projects enclosed in this thesis focus on the synthesis of heterologous metabolites in the scope of mammalian synthetic biology.

At first, Chapter I deals with the lack of a UV-A light inducible mammalian gene-regulation system. We engineered designer cells that respond to UV/blue-light and applied those as a cell-based screen for efficacy of commercial sunscreens.
Chapter II solves the problem of several reporter drawbacks (expensive, secreted, unstable, detection methods) in mammalian cells by the implementation of the production of the non-ribosomal peptide indigoidine, a blue-colored pigment, and its subsequent use as a reporter tool. Chapter III follows up on production of the heterologous metabolite tryptophan or the incretin GLP-1 for cell-cell communication to implement a gas-to-liquid converter of gaseous fragrances with subsequent digital processing. This solves the issue of the current limitation in complexity of synthetic biocomputational approaches implemented in single cells and enables modularization and interchangeability. Chapter IV tackles the lack of coupling of current synthetic oscillators in mammalian cell populations. We achieved this by the dynamic interconversion of the amino acid L-Tryptophan to indole and vice versa. This results in a common dynamic metabolic quorum for the entire cell consortium.

Chapter I: Engineered UV-A light-responsive gene expression system for measuring sun cream efficacy in mammalian cell culture

In this chapter, we designed and established a UV-A and blue-light inducible gene regulation system in a mammalian background. By combining the site-specific protease TEV with the blue-light heterodimerization system CRY2-C1B1 from *Arabidopsis thaliana* and engineering of a membrane-bound transcription factor tTA that translocates to the nucleus upon light-induced protease cleavage, we were able to establish a spatio-temporal controllable gene expression system via blue- and UV-light. This system was finally applied as a sunscreen-screening platform, scoring cell viability and UV-protection at the same time.

Chapter II: A novel reporter system for bacterial and mammalian cells based on the non-ribosomal peptide indigoidine

Production of natural compounds has so far been limited to prokaryotes. Chapter II describes the transfer of the indigoidine synthesis pathway to mammalian cells. This natural product is independent of mRNA and produced via a nonribosomal peptide synthase (NRPS). Co-expression of the indigoidine synthase BpsA from *Streptomyces lavendulae* and the 4'phosphopantetheinyl transferase (PPTase) Svp from *Streptomyces verticillus* enabled the production of the glutamine-derived pigment. Capitalizing on its blue color, the system could be applied as a novel visual and fluorescent reporter assay for bacteria and mammalian cells.

Chapter III: Designed cell consortia as fragrance-programmable analog-to-digital converters

In the human nose, fragrances are sensed by the olfactory cells. This perception is converted into a chemical signal, which is transmitted to the brain, processed and integrated. We used this system as a blueprint for the construction of a fragrance analog-to-digital converter with logics output. This was achieved by a mammalian designer consortium consisting of distinct cell lines for the discrimination of fragrances, which in turn produce intercellular communication compounds that signal to another cell population, which integrates and processes these intermediates in a digital manner with AND-, OR-, NOR-based arithmetics. Apart from the pioneering example of a mammalian analog-to-digital converter, we show the dissection of such a complex system to several single cell units as a working frame.

Chapter IV: A cell-communication-based human tissue oscillator

First mammalian oscillators have recently been described. The issue for possible applications however is the lack of coupling between single oscillating cells. In this last chapter, we describe the design of a mammalian tissue oscillator. The system is based on the interconversion of the joint metabolite L-tryptophan to indole and reverse. The oscillator consists of three distinct cell types, producer –converting indole to tryptophan-

, degrader –catalyzing the reverse reaction of L-tryptophan back to indole and reporter cells for visualization. In combination with descriptive system biology and microfluidic engineering we were able to construct a tissue-wide oscillatory system.

References

Auslander, D., et al. (2014a). "A synthetic multifunctional mammalian pH sensor and CO2 transgene-control device." Molecular Cell 55(3): 397-408.

Auslander, D., et al. (2014b). "A designer cell-based histamine-specific human allergy profiler." Nat Commun 5: 4408.

Auslander, D., M. Wieland, S. Auslander, M. Tigges and M. Fussenegger (2011). "Rational design of a small molecule-responsive intramer controlling transgene expression in mammalian cells." Nucleic Acids Research 39(22): e155.

Auslander, S., D. Auslander, M. Muller, M. Wieland and M. Fussenegger (2012a). "Programmable single-cell mammalian biocomputers." Nature 487(7405): 123-127.

Auslander, S., M. Wieland and M. Fussenegger (2012b). "Smart medication through combination of synthetic biology and cell microencapsulation." Metabolic engineering 14(3): 252-260.

Awan, A. R., W. M. Shaw and T. Ellis (2016). "Biosynthesis of therapeutic natural products using synthetic biology." Adv Drug Deliv Rev. 105(Pt A):96-106

Bade, R., H. F. Chan and J. Reynisson (2010). "Characteristics of known drug space. Natural products, their derivatives and synthetic drugs." Eur J Med Chem 45(12): 5646-5652.

Bailey, J. E. (1991). "Toward a science of metabolic engineering." Science 252(5013): 1668-1675.

Benam, K. H., et al. (2016). "Small airway-on-a-chip enables analysis of human lung inflammation and drug responses in vitro." Nat Methods 13(2): 151-157.

Benenson, Y. (2012). "Biomolecular computing systems: principles, progress and potential." Nat Rev Genet 13(7): 455-468.

Berens, C. and W. Hillen (2003). "Gene regulation by tetracyclines. Constraints of resistance regulation in bacteria shape TetR for application in eukaryotes." Eur J Biochem 270(15): 3109-3121.

Boorsma, M., et al. (2000). "A temperature-regulated replicon-based DNA expression system." Nat Biotechnol 18(4): 429-432.

Braff, D., D. Shis and J. J. Collins (2016). "Synthetic biology platform technologies for antimicrobial applications." Adv Drug Deliv Rev. 105(Pt A):35-43

Brune, K. D. and T. S. Bayer (2012). "Engineering microbial consortia to enhance biomining and bioremediation." Front Microbiol 3: 203.

Cuthbertson, L. and J. R. Nodwell (2013). "The TetR family of regulators." Microbiol Mol Biol Rev 77(3): 440-475.

Danino, T., O. Mondragon-Palomino, L. Tsimring and J. Hasty (2010). "A synchronized quorum of genetic clocks." Nature 463(7279): 326-330.

Danino, T., et al. (2015). "Programmable probiotics for detection of cancer in urine." Sci Transl Med 7(289): 289ra284.

Des Soye, B. J., J. R. Patel, F. J. Isaacs and M. C. Jewett (2015). "Repurposing the translation apparatus for synthetic biology." Curr Opin Chem Biol 28: 83-90.

Dominguez, A. A., W. A. Lim and L. S. Qi (2016). "Beyond editing: repurposing CRISPR-Cas9 for precision genome regulation and interrogation." Nat Rev Mol Cell Biol 17(1): 5-15.

Elowitz, M. B. and S. Leibler (2000). "A synthetic oscillatory network of transcriptional regulators." Nature 403(6767): 335-338.

Folcher, M., et al. (2014). "Mind-controlled transgene expression by a wireless-powered optogenetic designer cell implant." Nat Commun 5: 5392.

Fussenegger, M., et al. (2000). "Streptogramin-based gene regulation systems for mammalian cells." Nat Biotechnol 18(11): 1203-1208.

Gaber, R., et al. (2014). "Designable DNA-binding domains enable construction of logic circuits in mammalian cells." Nat Chem Biol 10(3): 203-208.

Galanie, S., K. Thodey, I. J. Trenchard, M. Filsinger Interrante and C. D. Smolke (2015). "Complete biosynthesis of opioids in yeast." Science 349(6252): 1095-1100.

Gao, F., X. Z. Shen, F. Jiang, Y. Wu and C. Han (2016). "DNA-guided genome editing using the Natronobacterium gregoryi Argonaute." Nat Biotechnol 34(7): 768-773.

Gardner, T. S., C. R. Cantor and J. J. Collins (2000). "Construction of a genetic toggle switch in Escherichia coli." Nature 403(6767): 339-342.

Gitzinger, M., C. Kemmer, M. D. El-Baba, W. Weber and M. Fussenegger (2009). Controlling transgene expression in subcutaneous implants using a skin lotion containing the apple metabolite phloretin. Proceedings of the National Academy of Sciences. 106**:** 10638-10643.

Gitzinger, M., et al. (2012). "The food additive vanillic acid controls transgene expression in mammalian cells and mice." Nucleic Acids Research 40(5): e37.

Gonsior, M., et al. (2015). "Biosynthesis of the Peptide Antibiotic Feglymycin by a Linear Nonribosomal Peptide Synthetase Mechanism." Chembiochem 16(18): 2610-2614.

Gossen, M. and H. Bujard (1992). "Tight control of gene expression in mammalian cells by tetracycline-responsive promoters." Proc Natl Acad Sci U S A 89(12): 5547-5551.

Haferburg, G. and E. Kothe (2010). "Metallomics: lessons for metalliferous soil remediation." Appl Microbiol Biotechnol 87(4): 1271-1280.

Hayden, E. C. (2014). "Synthetic-biology firms shift focus." Nature 505(7485): 598.

Heng, B. C., D. Aubel and M. Fussenegger (2015). "Prosthetic gene networks as an alternative to standard pharmacotherapies for metabolic disorders." Curr Opin Biotechnol 35: 37-45.

Hutchison, C. A., 3rd, et al. (2016). "Design and synthesis of a minimal bacterial genome." Science 351(6280): aad6253.

Kemmer, C., et al. (2011). "A designer network coordinating bovine artificial insemination by ovulation-triggered release of implanted sperms." J Control Release 150(1): 23-29.

Kemmer, C., et al. (2010). "Self-sufficient control of urate homeostasis in mice by a synthetic circuit." Nat Biotechnol 28(4): 355-360.

Khalil, A. S. and J. J. Collins (2010). "Synthetic biology: applications come of age." Nat Rev Genet 11(5): 367-379.

Kim, T., M. Folcher, G. Charpin-El Hamri and M. Fussenegger (2015a). "A synthetic cGMP-sensitive gene switch providing Viagra((R))-controlled gene expression in mammalian cells and mice." Metabolic engineering 29: 169-179.

Kim, T., M. Folcher, M. Doaud-El Baba and M. Fussenegger (2015b). "A synthetic erectile optogenetic stimulator enabling blue-light-inducible penile erection." Angew Chem Int Ed Engl 54(20): 5933-5938.

Kojima, R., D. Aubel and M. Fussenegger (2015). "Novel theranostic agents for next-generation personalized medicine: small molecules, nanoparticles, and engineered mammalian cells." Curr Opin Chem Biol 28: 29-38.

Kramer, B. P., C. Fischer and M. Fussenegger (2004a). "BioLogic gates enable logical transcription control in mammalian cells." Biotechnol Bioeng 87(4): 478-484.

Kramer, B. P. and M. Fussenegger (2005). "Hysteresis in a synthetic mammalian gene network." Proc Natl Acad Sci U S A 102(27): 9517-9522.

Kramer, B. P., et al. (2004b). "An engineered epigenetic transgene switch in mammalian cells." Nat Biotechnol 22(7): 867-870.

Meyer, S., et al. (2016). "Biochemical Dissection of the Natural Diversification of Microcystin Provides Lessons for Synthetic Biology of NRPS." Cell Chem Biol 23(4): 462-471.

Morsut, L., et al. (2016). "Engineering Customized Cell Sensing and Response Behaviors Using Synthetic Notch Receptors." Cell 164(4): 780-791.

Newman, D. J. and G. M. Cragg (2007). "Natural products as sources of new drugs over the last 25 years." J Nat Prod 70(3): 461-477.

Oakes, B. L., et al. (2016). "Profiling of engineering hotspots identifies an allosteric CRISPR-Cas9 switch." Nat Biotechnol 34(6): 646-651.

Pardee, K., et al. (2016). "Rapid, Low-Cost Detection of Zika Virus Using Programmable Biomolecular Components." Cell 165(5): 1255-1266.

Pinheiro, V. B. and P. Holliger (2012). "The XNA world: progress towards replication and evolution of synthetic genetic polymers." Curr Opin Chem Biol 16(3-4): 245-252.

Prochazka, L., B. Angelici, B. Haefliger and Y. Benenson (2014). "Highly modular bow-tie gene circuits with programmable dynamic behaviour." Nat Commun 5: 4729.

Purcell, O. and T. K. Lu (2014). "Synthetic analog and digital circuits for cellular computation and memory." Curr Opin Biotechnol 29: 146-155.

Reimer, J. M., M. N. Aloise, P. M. Harrison and T. M. Schmeing (2016). "Synthetic cycle of the initiation module of a formylating nonribosomal peptide synthetase." Nature 529(7585): 239-242.

Ro, D. K., et al. (2006). "Production of the antimalarial drug precursor artemisinic acid in engineered yeast." Nature 440(7086): 940-943.

Rossger, K., G. Charpin-El-Hamri and M. Fussenegger (2013). "A closed-loop synthetic gene circuit for the treatment of diet-induced obesity in mice." Nat Commun 4: 2825.

Roybal, K. T., et al. (2016). "Precision Tumor Recognition by T Cells With Combinatorial Antigen-Sensing Circuits." Cell 164(4): 770-779.

Rubens, J. R., G. Selvaggio and T. K. Lu (2016). "Synthetic mixed-signal computation in living cells." Nat Commun 7: 11658.

Saxena, P., G. Charpin-El Hamri, M. Folcher, H. Zulewski and M. Fussenegger (2016a). "Synthetic gene network restoring endogenous pituitary-thyroid feedback control in experimental Graves' disease." Proc Natl Acad Sci U S A 113(5): 1244-1249.

Saxena, P., et al. (2016b). "A programmable synthetic lineage-control network that differentiates human IPSCs into glucose-sensitive insulin-secreting beta-like cells." Nat Commun 7: 11247.

Schukur, L., B. Geering, G. Charpin-El Hamri and M. Fussenegger (2015). "Implantable synthetic cytokine converter cells with AND-gate logic treat experimental psoriasis." Sci Transl Med 7(318): 318ra201.

Slomovic, S., K. Pardee and J. J. Collins (2015). "Synthetic biology devices for in vitro and in vivo diagnostics." Proc Natl Acad Sci U S A 112(47): 14429-14435.

Smolke, C. D. and P. A. Silver (2011). "Informing biological design by integration of systems and synthetic biology." Cell 144(6): 855-859.

Stanley, S. A., et al. (2012). "Radio-wave heating of iron oxide nanoparticles can regulate plasma glucose in mice." Science 336(6081): 604-608.

Stephanopoulos, G. (2012). "Synthetic biology and metabolic engineering." ACS Synth Biol 1(11): 514-525.

Tastanova, A., et al. (2016). "Overexpression of YY1 increases the protein production in mammalian cells." J Biotechnol 219: 72-85.

Themeli, M. and M. Sadelain (2016). "Combinatorial Antigen Targeting: Ideal T-Cell Sensing and Anti-Tumor Response." Trends Mol Med 22(4): 271-273.

Tigges, M., N. Denervaud, D. Greber, J. Stelling and M. Fussenegger (2010). "A synthetic low-frequency mammalian oscillator." Nucleic Acids Research 38(8): 2702-2711.

Tigges, M., T. T. Marquez-Lago, J. Stelling and M. Fussenegger (2009). "A tunable synthetic mammalian oscillator." Nature 457(7227): 309-312.

Watanabe, K., et al. (2006). "Total biosynthesis of antitumor nonribosomal peptides in Escherichia coli." Nat Chem Biol 2(8): 423-428.

Weber, C. C., et al. (2005). "Broad-spectrum protein biosensors for class-specific detection of antibiotics." Biotechnol Bioeng 89(1): 9-17.

Weber, W., W. Bacchus, M. Daoud-El Baba and M. Fussenegger (2007). "Vitamin H-regulated transgene expression in mammalian cells." Nucleic Acids Research 35(17): e116.

Weber, W. and M. Fussenegger (2009). "The impact of synthetic biology on drug discovery." Drug Discov Today 14(19-20): 956-963.

Weber, W., et al. (2003). "Conditional human VEGF-mediated vascularization in chicken embryos using a novel temperature-inducible gene regulation (TIGR) system." Nucleic Acids Research 31(12): e69.

Xie, Z., L. Wroblewska, L. Prochazka, R. Weiss and Y. Benenson (2011). "Multi-input RNAi-based logic circuit for identification of specific cancer cells." Science 333(6047): 1307-1311.

Yang, L., et al. (2014). "Permanent genetic memory with >1-byte capacity." Nat Methods 11(12): 1261-1266.

Ye, H., M. Daoud-El Baba, R. W. Peng and M. Fussenegger (2011). "A synthetic optogenetic transcription device enhances blood-glucose homeostasis in mice." Science 332(6037): 1565-1568.

Zebec, Z., et al. (2016). "Towards synthesis of monoterpenes and derivatives using synthetic biology." Current opinion in chemical biology 34: 37-43.

Zetsche, B., et al. (2015). "Cpf1 is a single RNA-guided endonuclease of a class 2 CRISPR-Cas system." Cell 163(3): 759-771.

Zhao, H. and M. H. Medema (2016). "Standardization for natural product synthetic biology." Nat Prod Rep. 33(8):920-4

CHAPTER I

Engineered UV-A light-responsive gene expression system for measuring sun cream efficacy in mammalian cell culture

Marius Müller, Markus Wieland, Andreas Kyburz, Phillip Heissig, Sebastian Wekenmann, Franziska Stolz, Simon Ausländer, Martin Fussenegger

Journal of Biotechnology 189 (2014): 150-153

Abstract

Light-dependent gene regulation systems are advantageous as they allow for precise spatio-temporal control of target gene expression. In this paper, we present a novel UV-A and blue-light-inducible gene control system that is based on the light-dependent heterodimerization of the CRY2 and CIBN domains. Upon their interaction, a transcription factor is released from the cell membrane and initiates target gene expression. Capitalizing on that, sun cream UV-A protection properties were measured intracellularly.

Introduction

Light-responsive gene regulation systems in mammalian cells have recently attracted attention because they enable precise spatio-temporal and adjustable control of target gene expression. Additionally, their application saves costs and should not require any additional chemicals, which could potentially interfere with the host system (Bacchus and Fussenegger, 2012). To date, however, blue-light and red-light-dependent induction of gene expression in mammalian cells has been shown. We will expand this field with a flexible gene expression system that can be controlled by both UV-A and blue light and is easily compatible with many of the existing small molecule-responsive transcription regulation systems. We also highlight the potential of this setup by demonstrating its application as a cellular sun cream sensor.

The existing light-inducible gene expression systems in mammalian cells are based on different approaches: ectopically expressed light-responsive activators of an endogenous signaling cascade, which is rewired to a gene of interest, can be used to control target gene transcription as shown for the GPCR melanopsin (Ye et al., 2011), a photoactivated adenylyl cyclase (Schroder-Lang et al., 2007) and heterodimerization of phytochromes (Muller et al., 2013a; Muller et al., 2013b). Moreover, several proteins originating from the plant *Arabidopsis thaliana* have been demonstrated to heterodimerize upon light irradiation, including the flavin-binding kelch repeat f-box 1 (FKF1) protein with

GIGANTEA (GI) (Sawa et al., 2007) and cryptochrome 2 (CRY2) with the cryptochrome-interacting basic-helix–loop–helix (CIB1) (Liu et al., 2008). Capitalizing on this basic principle, artificial transcription regulators for mammalian cells were engineered by fusing GI to the Gal4 protein, which binds its respective operator site proximal to a minimal promoter, and FKF1 to the transcriptional activator domain VP16. Upon blue-light-mediated heterodimerization, FKF1-VP16 is recruited to Gal4 operator site, which induces target gene transcription (Yazawa et al., 2009). The blue-light-inducible homodimerization of Vivid was exploited similarly by fusing it to both the Gal4 and the transcriptional activator p65 domain. Again, this setup requires blue light irradiation in order to start target gene transcription (Wang et al., 2012).

Design and validation of the UV-A light-responsive gene expression system

In order to engineer a UV-A light-responsive gene expression system, we used the aforementioned proteins CRY2 and CIB1, which play a central role in the light regulation of plant flowering (Liu et al., 2008). In more detail, CRY2 is a conserved photolyase-like protein that binds a chromophore cofactor flavine adenine dinucleotide (FAD) (Liu et al., 2011) that exhibits two light absorption maxima, one in the UV-A (370 nm) and one in the blue-light (450 nm) range (Sang et al., 2005). Photoactivatable heterodimerization with CIB1 was observed in *Arabidopsis thaliana* (Liu et al., 2008) and also after transfer of these protein variants into mammalian HEK293-T cells (Kennedy et al., 2010; Lee et al., 2014). Furthermore, CRY2 and the truncated CIB1 variant CIBN retain blue-light-dependent interaction properties, even when fused to other proteins like GFP and localized to the cell membrane by the addition of a prenylation motif (Kennedy et al., 2010; Lee et al., 2014).

Capitalizing on this intriguing flexibility for protein design, we have engineered a novel gene expression system based on the photoactivatable CRY2-CIBN interaction. CRY2 was fused to the tobacco etch virus protease (TEV) (Kapust et al., 2001; Phan et al., 2002) and placed under the control of the human cytomegalovirus immediate early

promoter (P_{hCMV}; pPH16, P_{hCMV}-CRY2-TEV-pA). CIBN, on the other hand, was combined with an ubiquitinated variant of the tetracycline-dependent transactivator (tTA) (Gossen and Bujard, 1992), which increased the sensitivity of the system, followed by the TEV cleavage site (TCS) on the N-terminus, and a C-terminal transmembrane domain (TMD), which resulted in cell membrane localization (pSW214, P_{hCMV}-Ub-tTA-TCS-CIBN-TMD-pA). In this setup, the tTA-containing fusion protein cannot enter the nucleus, which prevents efficient transactivation of a tTA-dependent SEAP reporter (pMF111, *tet*O_7-$P_{hCMVmin}$-SEAP-pA) (Fussenegger et al., 1997). Only upon photoactivation-dependent CRY2-CIBN interaction is the TEV domain brought into proximity of its respective cleavage site. This leads to the liberation of tTA from its membrane site into the cytoplasm and eventually the nucleus, where it induces target gene expression (for a graphical overview of the system, see Fig. 1).

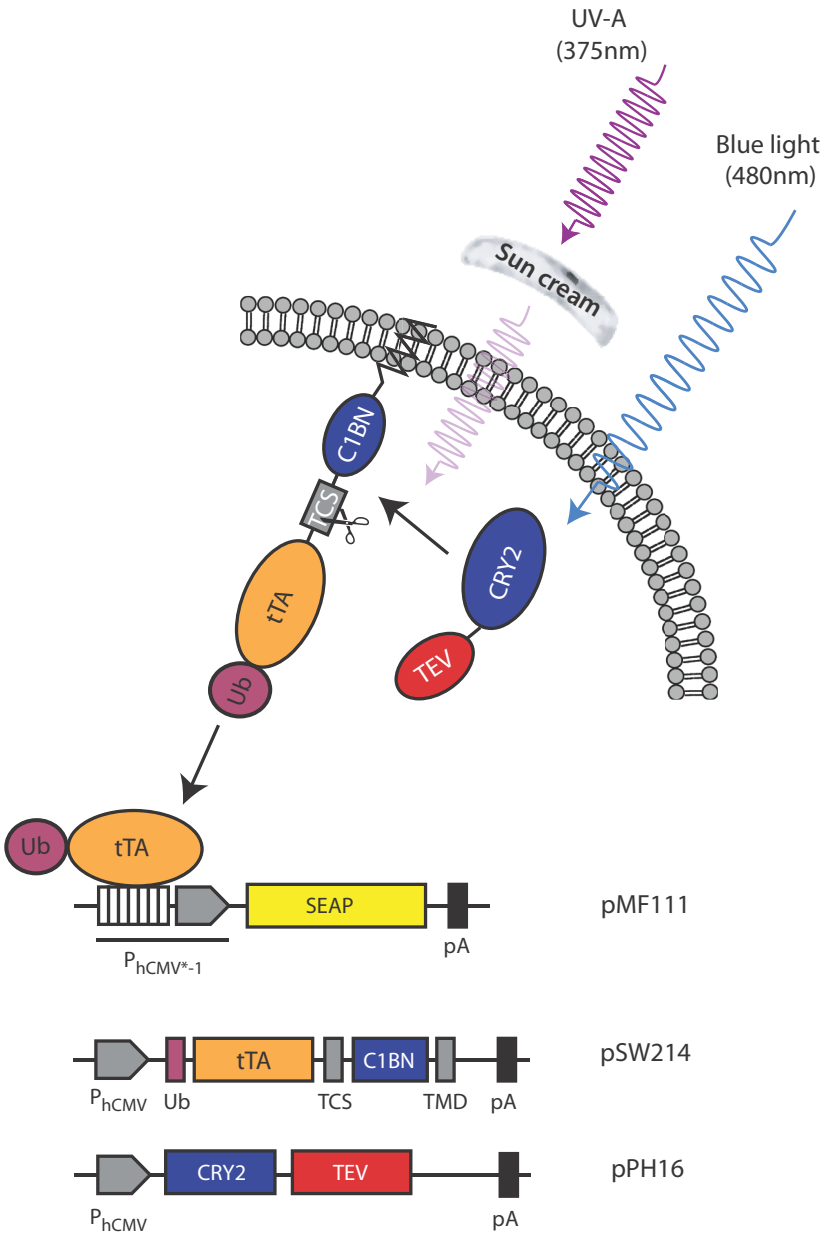

Figure 1. Proposed mechanism of the constructed UV-A and blue-light-responsive gene regulation system. The ubiquitinated tetracycline-dependent transactivator tTA is integrated into a multi-domain engineered protein that also harbors CIBN, which forms a photoactivatable heterodimer with CRY2, a TEV protease cleavage site and a transmembrane domain (TMD) responsible for membrane location of the fusion protein (pSW214, P_{hCMV}-Ub-tTA-TCS-CIBN-TMD-pA). Upon UV-A or blue-light irradiation, heterodimerization with the CRY2-TEV fusion protein (pPH16, P_{hCMV}-CRY2-TEV-pA) releases the tTA transactivator from the membrane, which binds to the tetracycline-responsive promoter ($P_{hCMV*-1}$) and induces target gene expression (e.g. SEAP). All constructs were ordered from Genscript (USA) and cloned into pcDNA3.1(+) vector for expression in mammalian cells. Complete DNA sequences of the constructs can be found in the supplementary information.

We validated this proposed mechanism in initial experiments by co-transfecting human embryonic kidney cells HEK293-T (American Type Culture Collection, ATCC) as described (Auslander et al., 2012) with 50 ng pPH16, 100 ng pSW214 and 100 ng of the pMF111 SEAP reporter plasmid. As expected, reporter gene expression was strongly induced upon UV-A irradiation using LEDs with a wavelength of λ = 375 nm. By removing either part of the system, SEAP expression levels were reduced to background levels and were no longer responsive to illumination; see Fig. 2a. In order to diminish UV-A-light-induced photodamage and toxicity to cells, we induced the cells with pulsed light (5 s light ON followed by 15 s light OFF for 20 h). Although a toxic side effect is still visible in the control experiments, it is compensated by the photo-induced gene expression when all plasmids are present (see Fig. 2a).

Since the performance of this system is strongly dependent on the photoactivatable heterodimerization of the CRY2 and CIBN domains, we first identified the optimal ratio of the two respective fusion proteins encoded on pPH16 and pSW214 plasmids. Accordingly, higher amounts of transfected pPH16 led to a total increase in SEAP production, both in the un-induced as well as in the induced state (see Fig. 2b). This could be explained by an increased probability of photo-independent heterodimerization events if higher concentrations of the heterodimer partners are present. Nevertheless, optimal induction behavior was identified for 50 ng pPH16, 100 ng pSW214, and 100 ng pMF111 plasmids transfected and was used in further experiments.

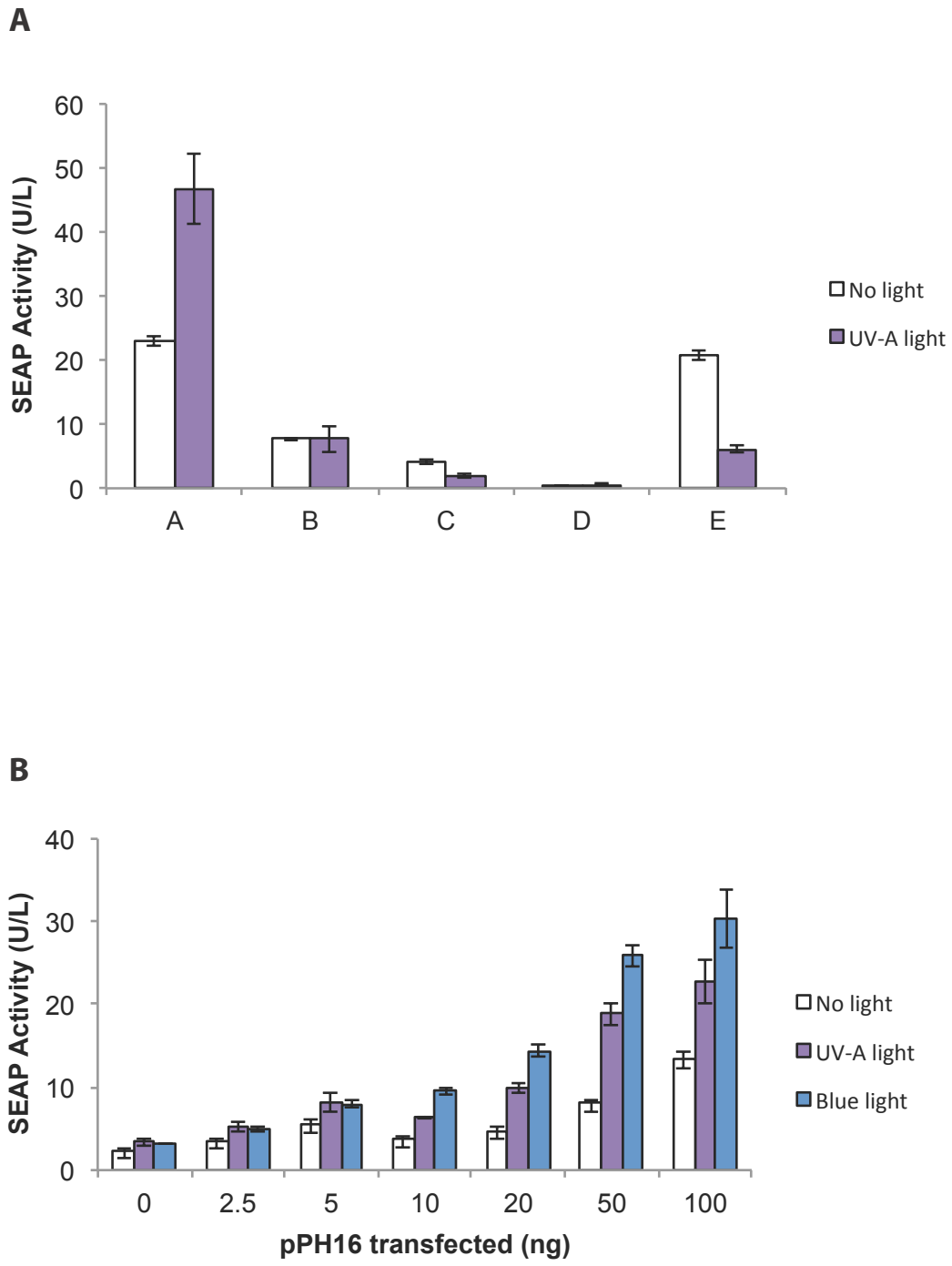

Figure 2. UV-A and blue-light-dependent activation of the engineered system. A. Cells were transfected with the complete gene network (**A**, 50 ng pPH16, 100 ng pSW214, 100 pMF111) or lacking either pPH16 (**B**), pSW214 (**C**) or pMF111 (**D**). UV-A induced cell toxicity was visualized by transfecting a constitutive SEAP expression vector (**E**, pSEAP2-Ctrl). B. pPH16 transfection amount was titrated to identify optimal system performance. If not stated otherwise, 50.000 engineered human HEK293-T cells were seeded per well of a 24-well plate (Nunclon, catalog no.142475, Thermofisher,

Wohlen, Switzerland) and cultivated in DMEM (Life Technologies Europe B.V., Zug, Switzerland) supplemented with 10% fetal calf serum (FCS; Bioconcept, Allschwil, Switzerland; lot no. PE01026P) for 12h at 37°C in a 5% CO_2-containing atmosphere prior to transfection using a standard PEI transfection protocol. Cells were transfected with 50 ng pPH16, 100 ng pSW214, 100 ng pMF111, 100 ng pSEAP2-Ctrl and filled up with empty pcDNA3.1(+) plasmid to 1 µg per transfection. After 18h, the medium was replaced by 500µL phenol red free-DMEM per 24-well. White bars denote no light, violet bars for LEDs with λ = 375 nm and blue bars for LEDs with λ = 480 nm. Upon illumination with UV-A (Custom-manufactured 24-UV-A-LED panel (λ = 375nm 4x6-LED-array, Solan AG, Basel, Switzerland)) or blue light (λ = 480 nm, Roithner, Austria) cells were arranged on an array with the same size as a standard 24-well cell culture plate. In order to diminish light-induced toxicity, cells were illuminated with pulsed light (5s light on, 25V; 15s light off) only. SEAP was measured and assessed as described (Muller et al., 2012) 24 h after medium change.

3. Cell-system-based evaluation of sun cream protection

As a next step, we planned to apply our optimized gene control system to evaluate sun cream UV-A protection on the cellular level. Sun cream protection usually relies on the absorption of high-energy UV light (UV-B and UV-A 290-400nm) and subsequent emission of longer-wave energies mediated by organic and inorganic, often TiO_2 or ZnO, substances. Currently, sun cream performance is indicated as sun protection factor (SPF), which quantifies the fraction of sunburn-producing UV-B light (290-320nm) that is blocked. The SPF is calculated based on the energy per unit area required to cause minimal redness of the skin known as the minimal erythemal dose. Current classification of sun-cream protection continues to be based on two pillars, (i) on optometrics quantifying spectral transmission *in vitro* and (ii) healthy volunteers whose skin is partially treated with sun cream prior to exposure to an artificial UV-A/B light source (290-400nm) and visual inspection of sun burn (Pelizzo et al., 2012). However, the *in vivo* assessment of sun cream performance is specific of the individuals' skin type, does not consider damaging UV-A (320-400nm) irradiation that fails to cause sunburn, is time consuming, expensive and remains ethically questionable.

In order to test and quantify the protection level of sun cream against irradiation of

light in the UV-A range on a cellular level, we capitalized on our engineered gene control system. To that end, we placed a defined layer of 1.75mg of broad-spectrum sun cream containing UV-A and UV-B protection filters (Daylong, Spirig Pharma AG, Egerkingen, Switzerland; SPF 6 to SPF50) circularly on the cover lid above the culture well using a T-formed spatule to generate a uniform concentric layer of sun cream (4.4 mg cm^{-2}) 5cm below our custom-manufactured 24-UV-A-LED panel (4x6 375nm LED-array, Solan AG, Basel, Switzerland) and our cells harboring the transfected plasmids pPH16, pSW214 and pMF111. Next, we irradiated the transfected cells for 2 h with a pulsed light as described before; SEAP levels were then determined after 24 h. As expected, SEAP expression levels were reduced in dependency of the applied SPF (see Fig. 3). While a SPF of 50 inhibited gene expression almost completely, increasing SEAP levels could be detected by lowering the SPF of the applied sun cream. Although cytotoxicity of the UV-A (375nm) irradiation as well as the inherent leakiness of the Tango-assay set-up (Barnea et al., 2008) and the basal expression of the tTA-specific promoter driving the reporter gene reduce the induction-fold of the sun-cream profiler, yet provide sufficient sensitivity to score commercial sun creams with a wide range of sun protection factors (SPF 0 to 50).

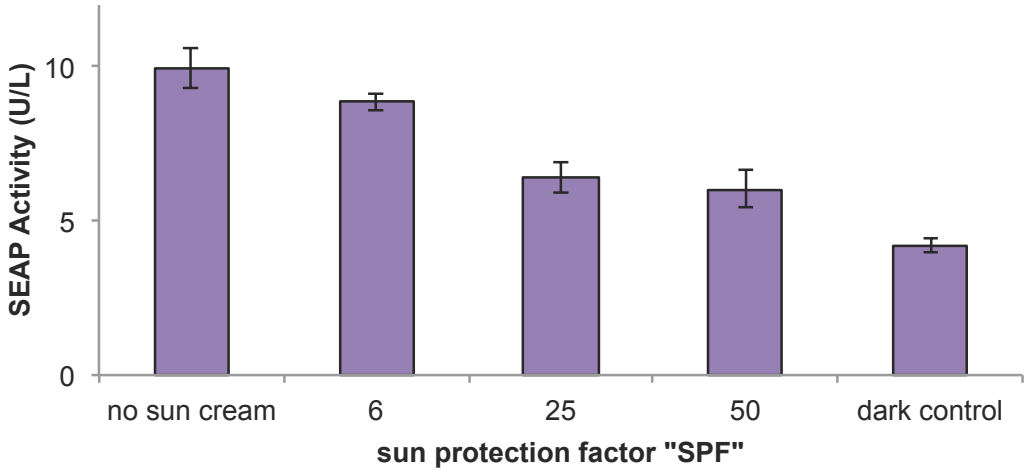

Figure 3. Sun-cream-mediated inhibition of UV-A light-induced SEAP expression. The higher the sun protection factor SPF, the more UV-A light is absorbed and the less reporter gene is expressed. Cells were transfected as described above with 50 ng pPH16, 100 ng pSW214 and 100 ng pMF111 and after

18h, the medium was replaced by 500µL phenol red-free DMEM per 24-well and 1.75mg of broad-spectrum sun cream containing UV-A and UV-B protection filters (Daylong, Spirig Pharma AG, Egerkingen, Switzerland; SPF 6 to SPF50) was circularly spread on the cover lid above the culture well using a T-formed spatule to generate a uniform concentric layer of sun cream (4.4 mg cm^{-2}). Standard Nivea® (Beiersdorf, Hamburg, Germany) cream was used as negative no sun cream control. The set-up was placed 5cm below a custom-manufactured 24-UV-A-LED panel (4x6 360nm LED-array, Solan AG, Basel, Switzerland) operated in intervals of 5s ON (360nm, 25V) and 15s OFF to minimize cytotoxicity. Reporter gene expression was evaluated 24 h after medium change.

In summary, we were able to design and engineer a UV-A and blue-light-inducible gene regulation system for mammalian cells. By exposing mammalian cells harboring this expression system, the transactivator tTA is liberated from the cell membrane and then starts to target gene transcription. We further demonstrated the application of this system as a novel *in vitro* method for quantifying the protection level of sun cream intracellularly. Moreover, the engineered system has a highly versatile setup that can be easily adapted to other mammalian transactivators by simply exchanging the tTA domain and replacing the reporter construct. This will allow for a simple integration into existing complex gene networks, thereby further expanding the potential of synthetic networks.

References

Auslander, S., Auslander, D., Muller, M., Wieland, M., Fussenegger, M., (2012) Programmable single-cell mammalian biocomputers. Nature 487, 123-127.

Bacchus, W., Fussenegger, M., (2012) The use of light for engineered control and reprogramming of cellular functions. Curr Opin Biotechnol 23, 695-702.

Barnea, G., Strapps, W., Herrada, G., Berman, Y., Ong, J., Kloss, B., Axel, R., Lee, K.J., (2008) The genetic design of signaling cascades to record receptor activation. Proc Natl Acad Sci U S A 105, 64-69.

Fussenegger, M., Mazur, X., Bailey, J.E., (1997) A novel cytostatic process enhances the productivity of Chinese hamster ovary cells. Biotechnol Bioeng 55, 927-939.

Gossen, M., Bujard, H., (1992) Tight control of gene expression in mammalian cells by tetracycline-responsive promoters. Proc Natl Acad Sci U S A 89, 5547-5551.

Kapust, R.B., Tozser, J., Fox, J.D., Anderson, D.E., Cherry, S., Copeland, T.D., Waugh, D.S., (2001) Tobacco etch virus protease: mechanism of autolysis and rational design of stable mutants with wild-type catalytic proficiency. Protein Eng 14, 993-1000.

Kennedy, M.J., Hughes, R.M., Peteya, L.A., Schwartz, J.W., Ehlers, M.D., Tucker, C.L., (2010) Rapid blue-light-mediated induction of protein interactions in living cells. Nat Methods 7, 973-975.

Lee, S., Park, H., Kyung, T., Kim, N.Y., Kim, S., Kim, J., Heo, W.D., (2014) Reversible protein inactivation by optogenetic trapping in cells. Nat Methods 11, 633-636.

Liu, H., Liu, B., Zhao, C., Pepper, M., Lin, C., (2011) The action mechanisms of plant cryptochromes. Trends Plant Sci 16, 684-691.

Liu, H., Yu, X., Li, K., Klejnot, J., Yang, H., Lisiero, D., Lin, C., (2008) Photoexcited CRY2 interacts with CIB1 to regulate transcription and floral initiation in Arabidopsis. Science 322, 1535-1539.

Muller, K., Engesser, R., Metzger, S., Schulz, S., Kampf, M.M., Busacker, M., Steinberg, T., Tomakidi, P., Ehrbar, M., Nagy, F., Timmer, J., Zubriggen, M.D., Weber, W., (2013a) A red/far-red light-responsive bi-stable toggle switch to control gene expression in mammalian cells. Nucleic Acids Res 41, e77.

Muller, K., Engesser, R., Schulz, S., Steinberg, T., Tomakidi, P., Weber, C.C., Ulm, R., Timmer, J., Zurbriggen, M.D., Weber, W., (2013b) Multi-chromatic control of mammalian gene expression and signaling. Nucleic Acids Res 41, e124.

Muller, M., Auslander, S., Auslander, D., Kemmer, C., Fussenegger, M., (2012) A novel reporter system for bacterial and mammalian cells based on the non-ribosomal peptide indigoidine. Metab Eng 14, 325-335.

Pelizzo, M., Zattra, E., Nicolosi, P., Peserico, A., Garoli, D., Alaibac, M., (2012) In vitro evaluation of sunscreens: an update for the clinicians. ISRN Dermatol 2012, 352135.

Phan, J., Zdanov, A., Evdokimov, A.G., Tropea, J.E., Peters, H.K., 3rd, Kapust, R.B., Li, M., Wlodawer, A., Waugh, D.S., (2002) Structural basis for the substrate specificity of tobacco etch virus protease. J Biol Chem 277, 50564-50572.

Sang, Y., Li, Q.H., Rubio, V., Zhang, Y.C., Mao, J., Deng, X.W., Yang, H.Q., (2005) N-terminal domain-mediated homodimerization is required for photoreceptor activity of Arabidopsis CRYPTOCHROME 1. Plant Cell 17, 1569-1584.

Sawa, M., Nusinow, D.A., Kay, S.A., Imaizumi, T., (2007) FKF1 and GIGANTEA complex formation is required for day-length measurement in Arabidopsis. Science 318, 261-265.

Schroder-Lang, S., Schwarzel, M., Seifert, R., Strunker, T., Kateriya, S., Looser, J., Watanabe, M., Kaupp, U.B., Hegemann, P., Nagel, G., (2007) Fast manipulation of cellular cAMP level by light in vivo. Nat Methods 4, 39-42.

Wang, X., Chen, X., Yang, Y., (2012) Spatiotemporal control of gene expression by a light-switchable transgene system. Nat Methods 9, 266-269.

Yazawa, M., Sadaghiani, A.M., Hsueh, B., Dolmetsch, R.E., (2009) Induction of protein-protein interactions in live cells using light. Nat Biotechnol 27, 941-945.

Ye, H., Daoud-El Baba, M., Peng, R.W., Fussenegger, M., (2011) A synthetic optogenetic transcription device enhances blood-glucose homeostasis in mice. Science 332, 1565-1568.

CHAPTER II

A novel reporter system for bacterial and mammalian cells based on the non-ribosomal peptide indigoidine

Marius Müller, Simon Ausländer, David Ausländer, Christian Kemmer, Martin Fussenegger

Metabolic Engineering 14, 325-335 (2012)

Abstract

The biosynthesis of non-ribosomal peptides, many of which have pharmaceutical activities, is an evolutionary privilege of microorganisms. Capitalizing on the universal set of the *Streptomyces lavendulae* non-ribosomal peptide synthase BpsA and the *Streptomyces verticillus* 4'phosphopantetheinyl transferase Svp, we have engineered *Escherichia coli* as well as mammalian cells, including human stem cells, to produce the blue 3,3'-bipyridyl pigment keto-indigoidine and the reduced colorless but fluorescent leuco-isoform. Detailed characterization of a tailored substrate-free chromogenic assay and FACS analysis showed that indigoidine's blue color and fluorescence could be reliably profiled in bacteria and mammalian cells using standard multiwell-compatible detection equipment. Besides serving as an inexpensive, reliable, versatile and easy-to-assay cross-kingdom reporter system, the potential of having mammalian cells produce non-ribosomal peptides, preferably ones with biopharmaceutical activities, may provide novel treatment opportunities in future gene- and cell-based therapies.

1. Introduction

Non-ribosomal peptides are exclusively produced by microorganisms and belong to a class of peptide secondary metabolites that includes some of the most valuable medical products such as immunosuppressants (e.g., cyclosporine A), antibiotics (e.g., vancomycin), antiviral compounds (e.g., luzopeptin A) and anticancer drugs (e.g., echinomycin) (Watanabe et al., 2006). Unlike RNA-encoded proteins that are assembled by ribosomes from a set of proteinogenic amino acids, each non-ribosomal peptide is produced by a specific non-ribosomal peptide synthase (NRPS). NRPS are very large proteins containing sets of modules, each consisting of various catalytic domains that form a chemical assembly line that synthesizes peptides in a sequential multi-step enzymatic process (Marahiel et al., 2009). NRPS is produced as an inactive apoform that requires activation by a superfamily of 4'phosphopantetheinyl transferases (PPTases),

which transfer the phosphopantetheinyl group of coenzyme A (CoA) to a conserved serine residue of their T-domain (Lambalot et al., 1996; Sanchez et al., 2001). The resulting holoform of NRPS activates individual amino acids as aminoacyl-adenylates that are fixed at the thiol group of the module's T-domain before it is condensed at the C-domain with the amino acid residues of adjacent modules. The growing peptide chain moves then from one module to the next until the final peptide is released by the catalysis of the thioesterase domain (Strieker et al., 2010). Since many non-ribosomal peptides are clinically relevant, several metabolic engineering-based approaches have been devised to increase production titer and simplify the synthesis in non-mammalian host systems (Kosec et al., 2012; Olano et al., 2008; Qiao et al., 2011) or to enable simplified production in heterologous hosts (Siewers et al., 2009; Watanabe et al., 2006).

The blue 3,3'-bipyridyl pigment indigoidine is a powerful radical scavenger which enables phytopathogens such as *Streptomyces lavendulae* to tolerate H_2O_2, organic peroxides and superoxides produced as part of the plant defense program (Reverchon et al., 2002). Indigoidine is synthesized by condensation of two L-glutamines by a PPTase-activated NRPS (Reverchon et al., 2002; Takahashi et al., 2007). Although NRPS and fatty acid synthases share common enzymatic principles and components of equivalent activities, mammalian cells have so far not been reported to produce any type of non-ribosomal peptides. Here we show that mammalian cells engineered for concomitant expression of the *S. lavendulae* blue pigment synthase A (BpsA) and the *Streptomyces verticillus* PPTase (Svp) are able to produce indigoidine. This blue pigment can be used as a visual indicator peptide, a FACS-compatible fluorescent marker and a reporter compound to precisely measure gene expression using a custom-designed simple, robust, cheap, scalable and high-throughput-compatible assay. Functioning in bacteria as well as in mammalian cells including human stem cells, the indigoidine-based reporter assay could be used as a universal cross-kingdom reporter system. Also, the pioneering example that engineered mammalian cells can in principle be engineered to produce the new compound class of non-ribosomal peptides,

many of which have therapeutic activities, may provide novel treatment opportunities for gene- and cell-based therapies.

2. Materials and Methods

2.1. Vector design. Comprehensive design and construction details for all expression vectors are provided in Table 1.

Plasmid	Description and Cloning Strategy	Reference or Source
pcDNA3.1	Mammalian expression vector (P_{hCMV}-MCS-pA).	Life Technologies, Carlsbad, CA
pCMV-GLuc	Constitutive GLuc expression vector (P_{hCMV}-GLuc-pA).	New England Biolabs, Ipswich, MA
pColaDuet-1	ColA replicon-based bacterial vector for P_{T7lac}-driven transgene expression.	Merck, Darmstadt, Germany
pETDuet-1	ColE1 replicon-based bacterial vector for P_{T7lac}-driven transgene expression.	Merck, Darmstadt, Germany
pMF111	Tetracycline-responsive SEAP expression vector ($P_{hCMV*-1}$-SEAP-pA).	Fussenegger et al., 1997
pSS158	Constitutive SAMY expression vector (P_{hCMV}-SAMY-pA).	Schlatter et al., 2002
pTet-ON	Constitutive rtTA expression vector (P_{hCMV}-rtTA-pA).	Clontech, Palo Alto, CA
pUC57	Bacterial expression vector.	GenScript, Piscataway, NJ
pDA43	Tetracycline-responsive GLuc expression vector ($P_{hCMV*-1}$-GLuc-pA). GLuc was excised from pCMV-GLuc using *BamH*I/*Not*I and cloned into the corresponding sites (*BamH*I/*Not*I) of pMF111.	This work
pMM45	pUC57-derived vector containing C-terminally HA-tagged BpsA (BpsA-HA). Insert synthesized by GenScript (Piscataway, NJ).	This work
pMM46	pUC57-derived vector containing C-terminally c-Myc-tagged Svp (Svp-c-Myc). Insert synthesized by GenScript (Piscataway, NJ).	This work
pMM47	Mammalian BpsA expression vector (P_{hCMV}-BpsA-HA-pA). BpsA-HA was excised from pMM45 using *Eco*RI/*Xba*I and cloned into the corresponding sites (*Eco*RI/*Xba*I) of pcDNA3.1.	This work
pMM48	Mammalian Svp expression vector (P_{hCMV}-Svp-c-Myc-pA). Svp-c-Myc was excised from pMM46 using *Eco*RI/*Xba*I and cloned into the corresponding sites (*Eco*RI/*Xba*I) of pcDNA3.1.	This work
pMM64	Bacterial BpsA expression vector (P_{T7lac}-BpsA-HA-pA). BpsA-HA was excised from pMM45 using *Eco*RI/*Hin*dIII and cloned into the corresponding sites (*Eco*RI/*Hin*dIII) of pETDuet-1.	This work

pMM65	Bacterial Svp expression vector (P_{T7lac}-Svp-c-Myc-pA). Svp-c-Myc was excised from pMM46 using (*Eco*RI/*Hin*dIII) and cloned into the corresponding sites (*Eco*RI/*Hin*dIII) of pColaDuet-1.	This work
pMM80	Tetracycline-responsive mammalian BpsA expression vector ($P_{hCMV*-1}$-BpsA-HA-pA). BpsA-HA was excised from pMM45 using *Eco*RI/*Hin*dIII and cloned into the corresponding sites (*Eco*RI/*Hin*dIII) of pMF111.	This work
pMM81	Tetracycline-responsive mammalian Svp expression vector ($P_{hCMV*-1}$-Svp-c-Myc-pA). Svp-c-Myc was excised from pMM45 using *Eco*RI/*Hin*dIII and cloned into the corresponding sites (*Eco*RI/*Hin*dIII) of pMF111.	This work
pMM95	Tetracycline-responsive SAMY expression vector ($P_{hCMV*-1}$-SAMY-pA). SAMY was excised from pSS158 using *SpeI*/*Hin*dIII and cloned into the complementary sites (*XbaI*/*Hin*dIII) of pMF111.	This work

Table 1. Plasmids used and designed in this study

Abbreviations: **BpsA**, blue pigment synthetase A of *Streptomyces lavendulae* (ATCC 11924) codon-optimized for *homo sapiens*; **c-Myc tag**, protein tag derived from the *c-myc* gene; **GLuc**, *Gaussia* Luciferase codon-optimized for *homo sapiens*; **HA tag**, protein tag derived from the human influenza hemagglutinin; **MCS,** multiple cloning site; **P_{hCMV},** human cytomegalovirus immediate early promoter; **$P_{hCMV*-1}$,** tetracycline-responsive promoter; **P_{T7lac},** lac-inducible variant of the Phage T7 RNA Polymerase promoter; **rtTA,** reverse tetacycline-dependent transactivator; **SAMY**, Bacillus stearothermoilus-derived heat-stable secreted α-amylase; **SEAP**, human placental secreted alkaline phosphatase; **Svp**, *Streptomyces verticillus* (ATCC 15003) 4'-phosphopantetheinyl transferase (PPTase) codon-optimized for *homo sapiens*.

2.2. Bacterial strains and indigoidine production. *Escherichia coli* strain XL10-Gold® (XL10-Gold® ultracompetent cells, Agilent Technologies, Basel, Switzerland; cat. no. 200314) was used for cloning and plasmid propagation. *E. coli* strain BL21 (DE3) Gold (Agilent Technologies; cat. no. 230132) was used for indigoidine production. All *E. coli* strains were grown at 37°C on LB agar plates or in liquid LB medium (Beckton Dickinson, NJ, USA; cat. no. 244610) supplemented with appropriate antibiotics (Ampicillin, 100mg/mL, cat. no. A9518; Kanamycin, 30mg/mL, cat. no. K1377, both from Sigma-Aldrich, Munich, Germany). In transgenic *E. coli* liquid cultures (10ml, cultivated for 4h) expression of the indigoidine-producing

enzymes BpsA and Svp was induced for 6h using 1mM isopropyl-1-thio-β-D-galactopyranoside (IPTG, Sigma-Aldrich, Munich, Germany; cat. no. I6758).

2.3. Cell culture and transfection. Human embryonic kidney cells (HEK293-T, ATCC: CRL-11268 (Mitta et al., 2002)) and human bone marrow stromal cells transgenic for the catalytic subunit of human telomerase (hMSC-TERT; (Simonsen et al., 2002)) were cultivated in Dulbecco's modified Eagle's medium (DMEM; Invitrogen, Basel, Switzerland; cat. no. 52100-039) supplemented with 10% (v/v) fetal calf serum (FCS; Bioconcept, Allschwil, Switzerland; cat. no. 2-01F10-I; lot no. PE01026P) and 1% (v/v) penicillin/streptomycin solution (Biowest, Nuaillé, France; cat. no. L0022-100). Human embryonic kidney cells adapted for growth in suspension (FreeStyle 293-F, Invitrogen, Carlsbad CA, USA) were cultivated in GIBCO® FreeStyle 293-F Expression Medium (Invitrogen, Carlsbad CA, USA; cat. no. 12338-018). All cell lines were cultivated at 37°C in a 5% CO_2-containing humidified atmosphere. Cells grown in suspension were cultivated on an orbital shaker (IKA KS 260 basic, IKA®-Werke GmbH & CO. KG, Staufen, Germany) at 100rpm. Whenever indicated, the culture medium was adjusted to specific pH and buffered using 25mM HEPES (AppliChem GmbH, Darmstadt, Germany; cat. no. A3724). The pH was monitored in real time using sensor dish-plates and the corresponding sensor dish reader (SDR SensorDish Reader, PreSens Precision Sensing GmbH, Regensburg, Germany; cat. no. 200000431).

All cell lines were transfected using an optimized polyethyleneimine (PEI)-based protocol. In brief, a transfection solution containing 1µg of plasmid DNA mixtures, 2µL PEI (PEI "max", 1mg/mL in water; Polysciences, Eppelheim, Germany; cat. no. 24765-2) was incubated for 30min at 37°C before it was added dropwise to $1x10^5$ cells ($5x10^5$ FreeStyle 293-F) seeded per well of a 24-well plate the day before transfection. Cells were counted and their viability was assessed using an electric field multi-channel cell counting device (Casy® Cell Counter and Analyser Model TT; Roche Diagnostics GmbH, Basel, Switzerland).

2.4. Indigoidine assay. The detailed protocol is illustrated in Figure 3B. A 24-well plate containing adherent mammalian cells was co-transfected with indigoidine

producer plasmids (pMM47 and pMM48). 48h after transfection, the cells were washed once with 1x PBS (Dulbecco's Phosphate-Buffered Saline; Invitrogen, Basel, Switzerland; cat. no. 21600-069). Alternatively, suspension cells were transferred to a 1.5ml Eppendorf tube, centrifuged for 3min at 100xg, washed once with 1x PBS and centrifuged again for 3min at 100xg. The cells were then lysed and indigoidine dissolved for 5min by the addition of 100µL DMSO supplemented with 5mM ascorbic acid (to stabilize indigoidine). The plate was then shaken at 50°C and 500rpm for 5min on a thermoshaker (Thermomixer comfort, Vaudaux-Eppendorf AG, Schönenbuch/Basel, Switzerland). A 100µL sample was transferred to a well of a transparent 96-well plate and absorbance was scored at 612nm relative to a sample containing 100µL DMSO and 5mM ascorbic acid for standardization using an Envision plate-reader (Envision 2104 Plate-reader, Perkin Elmer, MA, USA).

2.5. Bright field and fluorescence microscopy. Indigoidine-producing mammalian cells were visualized using a Leica DMI 6000B fluorescence microscope equipped with a Leica DC300 FX digital camera (Leica Microsystems AG, Heerbrugg, Switzerland) and a XF114 filter (Omega Optical Inc., Brattleboro, VT). Fluorescence micrographs of indigoidine-producing cells were taken using the same microscope equipped with a 420/30nm excitation and 465/20nm emission filter set (Blue, B/G/R, Leica Microsystems AG, Heerbrugg, Switzerland) and exposure times set to 500ms.

2.6. Western blot analysis. For Western blot analysis, $1x10^6$ HEK293-T cells were resuspended in lysis buffer (50mM Tris-HCl (pH 7.5), 0.15M KCl, 5mM $MgCl_2$, 0.2mM EDTA, 20% (v/v) glycerol containing 0.5mM DTT and a cocktail of protease inhibitors (Roche, Mannheim, Germany; cat. no. 11873580001)) and sonicated for 30s using a Bioruptor (Bioruptor, Diagenode, Liège, Belgium). The lysate was cleared from cell debris by centrifugation (4000xg for 10min at 4°C) and the protein content of the supernatant was quantified (Bio-Rad protein assay; Bio-Rad Laboratories, Hercules, CA, USA; cat. no. 500-0006). Samples of 25µg protein were mixed with 5x loading buffer (10% SDS, 1M Tris pH 6.8, 50% glycerol, 0.2% bromphenol blue, 0.5M DTT), resolved on a 10% SDS-PAGE and electroblotted (Trans-blot SD semi-dry transfer cell; Bio-Rad, Hercules, CA, USA) onto a polyvinylidene fluoride membrane (Immobilon-P,

Millipore, Billerica, MA, USA; cat. no. IPVH00010). BspA and Svp were visualized using anti-HA (Santa Cruz Biotechnology Inc., Santa Cruz, CA, USA; cat. no. sc-7392, lot no. H2410) and anti-c-Myc primary antibodies (Sigma-Aldrich, Munich, Germany; cat. no. M4439, lot no 119K4760), respectively, a horseradish peroxidase-conjugated anti-mouse secondary antibody (GE Healthcare, Buckinghamshire, UK; cat. no. NA931V, lot no. 399402) and ECL Plus Western blotting reagents (Amersham, GE Healthcare, Buckinghamshire, UK; cat. no. RPN2132). Actin was used as loading control (primary anti-actin antibody, Sigma-Aldrich, Munich, Germany; cat. no. A2066, lot no. 030M4844; secondary horseradish peroxidase-coupled anti-rabbit antibody, AbD Serotec, Oxford, UK; cat. no. STAR54, lot no. 291010).

2.7. SEAP assay. The protocol was adapted from Berger (Berger et al., 1988) as well as Schlatter and colleagues (Schlatter et al., 2002). In brief, 200µL cell culture supernatant were heat-inactivated for 30min at 65°C and centrifuged at 14.000xg for 15s. Subsequently, 80µl of the supernatant were transferred to a well of a 96-well plate containing 100µL 2xSEAP assay buffer (20mM homoarginine, 1mM $MgCl_2$, 21% diethanolamine pH 9.8). After addition of 20µl 120mM para-nitrophenylphosphate (pNPP disodium salt, hexahydrate, Acros Organics BVBA, Geel, Belgium; cat. no. 12886-0100) diluted in 1x SEAP assay buffer, the time-dependent increase in light absorbance was profiled at 405nm for 30min using a GeniosPro multi-well reader (TECAN AG, Maennedorf, Switzerland).

2.8. *Gaussia* luciferase assay. Activity of *Gaussia* Luciferase was assessed according to the manufacturer's protocol (BioLux *Gaussia* Luciferase Assay Kit, New England Biolabs Inc, Ipswich, MA, USA, cat. no. #3300S). In brief, 10µL of cell culture supernatant were transferred into a black 96-well plate. 50µL of reaction mix (containing 42µL BioLux Gluc Flex Assay Buffer, 8µL BioLux Gluc Flex Stabilizer and 0.1µL BioLux Gluc Flex Substrate) were added to the cell culture supernatant. *Gaussia* Luciferase levels were measured by integrating the luminescence signal for 2 seconds per well using an Envision plate-reader (Envision 2104 Plate-reader, Perkin Elmer, MA, USA).

2.9. SAMY assay. The protocol was adapted from Muscholl-Silberhorn (Muscholl-Silberhorn et al., 2000) and Schlatter and colleagues (Schlatter et al., 2002). In brief, 100µL of cell culture supernatant were centrifuged at 14.000xg for 2min. 50µL were transferred into an Eppendorf cup also containing 1mL substrate solution (45mg blue starch [1 Phadebas tablet, Pharmacia and Upjohn, Uppsala, Sweden, cat. no. 10-5380-32], 4mL ddH_2O) and incubated at 70° C for 15min. The reaction was stopped by the addition of 250µL of 0.5M NaOH, centrifuged for 5min at 14.000xg and 100µl of the supernatant were transferred into a transparent 96-well plate. α-amylase levels were measured at 620nm against samples using the supernatant of identical, but reporter-negative cell cultures using an Envision plate-reader (Envision 2104 Plate-reader, Perkin Elmer, MA, USA).

2.10. Photophysical analysis. To convert keto-indigoidine into the leuco-indigoidine isoform 1µl of a reducing agent (0.15g of sodium dithionate in 10mL of a 1M solution of sodium hydroxide) was added to DMSO-lysed/dissolved indigoidine-producing cells. Absorbance and fluorescence were analyzed using an Envision plate-reader (Envision 2104 Plate-reader, Perkin Elmer, MA, USA).

2.11. FACS analysis. Transfected and untransfected HEK293-T cells were analyzed using a Becton Dickinson LSR Fortessa flow cytometer (Becton Dickinson, Allschwil, Switzerland) equipped with a violet laser (405 nm laser, 520 nm longpass filter, 560/40 emission filter). The cells were gated to exclude cell doublets, dead cells and cell debris. At least 10.000 cells were recorded per data set and analyzed using FlowJo-877 software (Tree Star Inc., Ashland, OR, USA, version no. 7.6.3.).

3. Results

3.1. Design and characterization of an isogenic indigoidine reporter system for bacteria and mammalian cells. The non-ribosomal peptide indigoidine is a particularly attractive reporter compound since it is a naturally occurring metabolically inert blue pigment. It is produced from ubiquitous cellular L-glutamine involving the *Streptomyces lavendulae*-derived non-ribosomal peptide synthase (NRPS) BpsA (blue pigment synthase A), the 4'-phosphopantetheinyl transferase (PPTase) of *Streptomyces*

verticillus (Svp) and coenzyme A as a cofactor (Takahashi et al., 2007). In order to have a functional system, the inactive apo-BpsA needs to be activated by Svp via the addition of a coenzyme A-derived 4'phosphopantetheine moiety to the T (thiolation)-domain of the NRPS resulting in the holo-form of BpsA (Figure 1A; (Lambalot et al., 1996)). The activated NRPS is now able to convert L-glutamine by a sequential multi-step reaction into indigoidine (Figure 1B; (Reverchon et al., 2002))

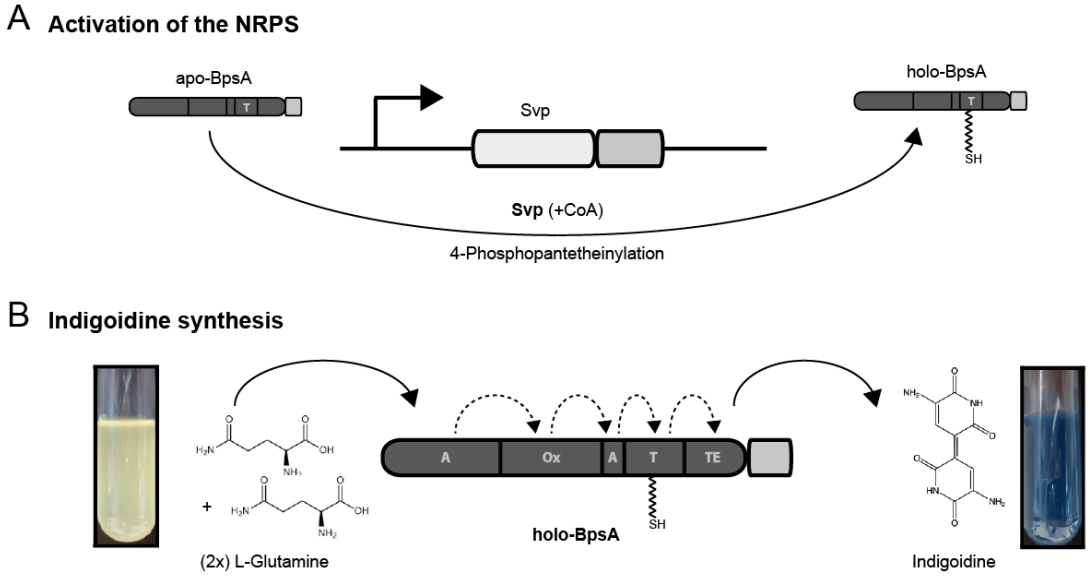

Figure 1 | Components and mechanism of the indigoidine reporter system. (**A**) Activation of the *Streptomyces lavendulae* non-ribosomal peptide synthase (NRPS) BpsA (blue pigment synthase A) by the *Streptomyces verticillus* 4'phosphopantetheinyl transferase (PPTase; Svp). BpsA is converted from an inactive apo-enzyme (apo-BpsA) to an active holo-isoform (holo-BpsA) by Svp-mediated transfer of a coenzyme A-derived moiety to the thiolation (T-) domain of the NRPS. (**B**) BpsA-mediated indigoidine synthesis. Active holo-BpsA converts two L-glutamines to one molecule of blue-pigment indigoidine by a sequential catalytic process involving adenylation (A), oxidation (Ox), thiolation (T) and thioesterase (TE) domains. The test tubes show wild-type (turbid) and BpsA and Svp-expressing (dark blue) *Escherichia coli* cultures.

We have designed a set of isogenic BpsA and Svp expression vectors that establishes indigoidine as a cross-kingdom reporter system to score gene expression in bacteria as well as in mammalian cells. Therefore, BpsA (pMM64, P_{T7lac}-BpsA-HA-pA) and Svp (pMM65, P_{T7lac}-Svp-c-Myc-pA) were tagged, codon-optimized for expression

in *Homo sapiens* and cloned into P_{T7lac}-driven expression units of compatible replicons to enable IPTG-triggered co-expression of the NRPS and PPTase in bacteria (Figure 2A). Indeed, when co-transformed into *Escherichia coli* pMM64/65-transgenic cultures turn blue due to high-level indigoidine production resulting from coordinated activities by the human codon-optimized BpsA and Svp variants (Figure 2B-C). The observation, that the supernatant of pelleted transgenic *E. coli* populations remains blue indicates that indigoidine is secreted by these bacteria (Figure 2B). Furthermore, colonies of pMM64/65-transformed *E. coli* turn blue suggesting that the indigoidine system may become an alternative to the proven lacZ-based blue/white screening system with the advantage that indigoidine production does not require additional substrates, such as 5-bromo-4-chloro-indolyl-galactopyranoside (X-gal) (Figure 2C).

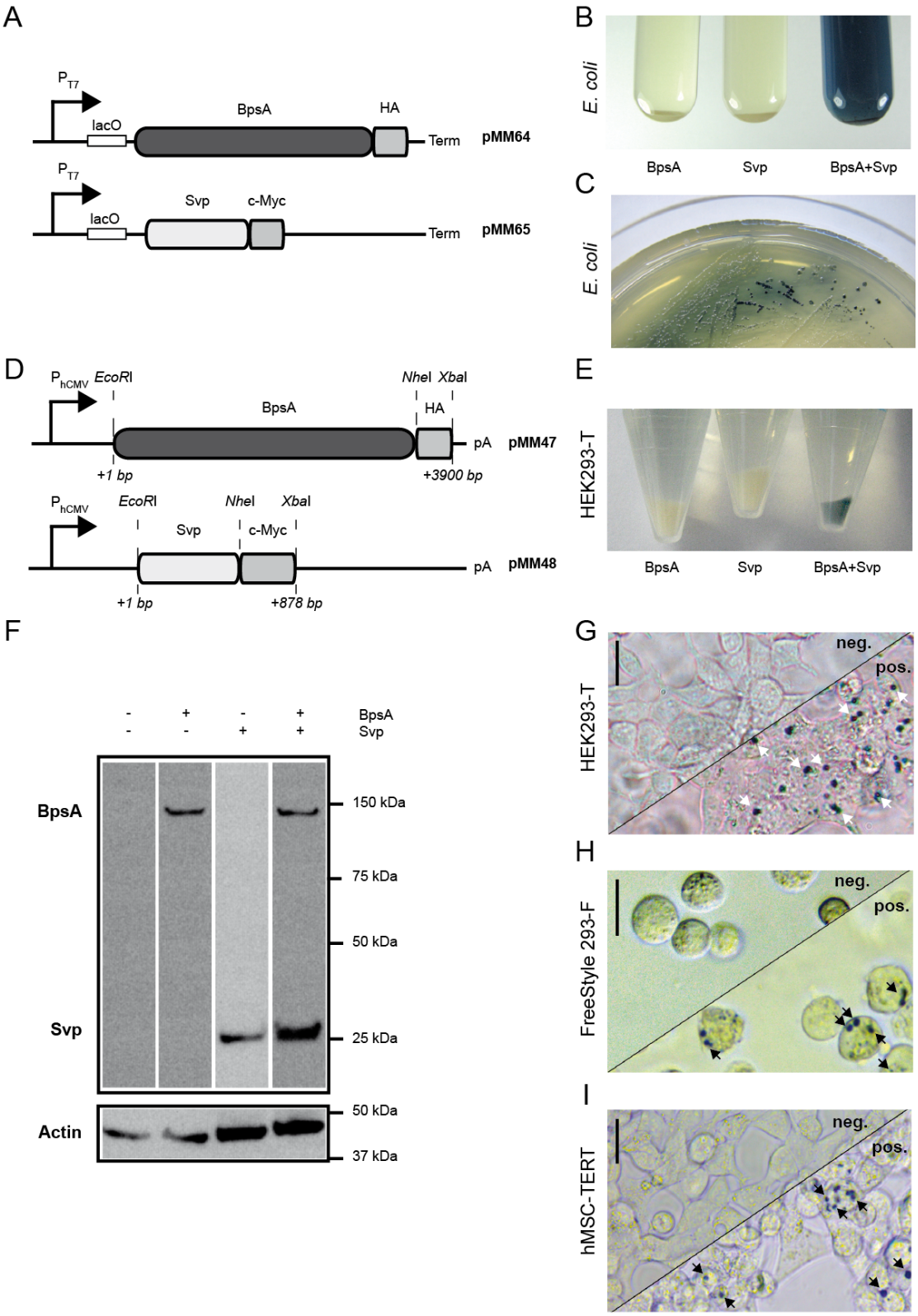

Figure 2 | Genetic design and validation of indigoidine production in bacteria and mammalian cells. (**A**) Design of bacterial indigoidine production vectors pMM64 and pMM65 (see Table 1). IPTG-inducible P_{T7lac} promoters consisting of the Phage T7 promoter with a 3' lactose operator (lacO), drive expression of HA-tagged BpsA (blue pigment synthase A) and c-Myc-tagged 4'phosphopantetheinyl transferase (PPTase; Svp). (**B**) Pelleted liquid cultures of *Escherichia coli* expressing either BpsA or Svp or both enzymes (BpsA + Svp) for indigoidine production. (**C**) *E. coli* colonies expressing BpsA

alone (white colonies) or BpsA and Svp (blue colonies). (**D**) Design of mammalian indigoidine production vectors pMM47 and pMM48 (see Table 1). The human cytomegalovirus immediate early promoters (P_{hCMV}) drive constitutive expression of HA-tagged BpsA (blue pigment synthase A) and c-Myc-tagged 4'phosphopantetheinyl transferase (PPTase; Svp). (**E**) Pelleted HEK293-T cells expressing either BpsA or Svp or both indigoidine production enzymes (BpsA + Svp). (**F**) Tag-specific Western blot analysis of mammalian cells expressing BpsA (pMM47; HA-tag) and Svp (pMM48; c-Myc-tag) alone or together (+/-). Actin was used as loading control. (**G-I**) pMM47 only (neg.) and pMM47/48-transfected (pos.) HEK293-T monolayer culture (**G**), FreeStyle 293-F suspension culture (**H**) and human stem cell (hMSC-TERT) monolayer culture (**I**). Intracellular blue indigoidine storage granules are indicated by arrows. All micrographs were taken 48h after transformation/transfection. Scale bar = 25µm.

Likewise, when cloned into an isogenic mammalian expression configuration driven by the constitutive cytomegalovirus immediate early promoter ($P_{hCMV;}$ pMM47, P_{hCMV}-BpsA-HA-pA; pMM48, P_{hCMV}-Svp-c-Myc-pA) (Figure 2D) and co-transfected into human embryonic kidney cells (HEK293-T) the cell pellet of pMM47/48-transgenic human cells was blue while the supernatant remained clear (Figure 2E). Western blot analysis of corresponding cell populations confirmed expression of BpsA and Svp in mammalian cells (Figure 2F). This indicated that mammalian cells could be successfully engineered for the production of non-ribosomal peptides, a synthetic activity that was so far limited to bacterial and lower eukaryotic species. Also, unlike bacteria, mammalian cells do not appear to secrete indigoidine (Figure 2E). Indeed, bright field micrographs of pMM47/48-co-transfected HEK293-T cells grown in monolayer (HEK293-T; Figure 2G) or suspension (FreeStyle 293-F; Figure 2H) cultures as well as human bone marrow stromal cells (hMSC-TERT; Figure 2I) revealed insoluble blue indigoidine storage granules inside cells (Figure 2G-I).

3.2. Development of a quantitative indigoidine reporter assay for mammalian cells. Design of a robust and reliable indigoidine-based assay for mammalian cells requires release, solubilization, stabilization and quantification of the blue pigment contained in intracellular storage granules. Extensive testing of different solvents showed that simple addition of DMSO to indigoidine-producing monolayer or pelleted

suspension cultures was able to lyse, extract and solubilize indigoidine in a way that enabled optimal light absorbance-based quantification of the blue pigment at 612nm (Figure 3A). Since the assay can be performed directly in the cultivation well without the need of complex handling, purification steps and substrates the indigoidine reporter system is simple, robust, cheap and scalable to a multi-well format (Figure 3B). Due to its chemical nature, indigoidine is an efficient radical scavenger that looses its blue color when it captures reactive oxygen species and radicals thereby compromising the assay readout (Reverchon et al., 2002). However, degradation of the blue color after DMSO-mediated extraction from mammalian inclusion bodies could be efficiently prevented by addition of inexpensive ascorbic acid (vitamin C). Since vitamin C is a more powerful radical scavenger compared to indigoidine it efficiently protects the blue pigment from loosing its color. Supplementing the assay cocktail with 5mM vitamin C stabilized indigoidine's peak absorbance at 612nm for more than 10h (Figure 3C). Including the stabilizer vitamin C in the standard indigoidine assay enabled reliable quantification of the blue pigment produced by human embryonic kidney cells grown as monolayer (HEK293-T) or suspension (FreeStyle 293-F) cultures or when expressed in human bone marrow stromal cells (hMSC-TERT) (Figure 3D).

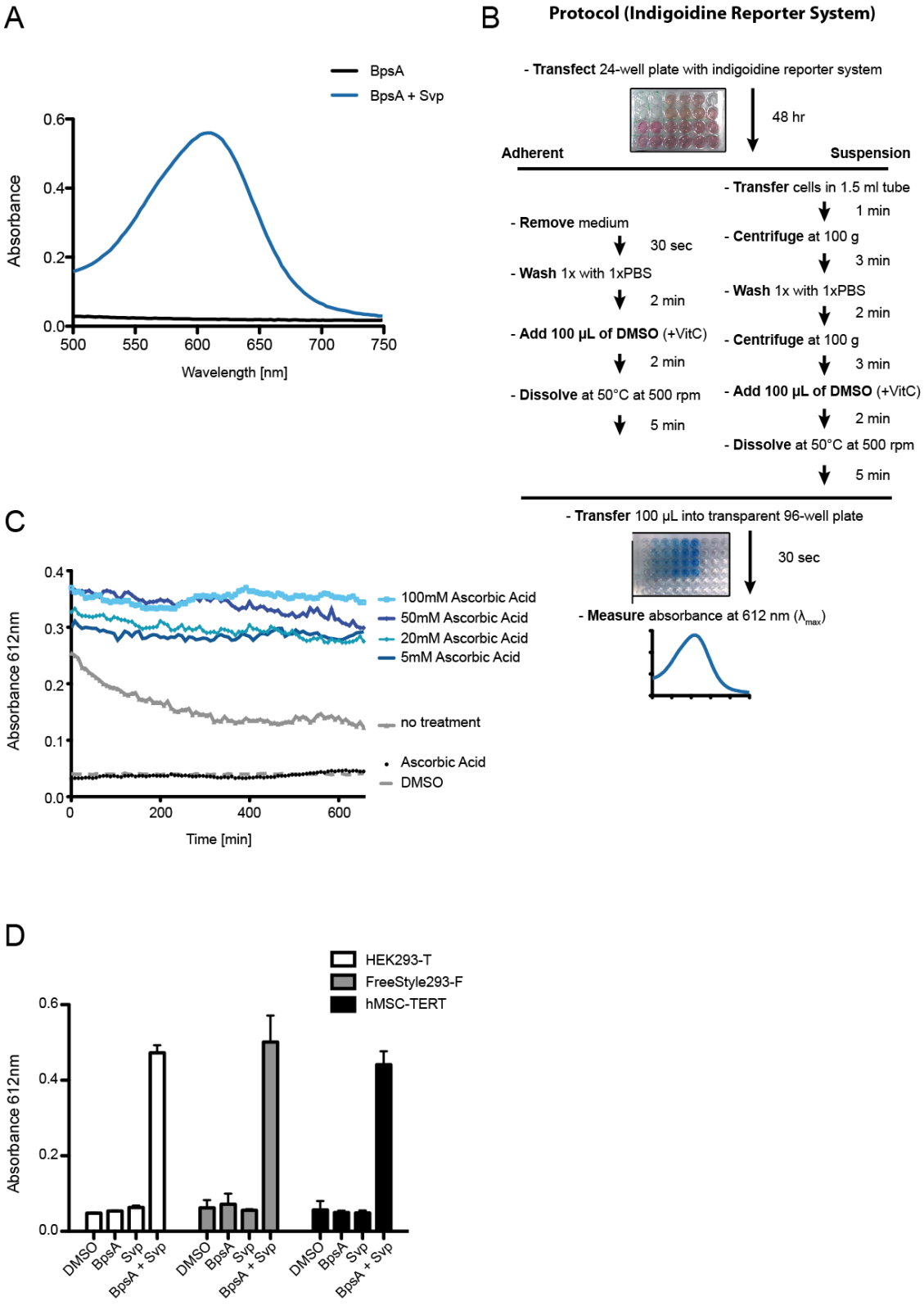

Figure 3 | Design and validation of the indigoidine-based absorbance assay. (**A**) Absorbance spectrum of DMSO-mediated lysates of HEK293-T 48h after transfection with vectors encoding only BpsA (BpsA, no indigoidine production) or BpsA and Svp (BpsA+Svp; indigoidine production). (**B**) Detailed protocol for quantitative analysis of indigoidine production in mammalian monolayer and suspension cultures. (**C**) Absorbance kinetics of DMSO-lysed/dissolved indigoidine-containing cell

lysates spiked with various concentrations of the stabilizer ascorbic acid. (**D**) Peak absorbance at 612nm of DMSO-lysed/dissolved indigoidine-containing cell lysates generated from HEK293-T, FreeStyle 293-F and hMSC-TERT cell lines transfected with either or both BpsA and Svp expression vectors. All assays were performed 48h after transfection of indigoidine-producing expression vectors pMM47 and/or pMM48.

3.3. Detailed characterization of indigoidine production parameters in mammalian cells. To characterize the indigoidine production in mammalian cells we analyzed various key parameters including the concentration of the substrate L-glutamine, the levels of ions that act as cofactors for glutamine synthase ($MnCl_2$; (Lambalot et al., 1996)) and PPTase ($MgSO_4$; (Lee et al., 2006)), pH of the culture medium, absolute and relative expression levels of NRPS and PPTase as well as the impact on cell viability.

With a standard L-glutamine concentration of 4mM, DMEM seems to already provide an optimal substrate concentration for the production of indigoidine (Figure 4A). The blue pigment levels could only be improved marginally by increasing L-glutamine in the culture medium up to 20mM (Figure 4A). Although manganese and magnesium ions had been reported to be important cofactors of glutamine synthase and PPTase, respectively (Lambalot et al., 1996; Lee et al., 2006), variation of the respective ion levels in the DMEM culture medium had no impact on the overall production of indigoidine. This confirms that L-glutamine levels are not a bottleneck and that PPTase activity is not a limiting factor in the production of indigoidine in mammalian cells either (Figure 4B-C). *In vitro* analysis of BpsA showed that this NRPS has its maximum enzymatic activity between pH 7.8 and pH 9.0 (Owen et al., 2011). Evaluation of different cell culture-compatible pH values on indigoidine production showed that the default physiologic pH of DMEM (range from pH 7.2 to pH 7.6) already enabled optimal performance of the reporter system (Figure 4D). Since BpsA and Svp team up to produce indigoidine, different absolute and relative expression levels may impact the cellular blue-pigment production capacity. In order to evaluate the contribution of various quantities of the single enzyme components we titrated the ratios of BpsA- and Svp-encoding plasmids from excess NRPS (20:1) to an excess of PPTase (1:20) (Figure

3E). The correlation of the highest indigoidine levels with maximum BspA expression suggested that BpsA rather than Svp was the bottleneck in the production of the blue pigment (Figure 4E). Importantly, the presence of intracellular indigoidine had no impact on the viability of mammalian cells as shown by flow cytometry (data not shown) and electric field multi-channel cell analysis (Figure 4F).

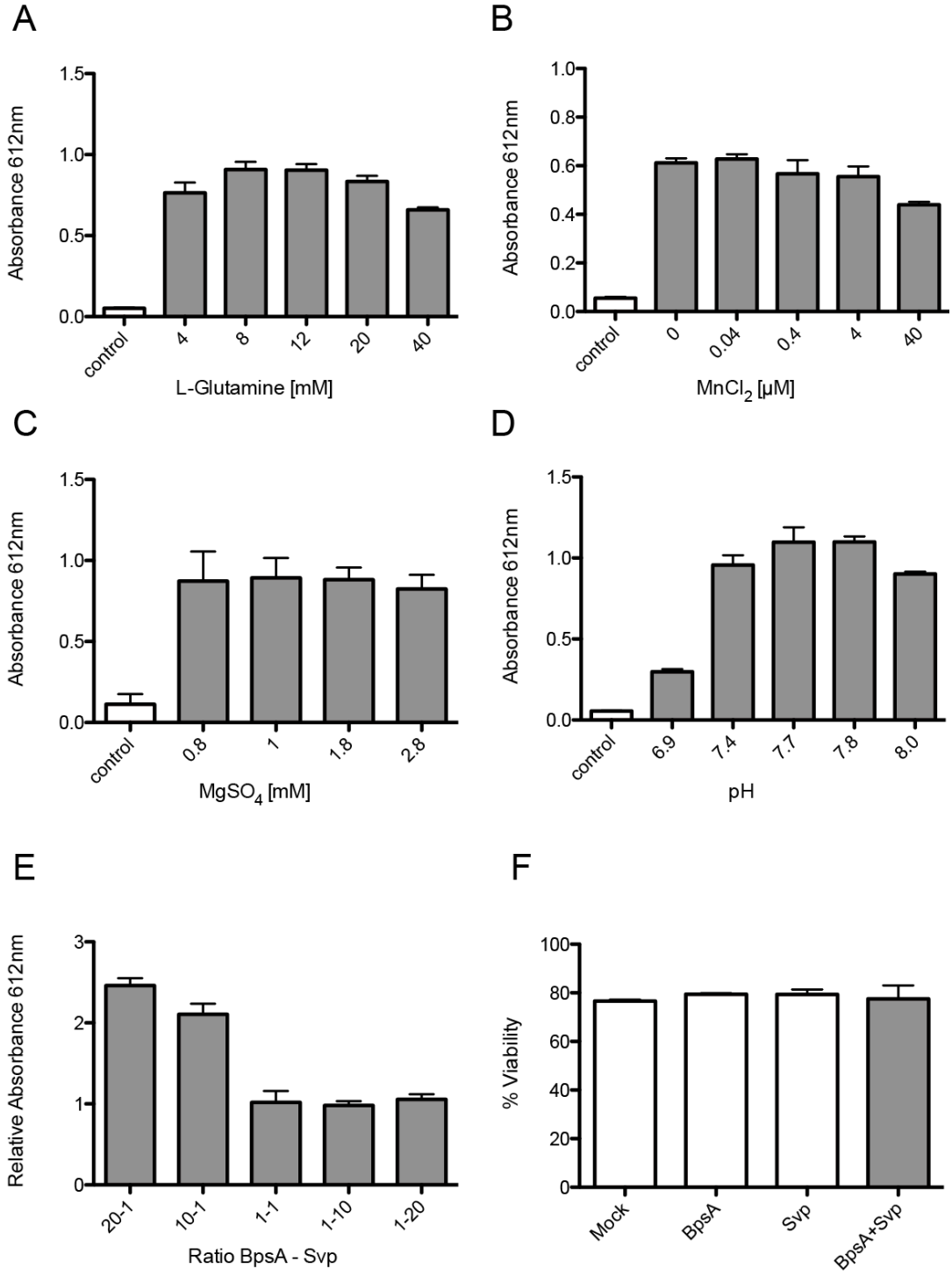

Figure 4 | Detailed characterization of the indigoidine reporter assay. (**A-D**) Indigoidine production of HEK293-T cells 48h after transfection with pMM47 and pMM48. Absorbance of DMSO-lysed/dissolved indigoidine-containing cell lysates generated from pMM47/48-transfected

HEK293-T and adjusted to different L-Glutamine (**A**) manganese (**B**) and magnesium (**C**) concentrations or pH (**D**). (**E**) Indigoidine levels produced by HEK293-T cells 48h after transfection with different ratios of BpsA- (pMM47-) and Svp- (pMM48-) encoding expression vectors. (**F**) Viability of HEK293-T cells 48h after transfection with an isogenic control vector (pcDNA3.1), BpsA- (pMM47-) and/or Svp- (pMM48-) encoding expression vectors.

3.4. Adjustability and compatibility of the indigoidine reporter system. Combinatorial gene expression profiling is an important tool for gene-function analysis in the post-genomic era. To validate the versatility of the indigoidine reporter system in this context, we tested its performance when adjustably expressed together with other reporter proteins. Therefore, the indigoidine-producer components BpsA (pMM80, $P_{hCMV*-1}$-BpsA-HA-pA) and Svp (pMM81, $P_{hCMV*-1}$-Svp-c-Myc-pA) as well as the human placental secreted alkaline phosphatase (SEAP; pMF111, $P_{hCMV*-1}$-SEAP-pA), the humanized form of the *Gaussia* Luciferase (GLuc; pDA43, $P_{hCMV*-1}$-GLuc-pA) or the *Bacillus stearothermophilus*-derived heat-stable secreted α-amylase (SAMY: pMM95; $P_{hCMV*-1}$-SAMY-pA) (Figure 5A) were cloned under the control of the tetracycline-responsive promoter ($P_{hCMV*-1}$). In this configuration, both indigoidine production and the expression of the secreted reporter proteins can be dose-dependently induced by doxycycline when all reporter units are co-induced by the reverse tetracycline-dependent transactivator (rtTA) (Gossen et al., 1995). Indeed, indigoidine production in HEK293-T cells, showed similar doxycycline-triggered induction kinetics when compared to classic reporter proteins such as SEAP, SAMY and GLuc. This confirms that the blue pigment is a reliable, robust and sensitive reporter compound that can be used together with other protein-based reporter tools (Figure 5B).

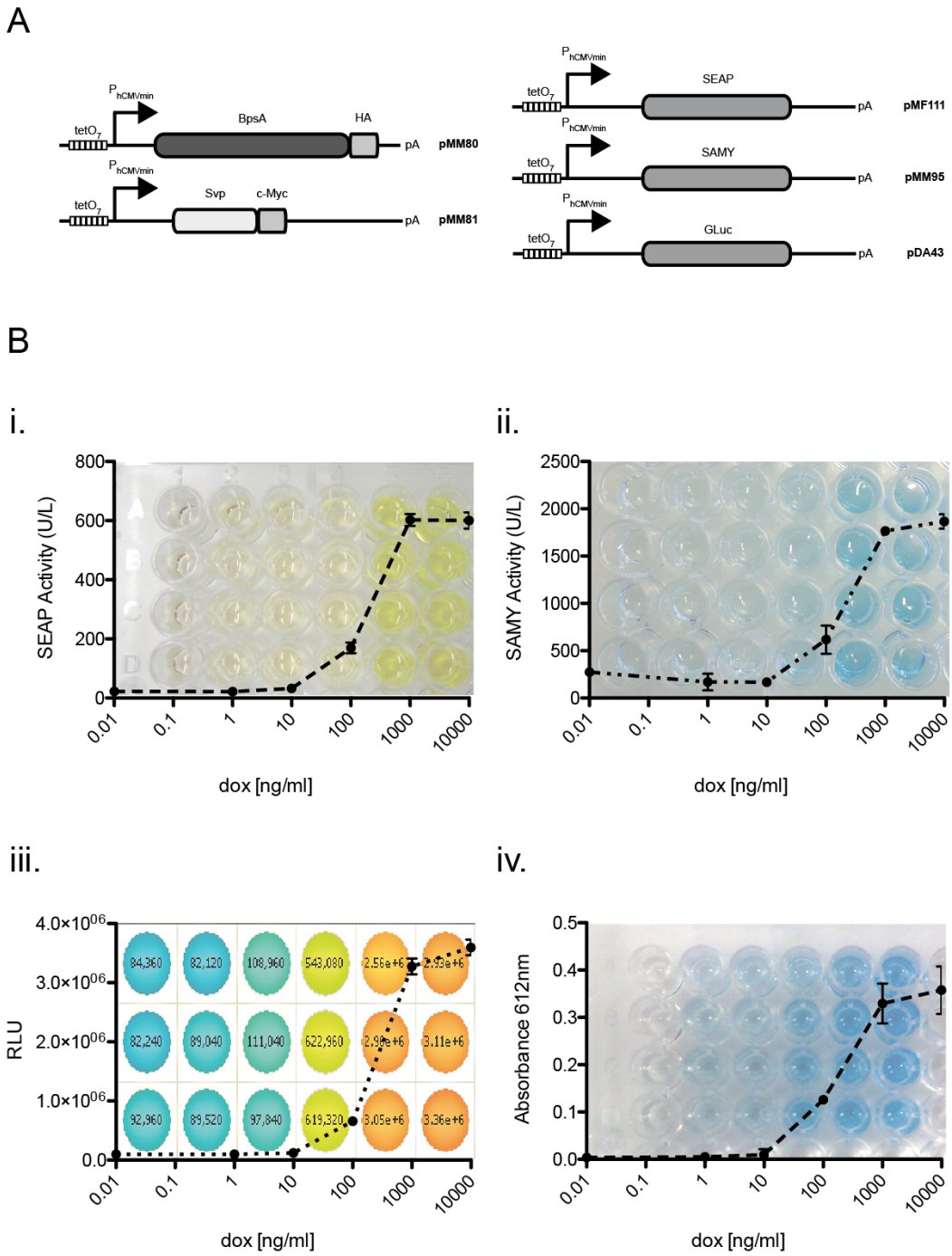

Figure 5 | Compatibility and adjustability of the indigoidine reporter system. (**A**) Design of the doxycycline-inducible reporter gene expression vectors. BpsA and Svp expression vectors are isogenic to the ones shown in Figure 2D but are driven by $P_{hCMV*-1}$, a synthetic promoter consisting of a heptameric operator sequence of the tetracycline operator ($tetO_7$) and a minimal version of the human cytomegalovirus immediate early promoter ($P_{hCMVmin}$). Equally driven by $P_{hCMV*-1}$ are the co-expressed secreted reporters the human placental secreted alkaline phosphatase (SEAP, pMF111), the *Bacillus stearothermophilus*-derived heat-stable secreted α-amylase (SAMY, pMM95) or the humanized form of the *Gaussia* Luciferase (GLuc, pDA43). $P_{hCMV*-1}$ is transactivated by the reverse tetracycline-

dependent transactivator (rtTA) in a doxycycline-inducible manner. (**B**) Simultaneous doxycycline-adjustable production of the secreted reporter proteins (**i**) SEAP, (**ii**) SAMY or (**iii**) GLuc, (all ribosomal peptides) and (**iv**) indigoidine (a non-ribosomal peptide) by HEK293-T co-transfected with pTet-ON (P_{hCMV}-rtTA-pA), pMM80 ($P_{hCMV*-1}$-BpsA-pA), pMM81 ($P_{hCMV*-1}$-Svp-pA) and either pMF111 ($P_{hCMV*-1}$-SEAP-pA), pDA43 ($P_{hCMV*-1}$-GLuc-pA) or pMM95 ($P_{hCMV*-1}$-SAMY-pA). Reporter levels were profiled 48 hours after transfection and blanked against reporter-negative cells.

3.5. Indigoidine is also a versatile fluorescence marker compatible with standard flow cytometric analysis. Live-cell flow cytometry allows for morphological analysis such as cell volume and granularity and enables accurate sorting of fluorescent reporter-positive cells (Ornatsky et al., 2010). Flow cytometric analysis of cell populations containing the indigoidine reporter system showed a higher percentage of cells with increased granularity and volume compared to isogenic controls of cells, which do not produce the blue pigment (Figure 6A).

Inspired by the photophysical and spectroscopic analysis of the blue dye indigo that revealed detectable fluorescence and significant quantum yields for its reduced colorless leuco form (Seixas de Melo et al., 2004), we tested whether the related pigment indigoidine also exists in two variants, the insoluble oxidized blue-colored keto species and the reduced water-soluble colorless leuco isoform. As shown by light absorbance spectroscopy, addition of a reducing agent (sodium dithionite in sodium hydroxide) to a cell-derived DMSO-dissolved blue indigoidine solution shifted the blue keto-indigoidine to the colorless soluble leuco-indigoidine isoform (Figure 6B). Furthermore, photophysical analysis of the indigoidine's leuco isoform revealed intrinsic fluorescence when excited at 415nm and recorded at 520nm (Figure 6C). Leuco-indigoidine could also be visualized by fluorescence microscopy of indigoidine-producing mammalian cells (Figure 6D) and was successfully used as a marker for flow cytometric analysis of indigoidine-producing cells when using a violet laser set-up for excitation (Figure 6E).

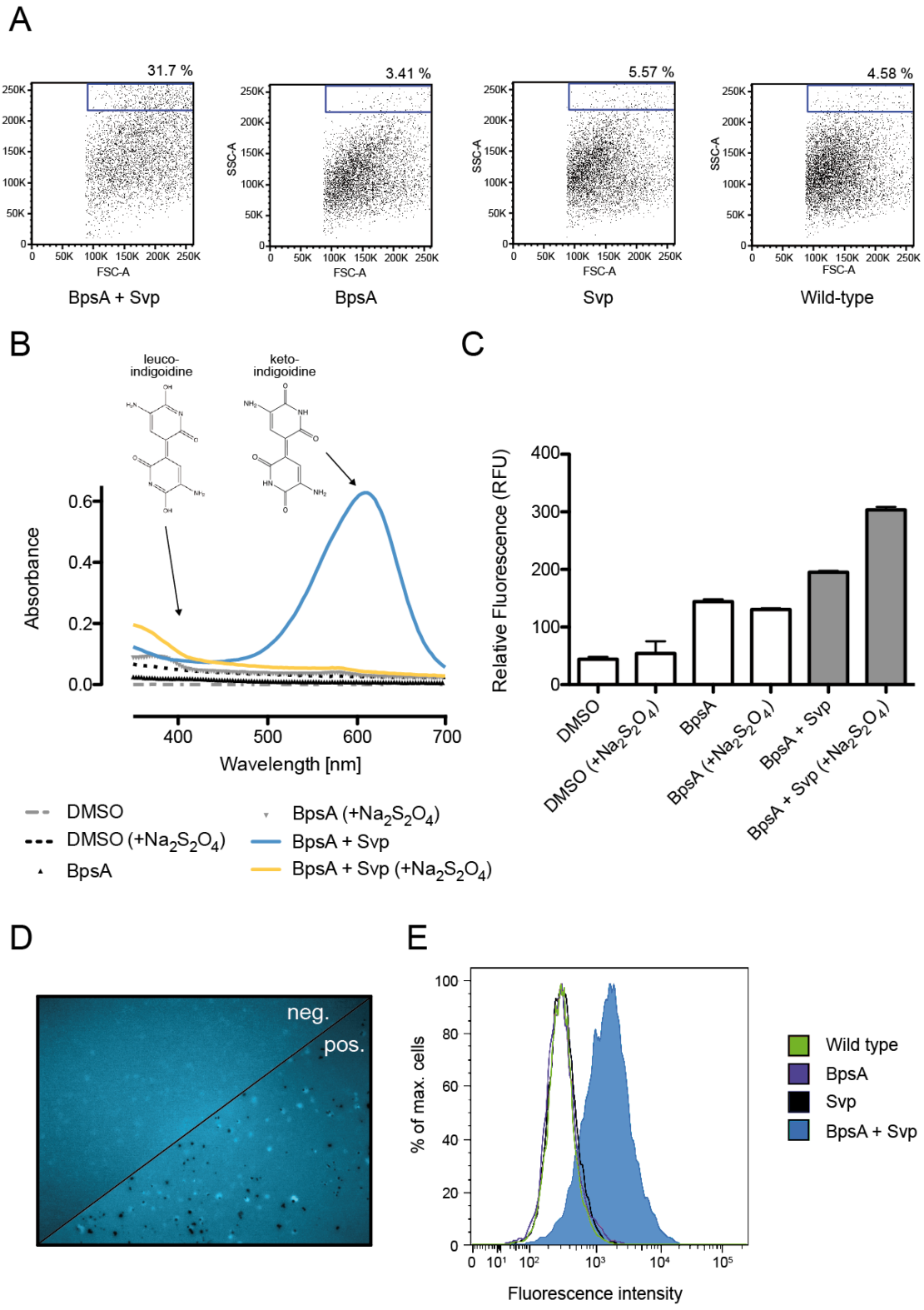

Figure 6 | Spectroscopic and flow cytometric analysis of indigoidine-producing mammalian cells. (**A**) Flow cytometric analysis of HEK293-T 48h after transfection with either or both BpsA and Svp expression vectors (pMM47 and pMM48). Untransfected wild-type HEK293-T were used as control. The cells were scored for high forward (FSC-A) and side (SSC-A) scatter (blue rectangle). (**B**) Absorbance spectra of the blue keto- and the colorless leuco-indigoidine isoforms produced for 48h by

pMM47-/pMM48-transfected HEK293-T cells. In order to increase the leuco-indigoidine isoform the cell lysate was spiked with the reducing agent sodium dithionite ($Na_2S_2O_4$). (**C**) Relative fluorescence of keto- and leuco-indigoidine isoforms produced by transfected HEK293-T cells (excitation, 415nm; emission, 520nm). The formation of leuco-indigoidine was increased by addition of $Na_2S_2O_4$ to cultured cells. (**D**) Fluorescence micrographs of HEK293-T cells transfected either with the BpsA expression vector (neg.) or co-transfected with BpsA and Svp (pos.) expression vectors. Please note, that both the keto-indigoidine (dark intracellular storage granules) and the fluorescent leuco-indigoidine isoforms (light cell staining) can be simultaneously visualized. (**E**) Leuco-indigoidine-specific flow cytometric analysis of HEK293-T cells 48h after transfection with indicated indigoidine expression vectors.

4. Discussion. Precise quantitative analysis of gene expression is essential for gene-function analysis in the postgenomic era (Weber et al., 2009), provides insights into the dynamic behavior of complex gene networks (Auslander et al., 2011; Gitzinger et al., 2009), enables the design of high-throughput drug screening assays (Fussenegger et al., 2000) and supports the quest for optimal product gene expression strategies in the biopharmaceutical manufacturing industry (Kemmer et al., 2010; Ye et al., 2011). Biological reporter systems differ in their detection characteristics, which range from substrate-free fluorescence (Wongsrikeao et al., 2011), to enzymatic assays scoring the conversion of chromogenic (Berger et al., 1988; Schlatter et al., 2002), bioluminescent (Wurdinger et al., 2008) or chemiluminescent (Kricka et al., 2000) substrates. Also, reporter proteins either remain inside the cell and can therefore be employed for single-cell analysis and spatiotemporal studies of individual cells in multicellular systems (Tigges et al., 2009) or they are secreted and used for screening assays (Weber et al., 2008) and upstream development in biopharmaceutical manufacturing scenarios (Peng et al., 2010). Besides these aforementioned considerations, which determine the choice of a detection technology for a specific application, an ideal reporter system technology should be (i) compatible with a variety of living species (e.g., prokaryotic and mammalian cells) and (ii) detection technologies (e.g., microscopy, FACS, enzymatic assay), (iii) involve reporter compounds that are (iv) stable and (v) functional over a wide range of physiologic conditions (e.g., pH, temperature) and can be reliably and

precisely quantified using a (vi) simple, preferably one-step, (vii) inexpensive (e.g., no or intrinsic substrate), and (viii) scalable assay that is compatible with a (ix) multiwell-plate format and (x) robotic handling. The indigoidine reporter system meets with all these characteristics at a high standard. When placing BpsA and Svp under respective constitutive or regulated promoters indigoidine is produced and can be quantified in *E. coli* as well as in a variety of mammalian cells including human stem cells. In bacteria, indigoidine colors colonies in blue suggesting that the system could be further developed as an alternative to the classic lacZ-based blue/white screening system which requires expensive substrates and inducer compounds (Vieira et al., 1982). When grown in liquid cultures, *E. coli* secrete indigoidine, which turns the supernatant into a ready-to-assay blue color. Suggesting a lack of such an active transport mechanism mammalian cells are unable to secrete the non-ribosomal peptide indigoidine, which resides in blue storage granules inside the cytoplasm. These granules can easily be quantified by flow cytometric analysis or prepared for spectroscopic analysis using a one-step DMSO-based cell lysis – indigoidine solution procedure. In contrast to the blue keto-indigoidine in storage granules the reduced leuco-isoform seems to readily dissolve in the cytosol of mammalian cells. Although leuco-indigoidine is colorless it can be detected by fluorescence microscopy and quantified by FACS analysis. Since both isoforms co-exist in the same cell, indigoidine is unique in providing a chromogenic as well as a fluorescent read-out making this reporter system highly versatile. Unlike established reporter systems, the indigoidine technology does not require expensive additional substrates since the blue pigment is produced from physiologically available L-glutamine. Conversion of L-glutamine to indigoidine seems not to lead to a metabolic bottleneck since the viability of mammalian cells producing the blue pigment remains unchanged.

Besides providing a novel, versatile and easy-to-assay cross-kingdom reporter technology, engineering mammalian cells to produce non-ribosomal peptides is a major achievement. Mammalian cells are widely used for biopharmaceutical manufacturing of protein therapeutics. Expanding the synthesis capacity of mammalian cells to non-

ribosomal peptides, many of which have therapeutic acitivities, may foster novel treatment strategies in future gene- and cell-based therapies.

Acknowledgments. We thank Marcel Tigges for generous advice and Verena Jäggin as well as Mark Dessing for assistance with flow cytometry. This work was supported by the Swiss National Science Foundation (grant no. 31003A-126022) and in part by the EC Framework 7 (Persist).

References

Auslander, D., Wieland, M., Auslander, S., Tigges, M., Fussenegger, M., 2011. Rational design of a small molecule-responsive intramer controlling transgene expression in mammalian cells. Nucleic Acids Res., 2011; 39 (22): e155.

Berger, J., Hauber, J., Hauber, R., Geiger, R., Cullen, B. R., 1988. Secreted placental alkaline phosphatase: a powerful new quantitative indicator of gene expression in eukaryotic cells. Gene. 66**,** 1-10.

Fussenegger, M., Morris, R. P., Fux, C., Rimann, M., von Stockar, B., Thompson, C. J., Bailey, J. E., 2000. Streptogramin-based gene regulation systems for mammalian cells. Nat Biotechnol. 18**,** 1203-8.

Gitzinger, M., Kemmer, C., El-Baba, M. D., Weber, W., Fussenegger, M., 2009. Controlling transgene expression in subcutaneous implants using a skin lotion containing the apple metabolite phloretin. Proc Natl Acad Sci U S A. 106**,** 10638-43.

Gossen, M., Freundlieb, S., Bender, G., Muller, G., Hillen, W., Bujard, H., 1995. Transcriptional activation by tetracyclines in mammalian cells. Science. 268**,** 1766-9.

Kemmer, C., Gitzinger, M., Daoud-El Baba, M., Djonov, V., Stelling, J., Fussenegger, M., 2010. Self-sufficient control of urate homeostasis in mice by a synthetic circuit. Nat Biotechnol. 28**,** 355-60.

Kosec, G., Goranovic, D., Mrak, P., Fujs, S., Kuscer, E., Horvat, J., Kopitar, G., Petkovic, H., 2012. Novel chemobiosynthetic approach for exclusive production of FK506. Metab Eng. 14, 39-46.

Kricka, L. J., Voyta, J. C., Bronstein, I., 2000. Chemiluminescent methods for detecting and quantitating enzyme activity. Methods Enzymol. 305**,** 370-90.

Lambalot, R. H., Gehring, A. M., Flugel, R. S., Zuber, P., LaCelle, M., Marahiel, M. A., Reid, R., Khosla, C., Walsh, C. T., 1996. A new enzyme superfamily - the phosphopantetheinyl transferases. Chem Biol. 3**,** 923-36.

Lee, Y.-A., Yu, C.-P., 2006. A differential medium for the isolation and rapid identification of a plant soft rot pathogen, *Erwinia chrysanthemi*. Journal of Microbiological Methods. 64**,** 200-206.

Marahiel, M. A., Essen, L. O., 2009. Chapter 13. Nonribosomal peptide synthetases mechanistic and structural aspects of essential domains. Methods Enzymol. 458**,** 337-51.

Mitta, B., Rimann, M., Ehrengruber, M. U., Ehrbar, M., Djonov, V., Kelm, J., Fussenegger, M., 2002. Advanced modular self-inactivating lentiviral expression vectors for multigene interventions in mammalian cells and in vivo transduction. Nucleic Acids Res. 30**,** e113.

Muscholl-Silberhorn, A. B., 2000. Pheromone-regulated expression of sex pheromone plasmid pAD1-encoded aggregation substance depends on at least six upstream genes and a cis-acting, orientation-dependent factor. J Bacteriol. 182, 3816-25.

Olano, C., Lombo, F., Mendez, C., Salas, J. A., 2008. Improving production of bioactive secondary metabolites in actinomycetes by metabolic engineering. Metab Eng. 10, 281-92.

Ornatsky, O., Bandura, D., Baranov, V., Nitz, M., Winnik, M. A., Tanner, S., 2010. Highly multiparametric analysis by mass cytometry. J Immunol Methods. 361**,** 1-20.

Owen, J. G., Copp, J. N., Ackerley, D. F., 2011. Rapid and flexible biochemical assays for evaluating 4'-phosphopantetheinyl transferase activity. Biochem J. 436**,** 709-17.

Peng, R. W., Guetg, C., Tigges, M., Fussenegger, M., 2010. The vesicle-trafficking protein munc18b increases the secretory capacity of mammalian cells. Metab Eng. 12**,** 18-25.

Qiao, K., Chooi, Y. H., Tang, Y., 2011. Identification and engineering of the cytochalasin gene cluster from Aspergillus clavatus NRRL 1. Metab Eng. 13, 723-32.

Reverchon, S., Rouanet, C., Expert, D., Nasser, W., 2002. Characterization of Indigoidine Biosynthetic Genes in *Erwinia chrysanthemi* and Role of This Blue Pigment in Pathogenicity. Journal of Bacteriology. 184**,** 654-665.

Sanchez, C., Du, L., Edwards, D. J., Toney, M. D., Shen, B., 2001. Cloning and characterization of a phosphopantetheinyl transferase from *Streptomyces verticillus* ATCC15003, the producer of the hybrid peptide-polyketide antitumor drug bleomycin. Chem Biol. 8**,** 725-38.

Schlatter, S., Rimann, M., Kelm, J., Fussenegger, M., 2002. SAMY, a novel mammalian reporter gene derived from *Bacillus stearothermophilus* alpha-amylase. Gene. 282**,** 19-31.

Seixas de Melo, J. S., Moura, A. P., Melo, M. J., 2004. Photophysical and spectroscopic studies of Indigo derivatives in their keto and leuco forms. Journal of Physical Chemistry A. 108**,** 6975-6981.

Siewers, V., Chen, X., Huang, L., Zhang, J., Nielsen, J., 2009. Heterologous production of non-ribosomal peptide LLD-ACV in Saccharomyces cerevisiae. Metab Eng. 11, 391-7.

Simonsen, J. L., Rosada, C., Serakinci, N., Justesen, J., Stenderup, K., Rattan, S. I., Jensen, T. G., Kassem, M., 2002. Telomerase expression extends the proliferative life-span and maintains the osteogenic potential of human bone marrow stromal cells. Nat Biotechnol. 20**,** 592-6.

Strieker, M., Tanovic, A., Marahiel, M. A., 2010. Nonribosomal peptide synthetases: structures and dynamics. Curr Opin Struct Biol. 20**,** 234-40.

Takahashi, H., Kumagai, T., Kitani, K., Mori, M., Matoba, Y., Sugiyama, M., 2007. Cloning and Characterization of a Streptomyces Single Module Type Non-ribosomal Peptide Synthetase Catalyzing a Blue Pigment Synthesis. Journal of Biological Chemistry. 282**,** 9073-9081.

Tigges, M., Marquez-Lago, T. T., Stelling, J., Fussenegger, M., 2009. A tunable synthetic mammalian oscillator. Nature. 457**,** 309-12.

Vieira, J., Messing, J., 1982. The pUC plasmids, an M13mp7-derived system for insertion mutagenesis and sequencing with synthetic universal primers. Gene. 19**,** 259-68.

Watanabe, K., Hotta, K., Praseuth, A. P., Koketsu, K., Migita, A., Boddy, C. N., Wang, C. C. C., Oguri, H., Oikawa, H., 2006. Total biosynthesis of antitumor nonribosomal peptides in *Escherichia coli*. Nature Chemical Biology. 2**,** 423-428.

Weber, W., Lienhart, C., Baba, M. D., Fussenegger, M., 2009. A biotin-triggered genetic switch in mammalian cells and mice. Metab Eng. 11**,** 117-24.

Weber, W., Schoenmakers, R., Keller, B., Gitzinger, M., Grau, T., Daoud-El Baba, M., Sander, P., Fussenegger, M., 2008. A synthetic mammalian gene circuit reveals antituberculosis compounds. Proc Natl Acad Sci U S A. 105**,** 9994-8.

Wongsrikeao, P., Saenz, D., Rinkoski, T., Otoi, T., Poeschla, E., 2011. Antiviral restriction factor transgenesis in the domestic cat. Nature Methods. 8**,** 853-859.

Wurdinger, T., Badr, C., Pike, L., de Kleine, R., Weissleder, R., Breakefield, X. O., Tannous, B. A., 2008. A secreted luciferase for ex vivo monitoring of in vivo processes. Nat Methods. 5**,** 171-3.

Ye, H., Daoud-El Baba, M., Peng, R. W., Fussenegger, M., 2011. A synthetic optogenetic transcription device enhances blood-glucose homeostasis in mice. Science. 332**,** 1565-8.

CHAPTER III

Designed cell consortia as fragrance-programmable analog-to-digital converters

Marius Müller, Simon Ausländer, Andrea Spinnler, David Ausländer, Julian Sikorski, Marc Folcher, Martin Fussenegger

Nat. Chem. Biol. (2016) accepted

Abstract

Synthetic biology advances the rational engineering of mammalian cells to achieve cell-based therapy goals. Synthetic gene networks have almost reached the complexity of digital electronic circuits and enable single cells to perform programmable arithmetic calculations or provide dynamic remote-control of transgenes by electromagnetic waves. We have designed a synthetic multi-layered gaseous fragrance-programmable analog-to-digital converter (ADC) providing remote control of digital gene expression with 2-bit AND, OR as well as NOR-gate logic in synchronized cell consortia. The ADC consists of multiple sampling and quantization modules sensing analog gaseous fragrance inputs, a gas-to-liquid transducer converting fragrance intensity into diffusible cell-to-cell signaling compounds and a digitization unit with a genetic amplifier circuit to improve signal-to-noise ratio and recombinase-based digital expression switches enabling 2-bit processing of logic gates. Synthetic ADCs remote-controlling cellular activities with digital precision may enable the development of novel biosensors and provide bio-electronic interfaces synchronizing analog metabolic pathways with digital electronics.

The principle of synthetic biology to rationally assemble standardized genetic parts to devices with novel, predictable, robust, reliable and useful functions has greatly advanced the design of synthetic signal-processing gene networks from interconnection of compatible trigger-inducible gene switches[1,2]. These gene switches are continuously refined to provide high-sensitivity gene expression within a wide dynamic range and in response to physiological compounds (cosmetics[3], food additives[4], vitamins[5]) or traceless physical cues (temperature[6,7], pH[8], electromagnetic[9] and brain waves[10]) to enable new bioprocessing[11] and therapy strategies[12]. Corresponding synthetic gene networks show increasingly complex design, processing capacity as well as control dynamics and are currently able to program mammalian cells to accomplish oscillating protein expression[13], perform arithmetic calculations[14], and execute logic operations

reminiscent of conventional electronics[15]. Synthetic gene networks have now reached a level of sophistication where they can synchronize early diagnosis of a pathologic situation with targeted therapeutic intervention in a closed-loop control manner[16]. For example, designer-cell implants with embedded therapeutic gene networks have been successfully used to diagnose, prevent and cure experimental gouty arthritis[17], obesity[18], Grave's disease[19] and psoriasis[20].

The execution of complex genetic programs amidst the cells' metabolic processes is by far more challenging than controlling the flow of electrons across metal wires in electronic devices[21]. The development of complex synthetic biocomputing devices may exceed the signal-processing capacity of single cells[22,23] and simultaneous activation of the same signaling pathways by different cell-surface receptors may lead to interference compromising their processing output[24]. Therefore, akin to the multi-core central processing units in today's personal computers and as evolved in multicellular organisms, the signal processing activities of synthetic gene networks need to be distributed among a synchronized consortium of different cells. With several hundreds of volatile compound-specific G protein-coupled olfactory receptors that manage analog integration of odorants and subsequent digital processing by olfactory neurons to constitute olfaction, the mammalian nose is a paradigm of a specialized cell consortium-based analog-to-digital converter.

We have chosen olfaction and conventional wired electronic circuits as blueprints for the design of a synthetic analog-to-digital converter (ADC) that enabled analog volatile fragrance-programmable control of 2-bit digital AND, OR as well as NOR gates by a synchronized consortium of chemically wired engineered cells. Thereby, sensor-sender cell populations record analog volatile fragrance inputs and produce soluble communication compounds that program the receiver-digitizer cells to execute product gene expression with Boolean logic. Digitization by the receiver-digitizer cells was achieved by recombinase-mediated excision of STOP cassettes or functional actuators which restored or prevented signal processing in a fragrance-inducible manner. Akin to electronic signal amplifiers, digitizers including a genetic signal-amplification loop showed improved induction dynamics, higher signal-to-noise ratios and higher

expression levels. Engineered genetic ADCs programming cellular activities may provide new insight into digital processing of natural systems and offer new opportunities for the design of bio-electronic interfaces.

RESULTS

Design of fragrance-programmable ADCs

We have designed a 2-bit interconnection between cell populations encoding a fragrance-sampling and -quantization module as well as a gas-to-liquid transducer and a digitization unit containing an optional genetic amplifier to improve the signal-to-noise ratio. The resulting ADC was successfully used to program gene expression with AND, OR and NOR logic (Fig. 1).

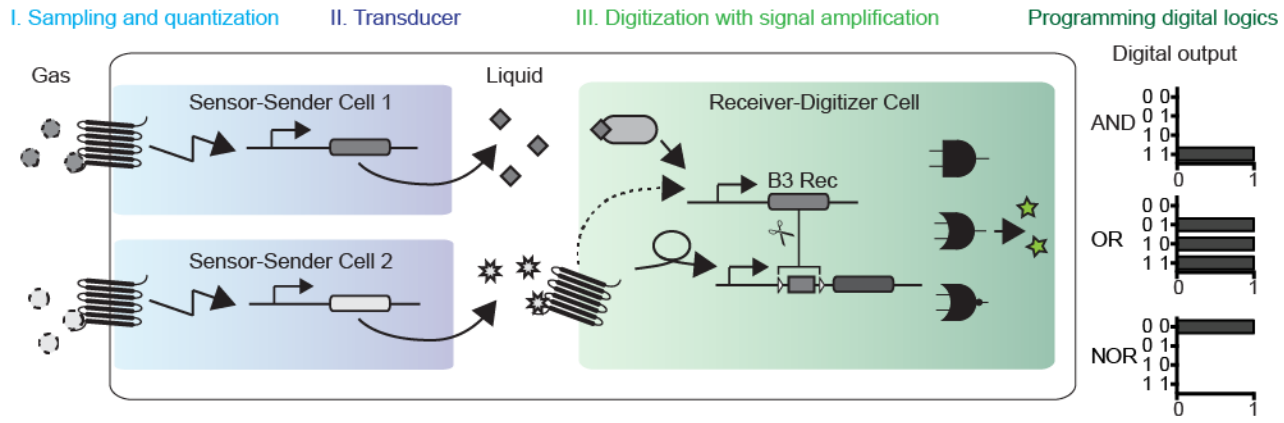

Figure 1

Figure 1 | Design of the fragrance-programmable analog-to-digital converter with Boolean expression logic. The fragrance-programmable analog-to-digital converter consists of three genetic modules distributed among different mammalian sensor-sender cell populations and receiver-digitizer cells that are interconnected via synthetic intra-cellular signaling cascades and inter-cellular communication devices: (i) Sampling and quantization module: Each sensor-sender cell population contains a volatile fragrance-sampling and -quantization module consisting of a specific odorant receptor, which constantly monitors the volatile level of a specific fragrance and dose-dependently activates the gas-to-liquid transduction module via its specific signaling cascade. (ii) Gas-to-liquid transducer: The sensor-sender cell populations also contain gas-to-liquid transducers, which convert volatile fragrance inputs into the soluble intercellular signaling compounds GLP-1 and L–tryptophan which are secreted by the sensor-sender cell populations and are broadcast to the receiver-digitizer cells. GLP-1 is directly produced and secreted by the sensor-sender cells. L–tryptophan is produced

from indole by the tryptophan synthase (TrpB) and diffuses to the receiver-digitizer cells. (iii) The digitizer module with signal amplifier: The receiver-digitizer cells monitor the input of the soluble intercellular signaling compounds GLP-1 and L–tryptophan via specific receptors and activate the digitizer module with integrated signal amplifier to improve the signal-to-noise ratio. The signal amplifier-containing digitizer module consists of a tetracycline-responsive transactivator (tTA) which feed-forward controls expression of a site-specific recombinase (B3) that removes a transcriptional stop cassette (STOP) flanked by the cognate recombination target sites (B3RT) thereby inducing reporter protein expression. The amplifier-containing digitizer module was set for 2-bit control of genetic AND, OR and NOR gates.

The fragrance-sampling and -quantization module consists of individual human cell populations each of which we engineered for the expression of a specific odorant receptor sampling the presence of a particular volatile compound as well as with the corresponding signaling cascade ($G_{\alpha olf}$-dependent cAMP signaling) that rewires odorant-receptor activation to transgene induction thereby quantifying odorant input (**Fig. 2a, Supplementary Results, Supplementary Fig. 1**). Since fragrance-sensitive olfactory receptors share the same cAMP-dependent signaling cascade, differential detection and interference-free processing of complex fragrance mixtures is only possible by a consortium of sensory designer cells in which individual cells have been engineered to detect a single olfactory compound. This is similar to the human nose, where individual olfactory neurons detect a specific olfactory compound and a consortium of olfactory neurons processes the resulting olfactory perception[25].

Detailed characterization of the cell-based fragrance-sampling and -quantization module using the odorant receptors specific for the different volatile fragrance compounds eugenol (OREG; pOREG, P_{SV40}-OREG-pA), coumarin (OR5P3; pCI-OR5P3, P_{hCMV}-OR5P3-pA), dihydrojasmone (OR1A1; pCI-OR1A1; P_{hCMV}-OR1A1-pA) and acetophenone (OR129-1; pCI-MOR129-1; P_{hCMV}-OR129-1-pA) linked to expression of the intracellular fluorescent protein mCherry (pMM222; P_{CRE}-mCherry-pA) or the human placental secreted alkaline phosphatase (SEAP; pSP16; P_{CREm}-SEAP-pA) confirmed concentration-(**Fig. 2b–e**) as well as distance-dependent odorant-inducible target gene expression (**Supplementary Fig. 2a–p**) at fragrance concentrations below

10^{-4}M. Above 10^{-4}M, the fragrance compounds eugenol, coumarin, dihydrojasmone, and acetophenone started to be cytotoxic for mammalian cells (**Supplementary Fig. 2q–t**).

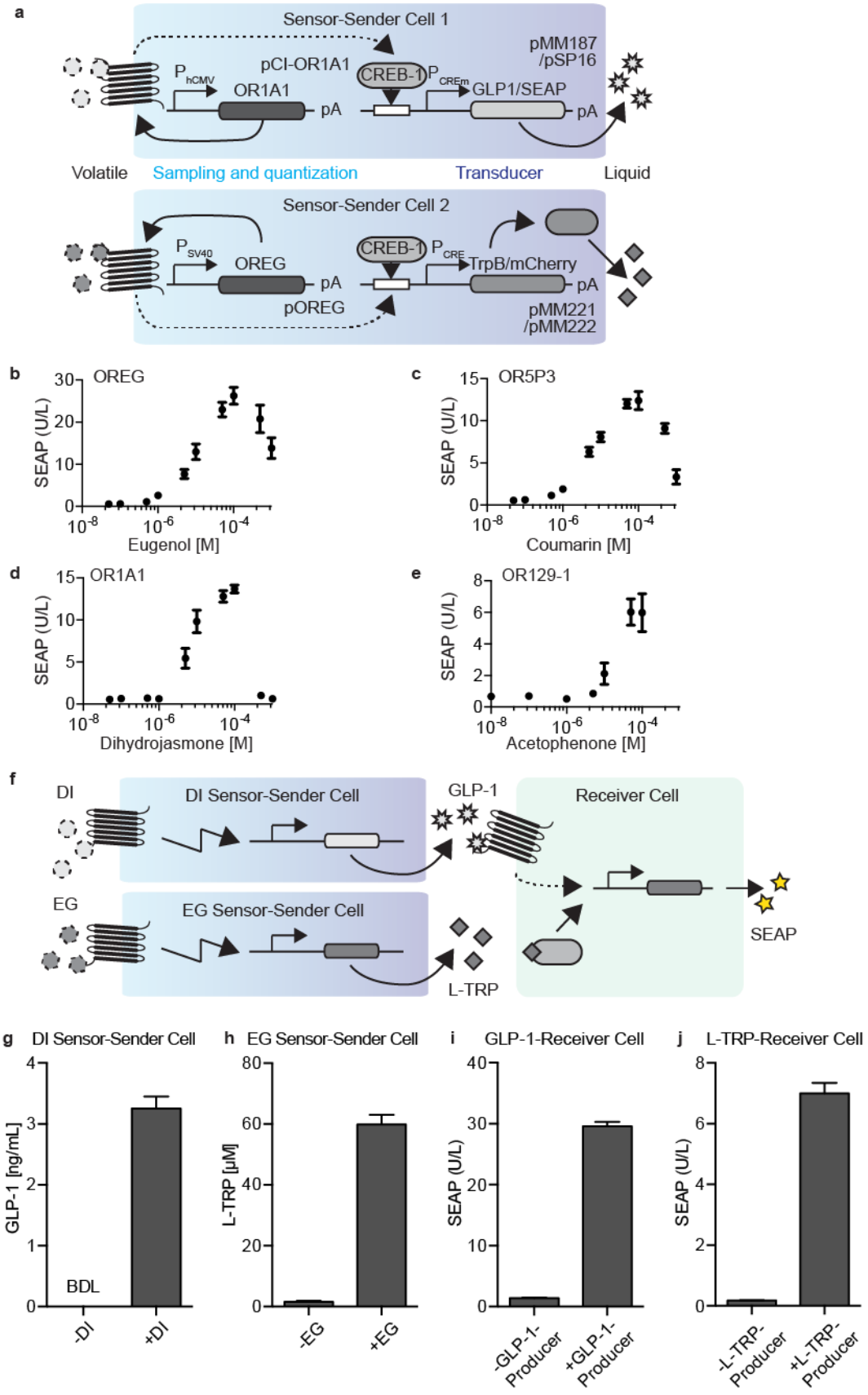

Figure 2

Figure 2 | Characterization of the fragrance-sampling and -quantization and the gas-to-liquid transduction modules. a Sensor-sender cells containing the fragrance-sampling and -quantization module as well as the gas-to-liquid transducer. These sensor-sender cells consist of distinct cell populations, each engineered to express a specific odorant receptor (OR1A1 and OREG) rewired to a synthetic signaling cascade controlling production of reporter proteins (mCherry, SEAP) or the secreted signaling compounds L–tryptophan (L–TRP) (produced from indole by the tryptophan synthase (TrpB)), or the glucagon-like peptide 1 (GLP-1). **b-e** Dose-response profiles of the fragrance-sampling and -quantization module exposed to different volatile fragrances (Supplementary Table 3). SEAP levels were profiled 48h after fragrance exposure. **f** Gas-to-liquid transducer. Dihydrojasmone- (DI-) or Eugenol- (EG-) programmable sensor-sender cells, containing the fragrance-sampling and -quantization module and the gas-to-liquid transducer convert volatile fragrances to soluble signaling compounds GLP-1 and L–tryptophan and broadcast them to the receiver cells where they trigger SEAP expression. **g,h** Fragrance-induced GLP-1 (**g**) and L–tryptophan (**h**) production (Supplementary Table 3). The transfected cells were induced by volatile fragrances and GLP-1 (BDL, below detection limit of 2.084 ng/mL for GLP-1) (**g**) and L–tryptophan (**h**) levels were profiled after 72h. Ethanol was used as negative control. **i,j** Inter-cellular communication via GLP-1 and L–tryptophan (Supplementary Table 3). Receiver cells were mixed with either GLP-1, tryptophan synthase-producing or negative control cells at ratio of 30:70 (receiver:producer cells) and SEAP was profiled after 48h. The data represent the mean ± SD of three independent experiments measured in triplicate.

Control experiments confirmed that odorant receptor-mediated induction of the P_{CRE} promoter was neither activated by unspecific trigger compounds nor activated by unrelated signaling cascades or endogenous GPCRs that share the same signaling pathway (**Supplementary Fig. 3**). Odorant receptor-based fragrance-sampling and -quantization was not limited to the aforementioned examples scoring pure fragrance compounds. This basic design could also be expanded to other odorant-receptor families and was successfully used to identify fragrance induction profiles of commercial perfume brands by differential sampling and quantization (**Supplementary Fig. 4**).While these fragrance-sampling and -quantization modules could be used as stand-alone gene switches for traceless gas-inducible remote-control of target gene expression over-the-air, odorant-sensitive cell

populations could also be combined to increase the processing complexity and multiplex the programming capacity of this fragrance-controlled device. For example, our synthetic fragrance-programmable ADC was designed by combining the dihydrojasmone- and eugenol- sampling and quantization modules. To transform the gaseous fragrance input into an output of soluble signaling molecules that diffuse to receiver cells for further signal integration and processing, we have included a gas-to-liquid transducer (**Fig. 2f**). Therefore, the dihydrojasmone-sampling and -quantization module was linked to the expression of the glucagon-like peptide 1 (GLP-1; pMM187, P_{CREm}-GLP-1-pA) (**Fig. 2g**) and the eugenol-sampling and -quantization module was connected to the expression of the tryptophan synthase (TrpB; pMM221, P_{CRE}-TrpB-pA) (**Fig. 2h**). Thus, GLP-1 is produced and secreted in response to dihydrojasmone and can directly be broadcast to the receiver cells (**Supplementary Fig. 5a**) where it binds to the GLP-1 receptor (GLP1R; pMM195; P_{SV40}-GLP1R-pA), activates the underlying signaling cascade and induces P_{CREm}-driven target gene expression (pSP16; P_{CREm}-SEAP-pA) (**Fig. 2i, Supplementary Fig. 5b,c**). By contrast, eugenol-triggered TrpB expression enabled the designer cell to convert indole to L–tryptophan which is then broadcast to the receiver cells (**Supplementary Fig. 5a**) and diffuses into the cell where it activates the L–tryptophan-dependent transactivator (TRT; pWB24, P_{SV40}-TRT-pA) to bind and induce P_{TRT}-driven target gene expression (pWB22, P_{TRT}-SEAP-pA) (**Fig. 2j, Supplementary Fig. 5d,e**). The distinct combination of a cell-surface receptor (GLP1R) with an intracellular receptor (TRT) enabled dual-input processing by the receiver cell without any observable crosstalk between the systems (**Supplementary Fig. 5b–f**).

Recombinase-based digitization

Site-specific recombinases such as Cre, Dre, KD or B3 provide a way to process information irreversibly on a genetic level and have therefore been used for advanced genomic editing[26,27] and for the design of memory devices[28] including counters[29] and time-delay circuits[30]. Additionally, irreversible high-precision switches are particularly suitable to target cancer cells. Non-limiting examples include the dual-recombinase system for targeting pancreatic cancer[31], the cancer cell

classifier[32] and cancer kill switches[33,34]. Detailed comparative performance analysis of several recombinases including KD, Dre and B3 revealed that the B3 recombinase of *Zygosaccharomyces bisporus*[35] exhibits high activity and low cytotoxicity[26] and is therefore best suited for site-specific recombination in mammalian cells (**Supplementary Fig. 6**).

The digitizer unit which converts a graded input signal into a digital expression response, was based on the expression of the B3 recombinase (pMM543; P_{hCMV}-B3-PEST-pA) that efficiently removes a transcriptional stop cassette (STOP) flanked by the B3 recombination target sites (B3RT), thereby inducing reporter protein expression (pMM207; P_{hCMV}-B3RT-STOP-B3RT-Citrine-pA)[26] (**Supplementary Fig. 7a,b**). To validate the digitization unit, we varied the amount of the B3 recombinase expression vector (pMM543; P_{hCMV}-B3-PEST-pA) co-transfected with pMM207 (P_{hCMV}-B3RT-STOP-B3RT-Citrine-pA) and observed maximum Citrine output over the entire concentration range of the B3 recombinase, which suggested that the digitization unit indeed provides the expected binary expression profile (**Supplementary Fig. 7c**). Direct control of B3-recombinase expression by the communication compound L–tryptophan (pWB24, P_{SV40}-TRT-pA; pMM189, P_{TRT2}-B3-PEST; pMM207, P_{hCMV}-B3RT-STOP-B3RT-Citrine-pA) confirmed trigger-inducible B3 recombinase-mediated digital expression switches in mammalian cells (**Fig. 3a–c**).

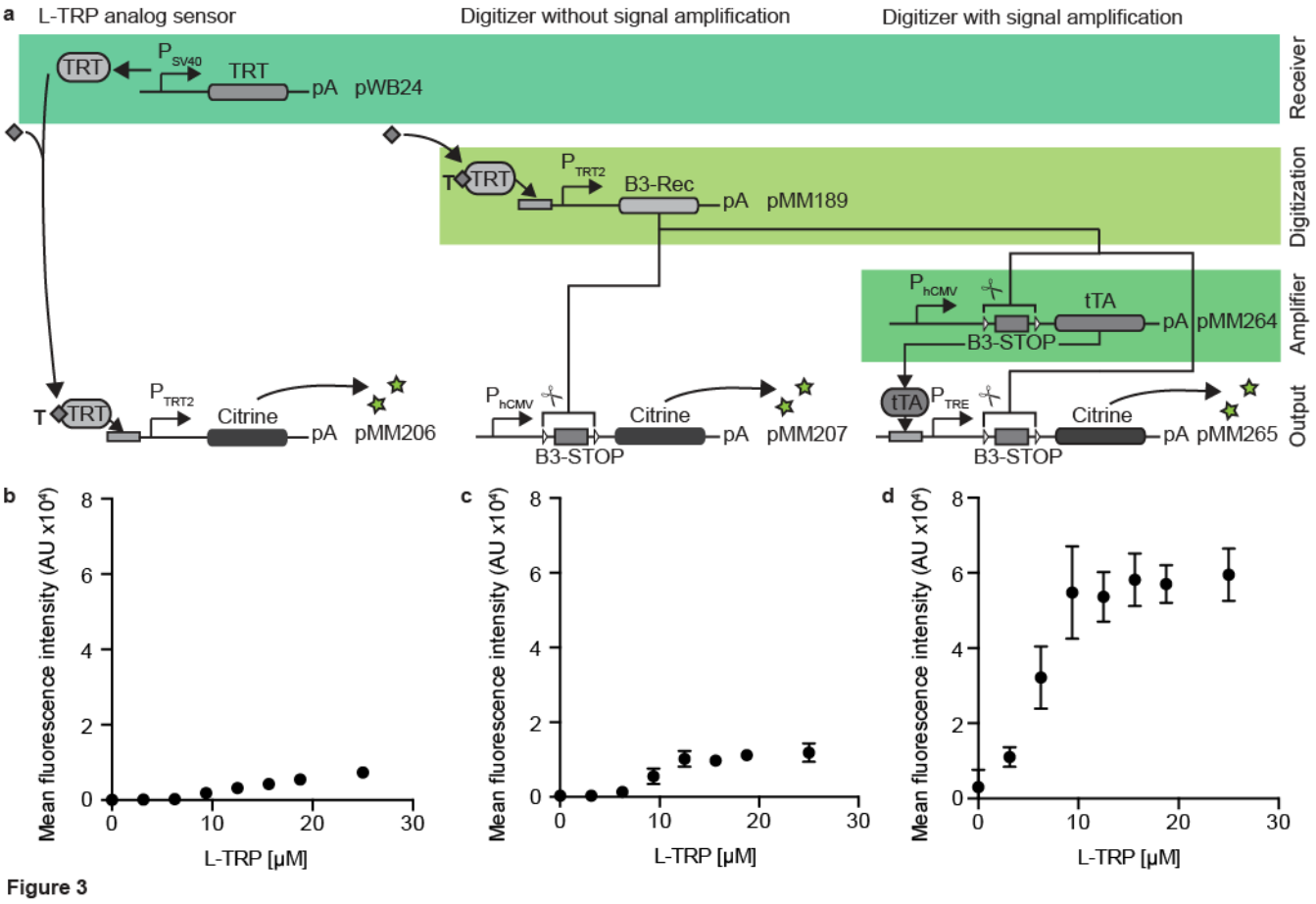

Figure 3

Figure 3 | Characterisation of the digitizer with integrated signal amplifier. a Step-wise assembly of the digitizer with integrated signal amplifier. Analog L–Tryptophan sensor: In the presence of L–tryptophan, the L–tryptophan-dependent transactivator (TRT) activates P_{TRT2}-driven Citrine expression. Digitizer without signal amplification: In the presence of L–tryptophan, TRT activates P_{TRT2}-driven expression of B3 recombinase which excises the STOP cassette, thereby inducing Citrine expression. Digitizer with signal amplification: In the presence of L–tryptophan, TRT activates P_{TRT2}-driven expression of B3 recombinase which excises the STOP cassette, thereby inducing expression of the tetracycline-dependent transactivator (tTA) and triggering tTA-amplified P_{TRE} (tetracycline-responsive promoter)-driven Citrine expression. Mean Citrine fluorescence intensity of the analog L–tryptophan sensor (**b**), the digitizer without signal amplification (**c**) and the digitizer with signal amplification (**d**) was profiled after 48 h by FACS analysis. Supplementary Table 3 provides an overview of cotransfected plasmids. The data represent the mean ± SD of three independent experiments measured in triplicate.

Electronic digitizers typically include signal amplifiers to improve signal-to-noise ratios[36,37]. To improve the sensitivity and expression output of the genetic digitizer unit we included a genetic amplification loop. Therefore, the digitizer unit (pWB24, P_{SV40}-TRT-pA; pMM189, P_{TRT2}-B3-PEST; pMM207, P_{hCMV}-B3RT-STOP-B3RT-Citrine-pA) was set for digital expression of the tetracycline-dependent transactivator (tTA; pMM264, P_{hCMV}-B3RT-STOP-B3RT-tTA-pA), which then drives amplified digital expression of the target gene (pMM265, P_{TRE}-B3RT-STOP-B3RT-Citrine-pA) (**Fig. 3a,d**). Integration of a signal amplifier into the digitizer unit provided significantly higher sensitivity and expression levels compared to the basic digitizer unit (**Fig. 3**).

Digital processing of Boolean expression logic

Having validated all framework components we set the amplifier-containing digitizer unit for 2-bit control of genetic AND, OR and NOR gates:

(i) The AND gate, which only provides digital Citrine expression in the presence of both input components glucagon-like peptide 1 (GLP-1) *and* L–tryptophan (L–TRP), was designed by combining L–TRP-inducible TRT (pWB24, P_{SV40}-TRT-pA) -mediated expression of tTA (pMM204, P_{TRT}-B3RT-STOP-B3RT-tTA-pA) and tTA-mediated amplification of Citrine expression (pMM265, P_{TRE}-B3RT-STOP-B3RT-Citrine-pA) with GLP-1-triggered activation of the GLP-1 receptor (GLP1R, pMM195, P_{SV40}-GLP1R-pA) and subsequent induction of the B3 recombinase (pMM174, P_{CREm}-B3-PEST-pA) (**Fig. 4a**). Digital expression of Citrine exclusively occured following L–TRP-mediated TRT-dependent P_{TRT}-driven induction of tTA and GLP-1-triggered activation of GLP1R, P_{CREm}-driven induction of B3 recombinase and B3 recombinase-mediated activation of tTA as well as tTA-mediated amplification of digital Citrine expression. Hence, Citrine expression occured in the presence of L–TRP *and* GLP-1 (**Fig. 4b**; **Supplementary Fig. 8; Supplementary Fig. 9a**).

(ii) The OR Gate, which provides digital Citrine expression in the presence of either L–TRP *or* GLP-1 or both inputs was designed by combining L–TRP-inducible TRT (pWB24, P_{SV40}-TRT-pA) -mediated expression of B3 recombinase (pMM189, P_{TRT2}-B3-PEST-pA), digital expression of tTA

(pMM204, P_{TRT}-B3RT-STOP-B3RT-tTA-pA) and tTA-mediated amplification of digital Citrine expression (pMM265, P_{TRE}-B3RT-STOP-B3RT-Citrine-pA) with GLP-1-triggered activation of the GLP-1 receptor (GLP1R, pMM195, P_{SV40}-GLP1R-pA) and subsequent induction of the B3 recombinase (pMM174, P_{CREm}-B3-PEST-pA), digital expression of tTA (pMM204, P_{TRT}-B3RT-STOP-B3RT-tTA-pA) and tTA-mediated amplification of digital Citrine expression (pMM265, P_{TRE}-B3RT-STOP-B3RT-Citrine-pA) (**Fig. 4c**). Digital expression of Citrine either occured following L–TRP-mediated TRT-dependent P_{TRT}-driven induction of B3 recombinase, B3 recombinase-mediated activation of tTA and tTA-mediated amplification of digital Citrine expression or GLP-1-triggered activation of GLP1R, P_{CREm}-driven induction of B3 recombinase, B3 recombinase-mediated activation of tTA and tTA-mediated amplification of digital Citrine expression. Hence, Citrine expression occured in the presence of either L–TRP *or* GLP-1 or both (**Fig. 4d**; **Supplementary Fig. 9b; Supplementary Fig. 10**).

(iii) The NOR Gate, which provides digital Citrine expression when neither L–TRP *nor* GLP-1 is present, was designed by combining L–TRP-inducible TRT (pWB24, P_{SV40}-TRT-pA) -mediated expression of B3 recombinase (pMM189, P_{TRT2}-B3-PEST-pA), digital excision of tTA (pMM267, P_{SV40}-B3RT-tTA-B3RT-pA) as well as the tTA-dependent P_{TRE}-driven amplification of digital Citrine expression (pMM262, P_{TRE}-B3RT-Citrine-B3RT-pA) with GLP-1-triggered activation of the GLP-1 receptor (GLP1R, pMM195, P_{SV40}-GLP1R-pA) and subsequent induction of the B3 recombinase (pMM212, P_{CRE}-B3-PEST-pA), digital excision of tTA (pMM267, P_{SV40}-B3RT-tTA-B3RT-pA) as well as the tTA-dependent P_{TRE}-driven amplification of digital Citrine expression (pMM262, P_{TRE}-B3RT-Citrine-B3RT-pA) (**Fig. 4e**). Digital expression of Citrine occured if neither P_{TRT}- nor P_{CRE}-driven B3 recombinase expression is activated. Hence, only when neither L–TRP *nor* GLP-1 was present (**Fig. 4f**, **Supplementary Fig. 9c; Supplementary Fig. 11**).

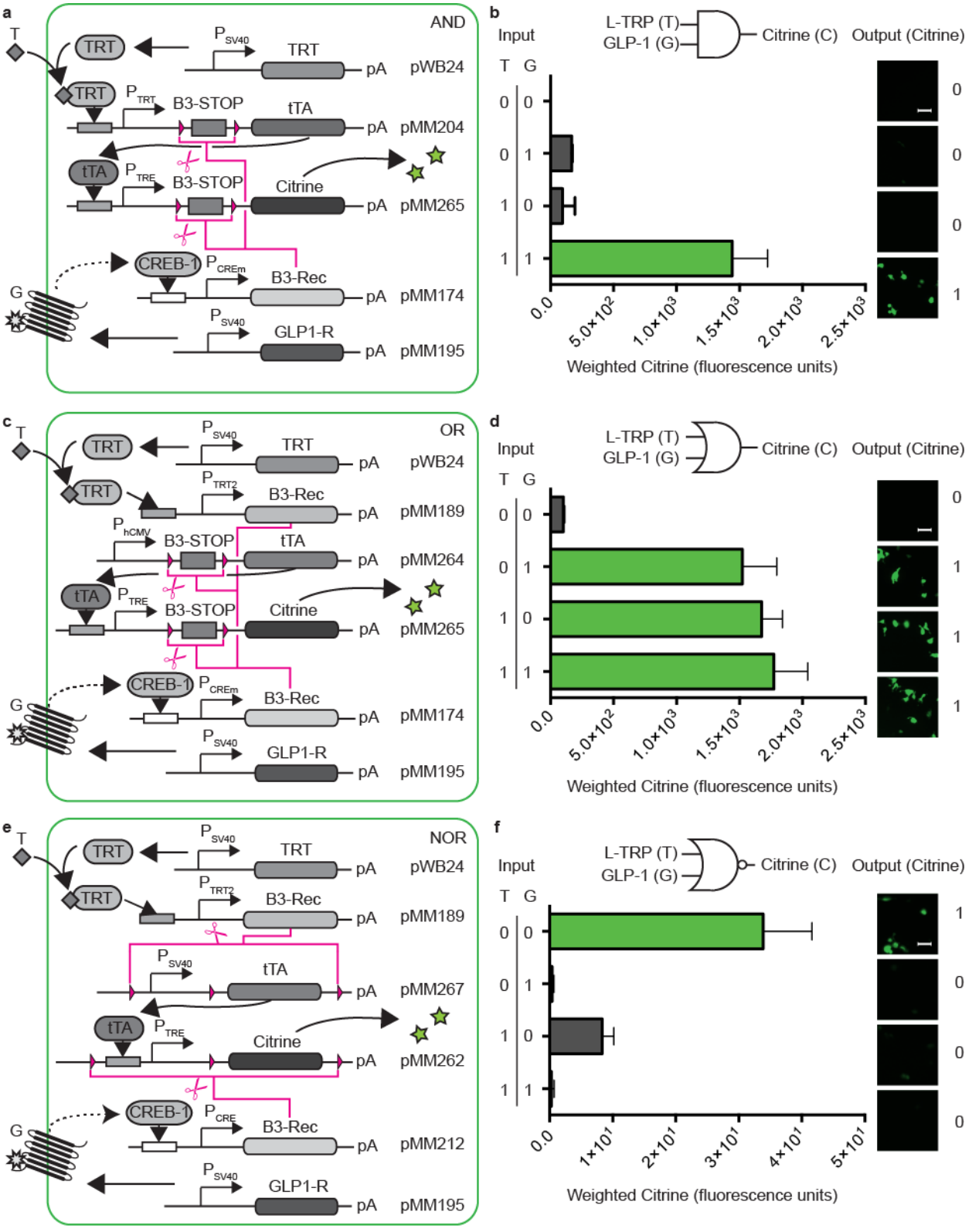

Figure 4

Figure 4 | Expression logic by receiver-digitizer cells. **a,b** Digital AND-gate. **a** In the presence of L–tryptophan (T), L–tryptophan-dependent transactivator (TRT) activates P_{TRT} (L–tryptophan-responsive promoter)-driven expression of a STOP cassette-containing tetracycline-dependent transactivator (tTA)-encoding expression unit. Upon excision of the STOP cassette by the B3 recombinase (B3), tTA is expressed and activates P_{TRE} (tetracycline-responsive promoter)-driven

expression of Citrine. Glucagon-like peptide 1 receptor (GLP1R) senses GLP-1 (G) and triggers P_{CREm}-driven expression of B3 which excises the STOP cassettes, thereby inducing and amplifying tTA-mediated P_{TRE}-driven Citrine expression. **b** Citrine fluorescence following exposure of the receiver-digitizer cells to the inducers was profiled by fluorescence microscopy and FACS. **c,d** Digital OR-gate. **c** In the presence of L–tryptophan, TRT activates P_{TRT2}-driven expression of B3 which excises the STOP cassettes in the tTA and Citrine expression units, inducing and amplifying tTA-mediated P_{TRE}-driven Citrine expression. GLP-1-mediated GLP1R activation triggers P_{CREm}-driven B3 expression. **d**. Citrine expression following exposure of the receiver-digitizer cells to the inducers was profiled by fluorescence microscopy and FACS. **e,f** Digital NOR-gate. In the presence of L–tryptophan, TRT activates P_{TRT2}-driven B3 expression. GLP1R senses GLP-1 and triggers P_{CRE}-driven B3 expression. In the presence of either inducer, production of B3 leads to excision of tTA and Citrine. **f**. Citrine fluorescence following exposure of the receiver-digitizer cells to the inducers was profiled by fluorescence microscopy and FACS. Scale bar = 75µm. Supplementary Table 3 provides an overview of cotransfected plasmids. The data represent the mean ± SD of three independent experiments measured in triplicate.

Fragrance-programmable ADCs controlling Boolean logics

Having characterized and validated each control module and cellular layer in great detail, we finally assembled the cell-consortium-based fragrance-programmable analog-to-digital converter. The fragrance-sampling and -quantization module, as well as the gas-to-liquid transducer, were combined in a set of sensor-sender cells, that sense the gaseous fragrances eugenol or dihydrojasmone and coordinate the respective production and secretion of L–tryptophan and GLP-1 (**Fig. 5a**). These communication compounds are broadcast to receiver-digitizer cells where they activate the respective signal-amplification and digitization unit that controls digital expression of Citrine with Boolean logic (**Fig. 5a**). Exposure of the sensor-sender and receiver-digitizer cell consortia to the volatile compounds eugenol and/or dihydrojasmone enabled fragrance-programmable ADC-based gene expression with AND (**Fig. 5b; Supplementary Fig. 12a**), OR (**Fig. 5c; Supplementary Fig. 12b**) and NOR (**Fig. 5d; Supplementary Fig. 12c**) logics.

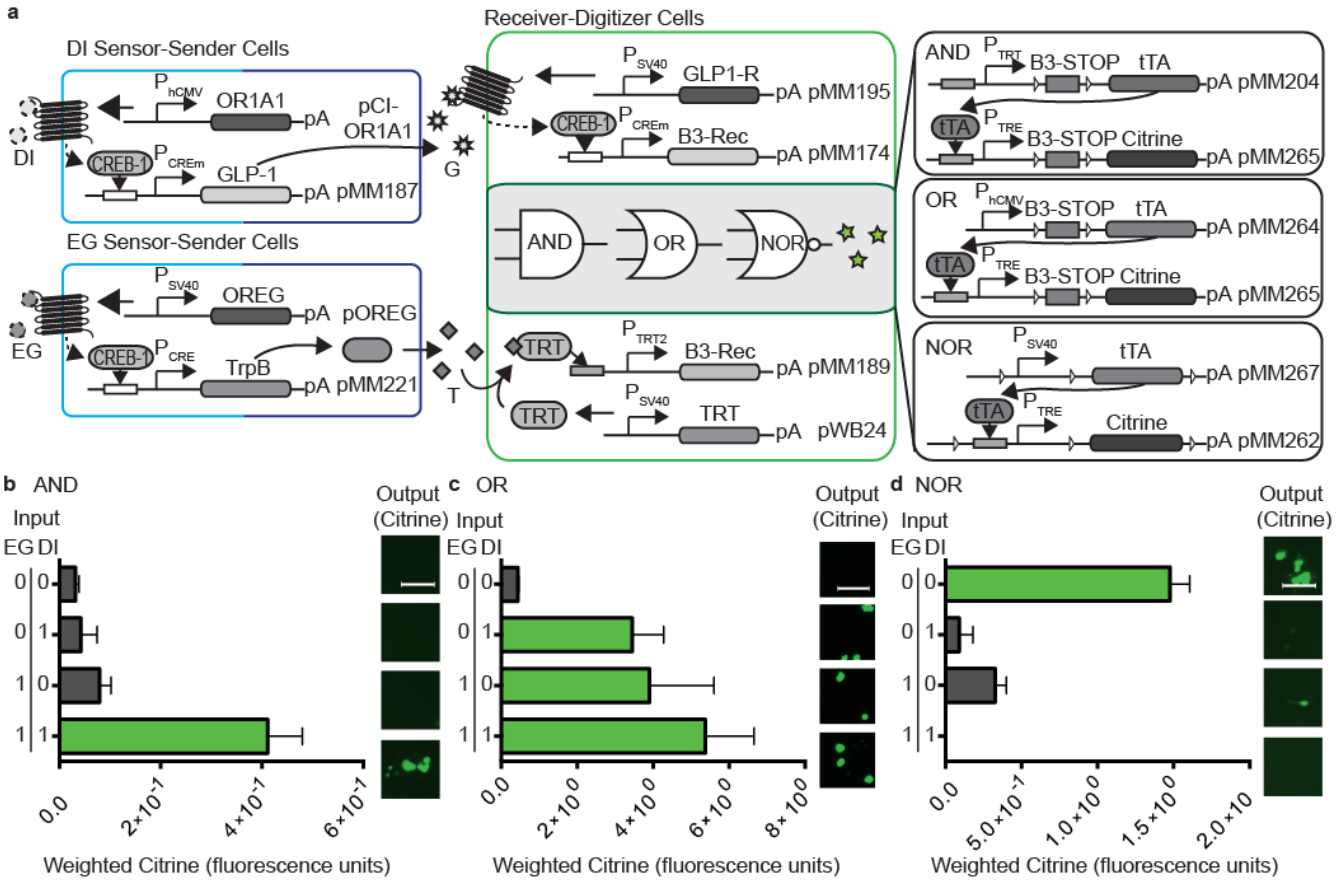

Figure 5

Figure 5 | Fragrance-programmable analog-to-digital conversion. a Fragrance-programmable analog-to-digital converter. Sensor-sender populations containing the fragrance-sampling and -quantization modules as well as the gas-to-liquid transducer. The soluble signaling compounds GLP-1 and L–tryptophan are broadcast to the co-cultivated receiver-digitizer cells. The receiver-digitizer cells contain the signal amplifier and the digitization unit, which detect GLP-1 and L–tryptophan and via specific receptors (TRT, GLP1R), amplify the input signals via a tTA-P_{TRE} (tetracycline-dependent transactivator-tetracycline-responsive promoter)-mediated feed-forward loop improving the signal-to-noise ratio and expressing the B3 recombinase for 2-bit processing of the AND, OR and NOR gates. **b,c,d** Fragrance-programmable analog-to-digital converter with AND (**b**), OR (**c**), and NOR (**d**)-gate logic. The two sensor-sender cell populations were mixed at a 2:1 ratio (DI Sensor cells:EG Sensor cells) and exposed for 24h to dihydrojasmone (DI) and eugenol (EG) and the receiver-digitizer cells were added to the sensor-sender-cells. Citrine expression was profiled by fluorescence microscopy and FACS. Scale bar = 75 µm. Supplementary Table 3 provides an overview of cotransfected plasmids. The data represent the mean ± SEM of three independent experiments measured in triplicate.

DISCUSSION

In digital nature, only two states exist: ‘0’ (OFF) and ‘1’ (ON). In practice, this condition is an abstraction of graded analog signals, whereas certain thresholds define the different states. However, most biologic systems follow analog proportional sensing, where an analog input signal leads to an analog output signal. Still, some important physiological controls have digital features, such as decision making in notch-delta signaling[38,39] or neuronal signaling in axons[40–42]. Another prominent example is the human nose which is able to distinguish a variety of over a trillion different odors due to the complex olfaction system[25]. During olfaction, odorants are inhaled via the nose and sensed by receptors of olfactory sensory neurons in the olfactory epithelium which produces electric signals that are finally integrated and processed in the olfactory bulb, part of the central nervous system and turned into olfactory perception[43].

Capitalizing on analog-to-digital converters, the transition from analog to digital signal processing has long been implemented in modern electronics. Electronic devices are controlled by binary calculations programmed exclusively by the input of electrons flowing through metal wires that are interconnected as multi-layered logic gates assembled in central processing units (CPUs). While these CPUs handle sequential calculations with enormous speed, the scalability to process streams of information simultaneously remains challenging and requires a multi-core architecture in combination with hyper-threading technology. By analogy, single mammalian cells are able to simultaneously process an enormous amount of analog metabolic information at rather slow speed but due to distribution of particular calculations among cell consortia and the scalability to tissue structures, mammalian biocomputers theoretically have unlimited parallel processing capacity. Examples of synthetic mammalian analog biocomputing devices which sense signal input and calculate a coordinated output, such as cancer kill switches[31–34,44], and molecular calculators[15,29], have first been tested in cell cultures. However, pioneering 1-bit control devices such as T-cell population controllers[45], artificial insemination devices[46], blue-light-triggered glucose rheostats[47] and closed-loop prosthetic networks for the treatment of hyperuricemic disorders[17], obesity[18] and Grave’s disease[19]

have been successfully used to perform therapeutic calculations when implanted and plugged into the metabolism of animals. Most recently, cytokine converters with 2-bit AND-gate logic converting proinflammatory cytokines into anti-inflammatory ones were able to treat experimental psoriasis[20]. However, it remains challenging to operate analog biocomputers processing metabolic information within the normal metabolic framework of a living cell without interferences[20]. Therefore, akin to the successful transition from analog to digital signal processing in the electronic world, the assembly of digital mammalian biocomputers that consist of a consortium of engineered cells which execute individual tasks and synchronize their processing activities by intercellular communication, could increase the sophistication, reliability and robustness of metabolic calculations. Mammalian biocomputers may foster the design of electro-genetic devices that enable the development of novel man-machine interfaces and therapeutic opportunities in the future. Although interfaces between electronic devices and electrogenic tissues such as muscle, heart as well as nerve fibers and the brain are well established and led to the development of pacemakers as well as brain-controlled prostheses and wheelchairs, it has only recently become possible to directly program gene activities by electromagnetic waves wirelessly transmitted by electronic devices[9] or brain activities[10]. However, the development of a truly cybernetic two-way communication interface between electronic devices and metabolic activities remains to be established. Analog-to-digital converters are the missing link and will play a pivotal role in such a development. In prokaryotes, digitization of synthetic gene networks has already been established and was successfully used for the design of different biocomputation devices such as signal converters and state-machines[48–50]. We have successfully designed a mammalian cell consortium-based analog-to-digital converter with integrated signal amplification to enable fragrance-programmable digital control of transgene expression in mammalian cells with AND, OR and NOR logic.

Acknowledgements. We thank Thomas Horn, Erica Montani, Telma Lopes and Verena Jaeggin for their support with microscopy and flow cytometry. We thank Ferdinand Sedlmayer, Vijay Viswam,

Sebastian Bürgel and Peter Buchmann for their generous advice and Oleg Chepurny, Hiroaki Matsunami, George Holz, Haifeng Ye and William Bacchus for providing plasmids and genetic components. This work was supported by the European Research Council (ERC) advanced grant (ProNet, no. 321381) and in part by the National Centre of Competence in Research (NCCR) for Molecular Systems Engineering awarded to M.F.

Author contributions. M.M., S.A., D.A., M.Fo. and M.F. designed the project and analyzed the results, M.M., J.S. and A.S. performed the experimental work and M.M. and M.F. wrote the manuscript.

Competing financial interests. The authors declare no competing financial interests.

References

1 Brophy, J. A. N. & Voigt, C. A. Principles of genetic circuit design. *Nature Methods* **11**, 508-520, (2014).

2 Moon, T. S., Lou, C., Tamsir, A., Stanton, B. C. & Voigt, C. A. Genetic programs constructed from layered logic gates in single cells. *Nature* **491**, 249-253, (2012).

3 Gitzinger, M., Kemmer, C., El-Baba, M. D., Weber, W. & Fussenegger, M. Controlling transgene expression in subcutaneous implants using a skin lotion containing the apple metabolite phloretin. *Proc Natl Acad Sci U S A* **106**, 10638-10643, (2009).

4 Gitzinger, M. *et al.* The food additive vanillic acid controls transgene expression in mammalian cells and mice. *Nucleic Acids Res* **40**, e37, (2012).

5 Weber, W., Bacchus, W., Daoud-El Baba, M. & Fussenegger, M. Vitamin H-regulated transgene expression in mammalian cells. *Nucleic Acids Res* **35**, e116, (2007).

6 Weber, W. *et al.* Conditional human VEGF-mediated vascularization in chicken embryos using a novel temperature-inducible gene regulation (TIGR) system. *Nucleic Acids Res* **31**, e69, (2003).

7 Boorsma, M. *et al.* A temperature-regulated replicon-based DNA expression system. *Nat Biotechnol* **18**, 429-432, (2000).

8 Auslander, D. *et al.* A Synthetic Multifunctional Mammalian pH Sensor and CO2 Transgene-Control Device. *Mol Cell* **55**, 397-408, (2014).

9 Stanley, S. A. *et al.* Radio-wave heating of iron oxide nanoparticles can regulate plasma glucose in mice. *Science* **336**, 604-608, (2012).

10 Folcher, M. *et al.* Mind-controlled transgene expression by a wireless-powered optogenetic designer cell implant. *Nat Commun* **5**, 5392, (2014).

11 Weber, W. & Fussenegger, M. Inducible product gene expression technology tailored to bioprocess engineering. *Curr Opin Biotechnol* **18**, 399-410, (2007).

12 Weber, W. & Fussenegger, M. Emerging biomedical applications of synthetic biology. *Nature Reviews Genetics* **13**, 21-35, (2012).

13 Tigges, M., Marquez-Lago, T. T., Stelling, J. & Fussenegger, M. A tunable synthetic mammalian oscillator. *Nature* **457**, 309-312, (2009).

14 Benenson, Y. Biomolecular computing systems: principles, progress and potential. *Nature Reviews Genetics* **13**, 455-468, (2012).

15 Auslander, S., Auslander, D., Muller, M., Wieland, M. & Fussenegger, M. Programmable single-cell mammalian biocomputers. *Nature* **487**, 123-7, (2012).

16 Auslander, S., Wieland, M. & Fussenegger, M. Smart medication through combination of synthetic biology and cell microencapsulation. *Metab Eng* **14**, 252-260, (2012).

17 Kemmer, C. *et al.* Self-sufficient control of urate homeostasis in mice by a synthetic circuit. *Nat Biotechnol* **28**, 355-360, (2010).

18 Rossger, K., Charpin-El-Hamri, G. & Fussenegger, M. Bile acid-controlled transgene expression in mammalian cells and mice. *Metab Eng* **21**, 81-90, (2014).

19 Saxena, P., Charpin-El Hamri, G., Folcher, M., Zulewski, H. & Fussenegger, M. Synthetic gene network restoring endogenous pituitary-thyroid feedback control in experimental Graves' disease. *Proc Natl Acad Sci U S A* **113**, 1244-1249, (2016).

20 Schukur, L., Geering, B., Charpin-El Hamri, G. & Fussenegger, M. Implantable synthetic cytokine converter cells with AND-gate logic treat experimental psoriasis. *Sci Transl Med* **7**, 318ra201, (2015).

21 Riccione, K. A., Smith, R. P., Lee, A. J. & You, L. A synthetic biology approach to understanding cellular information processing. *ACS Synth Biol* **1**, 389-402, (2012).

22 Regot, S. *et al.* Distributed biological computation with multicellular engineered networks. *Nature* **469**, 207-211, (2011).

23 Tamsir, A., Tabor, J. J. & Voigt, C. A. Robust multicellular computing using genetically encoded NOR gates and chemical 'wires'. *Nature* **469**, 212-215, (2011).

24 Tubio, M. R. *et al.* Expression of a G protein-coupled receptor (GPCR) leads to attenuation of signaling by other GPCRs: experimental evidence for a spontaneous GPCR constitutive inactive form. *J Biol Chem* **285**, 14990-14998, (2010).

25 Bushdid, C., Magnasco, M. O., Vosshall, L. B. & Keller, A. Humans can discriminate more than 1 trillion olfactory stimuli. *Science* **343**, 1370-1372, (2014).

26 Nern, A., Pfeiffer, B. D., Svoboda, K. & Rubin, G. M. Multiple new site-specific recombinases for use in manipulating animal genomes. *PNAS* **108**, 14198-14203, (2011).

27 Fenno, L. E. *et al.* Targeting cells with single vectors using multiple-feature Boolean logic. *Nature Methods* **11**, 763-772, (2014).

28 Yang, L. *et al.* Permanent genetic memory with >1-byte capacity. *Nature Methods* **11**, 1261-1266, (2014).

29 Friedland, A. E. *et al.* Synthetic Gene Networks That Count. *Science* **324**, 1199-1202, (2009).

30 Lapique, N. & Benenson, Y. Digital switching in a biosensor circuit via programmable timing of gene availability. *Nature Chemical Biology* **10**, 1020-7, (2014).

31 Schonhuber, N. *et al.* A next-generation dual-recombinase system for time- and host-specific targeting of pancreatic cancer. *Nat Med* **20**, 1340-1347, (2014).

32 Xie, Z., Wroblewska, L., Prochazka, L., Weiss, R. & Benenson, Y. Multi-Input RNAi-Based Logic Circuit for Identification of Specific Cancer Cells. *Science* **333**, 1307-1311, (2011).

33 Morel, M., Shtrahman, R., Rotter, V., Nissim, L. & Bar-Ziv, R. H. Cellular heterogeneity mediates inherent sensitivity-specificity tradeoff in cancer targeting by synthetic circuits. *Proc Natl Acad Sci U S A* **113**, 8133-8138, (2016).

34 Nissim, L. & Bar-Ziv, R. H. A tunable dual-promoter integrator for targeting of cancer cells. *Mol Syst Biol* **6**, 444, (2010).

35 Tohe, A. & Utatsu, I. Physical and Functional Structure of a Yeast Plasmid, Psb3, Isolated from Zygosaccharomyces-Bisporus. *Nucleic Acids Res* **13**, 4267-4283, (1985).

36 Bonnet, J., Yin, P., Ortiz, M. E., Subsoontorn, P. & Endy, D. Amplifying genetic logic gates. *Science* **340**, 599-603, (2013).

37 Hartwell, L. H., Hopfield, J. J., Leibler, S. & Murray, A. W. From molecular to modular cell biology. *Nature* **402**, C47-52, (1999).

38 Sprinzak, D. *et al.* Cis-interactions between Notch and Delta generate mutually exclusive signalling states. *Nature* **465**, 86-90, (2010).

39 Morsut, L. *et al.* Engineering Customized Cell Sensing and Response Behaviors Using Synthetic Notch Receptors. *Cell* **164**, 780-791, (2016).

40 Clark, B. & Hausser, M. Neural coding: hybrid analog and digital signalling in axons. *Curr Biol* **16**, R585-588, (2006).

41 Dreosti, E., Esposti, F., Baden, T. & Lagnado, L. In vivo evidence that retinal bipolar cells generate spikes modulated by light. *Nat Neurosci* **14**, 951-952, (2011).

42 Hahnloser, R. H., Sarpeshkar, R., Mahowald, M. A., Douglas, R. J. & Seung, H. S. Digital selection and analogue amplification coexist in a cortex-inspired silicon circuit. *Nature* **405**, 947-951, (2000).

43 Firestein, S. How the olfactory system makes sense of scents. *Nature* **413**, 211-218, (2001).

44 Roybal, K. T. *et al.* Precision Tumor Recognition by T Cells With Combinatorial Antigen-Sensing Circuits. *Cell* **164**, 770-779, (2016).

45 Chen, Y. Y., Jensen, M. C. & Smolke, C. D. Genetic control of mammalian T-cell proliferation with synthetic RNA regulatory systems. *Proc Natl Acad Sci U S A* **107**, 8531-8536, (2010).

46 Kemmer, C. *et al.* A designer network coordinating bovine artificial insemination by ovulation-triggered release of implanted sperms. *J Control Release* **150**, 23-29, (2011).

47 Ye, H., Daoud-El Baba, M., Peng, R. W. & Fussenegger, M. A synthetic optogenetic transcription device enhances blood-glucose homeostasis in mice. *Science* **332**, 1565-1568, (2011).

48 Roquet, N., Soleimany, A. P., Ferris, A. C., Aaronson, S. & Lu, T. K. Synthetic recombinase-based state machines in living cells. *Science* **353**, aad8559, (2016).

49 Siuti, P., Yazbek, J. & Lu, T. K. Synthetic circuits integrating logic and memory in living cells. *Nat Biotechnol* **31**, 448-452, (2013).

50 Rubens, J. R., Selvaggio, G. & Lu, T. K. Synthetic mixed-signal computation in living cells. *Nat Commun* **7**, 11658, (2016).

METHODS

Components of the fragrance-programmed analog-to-digital converter with Boolean expression logic. Comprehensive design and construction details for the expression vectors are provided in Supplementary Table 1. The key components of the fragrance-programmable analog-to-digital converter consists of (i) the sampling and quantization module sensing gaseous fragrance compounds such as eugenol, coumarin, dihydrojasmone and acetophenone, by corresponding odorant receptors OREG (**pOREG** [P_{SV40}-OR-EG-pA]), OR5P3 (**pCI-OR5P3** [P_{hCMV}-OR5P3-pA]), OR1A1 (**pCI-OR1A1** [P_{hCMV}-OR1A1-pA]) and OR129-1 (**pCI-MOR129-1** [P_{hCMV}-OR129-1-pA]), (ii) the gas-to-liquid transducer producing soluble signaling compounds such as GLP-1 (**pMM187** [P_{CREm}-GLP-1-Fc_{mIgG}-pA]) and L–tryptophan (via conversion of indole by TrpB) (**pMM221** [P_{CRE}-TrpB-pA]) in response to fragrance input and (iii) the digitization unit which produces recombinases in response to the liquid trigger compounds GLP-1 and L–tryptophan (**pMM195** [P_{SV40}-GLP1R-pA] GenBank ID KY053832, **pWB24** [P_{SV40}-TRT-pA], **pMM212** [P_{CRE}-B3-PEST-pA] or **pMM174** [P_{CREm}-B3-PEST-

pA] GenBank ID KY053830 and **pMM189** [P_{TRT2}-B3-PEST-pA] GenBank ID KY053831. The analog-to-digital converter is set to control AND (**pMM204** [P_{TRT}-B3RT-STOP-B3RT-Ub-tTA-pA] GenBank ID KY053833, **pMM265** [P_{TRE}-B3RT-STOP-B3RT-Citrine-pA] GenBank ID KY053834), OR (**pMM264** [P_{hCMV}-B3RT-STOP-B3RT-tTA-pA], **pMM265** [P_{TRE}-B3RT-STOP-B3RT-Citrine-pA] GenBank ID KY053834) and NOR (**pMM267** [B3RT-P_{SV40}-B3RT-tTA-B3RT-pA], **pMM262** [B3RT-P_{TRE}-B3RT-Citrine-PEST-B3RT-pA]) gates.

Cell culture and transfection. Human embryonic kidney cells (HEK-293T, ATCC: CRL-11268) and HEK-293-derived Hana3A cells[51] constitutively expressing RTP1, RTP2, REEP1, and $G_{\alpha olf}$ were cultivated at 37°C in Dulbecco's modified Eagle's medium (DMEM; Invitrogen) supplemented with 10% fetal calf serum (FCS; Sigma-Aldrich; cat. no. F7524, lot no. 022M3395) and 1% penicillin/streptomycin solution (Sigma-Aldrich) in a humidified atmosphere containing 5% CO_2. HEK-293T and Hana3A cells were cotransfected using an optimized polyethyleneimine-based protocol. In brief, the culture medium of $4x10^5$ HEK-293T or Hana3A cells, cultivated per well of a 6-well plate for 16 h, was replaced with low-L–tryptophan medium (5 µM; Cell Culture Technologies LLC) to repress the L–tryptophan-inducible promoter P_{TRT}, while maintaining high cell viability before the cells were cotransfected by dropwise addition of a transfection solution containing 4 µg of total plasmid DNA, 600 µL FCS-free DMEM and 12 µL polyethyleneimine (1 mg mL^{-1} in ddH_2O; Polysciences) and were incubated for 30 min at 22°C. After 6 h, the cells were detached using 200 µL of trypsin/EDTA (Sigma-Aldrich), washed once with 1.8 mL FCS-containing DMEM, resuspended in 0.75 mL of FCS-containing DMEM, re-seeded in a 96-well plate (25,000 cells/well) containing 25mM HEPES (AppliChem GmbH) as well as different L–tryptophan concentrations and cultivated for up to 48 h before analysis. Gaseous fragrance- and perfume-based remote control of cellular behavior was achieved by placing the compounds in the adjacent well followed by airtight sealing of the entire plate.

Chemical compounds and fragrances. L–tryptophan (stock solution 25 mM in ddH_2O; Sigma-Aldrich) and indole (stock solution 100 mM in 50% ethanol; Sigma-Aldrich) were used to supplement the L–tryptophan-free DMEM (Cell Culture Technologies LLC). Low-L–tryptophan DMEM contained 5 µM L–tryptophan and 400 µM indole. High-L–tryptophan medium contained 25 µM L–tryptophan. Commercial perfume brands listed in Supplementary Table 2 were diluted 1:10 in ethanol for gaseous induction. The pure fragrances eugenol, coumarin, dihydrojasmone and acetophenone were prepared as 100 mM stock solutions in ethanol and used at 10 mM for gaseous induction. The GLP-1 analogue Exendin-4 (Sigma-Aldrich) was used at 50 nM for receptor activation. L–norepinephrine hydrochloride (10mM stock solution in ddH_2O; Sigma-Aldrich, cat. no. 74480), lithocholic acid (10mM stock solution in DMSO; Sigma-Aldrich, cat. no. L6250) and stromal cell-derived factor 1 alpha (1 µM stock solution in PBS, R&D Systems, cat. no. 350-NS) were directly added to the cell culture media.

Flow cytometry. Cell populations were analyzed with a LSRII Fortessa flow cytometer (Becton Dickinson) equipped for Citrine (488 nm laser, 505 nm longpass filter and 530/11 emission filter [passband 530 nm; width 11 nm]) and mCherry (561 nm laser, 600 nm longpass filter and 610/20 emission filter) detection and set to exclude dead cells and cell doublets. Each sample run was spiked with AlignFlow alignment beads (A-7302; Life Technologies, lot: 1252789) as an internal control, ensuring consistency of the flow cytometry settings between different circuits and independent experiments. At least 3 × 10,000 cells were recorded per data set and were analyzed with FACSDiva software (version no. 8.0.1; BD Biosciences). Transfected HEK-293T populations were gated for cell fluorescence compared to mock-transfected cells (pcDNA3.1). The percentage of gated cells was multiplied by their mean fluorescence, resulting in a weighted Citrine expression value that correlates fluorescence intensity with cell number. FACS profiles and gates are shown in **Supplementary Fig. 13**.

Fluorescence imaging. Fluorescence microscopy was performed using an inverted fluorescence microscope (Nikon Ti-E; Nikon) equipped with an incubation chamber, an Orca Flash-4 digital camera (Hamamatsu), a pE-100-LED (CoolLED) as the transmission light source, a Spectra X (Lumencor) as the fluorescent light source and a 10× objective (Plan Apo λ N/A: 0.45; DIC N1; WD:4). Brightfield (3% intensity; 5 ms exposure), citrine (excitation 470 nm; 12% intensity; 200 ms exposure; YFP ET Filter: Dichroic 515 nm; emission: 535/30 nm), and mCherry (excitation 555 nm; 10% intensity; 500 ms exposure; CY3 HC: Dichroic 560 nm; emission 595/50) were detected. A binning of 2×2 was used.

Analytical assays. SEAP production levels were quantified in the cell-culture supernatants using a p-nitrophenylphosphate-based light-absorbance time course. In brief, 100 µL of cell culture supernatant was heat-inactivated for 30 min at 65°C. Subsequently, 80 µL of the supernatant was transferred to a well of a 96-well plate containing 100 µL 2× SEAP assay buffer (20 mM homoarginine, 1 mM $MgCl_2$, 21% (v/v) diethanolamine, pH 9.8). After the addition of 20 µL of 120 mM para-nitrophenylphosphate (pNPP disodium salt, hexahydrate, Acros Organics BVBA) and dilution in 1× SEAP assay buffer, the time-dependent increase in light absorbance was profiled at 405 nm for 30 min using a GeniosPro multi-well reader (Tecan). L–tryptophan levels in the culture supernatant were profiled using a fluorescence-based assay kit (Mediomics, cat. no. 1-1-1001B). Glucagon-like peptide-1 (GLP-1) levels in the culture supernatant were quantified using a Mouse IgG enzyme-linked immunosorbent assay (ELISA) kit (Immunology Consultants Laboratory Inc., cat. no. E-90G).

51 Saito, H., Kubota, M., Roberts, R. W., Chi, Q. & Matsunami, H. RTP family members induce functional expression of mammalian odorant receptors. *Cell* 119, 679-691, (2004).

Data availability. GenBank accession codes: pMM174, KY053830; pMM189, KY053831; pMM195, KY053832; pMM204, KY053833; pMM265, KY053834.

Supplementary Information

Designed cell consortia as fragrance-programmable analog-to-digital converters

Marius Müller[1], Simon Ausländer[1], Andrea Spinnler[1], David Ausländer[1], Julian Sikorski[1], Marc Folcher[1], Martin Fussenegger[1,2,*]

*[1]Department of Biosystems Science and Engineering, ETH Zurich, Mattenstrasse 26, CH-4058 Basel, Switzerland; [2]Faculty of Science, University of Basel, Mattenstrasse 26, CH-4058 Basel, Switzerland; *To whom correspondence should be addressed: Tel.: +41 61 387 31 60, Fax: +41 61 387 39 88, E-mail: fussenegger@bsse.ethz.ch.*

Supplementary Results

Supplementary Tables

Supplementary Table 1. Plasmids used and designed in this study

Plasmid	Description and Cloning Strategy	Reference or Source
pJFRC157-20XUAS-IVS-B3::PEST	B3-PEST expression vector (UAS_{20}-P_{HSP70}-B3-PEST-pA).	Nern et al., 2011
pJFRC160-21XUAS-B3RT>-dSTOP-B3RT>-myr::RFP	myr-RFP expression vector containing a STOP cassette flanked by B3RT (UAS_{21}-P_{HSP70}-B3RT-STOP-B3RT-myr-RFP-pA).	Nern et al., 2011
pcDNA3.1(+)	Constitutive mammalian expression vector (P_{hCMV}-MCS-pA).	Life Technologies, Carlsbad, CA
pCRE-Luc	P_{CRE}-driven Luc expression vector (P_{CRE}-Luc-pA).	Clontech, Mountain View, CA
pColaDuet^{TM}-1	Prokaryotic expression vector used as filler plasmid.	Merck, Darmstadt, Germany
pCI-MOR9-1	Constitutive vanillic acid-inducible OR9-1 expression vector (P_{hCMV}-OR9-1-pA).	Saito et al., 2009
pCI-MOR31-1	Constitutive heptanoic acid-inducible OR31-1 expression vector (P_{hCMV}-OR31-1-pA).	Saito et al., 2009
pCI-MOR129-1	Constitutive acetophenone-inducible OR129-1 expression vector (P_{hCMV}-OR129-1-pA).	Saito et al., 2009
pCI-MOR261-1	Constitutive 1-octanol-inducible OR261-1 expression vector (P_{hCMV}-OR261-1-pA).	Saito et al., 2009
pCI-MOR271-1	Constitutive benzyl acetate-inducible OR271-1 expression vector (P_{hCMV}-OR271-1-pA).	Saito et al., 2009
pCI-OR1A1	Constitutive dihydrojasmone-inducible OR1A1 expression vector (P_{hCMV}-OR1A1-pA).	Saito et al., 2009
pCI-OR2J2	Constitutive 1-nonanol-inducible OR2J2 expression vector (P_{hCMV}-OR2J2-pA).	Saito et al., 2009
pCI-OR2W1	Constitutive 2-heptanone-inducible OR2W1 expression vector (P_{hCMV}-OR2W1-pA).	Saito et al., 2009
pCI-OR5P3	Constitutive coumarin-inducible OR5P3 expression vector (P_{hCMV}-OR5P3-pA).	Saito et al., 2009
pCI-OR51E2	Constitutive propionic acid-inducible OR51E2 expression vector (P_{hCMV}-OR51E2-pA).	Saito et al., 2009
pCK53	P_{CRE}-driven SEAP expression vector (P_{CRE}-SEAP-pA).	Kemmer et al., 2011
pCK91	P_{CRE}-driven YFP expression vector (P_{CRE}-YFP-pA).	Kemmer et al., 2011
pCK120	Constitutive HRH2 expression vector ($P_{EF1\alpha}$-HRH2-pA).	Auslaender et al., 2014
pDA134	P_{CREm}-driven Citrine expression vector (P_{CREm}-Citrine-pA).	Auslaender et al., 2014
pFS29	Constitutive mCherry expression vector (P_{SV40}-	Auslaender et

	mCherry-pA).	al., 2014
pGLP-1-R	Constitutive GLP1R expression vector (P_{hCMV}-GLP1R-pA).	Chepurny et al., 2002
pHY69	P_{CRE}-driven GLP-1-Fc_{mIgG}-Leptin expression vector (P_{CRE}-GLP-1-Fc_{mIgG}-Leptin-pA).	Ye et al., 2013
piRFP670-N1	Constitutive iRFP670 expression vector (P_{hCMV}-iRFP670-pA).	Shcherbakova et al., 2013
pOR7D4	Constitutive androstenone-inducible OR7D4 expression vector (P_{hCMV}-OR7D4-pA).	Folcher et al., unpublished
pOREG	Constitutive eugenol-inducible OREG expression vector (P_{SV40}-OREG-pA).	Baud et al., 2010
pMT100	$P_{hCMV*-1}$-driven Ub-GFP expression vector ($P_{hCMV*-1}$-Ub-GFP-pA).	Tigges et al., 2009
pSAM200	Constitutive tTA expression vector (P_{SV40}-tTA-pA).	Fussenegger et al., 2000
pSEAP2-Basic	SEAP-encoding vector (MCS-SEAP-pA).	Clontech, Mountain View, CA
pSEAP2-Control	Constitutive SEAP expression vector (P_{SV40}-SEAP-pA).	Clontech, Mountain View, CA
pSP16	P_{CREm}-driven SEAP expression vector (P_{CREm}-SEAP-pA).	Saxena et al., unpublished
pTRE3G-bi	Bidirectional P_{TRE}-driven expression vector (pA-MCS2-P_{TRE}-MCS1-pA).	Clontech, Mountain View, CA
pWB22	L-tryptophan-inducible P_{TRT}-driven SEAP expression vector (P_{TRT}-SEAP-pA).	Bacchus et al., 2012
pWB24	Constitutive TRT expression vector (P_{SV40}-TRT-pA).	Bacchus et al., 2012
pWB32	Constitutive TrpB expression vector (P_{hCMV}-TrpB-pA).	Bacchus et al., 2012
pMM1	pcDNA3.1(+)-derived expression vector containing a modified MCS (P_{hCMV}-MCS-pA; MCS, *Eco*RI-ATG-*Spe*I-*Nhe*I-*Bam*HI-STOP-*Xba*I-*Hind*III-*Fse*I-pA). pcDNA3.1(+) was PCR-amplified using oligonucleotides OMM1 (5'-cggatccaccggtgtctagaaagctttgaggccggcctgcaggGATCAGCCTCGACTGTGCCTTC-3') and OMM2 (5'-ctagcactagtcatggtgaattcgattaatcaattgacgcgtGGAGATCTCCCGATCCGTC-3') and self-ligated.	This work
pMM146	L-tryptophan-inducible P_{TRT2}-driven SEAP expression vector (P_{TRT2}-SEAP-pA). pWB22 was PCR-amplified using the P_{min}-containing oligonucleotide OMM131 (5'-**tagagggtatataatggaagctcgacttccag**GAATTCGAGCTCGCCCGGGG-3') and OMM132 (5'Phos-CCTGCAGGATCCTTGTAATG-3') and self-ligated.	This work
pMM163	B3 recombinase-inducible P_{hCMV}-driven RFP expression vector (P_{hCMV}-B3RT-STOP-B3RT-myr-RFP-pA). B3RT-STOP-B3RT-myr-RFP was excised from pJFRC160-21XUAS-B3RT-STOP-B3RT-	This work

	myr::RFP using *Bgl*II/*Xba*I and ligated into the compatible sites (*Bam*HI/*Xba*I) of pcDNA3.1(+).	
pMM172	B3 recombinase-inducible P_{CRE}-driven RFP expression vector (P_{CRE}-B3RT-STOP-B3RT-myr-RFP-pA). B3RT-STOP-B3RT-myr-RFP was excised from pMM163 using *Hin*dIII/*Xba*I and ligated into the corresponding sites (*Hin*dIII/*Xba*I) of pCRE-Luc.	This work
pMM174	P_{CREm}-driven B3-PEST expression vector (P_{CREm}-B3-PEST-pA). B3-PEST was excised from pMM543 using *Eco*RI/*Bam*HI and ligated into the corresponding sites (*Eco*RI/*Bam*HI) of pSP16.	This work
pMM184	Constitutive Citrine expression vector containing a B3RT in the 3'UTR (P_{hCMV}-Citrine-B3RT-pA). B3RT was excised from pMM163 using *Nhe*I/*Hin*dIII and ligated into the corresponding sites (*Nhe*I/*Hin*dIII) of pMM545.	This work
pMM187	P_{CREm}-driven GLP-1-Fc_{mIgG} expression vector (P_{CREm}-GLP-1-Fc_{mIgG}-pA). GLP-1-Fc_{mIgG} was excised from pHY69 using *Eco*RI/*Hin*dIII and ligated into the corresponding sites (*Eco*RI/*Hin*dIII) of pSP16.	This work
pMM188	P_{CREm}-driven TrpB expression vector containing (P_{CREm}-TrpB-pA). TrpB was excised from pWB32 using *Eco*RI/*Xba*I and ligated into the corresponding sites (*Eco*RI/*Xba*I) of pSP16.	This work
pMM189	L-tryptophan-inducible P_{TRT2}-driven B3-PEST expression vector (P_{TRT2}-B3-PEST-pA). B3-PEST was excised from pMM543 using *Eco*RI/*Xba*I and ligated into the corresponding sites (*Eco*RI/*Xba*I) of pMM146.	This work
pMM190	L-tryptophan-inducible P_{TRT}-driven B3-PEST expression vector (P_{TRT}-B3-PEST-pA). B3-PEST was excised from pMM543 using *Eco*RI/*Xba*I and ligated into the corresponding sites (*Eco*RI/*Xba*I) of pWB22.	This work
pMM191	B3 recombinase-inducible P_{hCMV}-driven RFP expression vector (P_{hCMV}-B3RT-STOP-B3RT-myr-RFP-pA). pMM163 was PCR-amplified using oligonucleotides OMM175 (5'-GAATGAATTGTTGTTGTTAACTTGTTTATTGCAGC-3') and OMM176 (5'Phos-ATTTTATGTTTCAGGTTCAGGGGGAGG-3') to remove the *Mfe*I restriction site and self-ligated.	This work
pMM193	Constitutive GLP-1-Fc_{mIgG} expression vector (P_{hCMV}-GLP-1-Fc_{mIgG}-pA). GLP1-Fc_{mIgG} was excised from pHY69 using *Eco*RI/*Hin*dIII and ligated into the corresponding sites (*Eco*RI/*Hin*dIII) of pMM1.	This work
pMM195	Constitutive GLP1R expression vector (P_{SV40}-GLP1R-pA). GLP1R was excised from pGLP-1-R using *Hin*dIII/*Xba*I and ligated into the corresponding sites (*Hin*dIII/*Xba*I) of pSEAP2-Control.	This work
pMM197	L-tryptophan-inducible P_{TRT}-driven Citrine expression vector (P_{TRT}-Citrine-pA). Citrine was excised from pMM545 using *Eco*RI/*Xba*I and ligated into the	This work

	corresponding sites (*Eco*RI/*Xba*I) of pWB22.	
pMM198	Constitutive B3 recombinase-excisable Citrine expression vector (P_{SV40}-B3RT-Citrine-B3RT-pA). B3RT was PCR-amplified from pSEAP2-Control using the B3RT-containing oligonucleotide OMM169 (5'-gcggaattccgtta**ggttgcttaagaattacttattcttaagcaacc**agatcCGATTCGTAGCTTTTTGCAAAAGCC -3') and OMM170 (5'-gcgctctagataagcttggccggccGATACATTGATGAGTTTGGAC -3'), digested with *Eco*RI/*Xba*I and ligated into the corresponding sites (*Eco*RI/*Xba*I) of pMM184.	This work
pMM200	B3 recombinase-inducible P_{TRT}-driven Citrine expression vector (P_{TRT}-B3RT-STOP-B3RT-Citrine-pA). B3RT-STOP-B3RT was PCR-amplified from pMM163 using oligonucleotides OMM179 (5'-gcgaattcGCGTTTAAACTTATGCTTGGTACCGAGCTCGGATC -3') and OMM180 (5'-cgcgcttctagaggcCATTTGTTGCCGATTTTGATTCTCGAG -3'), digested using *Eco*RI/*Xba*I and ligated into the compatible sites (*Eco*RI/*Spe*I) of pMM197.	This work
pMM203	L-tryptophan-inducible P_{TRT}-driven destabilized tTA expression vector (P_{TRT}-Ub-tTA-pA). Ub-tTA was excised from pMM509 using *Eco*RI/*Xba*I and ligated into the corresponding sites (*Eco*RI/*Xba*I) of pWB22.	This work
pMM204	B3 recombinase-inducible P_{TRT}-driven destabilized tTA expression vector (P_{TRT}-B3RT-STOP-B3RT-Ub-tTA-pA). B3RT-STOP-B3RT was PCR-amplified from pMM163 using oligonucleotides OMM179 (5'-gcgaattcGCGTTTAAACTTATGCTTGGTACCGAGCTCGGATC -3') and OMM180 (5'-cgcgcttctagaggcCATTTGTTGCCGATTTTGATTCTCGAG -3'), digested using *Eco*RI/*Xba*I and ligated into the compatible sites (*Eco*RI/*Spe*I) of pMM203.	This work
pMM206	L-tryptophan-inducible P_{TRT2}-driven Citrine expression vector (P_{TRT2}-Citrine-pA). Citrine was excised from pMM545 using *Eco*RI/*Xba*I and ligated into the corresponding sites (*Eco*RI/*Xba*I) of pMM146.	This work
pMM207	B3 recombinase-inducible P_{hCMV}-driven Citrine expression vector (P_{hCMV}-B3RT-STOP-B3RT-Citrine-pA). B3RT-STOP-B3RT-Citrine was excised from pMM200 using *Eco*RI/*Xba*I and ligated into the corresponding sites (*Eco*RI/*Xba*I) of pMM1.	This work
pMM211	P_{CRE}-driven SEAP expression vector (P_{CRE}-SEAP-pA). pCK53 was PCR-amplified using oligonucleotides OMM187 (5'Phos-GCCAATGACAAGACGCTGGG-3') and OMM188 (5'- GAATTgGAACACGCAGATGCAG-3') and self-ligated.	This work
pMM212	P_{CRE}-driven B3-PEST expression vector (P_{CRE}-B3-	This work

	PEST-pA). B3-PEST was excised from pMM543 using *Eco*RI/*Xba*I and ligated into the corresponding sites (*Eco*RI/*Xba*I) of pMM211.	
pMM216	Constitutive B3 recombinase-excisable Citrine expression vector (B3RT-P_{SV40}-B3RT-Citrine-B3RT-pA). B3RT was PCR-amplified from pSEAP2-Control using oligonucleotides OMM203 (5'-GGTACTTGGAGCGGCCGCAATAAAATATC-3') and the B3RT-containing oligonucleotide OMM204 (5'-gccgcagatct**ggttgcttaagaattacttattcttaagcaacc**CGAGCCCGGGCTAGCACGCGTAAG -3') digested with *Not*I/*Bgl*II and ligated into the corresponding sites (*Not*I/*Bgl*II) of pMM198.	This work
pMM221	P_{CRE}-driven TrpB expression vector (P_{CRE}-TrpB-pA). TrpB was excised from pWB32 using *Eco*RI/*Xba*I and ligated into the corresponding sites (*Eco*RI/*Xba*I) of pMM211.	This work
pMM222	P_{CRE}-driven mCherry expression vector (P_{CRE}-mCherry-pA). mCherry was excised from pMM573 using *Eco*RI/*Xba*I and ligated into the corresponding sites (*Eco*RI/*Xba*I) of pMM211.	This work
pMM224	L-tryptophan-inducible P_{TRT}-driven mCherry expression vector (P_{TRT}-mCherry-pA). mCherry was excised from pMM573 using *Eco*RI/*Xba*I and ligated into the corresponding sites (*Eco*RI/*Xba*I) of pWB22.	This work
pMM229	P_{CRE}-driven iRFP670 expression vector (P_{CRE}-iRFP670-pA). iRFP670 was excised from pMM581 using *Eco*RI/*Xba*I and ligated into the corresponding sites (*Eco*RI/*Xba*I) of pMM211.	This work
pMM242	Constitutive B3 recombinase-excisable destabilized Citrine expression vector (B3RT-P_{SV40}-B3RT-Citrine-PEST-B3RT-pA). Citrine-PEST was excised from pMM588 using *Eco*RI/*Hin*dIII and ligated into the corresponding sites (*Eco*RI/*Hin*dIII) of pMM216.	This work
pMM262	Tetracycline-responsive B3 recombinase-excisable destabilized Citrine expression vector (B3RT-P_{TRE}-B3RT-Citrine-PEST-B3RT-pA). P_{TRE} was PCR-amplified from pTRE3G-bi using oligonucleotides OMM242 (5'-gaagatctCGACATACTCGAGTTTACTCCC-3') and OMM243 (5'-gccggatatcctaggTGTCGACTTTACGAGGGTAGG-3´), restricted with *Bgl*II/*Avr*II and ligated into the corresponding sites (*Bgl*II/*Avr*II) of pMM242.	This work
pMM264	Constitutive B3 recombinase-inducible destabilized tTA expression vector (P_{hCMV}-B3RT-STOP-B3RT-Ub-tTA-pA). P_{hCMV} was excised from pMM1 using *Bgl*II/*Eco*RI and ligated into the corresponding sites (*Bgl*II/*Eco*RI) of pMM204.	This work
pMM265	B3 recombinase-inducible P_{TRE}-driven Citrine expression vector (P_{TRE}-B3RT-STOP-B3RT-Citrine-	This work

	pA). P_{TRE} was excised from pTRE3G-bi using *Bgl*II/*Eco*RI and ligated into the corresponding sites (*Bgl*II/*Eco*RI) of pMM200.	
pMM267	Constitutive B3 recombinase-excisable destabilized tTA expression vector (B3RT-P_{SV40}-B3RT-Ub-tTA-B3RT-pA). Ub-tTA was excised from pMM509 using *Eco*RI/*Sbf*I and ligated into the compatible sites (*Eco*RI/*Pst*I) of pMM242.	This work
pMM506	Constitutive tTA expression vector (P_{hCMV}-tTA-pA). tTA was PCR-amplified from pSAM200 using oligonucleotides OMM77 (5'-gcgaattcaccatgactagtTCCAGATTAGATAAAAGTAAAG-3') and OMM78 (5'-gctctagacaccggtggatccgctagcCCCACCGTACTCGTCAATTC -3´), restricted with *Eco*RI/*Xba*I and ligated into the corresponding sites (*Eco*RI/*Xba*I) of pMM1.	This work
pMM509	Constitutive destabilized tTA expression vector (P_{hCMV}-Ub-tTA-pA). Ubiquitin was PCR-amplified from pMT100 using oligonucleotides OMM67 (5'-gcgaattcaccatgactagtCAGATTTTCGTGAAGACCCTG-3') and OMM76 (5'-gctctagacggatccgctagcaggGCCACCTCTCAGGCGAAG-3') restricted with *Eco*RI/*Nhe*I and ligated into compatible sites (*Eco*RI/*Spe*I) of pMM506.	This work
pMM516	Constitutive TRT expression vector (P_{hCMV}-TRT-pA). TRT was PCR-amplified from pWB24 using oligonucleotides OMM98 (5'-gcgaattcaccatgactagtAAAAATCAAGAGGAGTCTGGC-3') and OMM78 (5'-gctctagacaccggtggatccgctagcCCCACCGTACTCGTCAATTC -3´), restricted with *Eco*RI/*Xba*I and ligated into the corresponding sites (*Eco*RI/*Xba*I) of pMM1.	This work
pMM543	Constitutive B3-PEST expression vector (P_{hCMV}-B3-PEST-pA). B3-PEST was PCR-amplified from pB3-PEST using oligonucleotides OMM137 (5'-gcgaattcaccatgactagtAGCTCGTATATGGATCTTGTTG-3') and OMM110 (5'-aagcttttctagacaccggtggatccgctagcCACATTGATCCTAGCAGAAGC -3´), restricted with *Eco*RI/*Xba*I and ligated into the corresponding sites (*Eco*RI/*Xba*I) of pMM1.	This work
pMM545	Constitutive Citrine expression vector (P_{hCMV}-Citrine-pA). Citrine was PCR-amplified from pDA134 using oligonucleotides OMM139 (5'-gcggaattcaccatgactagtGGTGGTTCTGGTGTGAGCAAGGGCGAGGAGCTG-3') and OMM140 (5'-aagcttttctagacaccggtggatccgctagcAGAACCCTTGTACAGCTCGTCCATGCC-3'), restricted with *Eco*RI/*Xba*I and ligated into the corresponding sites (*Eco*RI/*Xba*I) of pMM1.	This work
pMM573	Constitutive mCherry expression vector (P_{hCMV}-mCherry-pA). mCherry was PCR-amplified from	This work

	pFS29 using oligonucleotides OMM197 (5'-cggaattcaccatgactagtGTGAGCAAGGGCGAGGAGGATAAC-3') and OMM198 (5'-aagctttctagacaccggtggatccgctagcTCCAGACTTGTACAGCTCGTCC-3'), restricted with *Eco*RI/*Xba*I and ligated into the corresponding sites (*Eco*RI/*Xba*I) of pMM1.	
pMM581	Constitutive iRFP670 expression vector (P_{hCMV}-iRFP670-pA). iRFP670 was PCR-amplified from piRFP670-N1 using oligonucleotides OMM206 (5'-gcgaattcaccatgactagtGCGCGTAAGGTCGATCTCACC-3') and OMM207 (5'-aagctttctagacaccggtggatccgctagcGCGTTGGTGGTGGGCGGC-3'), restricted with *Eco*RI/*Xba*I and ligated into the corresponding sites (*Eco*RI/*Xba*I) of pMM1.	This work
pMM588	Constitutive destabilized Citrine expression vector (P_{hCMV}-Citrine-PEST-pA). PEST was PCR-amplified from d2EYFP using oligonucleotides OMM109 (5'-gcgaattcaccatgactagtAGCCATGGCTTCCCGCCGG-3') and OMM110 (5'-aagctttctagacaccggtggatccgctagcCACATTGATCCTAGCAGAAGC-3'), restricted with *Spe*I/*BamH*I and ligated into the compatible sites (*Nhe*I/*BamH*I) of pMM545.	This work

Abbreviations: **B3,** *Zygosaccharomyces bisporus* recombinase; **B3RT,** B3 recombination target site; **cAMP**, cyclic adenosine monophosphate; **Citrine**, improved version of EYFP; **CRE**, cAMP-response element**; d2EYFP**, destabilized EYFP variant; **EYFP**, enhanced yellow fluorescent protein; **Fc**, fragment crystallizable region of an antibody that interacts with the Fc cell surface receptors; **Fc_{mIgG}**, mouse IgG-derived Fc linker; **GAL4**, *Saccharomyces cerevisiae* transcription activator; **GFP**, green fluorescent protein; **GLP-1**, Glucagon-like peptide 1; **GLP-1-Fc_{mIgG}-Leptin**, bifunctional therapeutic peptide hormone combining GLP-1 and leptin; **GLP1R**, GLP-1 receptor; **hsp70**, heat shock protein 70; **iRFP670**, near-infrared-red fluorescent protein with excitation at 670nm; **KRAB**, Krueppel-associated box protein of the human kox-1 gene; **HRH2**, human histamine receptor H2; **Luc**. *Photinus pyralis* firefly luciferase; **mCherry**, *Discosoma*-derived red fluorescent protein; **MCS**, multiple cloning site; **myr-RFP**, myristoylated RFP; **OR**, Odorant receptor; **OR1A1**, dihydrojasmone-responsive human OR; **OR2J2**, octanol-responsive human OR; **OR2W1**, hexanal-responsive human OR; **OR5P3**, cumarin-responsive human OR; **OR51E2**, propionic acid-responsive human OR; OR7D4, androstenone-responsive human OR; **OR9-1**, vanillic acid-responsive mouse OR; **OR31-1**, heptanoic acid-responsive mouse OR; **OR129-1**, acetophenone-responsive mouse OR; **OR261-1**, octanol-responsive mouse OR; **OR271-1**, benzyl acetate-responsive mouse OR; **OREG**, eugenol-responsive mouse OR; **$(O_{Trp})_2$**, dimeric TrpR-/TRT-specific operator site; **pA**, polyadenylation signal; **P_{CRE}**, synthetic mammalian promoter containing a cAMP-response element (CRE-$P_{hCMVmin}$); **P_{CREm}**, modified P_{CRE}; **PEST**, mouse ornithine decarboxylase-derived peptide sequence rich in proline (P), glutamic acid (E), serine (S) and threonine (T) acting as protein degradation signal; **P_{hCMV}**, human cytomegalovirus immediate early promoter; **$P_{hCMV*-1}$**, tTA-specific tetracycline-responsive promoter ; **$P_{hCMVmin}$**, minimal version of P_{hCMV}; **$P_{EF1\alpha}$**, human elongation factor 1 alpha promoter; **P_{HSP70}**, *Drosophila melanogaster* heat shock protein 70 promoter; **P_{min}**, synthetic minimal mammalian promoter; **P_{SV40}**, simian virus 40 promoter; **P_{TRE}**, **enhanced** tTA-specific tetracycline-responsive promoter; **P_{TRT}**, TRT-specific L-tryptophan-inducible promoter ($(O_{TRP})_2$-$P_{hCMVmin}$); **P_{TRT2}**, TRT-specific L-tryptophan-inducible

promoter ($(O_{Trp})_2$-P_{min}); **RFP**, Acropora *millepora*-derived red fluorescent protein; **SEAP**, human placental secreted alkaline phosphatase; **STOP**, transcriptional STOP cassette consisting of tandem hsp70 and SV40 transcriptional terminators; **SV40**, simian virus 40; **tetR**, *Escherichia.coli Tn*10-derived tetracycline repressor; **TRE**, tetracycline responsive element; **TrpB**, *Escherichia coli*-derived tryptophan synthase *β*-subunit; **TrpR**, *Chlamydia trachomatis*-derived tryptophan repressor; **TRT**, L-tryptophan-dependent transactivator (TrpR-VP16); **tTA**, tetracycline-dependent transactivator (tetR-VP16); **UAS_n**, n tandem repeats of the GAL4-specific upstream activation sequence; **Ub**, Ubiquitin degradation signal; **UTR**, untranslated region; **VP16**, *Herpes simplex*-derived transactivation domain.

Oligonucleotides: Restriction endonuclease-specific sites are underlined, annealing basepairs are shown in capital letters and B3RT is indicated in bold.

Supplementary Table 2. Perfumes used in this study

Number	Name	Gender	Brand
1	Chanel n°5 (EdT)	female	Chanel
2	Chanel n°19 (EdT)	female	Chanel
3	Coco (EdT)	female	Chanel
4	Cristalle (EdT)	female	Chanel
5	Chanel n°5 (EdP)	female	Chanel
6	Xeryus	male	Givenchy
7	Mumure	female	Van Cleef & Arpels
8	Magnetism (EdP)	female	Escada
9	Opium	female	Yves Saint Laurent
10	Reminiscence	male	Reminiscence
11	Eden	female	Cacharel
12	Rocabar	female	Hermès
13	Acqua Allegoria Pampelune	female	Guerlain
14	Cristobal	female	Balenciaga
15	Habit Rouge (EdT)	male	Guerlain
16	Ines de la Fressanges	female	Inès de la Fressanges
17	Lolita lempicka	male	Les Magnolias
18	Cerruti Image	male	Cerrutti
19	Folies de Saisons	female	Yves Rocher
20	Façonnable	female	Façonnable
21	Chrome	female	Azzaro
22	Romance	female	Ralph Lauren
23	Bulgari (EdP)	female	Eau de Cologne
24	Envy	female	Gucci
25	Ô de Lancôme (EdT)	female	Lancôme
26	Pivoine	female	Yves Rocher
27	Egoiste (EdT)	male	Chanel
28	Knowing	female	Estée Lauder
29	Aromatic Elixir	female	Laboratoires clinique
30	Chic	female	Carolina Herrera
31	Opium	male	Yves Saint Laurent
32	Only	female	Julio Iglesias
33	First	female	Van Cleef & Arpels
34	Trésor	female	Lancôme
35	Lacoste (EdT)	male	Lacoste

36	Eau Sauvage	male	Christian Dior
37	Must de Cartier	male	Cartier
38	Venise	female	Yves Rocher
39	Luna	female	Souleiado
40	Boucheron (EdT)	male	Boucheron
41	Rochas (EdP)	female	Rochas
42	Rochas Paris (EdT)	female	Rochas
43	8ème jour	female	Yves Rocher
44	Pourpre	female	Tan Giudicelli
45	Armani	male	Armani
46	Le B	female	Agnès B.
47	Cantate	female	Yves Rocher
48	Shafali Fleur rare	female	Yves Rocher
49	Prada	female	Prada
50	Good Life	female	Davidoff
51	Silver Rain	female	Clarins
52	Flower Bomb	female	Victor & Rolf
53	Chance (EdP)	female	Chanel
54	Elixir des Merveilles (EdP)	female	Hermès
55	Narcisso Rodrigues for HER	female	Narciso Rodriguez
56	Light Blue	female	Dolce & Gabbana
57	Flora	female	Gucci
58	Sentiment	female	Escada
59	Ibiza Hippie	female	Escada
60	UB (EdT)	female	Club des Créateurs
61	Lettre à Anna	female	Isabel Derroisné
62	Love de Lune	female	Hubert Isabelle d'Ornano
63	Miss me	female	Stella Cadente
65	Rose ispahan	female	Yves Rocher
66	Homme de Café	male	Parfums Café
67	LouLou	female	Cacharel
69	Adidas	female	Adidas
70	Orchidee	female	Yves Rocher
71	Vie privée	female	Yves Rocher
72	Nature	female	Yves Rocher
73	Ispahan	female	Yves Rocher
74	Vent Vert	female	Pierre Balmain
75	Coco Mademoiselle (EdP)	female	Chanel
76	Ma Griffe	female	Carven
77	Amarige	female	Givenchy
78	Escada pour homme	male	Escada
80	Givenchy III	female	Givenchy
82	Tsar	male	Van Cleef & Arpels
83	Turbulences	female	Revillion

Abbreviations: **EdP,** Eau de Perfume; **EdT,** Eau de Toilette.

Supplementary Table 3. Composition of the transfected components in this work

Composition sampling and quantization module characterisation (Figure 2b-i)

Hana3A cells		
Plasmid (ng/6well)	Plasmid name	Description
400 (100)	pOREG or pCI-OR5P3 or pCI-OR1A1 or (pCI-MOR129-1)	P_{SV40}-OREG-pA or P_{hCMV}-OR5P3-pA or P_{hCMV}-OR1A1-pA or P_{hCMV}-OR129-1-pA
400	pSP16	P_{CREm}-SEAP-pA
400	pMM222	P_{CRE}-mCherry-pA
1200 (1500)	pColaDuet-1	Filler Plasmid

Composition sender-sensor cells characterisation (Figure 2k,l)

Hana3A cells	**DI-sensor-sender cells**	
Plasmid (ng/6well)	Plasmid name	Description
400	pCI-OR1A1	P_{hCMV}-OR1A1-pA
400	pMM187	P_{CREm}-GLP-1-Fc_{mIgG}-pA
1400	pColaDuet-1	Filler Plasmid
Hana3A cells	**EG-sensor-sender cells**	
Plasmid (ng/6well)	Plasmid name	Description
400	pOREG	P_{SV40}-OREG-pA
400	pMM221	P_{CRE}-TrpB-pA
1400	pColaDuet-1	Filler Plasmid

Composition transducer module characterisation (Figure 2m,n)

HEK-293T cells	**GLP-1 Receiver**	
Plasmid (ng/6well)	Plasmid name	Description
1000	pMM195	P_{SV40}-GLP1R-pA
1000	pSP16	P_{CREm}-SEAP-pA
Hana3A cells	**GLP-1 Producer**	
Plasmid (ng/6well)	Plasmid name	Description
2000	pMM193	P_{hCMV}-GLP-1-Fc_{mIgG}-pA
Hana3A cells	**Mock**	
Plasmid (ng/6well)	Plasmid name	Description
2000	pcDNA3.1	P_{hCMV}-MCS-pA

HEK-293T cells	**L-TRP Receiver**	
Plasmid (ng/6well)	Plasmid name	Description
400	pMM516	P_{hCMV}-TRT-pA
400	pWB22	P_{TRT}-SEAP-pA
1200	pColaDuet-1	Filler Plasmid
Hana3A cells	**L-TRP Producer**	
Plasmid (ng/6well)	Plasmid name	Description
2000	pWB32	P_{hCMV}-TrpB-pA
Hana3A cells	**Mock**	
Plasmid (ng/6well)	Plasmid name	Description
2000	pcDNA3.1	P_{hCMV}-MCS-pA

Composition Digitization-cells characterisation (Figure 3b)

HEK-293T cells	**Control**	
Plasmid (ng/6well)	Plasmid name	Description
1200	pcDNA3.1	P_{hCMV}-MCS-pA
400	pMM573	P_{hCMV}-mCherry-pA
HEK-293T cells	**-Recombinase**	
Plasmid (ng/6well)	Plasmid name	Description
800	pMM207	P_{hCMV}-B3RT-STOP-B3RT-Citrine-pA
400	pcDNA3.1	P_{hCMV}-MCS-pA
400	pMM573	P_{hCMV}-mCherry-pA
HEK-293T cells	**+Recombinase**	
Plasmid (ng/6well)	Plasmid name	Description
800	pMM207	P_{hCMV}-B3RT-STOP-B3RT-Citrine-pA
400	pMM543	P_{hCMV}-B3-PEST-pA
400	pMM573	P_{hCMV}-mCherry-pA

Composition Digitization-cells characterisation (Figure 3c)

HEK-293T cells		
Plasmid (ng/6well)	Plasmid name	Description
400	pMM207	P_{hCMV}-B3RT-STOP-B3RT-Citrine-pA
0,20,100,200,400,800	pMM543	P_{hCMV}-B3-PEST-pA
800,780,700,600,400,0	pcDNA3.1	P_{hCMV}-MCS-pA
800	pColaDuet-1	Filler Plasmid

Composition Digitization unit with signal amplification characterisation (Figure 4)

HEK-293T cells	**Direct sensing**	
Plasmid (ng/6well)	Plasmid name	Description
800	pWB24	P_{SV40}-TRT-pA
400	pMM206	P_{TRT2}-Citrine-pA
800	pColaDuet-1	Filler Plasmid
HEK-293T cells	**Digitizer without signal amplification**	
Plasmid (ng/6well)	Plasmid name	Description
800	pWB24	P_{SV40}-TRT-pA
400	pMM189	P_{TRT2}-B3-PEST-pA
400	pMM207	P_{hCMV}-B3RT-STOP-B3RT-Citrine-pA
400	pColaDuet-1	Filler Plasmid
HEK-293T cells	**Digitizer with signal amplification**	
Plasmid (ng/6well)	Plasmid name	Description
800	pWB24	P_{SV40}-TRT-pA
400	pMM189	P_{TRT2}-B3-PEST-pA
400	pMM264	P_{hCMV}-B3RT-STOP-B3RT-Ub-tTA-pA
400	pMM265	P_{TRE}-B3RT-STOP-B3RT-Citrine-pA

Composition Receiver-digitization cells with AND-Gate logic (Figure 5,6)

HEK-293T cells		
Plasmid (ng/6well)	Plasmid name	Description
800	pMM195	P_{SV40}-GLP1R-pA
800	pWB24	P_{SV40}-TRT-pA
80	pMM174	P_{CREm}-B3-PEST-pA
80	pMM204	P_{TRT}-B3RT-STOP-B3RT-Ub-tTA-pA
400	pMM265	P_{TRE}-B3RT-STOP-B3RT-Citrine-pA

Composition Receiver-digitization cells with OR-Gate logic (Figure 5,6)

HEK-293T cells		
Plasmid (ng/6well)	Plasmid name	Description
800	pMM195	P_{SV40}-GLP1R-pA
400	pWB24	P_{SV40}-TRT-pA
40	pMM174	P_{CREm}-B3-PEST-pA
400	pMM189	P_{TRT2}-B3-PEST-pA
720	pMM264	P_{hCMV}-B3RT-STOP-B3RT-Ub-tTA-pA
400	pMM265	P_{TRE}-B3RT-STOP-B3RT-Citrine-pA

Composition Receiver-digitization cells with NOR-Gate logic (Figure 5,6)

HEK-293T cells		
Plasmid (ng/6well)	Plasmid name	Description
800	pMM195	P_{SV40}-GLP1R-pA
800	pWB24	P_{SV40}-TRT-pA
80	pMM212	P_{CRE}-B3-PEST-pA
400	pMM189	P_{TRT2}-B3-PEST-pA
80	pMM267	B3RT-P_{SV40}-B3RT-Ub-tTA-B3RT-pA
400	pMM262	B3RT-P_{TRE}-B3RT-Citrine-PEST-B3RT-pA

Composition DI-sensor-sender cells (Figure 6)

Hana3A cells		
Plasmid (ng/6well)	Plasmid name	Description
400	pCI-OR1A1	P_{hCMV}-OR1A1-pA
400	pSP16	P_{CREm}-SEAP-pA
400	pMM222	P_{CRE}-mCherry-pA
400	pMM187	P_{CREm}-GLP-1-Fc_{mIgG}-pA
400	pColaDuet-1	Filler Plasmid

Composition EG-sensor-sender cells (Figure 6)

Hana3A cells		
Plasmid (ng/6well)	Plasmid name	Description
400	pOREG	P_{SV40}-OREG-pA
400	pSP16	P_{CREm}-SEAP-pA
400	pMM223	P_{CREm}-mCherry-pA
400	pMM221	P_{CRE}-TrpB-pA
400	pColaDuet-1	Filler Plasmid

Abbreviations: **B3,** *Zygosaccharomyces bisporus* recombinase; **B3RT,** B3 recombination target site; **cAMP**, cyclic adenosine monophosphate; **Citrine**, improved version of EYFP; **CRE**, cAMP-response element**; Di**,

fragrance dihydrojasmone; **Eg**, fragrance eugenol; **EYFP**, enhanced yellow fluorescent protein; **Fc**, fragment crystallizable region of an antibody that interacts with the Fc cell surface receptors; **Fc_{mIgG}**, mouse IgG-derived Fc linker; **GLP-1**, Glucagon-like peptide 1; **GLP1R**, GLP-1 receptor; **iRFP670**, near-infrared-red fluorescent protein with excitation at 670nm; **mCherry**, *Discosoma*-derived red fluorescent protein; **MCS**, multiple cloning site; **OR**, Odorant receptor; **OR1A1**, dihydrojasmone-responsive human OR; **OR5P3**, cumarin-responsive human OR; **OR129-1**, acetophenone-responsive mouse OR; **OREG**, eugenol-responsive mouse OR; **$(O_{Trp})_2$**, dimeric TrpR-/TRT-specific operator site; **pA**, polyadenylation signal; **P_{CRE}**, synthetic mammalian promoter containing a cAMP-response element (CRE-$P_{hCMVmin}$); **P_{CREm}**, modified P_{CRE}; **PEST**, mouse ornithine decarboxylase-derived peptide sequence rich in proline (P), glutamic acid (E), serine (S) and threonine (T) acting as protein degradation signal; **P_{hCMV}**, human cytomegalovirus immediate early promoter; **$P_{hCMVmin}$**, minimal version of P_{hCMV}; **P_{min}**, synthetic minimal mammalian promoter; **P_{SV40}**, simian virus 40 promoter; **P_{TRE}**, tTA-specific tetracycline-responsive promoter; **P_{TRT}**, TRT-specific L-tryptophan-inducible promoter ($(O_{TRP})_2$-$P_{hCMVmin}$); **P_{TRT2}**, TRT-specific L-tryptophan-inducible promoter ($(O_{Trp})_2$-P_{min}); **SEAP**, human placental secreted alkaline phosphatase; **STOP**, transcriptional STOP cassette consisting of tandem hsp70 and SV40 transcriptional terminators; **SV40**, simian virus 40; **tetR**, *Escherichia.Coli Tn*10-derived tetracycline repressor; **TRE**, tetracycline responsive element; **TrpB**, *Escherichia coli*-derived tryptophan synthase *β*-subunit; **TrpR**, *Chlamydia trachomatis*-derived tryptophan repressor; **TRT**, L-tryptophan-dependent transactivator (TrpR-VP16); **tTA**, tetracycline-dependent transactivator (tetR-VP16); **Ub**, Ubiquitin degradation signal; **VP16**, *Herpes simplex*-derived transactivation domain.

Supplementary Figures

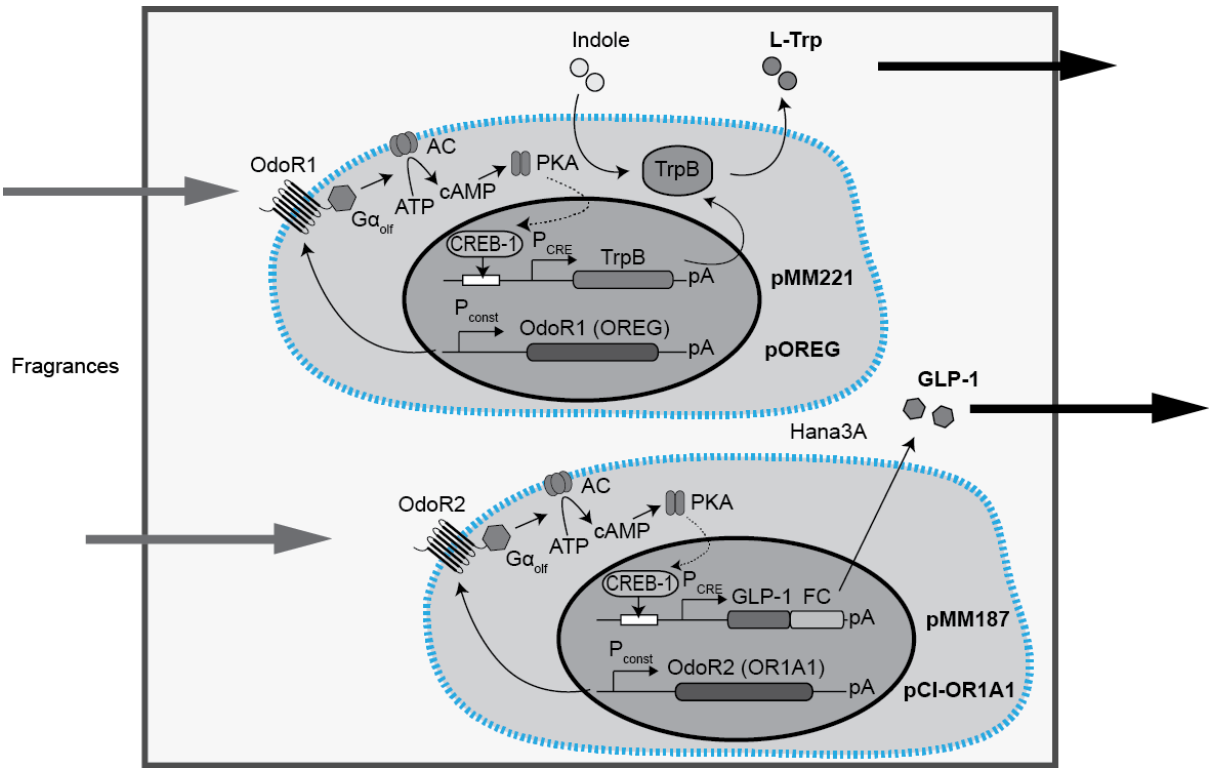

Supplementary Figure 1. Schematic of the sensor-sender cells. Diagram of the sensor-sender cells consisting of a fragrance-sampling and -quantization module and a gas-to-liquid transducer converting gaseous fragrances into secreted L-Tryptophan and GLP-1. The constitutively expressed G protein-coupled odorant receptors (OdoR1/2; e.g., OREG (pOREG) and OR1A1 (pCI-OR1A1)) detect and quantify specific fragrances and activate, via a specific G protein ($G\alpha_{olf}$), the membrane-bound adenylyl cyclase (AC) that converts ATP into the second messenger cyclic AMP (cAMP). The intracellular cAMP surge activates the protein kinase A (PKA), whose regulatory subunits are released and translocate into the nucleus where they phosphorylate and activate the cAMP-responsive element-binding protein 1 (CREB-1). Activated CREB-1 binds to synthetic promoters (P_{CRE}, P_{CREm}) containing cAMP-response elements (CRE) and induces P_{CRE}-driven expression of the tryptophan synthase (TrpB; pMM221) that converts indole into L-Tryptophan or the secreted glucagon-like peptide (GLP-1; pMM187).

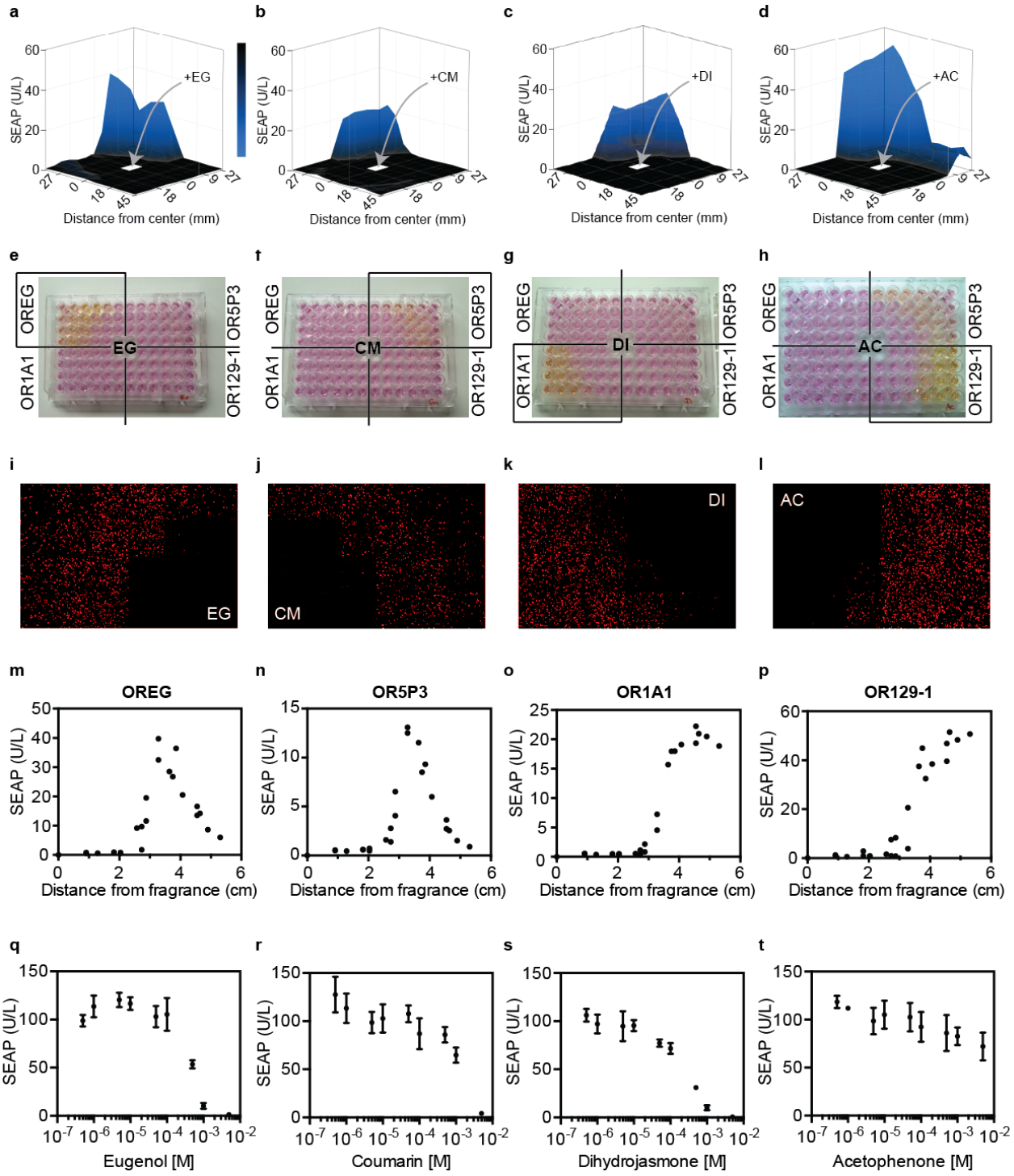

Supplementary Figure 2. Gaseous fragrance-triggered induction of the sampling and quantization module. (a-p) Distance-dependent induction of the sampling and quantization module by different volatile fragrances. Hana3A cells were cotransfected with the odorant receptor-encoding expression vectors pOREG (OREG, 400ng), pCI-OR5P3 (OR5P3, 400ng), pCI-OR1A1 (OR1A1, 400ng) or pCI-MOR129-1 (OR129-1, 100ng) as well as the P_{CREm}-driven SEAP expression vector (pSP16, 400ng) and the P_{CRE}-driven mCherry (pMM222, 400ng) reporter plasmid and seeded into quadrants of 96-well plates. The reprogrammed cells were induced with 10 mM of the corresponding

fragrances eugenol (EG) **(a,e)**, coumarin (CM) **(b,f)**, dihydrojasmone (DI) **(c,g)**, acetophenone (AC) **(d,k)** in the 4 center wells and resulting SEAP levels were quantified (**a-d**) and profiled chromogenically in the culture supernatant 48h after induction (**e-h**; yellow color) to provide a distance-dependent profile of gaseous transgene control. (**i-l**) Corresponding fluorescence micrographs of the respective 96-well plate quadrants of **(a-h)** showing mCherry-specific fluorescence 48h after fragrance exposure. **(m-p)** Resulting SEAP levels were profiled in the culture supernatant 48h after induction and correlated with the distance to the fragrance inducing well (**a-h**). **(q-t)** Cytotoxicity of fragrance compounds. HEK293-T cells were transfected with the constitutive SEAP expression vector pSEAP2-Control (800ng) and exposed to different concentrations of the fragrance compounds eugenol (EG, **q**), coumarin (CM, **r**), dihydrojasmone (DI, **s**), acetophenone (AC, **t**) for 48h before SEAP levels were profiled in the culture supernatant.

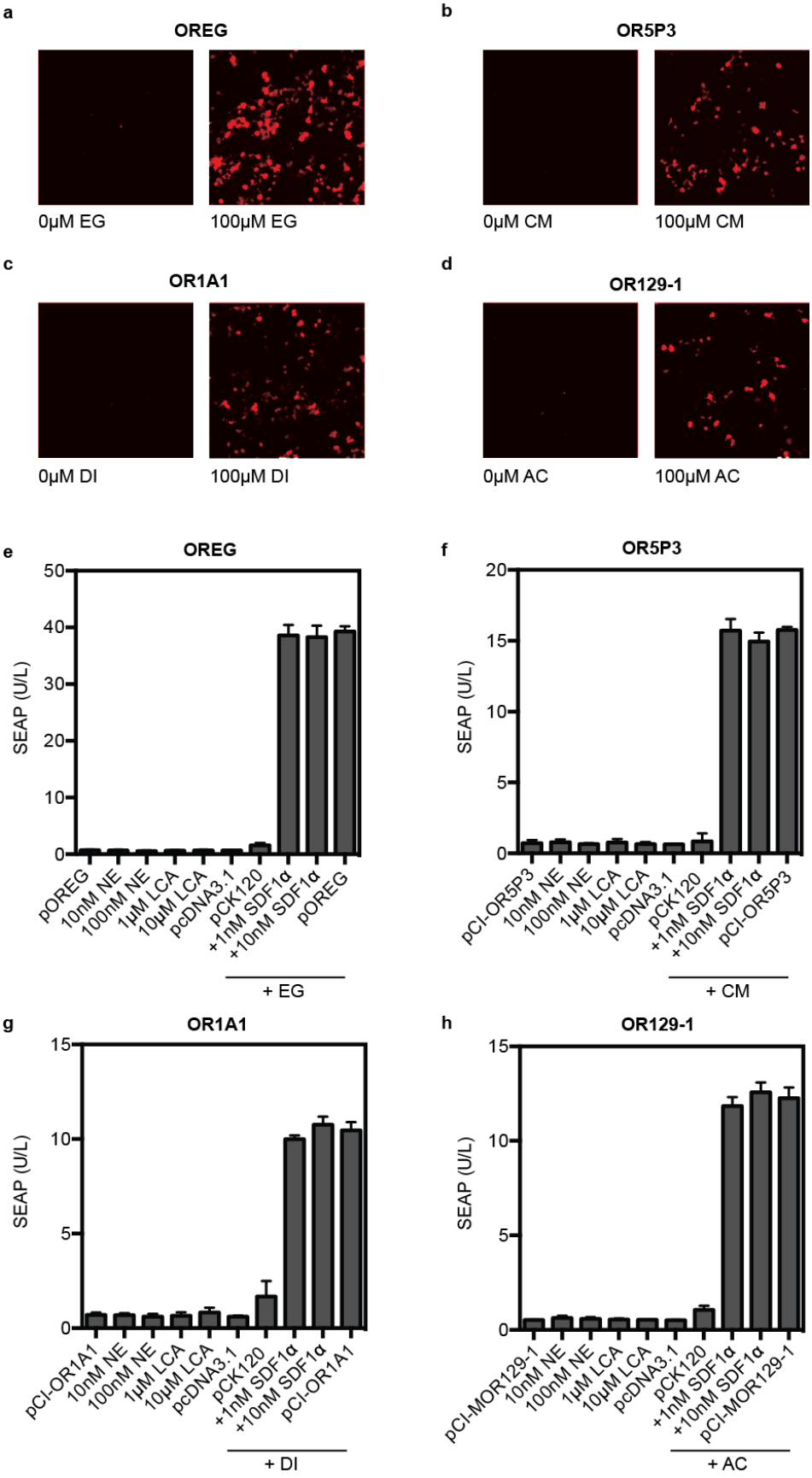

Supplementary Figure 3. Characterization of the sampling and quantization module.

(a-d) Hana3A cells were cotransfected with the odorant receptor-encoding expression vectors **(a)** pOREG (OREG, 400ng), **(b)** pCI-OR5P3 (OR5P3, 400ng), **(c)** pCI-OR1A1 (OR1A1, 400ng) or **(d)**

pCI-MOR129-1 (OR129-1, 100ng) as well as the P_{CREm}-driven SEAP expression vector (pSP16, 400ng) and the P_{CRE}-driven mCherry (pMM222, 400ng) reporter plasmid. The cells were exposed to 0µM and 100µM of the corresponding fragrances (eugenol (EG), coumarin (CM), dihydrojasmone (DI), acetophenone (AC)) and mCherry-fluorescence was profiled after 48h. **(e-h)** HEK-293T expressing endogenous GPCRs such as adrenoceptor alpha 1B (ADRA1B), G protein-coupled bile acid receptor 1 (GPBAR1) and chemokine (C-X-C motif) receptor 4 (CXCR4) which share the same cAMP-based signaling pathway and may therefore in principle interfere with the sampling and quantization module following co-induction by their specific agonists L-norepinephrine, lithocholic acid and stromal cell-derived factor 1 alpha (SDF1α) and the corresponding fragrances, respectively. We have therefore exposed HEK-293T containing the different sampling and quantization modules **(e-h)** to different concentrations of L-norepinephrine (NE; 10nM, 100nM), lithocholic acid (LCA; 1µM, 10µM) or 100µM of the corresponding fragrances (eugenol (EG), coumarin (CM), dihydrojasmone (DI), acetophenone (AC)). To confirm the specificity of the sampling and quantization modules, the corresponding olfactory receptors were replaced by the parental control vector (pcDNA3.1, 400ng) or an unrelated GPCR (pCK120, 400ng, encoding histamine-specific HRH2). SDF1α (1nM, 10nM) was directly added to the inducer fragrances (100µM). SEAP expression levels were recorded 48h after induction.

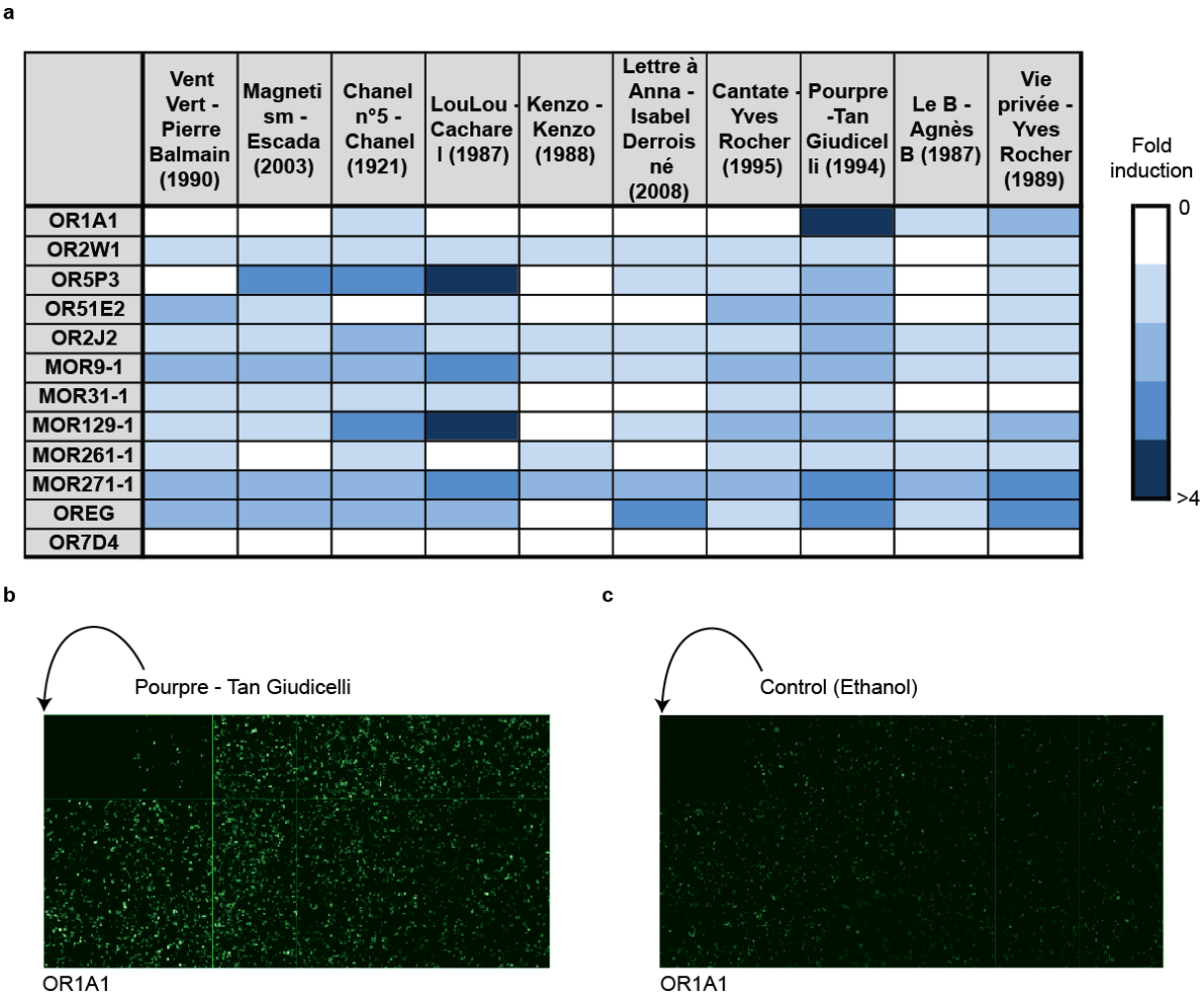

Supplementary Figure 4. Perfume-triggered induction of the sampling and quantization module. **(a)** Profiling of perfume-based gaseous induction of the sampling and quantization module. Hana3A cells were cotransfected with different odorant receptor-encoding expression vectors (pCI-OR1A1, pCI-OR2w1, pCI-OR5P3, pCI-OR51E2, pCI-OR2J2, pCI-MOR9-1, pCI-MOR31-1, pCI-MOR129-1, pCI-MOR261-1, pCI-MOR271-1, pOREG, pOR7D4; 100ng) and the P_{CREm}-driven SEAP reporter plasmid (pSP16, 600ng), seeded into the wells of a 96-well and exposed to different perfume brands (1:3 dilution in DMSO) to enable gaseous fragrance-induced SEAP expression that was profiled after 24h. **(b,c)** Fluorescence micrographs of volatile perfume-based induction of the sampling and quantization module. Hana3A cells were cotransfected with pCI-OR1A1 (400ng) and the P_{CREm}-driven Citrine reporter plasmid (pDA134, 400ng), seeded into the wells of a 96-well plate containing **(b)** a 1:10 dilution of the perfume Pourpre Tan Giudicelli or **(c)** ethanol (negative control) in the top left well and resulting Citrine-based fluorescence was profiled by fluorescence microscopy after 48h.

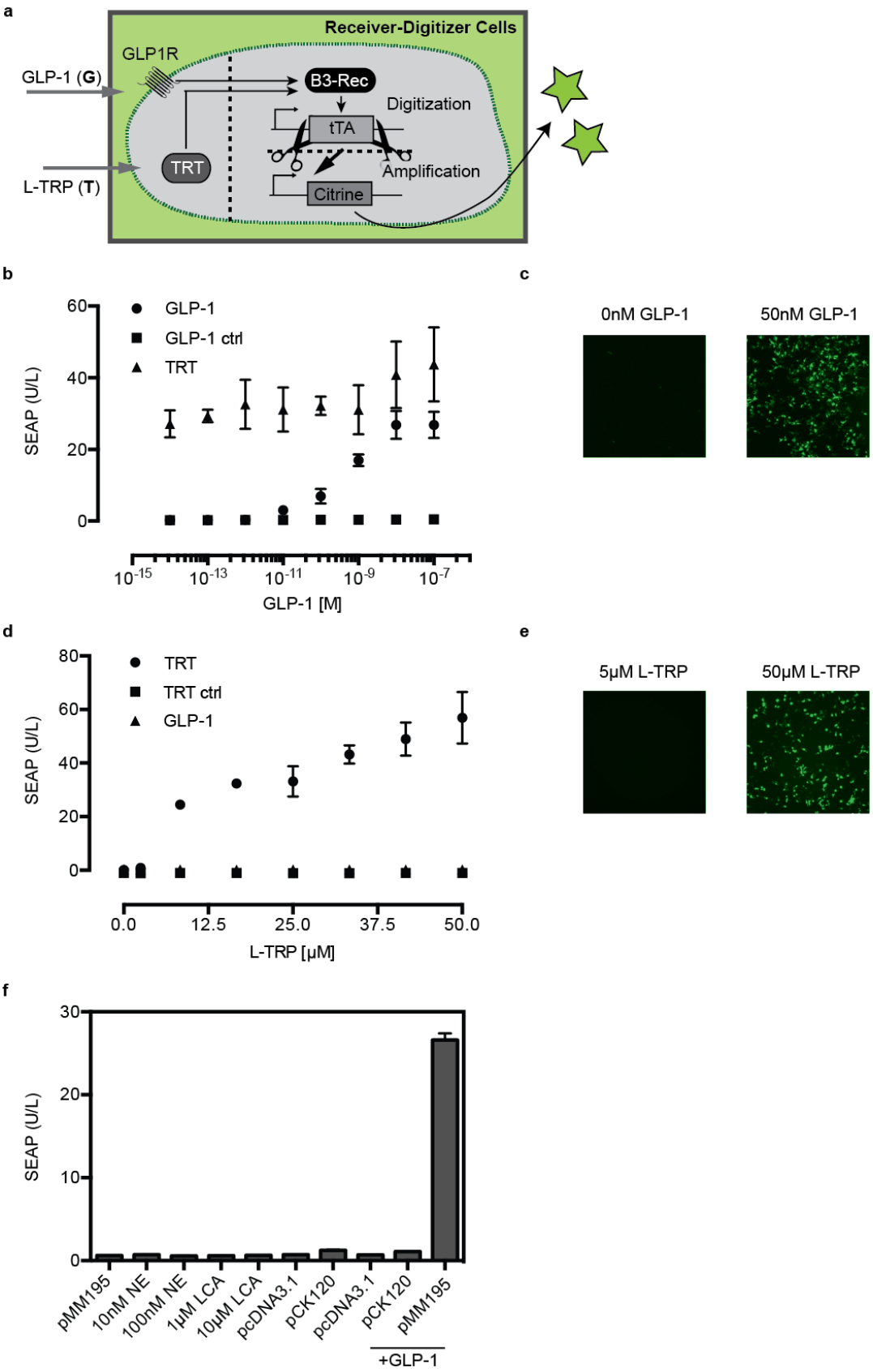

Supplementary Figure 5. Characterisation of the receiver-digitizer cells. (a) Diagram of the receiver-digitizer cells. The signalling compounds GLP-1 (G) and L-Tryptophan (T) broadcast by the sensor-sender cells are detected by the receiver-digitizer cells via specific receptors, the G protein-

coupled receptor GLP1R and the transcription factor TRT, respectively, which trigger expression of the B3 recombinase using distinct downstream pathways. The B3 recombinase manages analog-to-digital conversion and processes the expression of tTA which feed-forward controls and amplifies expression of Citrine. **(b)** Characterisation of the GLP1R component of the digitizer module. HEK-293T cells were cotransfected with the GLP1R-encoding expression vector (pMM195, 800ng) and the specific P_{CREm}-driven SEAP reporter plasmid (pSP16, 400ng) and cultivated for 48h in the presence of different concentrations of GLP-1 before SEAP levels were quantified in the culture supernatant. HEK-293T cells cotransfected with the unrelated olfactory receptor OREG (pOREG, 400ng) and pSP16 (400ng) were used as negative control (GLP-1 ctrl). Likewise, HEK-293T cotransfected with the constitutive TRT expression vector (pMM516, 400ng) and P_{TRT}-driven SEAP expression plasmid (pWB22, 400ng) was used as specificity control (TRT). **(c)** Fluorescence micrographs of GLP-1-responsive gene expression in receiver-digitizer cells. HEK-293T cells were cotransfected with the GLP1R-encoding expression vector (pMM195, 800ng) and the specific P_{CREm}-driven Citrine reporter plasmid (pDA134, 400ng) and cultivated for 48h in the presence (50nM) or absence of GLP-1 before Citrine fluorescence was recorded by fluorescence microscopy. **(d)** Characterisation of the TRT component of the digitizer module. HEK-293T cells were cotransfected with the constitutive TRT expression vector (pMM516, 400ng) and the P_{TRT}-driven SEAP expression plasmid (pWB22, 400ng) and cultivated for 48h in the presence of different concentrations of L-Tryptophan before SEAP levels were quantified in the culture supernatant. HEK-293T cells cotransfected with the unrelated transcription factor tTA (pMM506, 400ng) and pWB22 (400ng) were used as negative control (TRT ctrl). Likewise, cotransfected with the constitutive GLP1R expression vector (pMM195, 800ng) and P_{TRT}-driven SEAP expression plasmid (pWB22, 400ng) and the P_{CREm}-inducible SEAP reporter plasmid (pSP16, 400ng) was used as specificity control (GLP-1). **(e)** Fluorescence micrographs of L-Tryptophan-responsive gene expression in receiver-digitizer cells. HEK-293T cells were cotransfected with the TRT-encoding expression vector (pMM516, 400ng) and the specific P_{TRT}-driven Citrine reporter plasmid (pMM206, 400ng) and cultivated for 48h in the presence (50µM) or absence of L-Tryptophan before Citrine fluorescence was recorded by fluorescence microscopy. **(f)** GLP1R specificity of receiver-digitizer cells. HEK-293T were cotransfected with the GLP1R-encoding expression vector (pMM195, 800ng) and the specific P_{CREm}-driven SEAP reporter plasmid (pSP16, 400ng) and exposed to either L-norepinephrine (NE; 10nM, 100nM), lithocholic Acid (LCA; 1µM, 10µM) or GLP-1 (50nM) for 48h before SEAP levels were profiled in the culture supernatant. To confirm the specificity of the receiver-digitizer cells, the GLP1R expression vector was either replaced by the parental control vector (pcDNA3.1, 400ng) or an unrelated GPCR (pCK120, 400ng, encoding histamine-specific HRH2).

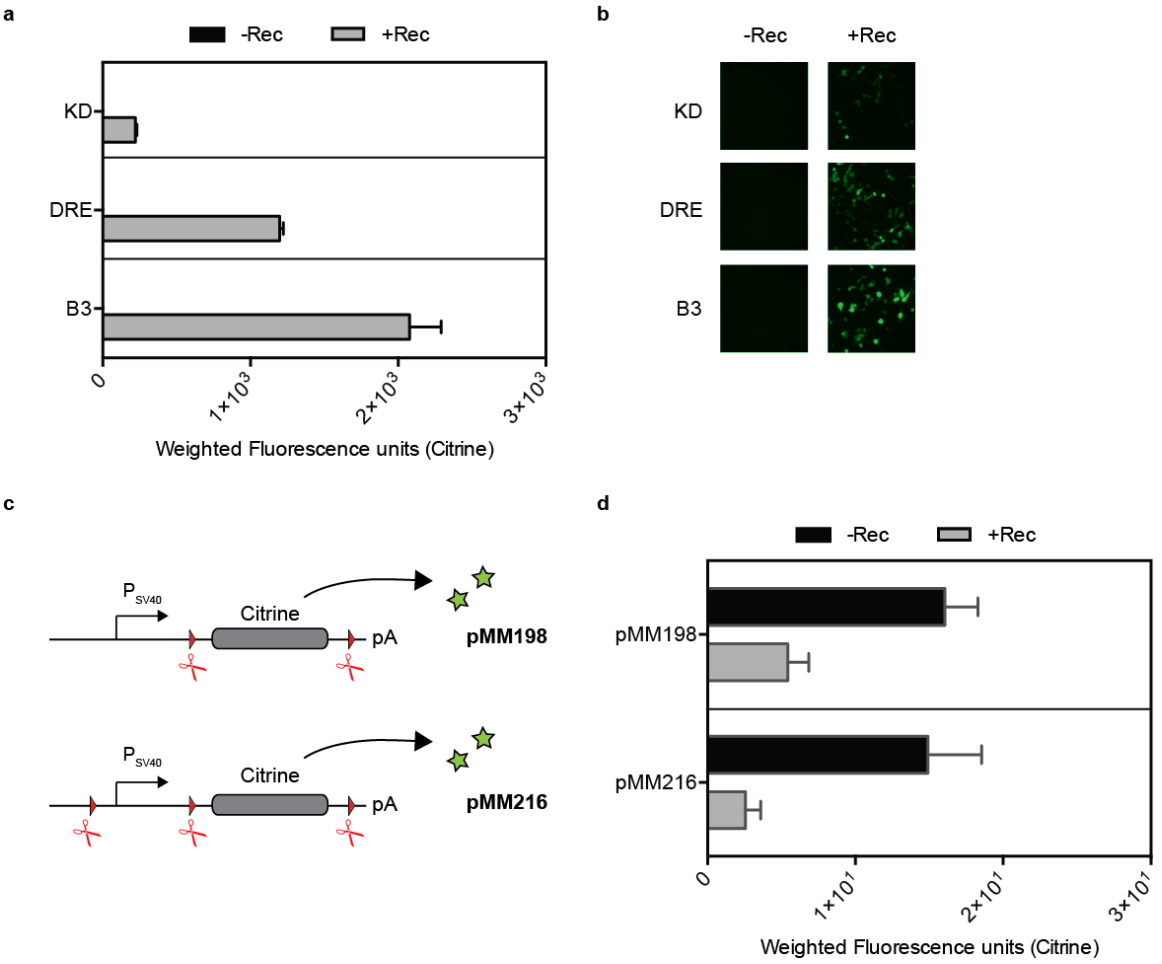

Supplementary Figure 6. Optimization of the digitization unit. (a,b) Performance analysis of different recombinases. HEK-293T cells were cotransfected with either of the recombinase-encoding expression vectors pMM544 (KD, 400ng), pMM581 (DRE, 400ng), pMM543 (B3, 400ng), or pcDNA3.1(+) (-Rec, 400ng) as well as the corresponding reporter construct containing the Citrine gene flanked by the specific recombinase target sites (KD, pMM208, 400ng; DRE, pMM251, 400ng; B3, pMM207, 400ng). Resulting Citrine expression levels were profiled by FACS analysis (**a**) as well as fluorescence microscopy (**b**) 48h after cotransfection. (**c,d**) Optimization of the B3-specific reporter plasmid. Whereas pMM198 contains two B3-specific target sites flanking the Citrine gene, pMM216 harbors a third B3-specific target site 5' of the constitutive promoter P_{SV40}. (**d**) Comparative performance analysis of the B3-specific reporter constructs pMM198 and pMM216. HEK-293T cells were cotransfected with either the B3 recombinase-encoding expression vector (+Rec; pMM543, 400ng) or the negative parental control vector pcDNA3.1(+) (-Rec; pcDNA3.1(+), 400ng) and either of the Citrine-encoding reporter plasmids pMM198 (400ng) or pMM216 (400ng). Resulting Citrine expression levels were profiled by FACS analysis 48h after cotransfection.

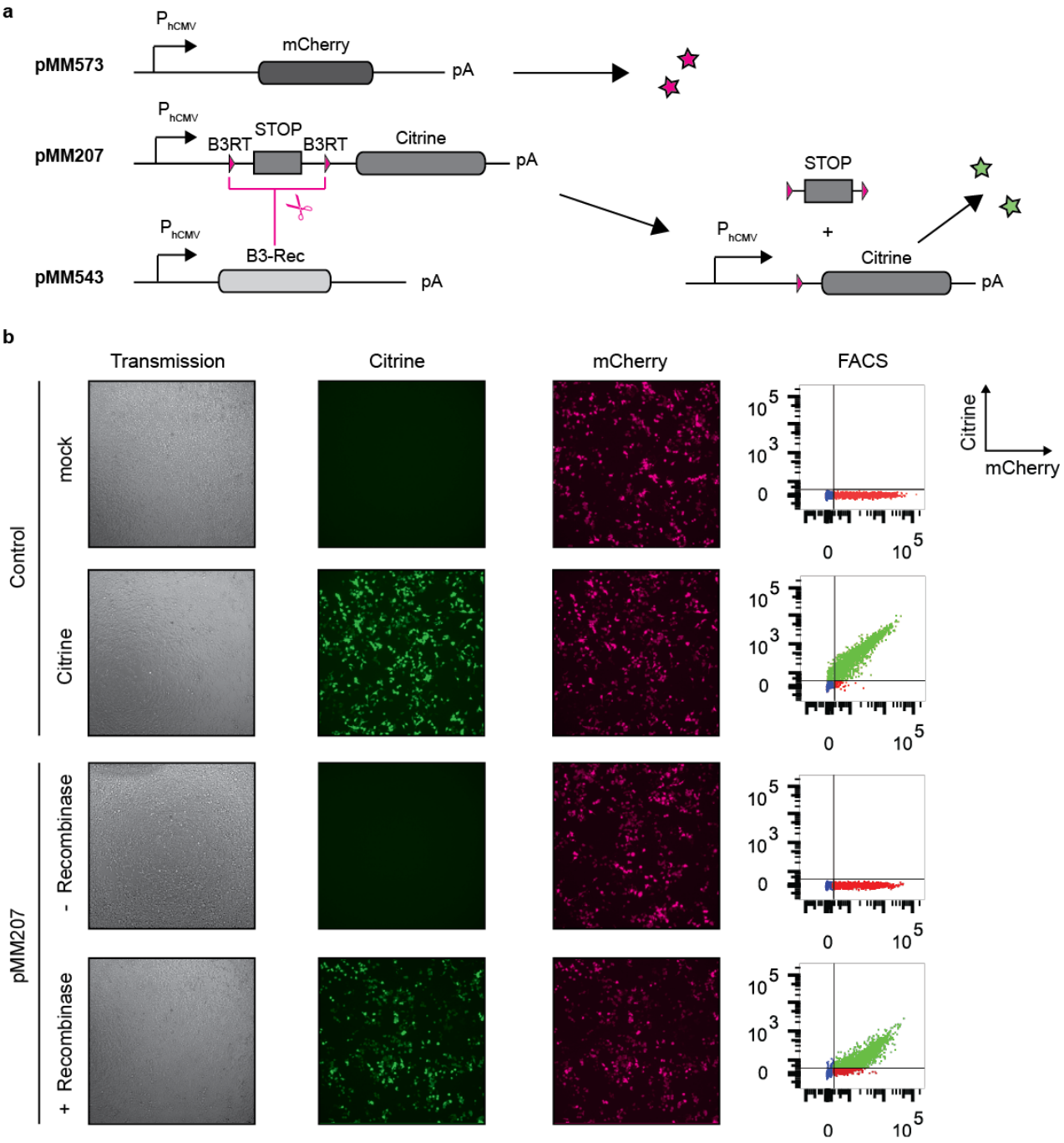
a
pMM573
P hCMV
mCherry
pA
pMM207
P hCMV
B3RT
STOP
B3RT
Citrine
pA
pMM543
P hCMV
B3-Rec
pA
STOP
P hCMV
+
Citrine
pA
b
Transmission
Citrine
mCherry
FACS
Control
mock
Citrine
pMM207
- Recombinase
+ Recombinase
Citrine
mCherry
10 5
10 3
0
0
10 5

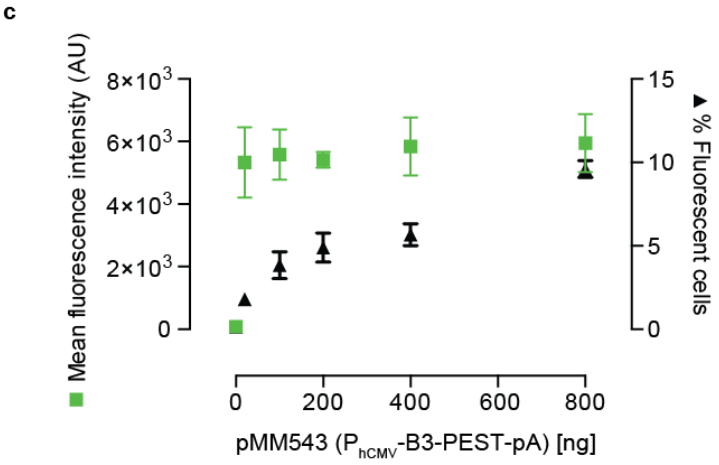
c
Mean fluorescence intensity (AU)
8×10 3
6×10 3
4×10 3
2×10 3
0
15
10
5
0
▲ % Fluorescent cells
0
200
400
600
800
pMM543 (P hCMV-B3-PEST-pA) [ng]

Supplementary Figure 7. Characterisation of the recombinase-based digitization module. a Genetic switchboard of the recombinase-based digitization module. Constitutively expressed B3 recombinase (pMM543, P_{hCMV}-B3-PEST-pA) efficiently excises a transcriptional stop cassette (STOP) flanked by the B3 recombination target sites (B3RT, red triangles) from a constitutive expression unit thereby inducing expression of the reporter protein Citrine (pMM207, P_{hCMV}-B3RT-STOP-B3RT-Citrine-pA). Constitutive expression of reporter protein mCherry (pMM573, P_{hCMV}-mCherry-pA) in the same cell is used as a negative control. **b** Basic validation of the digitization module. HEK-293T cells were cotransfected with vectors encoding the digitization unit along with the internal mCherry control (+Recombinase; pMM543, 400ng; pMM207, 800ng; pMM573; 400ng), the recombinase-free digitization unit (-Recombinase; pcDNA3.1, 400ng; pMM207, 800ng; pMM573, 400ng) or the negative (Mock; pcDNA3.1, 800ng; pMM543, 400ng; pMM573, 400ng) and positive (Citrine; pMM545, 800ng; pMM543, 400ng; pMM573, 400ng) control vectors and Citrine as well as mCherry fluorescence was visualized by fluorescence microscopy or profiled by FACS analysis (Citrine filter set vs. mCherry filter set). By normalizing the percentage of citrine-positive cells (+Recombinase; 10.7% ±0.4) to the constitutive citrine reference (Control+; 16.0% ±0.2), the B3 recombinase efficacy was calculated to be 67.0% ±3.3. **c** B3 recombinase-mediated digitization. HEK-293T cells were cotransfected with components of the digitization unit including various amounts of the B3 recombinase expression vector (pMM543, P_{hCMV}-B3-PEST-pA, 0-800ng) and a Citrine-expression vector containing a B3-excisable STOP cassette (pMM207, P_{hCMV}-B3RT-STOP-B3RT-Citrine-pA, 400ng). The resulting mean fluorescence intensity and percentage of Citrine-positive cells were profiled after 48 h by FACS analysis.

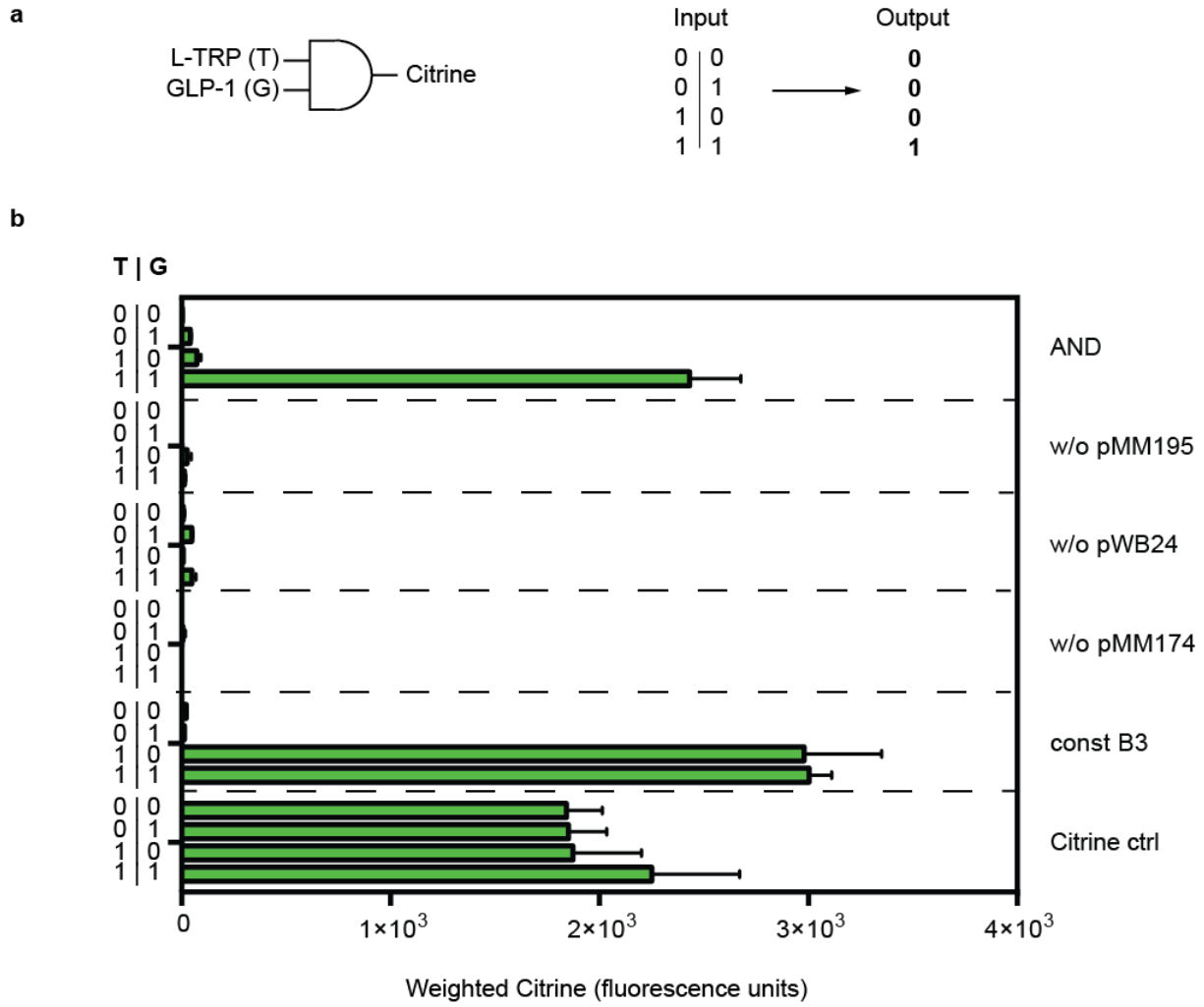

Supplementary Figure 8. Digital AND-gate expression logic by receiver-digitizer cells. (a) The combination of the two input signals L-TRP (T) and GLP-1 (G) according to the truth table programs digital AND-gate expression by receiver-digitizer cells: Citrine expression is exclusively switched ON in the presence of both input signals L-TRP and GLP-1. **(b)** Input-programmable AND-gate expression logic by receiver-digitizer cells. HEK-293T cells were cotransfected with all components of the digital AND-gate (AND; Supplementary Table 3). Control configurations had either individual components removed (w/o), included constitutive expression of the B3 recombinase (const B3) or had the P_{TRE}-driven Citrine expression vector pMM265 replaced by the constitutive Citrine expression vector pMM545 (P_{hCMV}-Citrine-pA; Citrine ctrl). While removal of either GLP1R (w/o pMM195), TRT (w/o pWB24) and P_{CRE}-inducible B3 recombinase (w/o pMM174) expression vectors abolished AND-gate control of Citrine, constitutive coexpression of B3 recombinase mediated L-Tryptophan-triggered Citrine expression independent of the presence or absence of GLP-1. Weighted Citrine fluorescence was scored after 48h by FACS analysis.

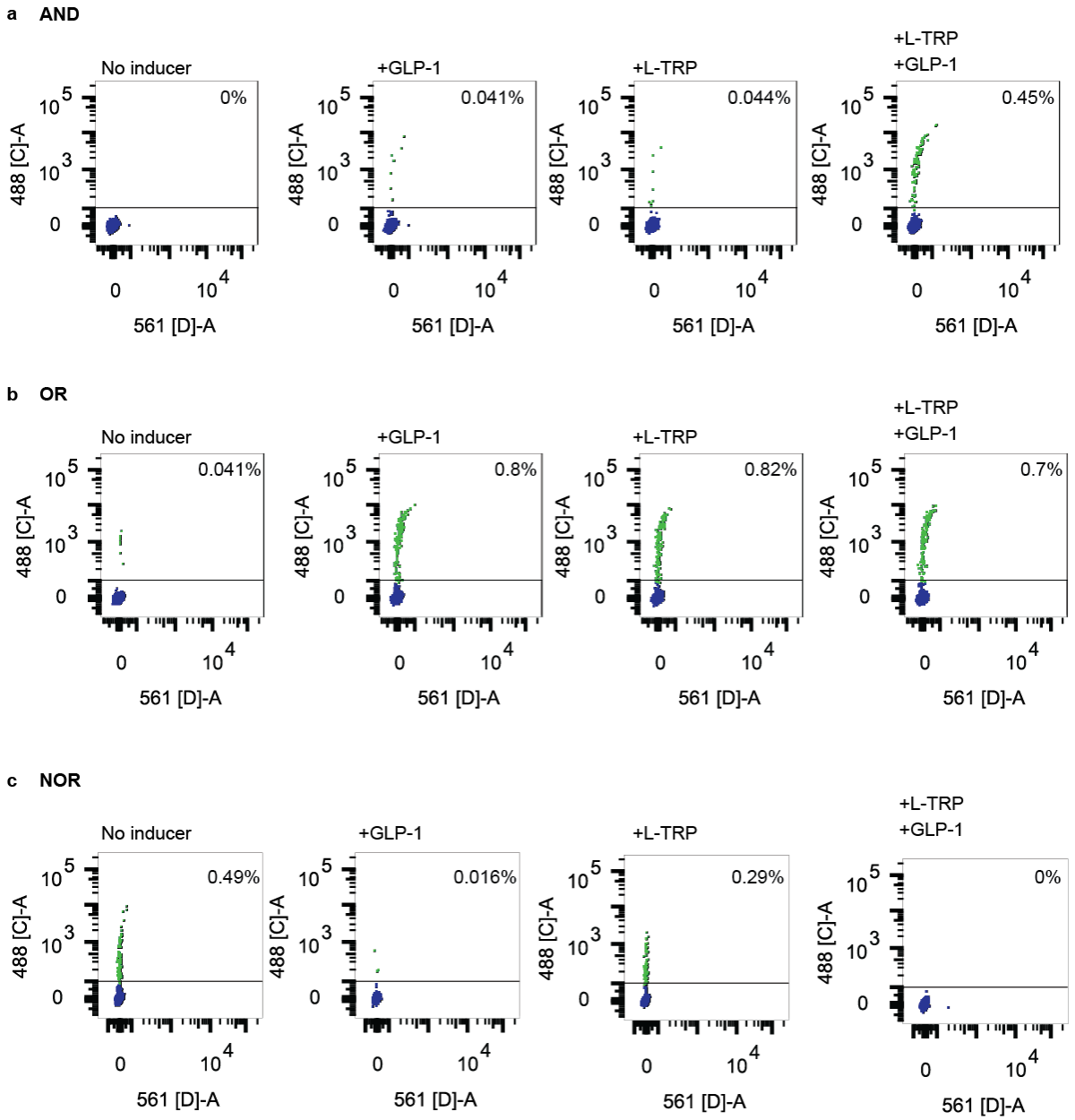

Supplementary Figure 9. Raw flow cytometry data of receiver-digitizer cells processing logic gates. Receiver-digitizer cells transfected with AND- **(a)**, OR- **(b)** and NOR- **(c)** gate components (Supplementary Table 3) were exposed to L-TRP and/or GLP-1 and resulting Citrine fluorescence was analysed by FACS after 48h.

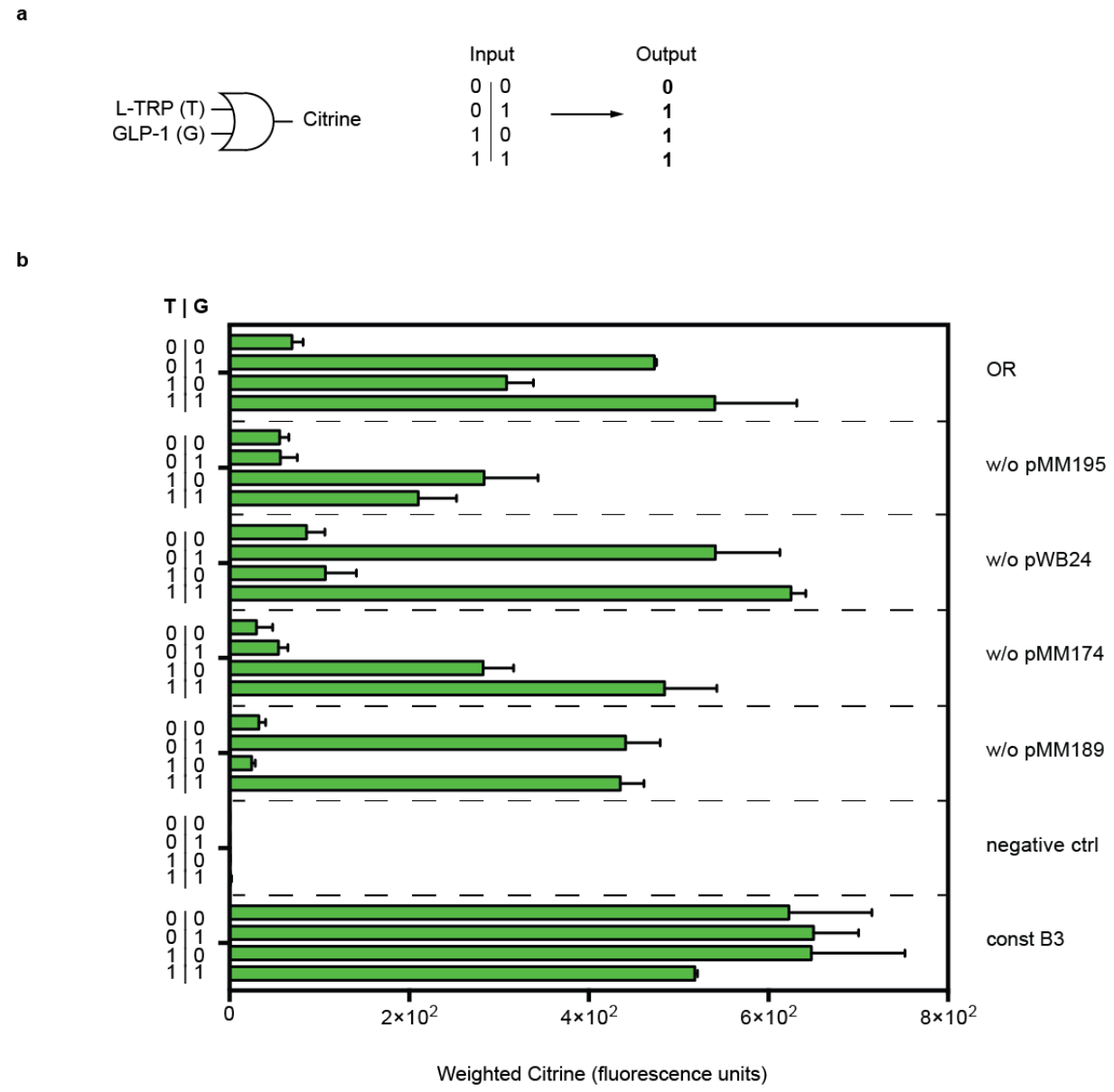

Supplementary Figure 10. Digital OR-gate expression logic by receiver-digitizer cells. (a) The combination of the two input signals L-TRP (T) and GLP-1 (G) according to the truth table, programs digital OR-gate expression by receiver-digitizer cells: Citrine expression is switched ON in the presence of either input signals L-TRP or GLP-1 or both input signals. **(b)** Input-programmable OR-gate expression logic by receiver-digitizer cells. HEK-293T cells were cotransfected with all components of the digital OR-gate (OR; Supplementary Table 3). Control configurations had either individual components removed (w/o), included constitutive expression of the B3 recombinase (const B3) or were based on exclusive transfection of the P_{TRE}-driven Citrine expression vector pMM265 (P_{TRE}-B3RT-STOP-B3RT-Citrine-pA; negative ctrl). While removal of GLP1R (w/o pMM195), TRT (w/o pWB24), P_{CREm}-inducible B3 recombinase (w/o pMM174) or P_{TRT}-driven B3 recombinase (w/o pMM189) expression vectors abolished OR-gate control of Citrine, cotransfection of constitutive B3

recombinase mediated Citrine expression for all combinations of L-tryptophan and GLP-1. Weighted Citrine fluorescence was scored after 48h via FACS analysis.

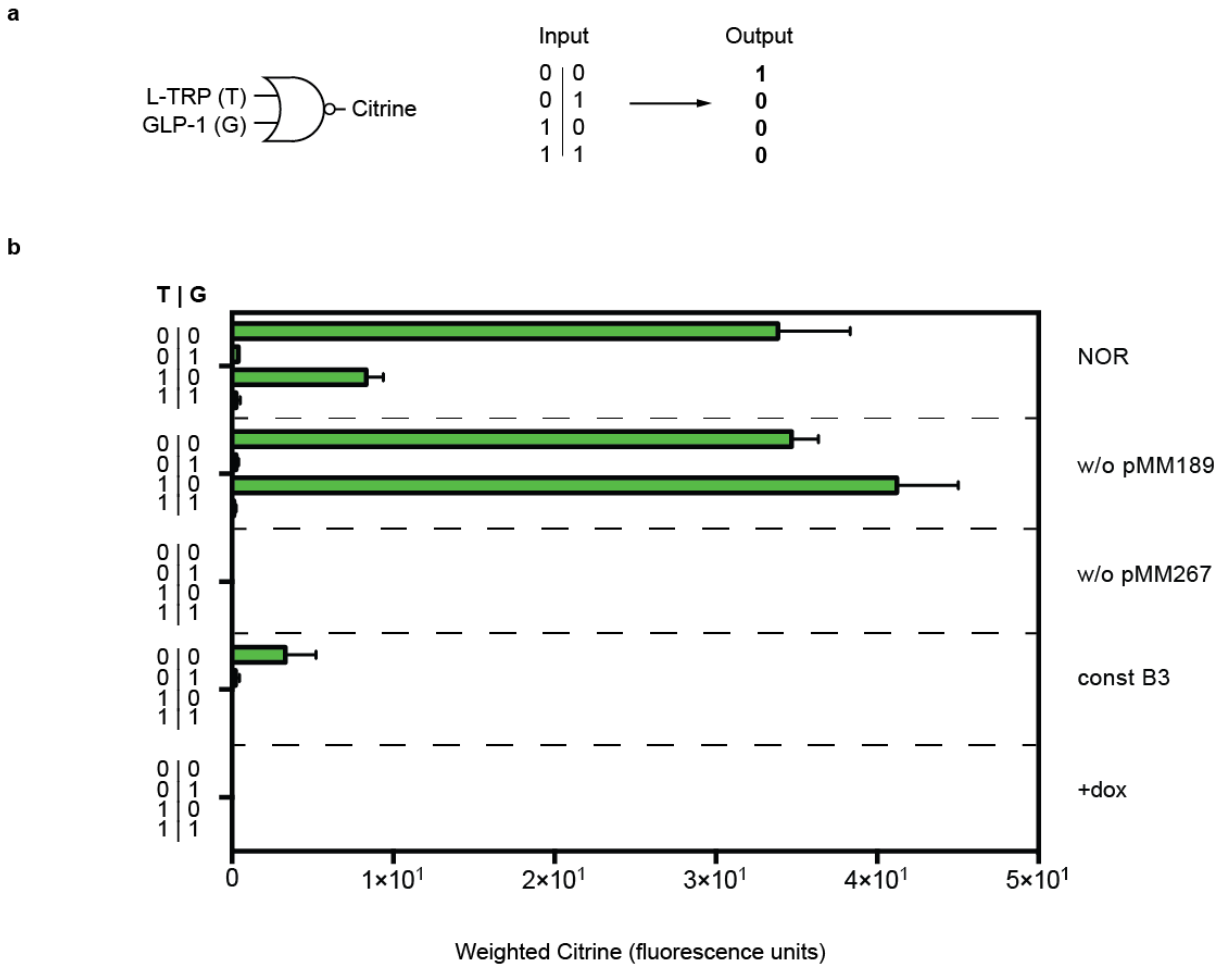

Supplementary Figure 11. Digital NOR-gate expression logic by receiver-digitizer cells. (a) The combination of the two input signals L-TRP (T) and GLP-1 (G) according to the truth table, programs digital NOR-gate expression by receiver-digitizer cells: Citrine expression is switched ON in the presence of neither input signals L-TRP nor GLP-1. **(b)** Input-programmable NOR-gate expression logic by receiver-digitizer cells. HEK-293T cells were cotransfected with all components of the digital NOR gate (NOR; Supplementary Table 3). Control configurations had either individual components removed (w/o) such as the P_{TRT}-driven B3 recombinase expression vector (w/o pMM189) or the signal amplification plasmid pMM267 (w/o pMM267), included constitutive expression of the B3 recombinase (const B3) or exposure to doxycycline, all of which abolished NOR-gate control. Weighted Citrine fluorescence was scored after 48h via FACS analysis.

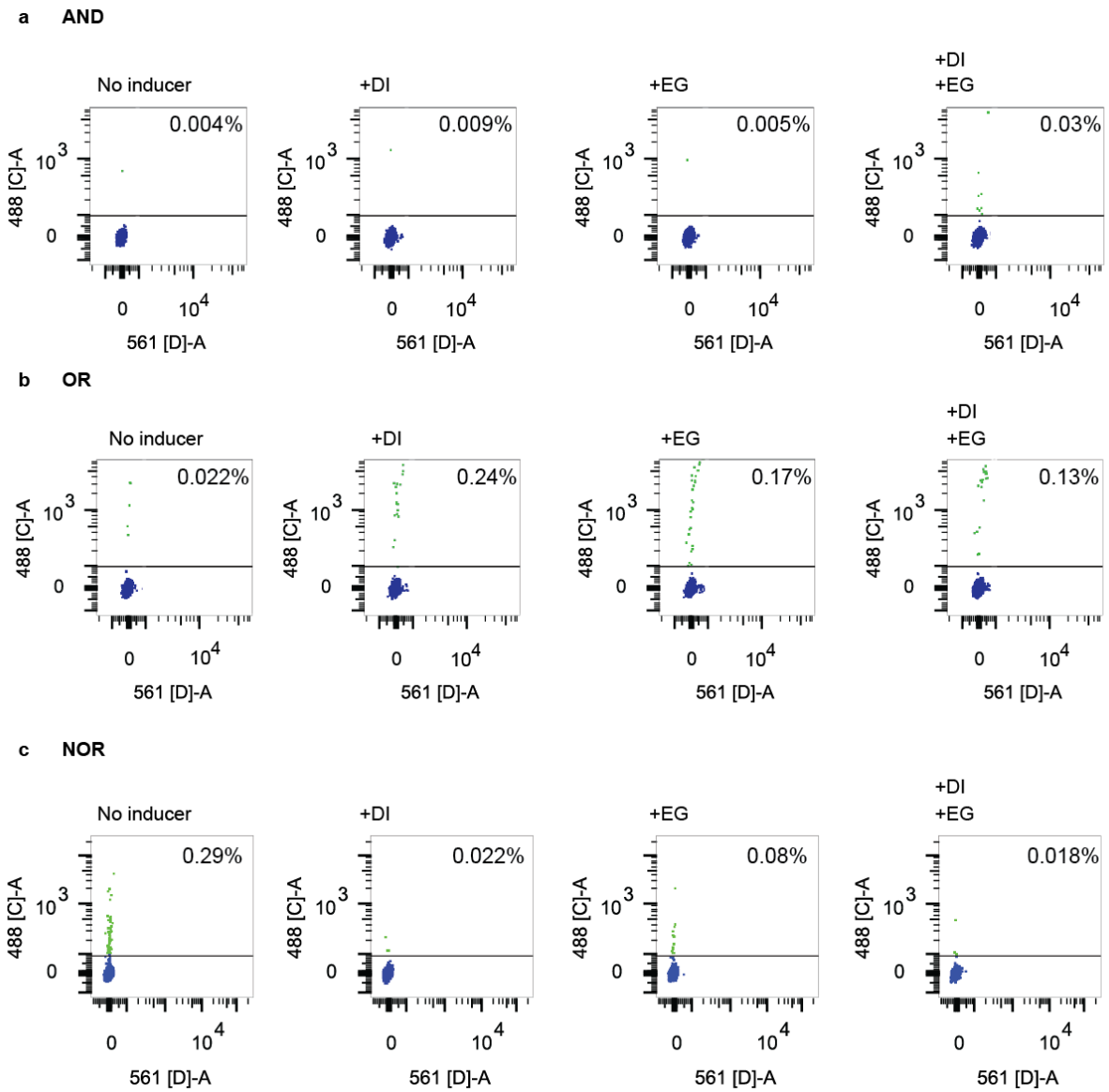

Supplementary Figure 12. Raw flow cytometry data of the fragrance-programmable analog-to-digital converter controlling Boolean expression logic (a-c) Sensor-sender cells and receiver-digitizer cell populations containing the fragrance-programmable analog-to-digital converter components (Supplementary Table 3) were exposed 10mM of the volatile fragrances dihydrojasmone (DI) and/or eugenol (EG) and the digital AND- **(a)**, OR- **(b)** and NOR- **(c)** expression of Citrine by the receiver-digitizer cells was analysed by FACS after 72h.

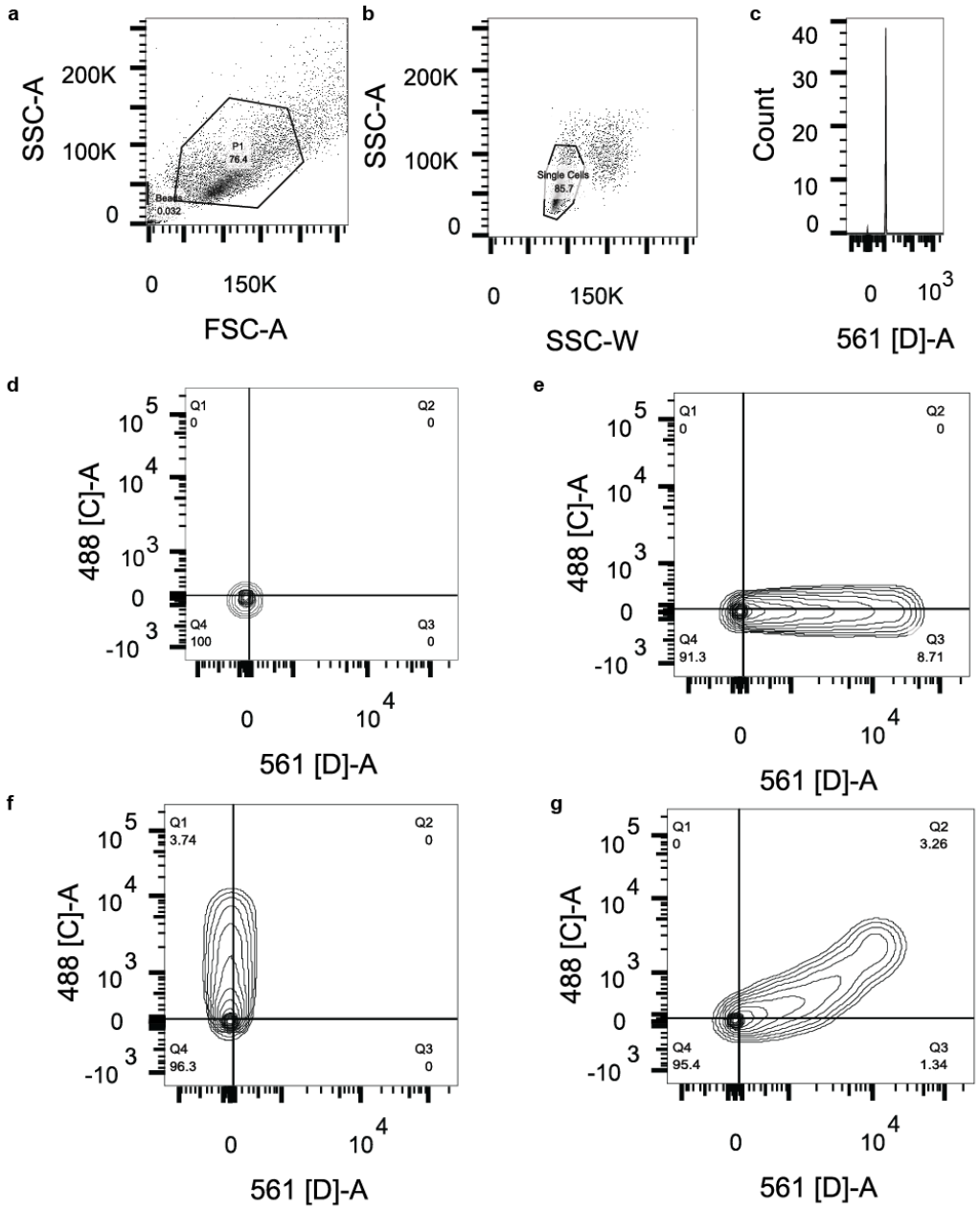

Supplementary Figure 13. FACS gating. (a) Representative gating for viable HEK-293T cells via side scatter-area (SSC-A) and front scatter-area (FSC-A) resulting in population P1. Internal control beads were also gated by size. **(b)** Viable cells in gate P1 were gated to exclude cell doublets via side scatter-area (SSC-A) and side scatter-width (SSC-W). This results in population P2 consisting of viable single cells. **(c)** Representative fluorescence histogram of gated beads (561nm filter sets). **(d)** Fluorescence of mock (pcDNA3.1) -transfected cells inside gate P2 shown for Citrine- (488nm) and mCherry- (561nm) filter sets and within respective quadrants. **(e)** Fluorescence of mCherry (pMM573) -transfected cells inside gate P2 shown for Citrine- (488nm) and mCherry- (561nm) filter sets and within respective quadrants. **(f)** Fluorescence of Citrine (pMM545) -transfected cells inside Gate P2 shown for Citrine- (488nm) and mCherry- (561nm) filter sets and within respective quadrants. **(g)** Fluorescence of Citrine- (pMM545) and mCherry (pMM573)-cotransfected cells inside gate P2 shown

for Citrine- (488nm) and mCherry- (561nm) filter sets and within respective quadrants. Cells were analysed by flow cytometry 48h after transfection.

CHAPTER IV

A cell-communication-based human tissue oscillator

Marius Müller, Jörg Stelling, Martin Fussenegger *et al.*

in preparation

Abstract

Biological timekeepers are of major importance for human physiological mechanisms and metabolism, on defined temporal scales ranging from short-term oscillations such as the daily circadian clock to long-term oscillations such as hormone secretion or hibernation. An important ability in natural pacemakers is the tight and cell-wide interconnection. However, its synthetic counterparts engineered in mammalian cells, still lack this feature.

Here we present a cell-communication-based mammalian tissue oscillator that is uncoupled from the circadian clock. This synthetic oscillator is based on a multicellular interplay of fine-tuned producer, degrader and reporter cell populations, which rely on the interconversion of the joint metabolite L-Tryptophan, serving at the same time as a cell-to-cell signalling molecule transmitting information about the oscillatory phase. Combining transcriptional and translational control modules to achieve inter- and extracellular time-delayed negative feedback circuits together with a microfluidic tissue perfusion system enabled oscillatory patterns in entire tissues. Computational modelling along with experimental analysis of the system allowed for stepwise design optimization and reliable prediction of the oscillatory space.

This artificial dynamic system paves the way for insights into rhythmic expression networks in mammalian cells and provides a basis for future design principles. Application of this strategy to cell therapies based on cell implants or tissue engineering could enable periodic protein expression such as insulin.

Introduction

Natural oscillators -conserved throughout all kingdoms of life, from cyanobacteria over plants to humans- are of importance for orchestrating physiological and metabolic processes such as hormone secretion to circadian gene expression governing the day-night rhythm. An important feature of these biological pacemakers is the ability to synchronize amongst cells and tissues, where the suprachiasmatic nucleus in mammalian brains is the central organ remote controlling peripheral cells.

Although this robust and tuneable clock is capable of integrating and adapting environmental influences such as temperature and light[1-4], asynchrony or malfunction in the oscillatory system can lead to severe pathological states including obesity and diabetes[5,6], as well as epileptic seizures and neuronal diseases such as Alzheimer and Parkinson[7-9]. Synthetic counterparts that mimic and model this complex dynamic behaviour provide valuable insights into how these cellular clocks operate: first success started in the last decade with the *de novo* implementation of a synthetic toggle switch[10] and the daisy-chain repressilator[11] in prokaryotes, both accompanied with descriptive models that initialised the synergy between systems and synthetic biology. This resulted in more robust and tuneable time-keepers on the single cell level[12] to eventually first artificial oscillators in mammalian cells[13,14], which relied on the implementation of negative feedback loops of transcription- and translation-based synthetic modules. However, these genetic clocks behaved asynchronous on a population-scale due to the lack of successful cell-cell coupling. In bacteria, this could be achieved by linking to an external entrainment source[15] or an autonomous common quorum[16], which resulted in synchronized oscillatory dynamics on a population-wide scale.

Multicellular interconnected synthetic networks –similar to cellular consortia that occur in nature– have enabled researchers to increase the complexity of designer topologies[17-19] as well as to allow for spatial-temporal expression as seen for various pattern formations[20], edge detection[21], logic gates[22,23], interkingdom transmission systems[24] and mammalian two-way communication systems[18,25]. The later relies on the common metabolite and essential amino acid L-Tryptophan, which could be interconverted by a

producer cell line from its precursor indole via the tryptophan-synthase TrpB and sensed by another receiver cell line -via the bacterial transcription factor TrpR- that could translate the tryptophan-concentration in the environment to desired gene expression.
In this study, we present a synthetic mammalian oscillator in a multipopulation tissue, uncoupled from the circadian clock, based on the joint metabolite L-Tryptophan. This was achieved by the implementation of a fast fluorescent timer, cell-cell communication, artificial 3D-microtissue technologies with a corresponding microfluidic perfusion system and an adjacent descriptive mathematical model. Apart from giving valuable insights into the field of biological clocks, this rhythmic gene expression could be applied for therapeutic proteins such as cortisone or insulin.

Oscillator design and cell populations assembly

In our synthetic tissue oscillator, dynamic gene expression depends on the reversible, circled interconversion of the shared pool of the metabolites indole (Ind) and L–Tryptophan (Trp) named synthetic metabolic circle. The core oscillator unit (Fig. 1a) consists of three distinct engineered mammalian HEK-293T cell populations, regulated by the common metabolite Trp: (i) the producer population (P) converts Ind to Trp at low Trp concentrations, (ii) the degrader population (D) counteracts the producer by converting Trp back to Ind at high levels of Trp, and (iii) the fluorescent reporter population (R) that directly allows for dynamic and real-time-quantification of tryptophan.
Oscillations occur due to the impairing time-delayed cyclic negative-feedback loop circuits of the producer and degrader populations: the producer OFF-Type regulation relies on the tryptophan-dependent transactivator TRT combined with a negative inverter-circuit, that converts an enhancing signal (Trp) to a repressing output (TrpB). This was achieved by the RNA-binding protein L7Ae[26], which inhibits translation upon binding. This composition resulted in an inverted tryptophan-inducible transgene expression profile (ON for low tryptophan concentrations, OFF for high levels), which was illustrated via the secreted reporter SEAP (Fig. S1a,b). In the final setup, the SEAP

cassette is replaced by the β-subunit of the Tryptophan-Synthase TrpB from *Escherichia coli* converting Ind to Trp (Fig. 1a; Producer (P)).

In contrast, the degrader population shows induction of gene expression exclusively for high levels of tryptophan (Fig. S1c,d). To achieve high degrader expression levels, the L-tryptophan-dependent transactivator TRT was combined with an amplification-cascade using the orthologous tetracycline-responsive system[27]. Subsequent promoter-optimization (Fig. S1e) lead to the low-leakiness high-induction degrader cell population (Fig. S1f). The negative feedback loop results from the expression of the Tryptophanase enzyme TnaA (also from *E. coli*) that hydrolyses Trp back to Ind, thereby closing the synthetic metabolic circle (Fig. 1a; Degrader (D)).

The reporter cell population harbours the TRT that –dependent on tryptophan– directly drives the expression of the reporter -illustrated by the SEAP reporter (Fig. S2a,b). To visualize the dynamic interconversion, a monomeric fast-maturing blue-to-red-fluorescent-timer is used as readout, which upon folding exhibits characteristics (excitation and emission) of a blue fluorescent protein (unmaturated variant). As the chromophore centre undergoes maturation due to oxidation, the fluorescent protein characteristics change over time to those of a red fluorescent protein (maturated variant). Therefore, blue-to-red-transition is independent of the cellular degradation machinery[28]. Reversibility analysis revealed superior characteristics of the fluorescent timer compared to PEST-destabilized GFP (Fig. S2c) and Ubiquitin-destabilized GFP (Fig. S2d), and was therefore chosen as the ideal reporter for the dynamic system (Fig. S2e; Fig. 1a; Reporter (R)).

To achieve high spatial cell density, shown to be crucial for rapid and robust cellular coupling (evaluated via the deterministic model and from literature[29]), the different cellular populations constituting the oscillator were clustered to synthetic 3D-microtissues by gravity-enforced cell assembly[30] (Fig. 1b, Supplementary Movie1).

a)

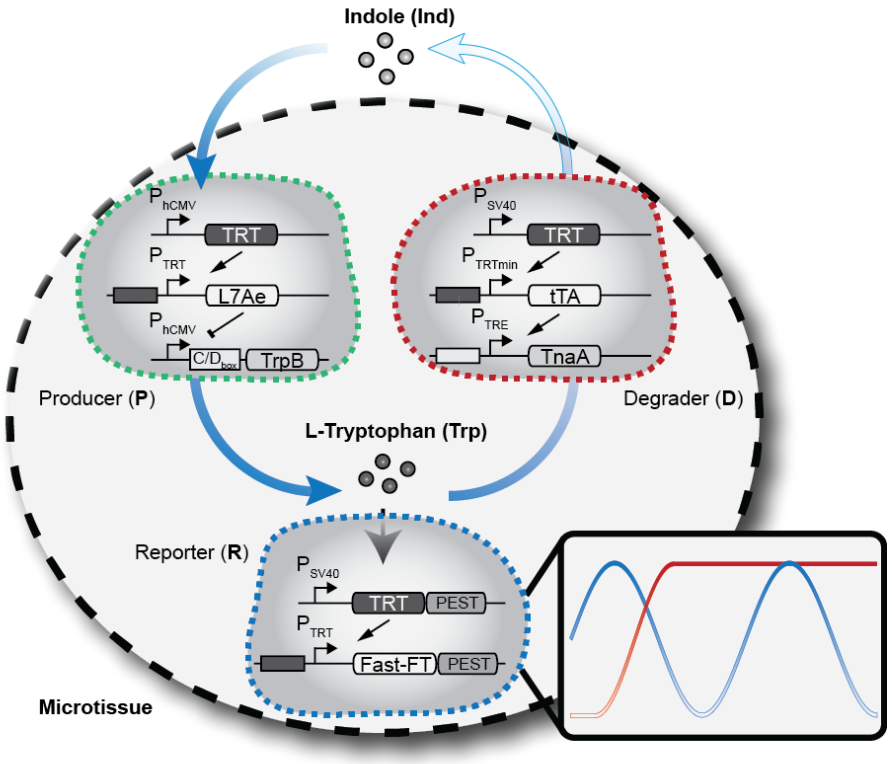

b)

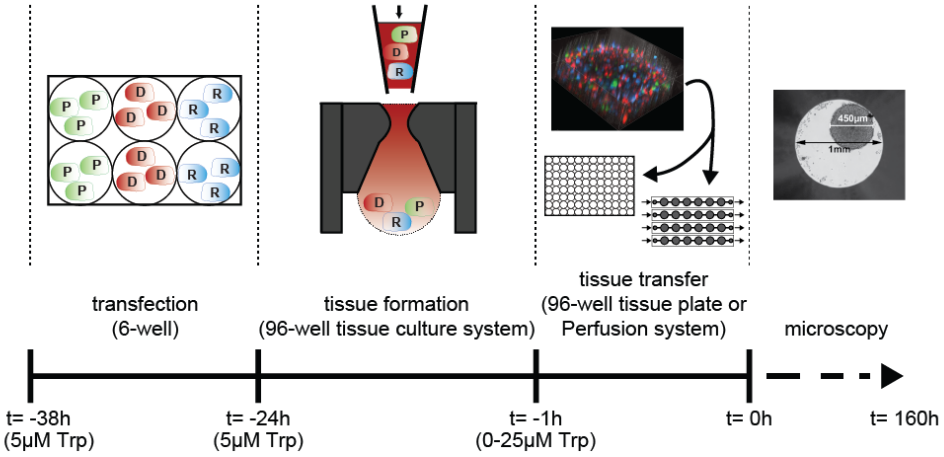

Figure 1. Oscillator design and experimental setup

a) The core oscillator consists of three mammalian cell populations (Producer (P), Degrader (D), Reporter(R)) clustered in a microtissue. The producer cells (green) are composed of the tryptophan responsive transactivator (TRT), which upon activation drives the expression of the RNA-binding protein L7Ae that in turn inhibits expression of the tryptophan-synthase TrpB, converting indole to the common-sensed metabolite L–Tryptophan. The counteracting degrader cells (red) also consist of the TRT. While tryptophan is present, the expression gets amplified via the additional transactivator tTA (tetracycline-responsive transactivator), which binds to its cognate promoter (P_{TRE}) and drives the expression of the Tryptophanase TnaA. TnaA closes the synthetic metabolic circle by converting

tryptophan back to indole. This circled conversion can be visualised by the reporter cells (blue), where TRT directly activates a fast fluorescent timer (Fast-FT) resulting in a dynamic blue and a steady red fluorescent signal.

b) Schematic illustration of the experimental process. In a first step HEK293-T cells are transfected with the cognate components (Table S2). After the transfection procedure, the cell populations are mixed in various ratios and tissues are formed by gravity-enforced cell assembly (15.000 cells per 40µL drop; for details see Materials and Methods section). The final tissues are transferred to a 96-well tissue plate (closed oscillator setup) or into a spheroid perfusion system (perfusion oscillator setup), followed by time-lapse microscopy.

Designer cells analysis

Preliminary analysis included evaluation of the single synthetic parts and cell systems such as the blue-to-red fluorescent timer in concert with the tryptophan-responsive system for its fundamental reversible behaviour (Table S2). In a first experiment, the system was induced for 24h with tryptophan and then changed to tryptophan-free media. This entrainment proved the applicability as a dynamic reporter cell system. As the system is based on the tissue-scale interconversion of a joint metabolite, the reporter cell population with either only the producer population (Fig. 2b) or the degrader population (Fig. 2c) were combined with wildtype cells (Table S2) in various ratios. The more producer/degrader cells were present the more/less reporter expression could be detected, indicating the principal modularity of the shared metabolite tryptophan in a multicellular environment. Additionally, we could show that conversion exclusively takes place in the presence of the substrate (Ind/Trp) and that the reaction is unidirectional: no induction of the reporter system could be observed in combination with the degrader cells at high levels of indole but without Tryptophan (0µM)(Fig. S3a) and no induction for the producer cells in the absence of indole (Fig. S3b).

As a critical cell density is required for common functional metabolite sensing networks and as no dynamic gene expression could be observed in a monolayer-culture, we increased the local cell density by the formation of multipopulation 3D-microtissues (consisting of the producer, degrader and reporter populations). Preliminary experiments

showed that cells get distributed equally (Fig. S4) in the tissue after formation process (Fig. S5).

We then confirmed applicability of the reporter and producer populations (Table S2) in a 3D-environment. First we showed tryptophan-dependent reporter induction within the entire tissue (Fig. 2d,f) for the unmaturated (Fig. 2e) and maturated variant (Fig. 2f), which was coherent with the data obtained from the initial component analysis and proved interconversion of Ind to Trp by combining the producer and reporter populations (Table S2) in a tissue. As expected, we could observe fluorescence also for no (0μM) and low (8μM) concentrations of Trp (Fig. 2g,h).

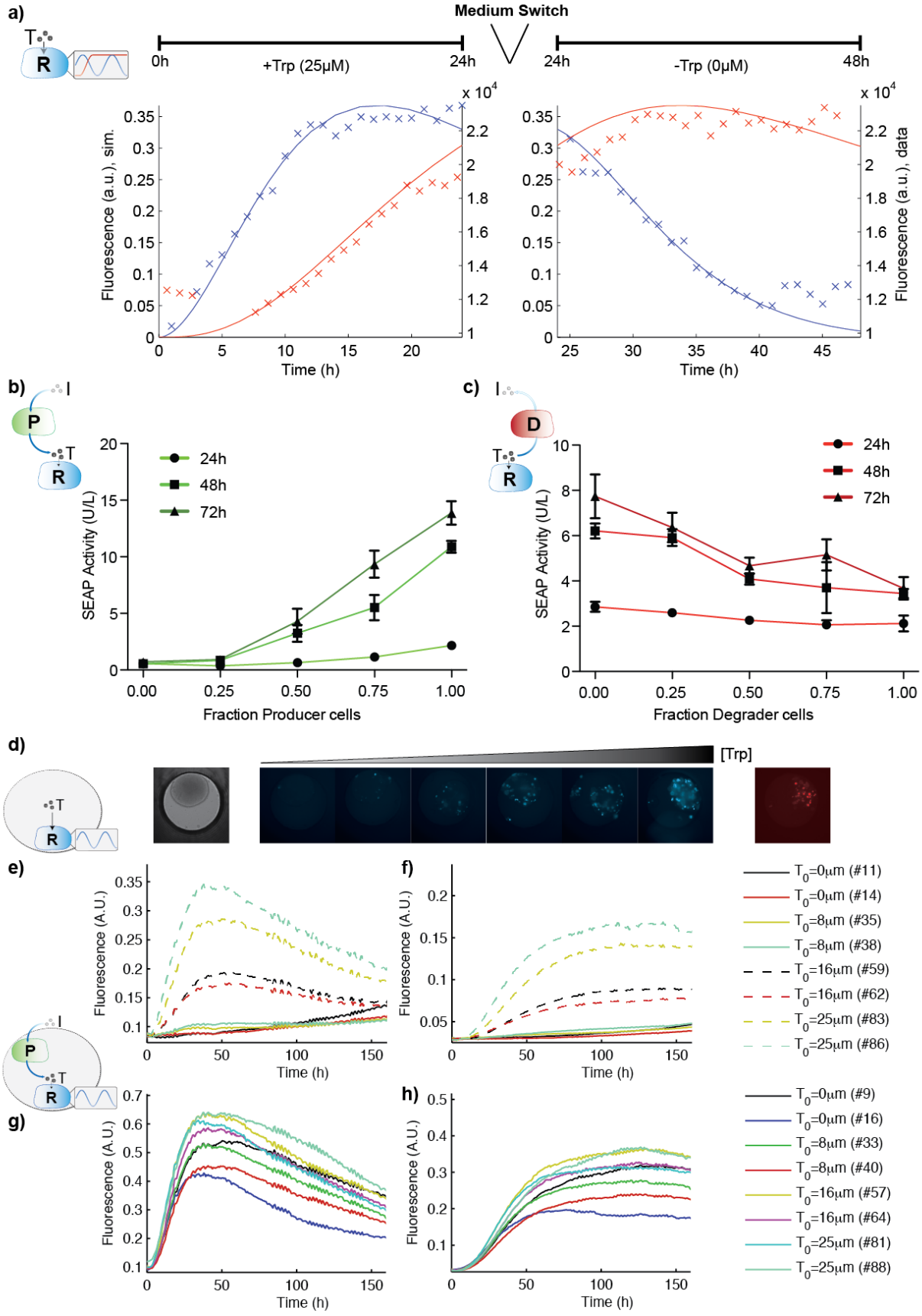

Figure 2. Component analysis and validation

a) Dynamic and reversible behaviour of the reporter cells. HEK293-T cells, transfected with the reporter components (Table S2) were induced with tryptophan (25µM). After 24h the system was shut off by switching to tryptophan-free media (0µM). Every 1h the unmaturated (blue) and maturated (red)

variant of the fluorescent timer were monitored via fluorescent time-lapse microscopy. Single points mark experimental data, curves represent simulated data. **b)**,**c)** Multicellular producer (**b**) and degrader (**c**) cells evaluation. Combination of the SEAP reporter cells with various fraction of producer (**b**) or degrader (**c**) cells to wild type HEK293-T cells. Initial Tryptophan levels were 0µM Tryptophan for producer cells (**b**) and 25µM for Degrader cells (**c**). The secreted SEAP reporter was scored every 24h. Error bars represent s.d.; n=3.

d-f) Reporter cell performance in microtissues. Transgenic reporter cells and wildtype cells (Table S2) were clustered to microtissues as described (see Materials and Methods section) and exposed to various concentrations of Tryptophan ranging from 0µM to 50µM. **d)** Representative brightfield and fluorescence (blue and red) images were assessed after 48h. Quantified fluorescence for the unmaturated variant (**e**) and the maturated variant (**f**) over time.

g,h) Reporter and producer cells combined in microtissues. Transgenic reporter and producer cells (Table S2) were clustered into microtissues as described and exposed to various concentrations of Tryptophan. Quantified fluorescence for the unmaturated variant (**g**) and the maturated variant (**h**) over time.

Tissue-wide dynamic reporter expression

Having verified and optimized the single components, assembled them to the specified cell populations (Fig. 1a), we formed autonomous tissues including all designer populations (producer, degrader and reporter) (Table S2) at optimal producer-degrader ratios evaluated by the mathematical model. After the tissue formation process, tissues exhibited dynamic oscillatory patterns illustrated by several tissue trajectories (Fig. 3a + Supplementary Movie 1). Thereby the producer population (precultivated in minimal Trp without Ind) converts Ind to Trp resulting in the first oscillatory peak. As Trp levels in the tissue increase, the Degrader population counteracts the producer (which additionally gets shut off at high Trp-levels) by converting Trp back to indole resulting in decreased fluorescence of the reporter population. After interconversion, the synthetic metabolic circle starts over again, resulting in the second fluorescent peak (Fig. 3b,c). In contrast the matured fluorescent variant (red) only showed steady increase without oscillatory patterns as expected. This was illustrated by a representative trajectory (Fig. 3d) as well as homogeneous distribution over the tissue and time (Fig.

3e,f), as control. However, we could not observe sustained oscillatory patterns, likely due to nutrition limitation in the closed batch system.

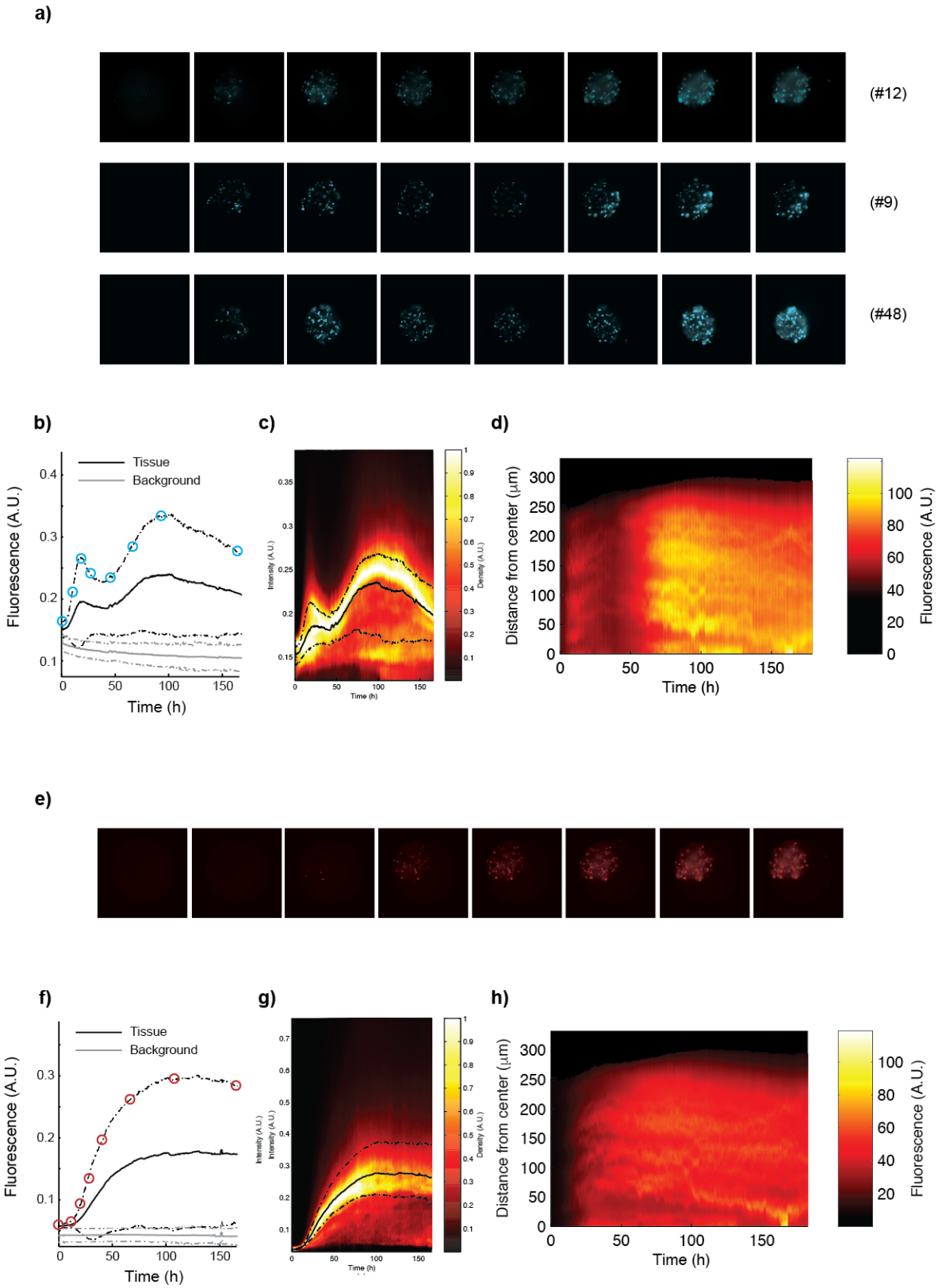

Figure 3. Dynamic expression in microtissues.

a),**e)** Representative fluorescent trajectories for the unmaturated (blue) (a)/ maturated (red) (e) variant of the full oscillator setup (consistent of the producer (52.5%), degrader (17.5%) and reporter (30%) cells; Table S2) in a 3D-microtissue demonstrating dynamic oscillatory behaviour (Supplementary movie). **b)**,**f)** Corresponding quantified fluorescence for the unmaturated (blue) (**b**)/ maturated (red) (**f**) variant as a function of time for the representative experiment. Dashed black lines indicate lower and upper quartiles, black line illustrates mean fluorescence. Grey lines indicate background fluorescence.
c),**g)** Intensity-density diagram showing fluorescence intensity distribution for the unmaturated (**c**) / maturated (**g**) variant over time and cell density. White plots indicate high cellular density proving synchronized behaviour.
d),**h)** Spatial distribution diagram showing fluorescence of the unmaturated (**d**) / maturated (**h**) variant within a microtissue along the centre over time. a.u., arbitrary units

Sustained dynamics in a tissue-perfusion system

Tissues in the human body are under constant supply of nutrition by the blood and vessel perfusion system. Similarly, we sought to overcome the nutrition limitation of our closed system by introducing a spheroid microfluidic system. The microfluidic system consists of 4x 5 chambers for simultaneous real-time monitoring of different conditions (Fig. 4a).

In our synthetic metabolic cycle, we substituted the producer population with a constant flow of tryptophan-containing media. Dynamic expression takes place as a result of the degrader population and the intrinsic genetic feed-back (Fig 4a).

After evaluating the functional parameter space, we observed periodic expression patterns (Fig. 4b; Fig. S6; Supplementary Movie 3). Thereby, the system (precultivated in minimal Trp without Ind) is turned on by perfusion of Trp-containing media, resulting in the first reporter expression peak. As Trp levels in the tissue increase, the Degrader population counteracts the Trp in the media by converting Trp to indole resulting in decreased fluorescence levels of the reporter cell system. After interconversion, the Degrader population is shut off at low Trp levels and the synthetic metabolic circle starts over again, resulting in sustained periodic expression patterns. These dynamics only occur when degrader cells are present and thus independent of the microfluidic setup as confirmed for constitutive fluorescence reporter expression (Fig. S6a) and for microtissues lacking the degrader cell population (Fig. S6b). These dynamics in

expression do not show the same amplitude and frequency as in the batch setup. Instead, the oscillatory frequency is higher and we observe local wave-like patterns in the unmaturated fluorescent variant (Fig. 4b,c, Fig S6c). In contrast the matured fluorescent variant shows a constant increase in intensity of the entire tissue (Fig. 4d,e, Fig S6c).

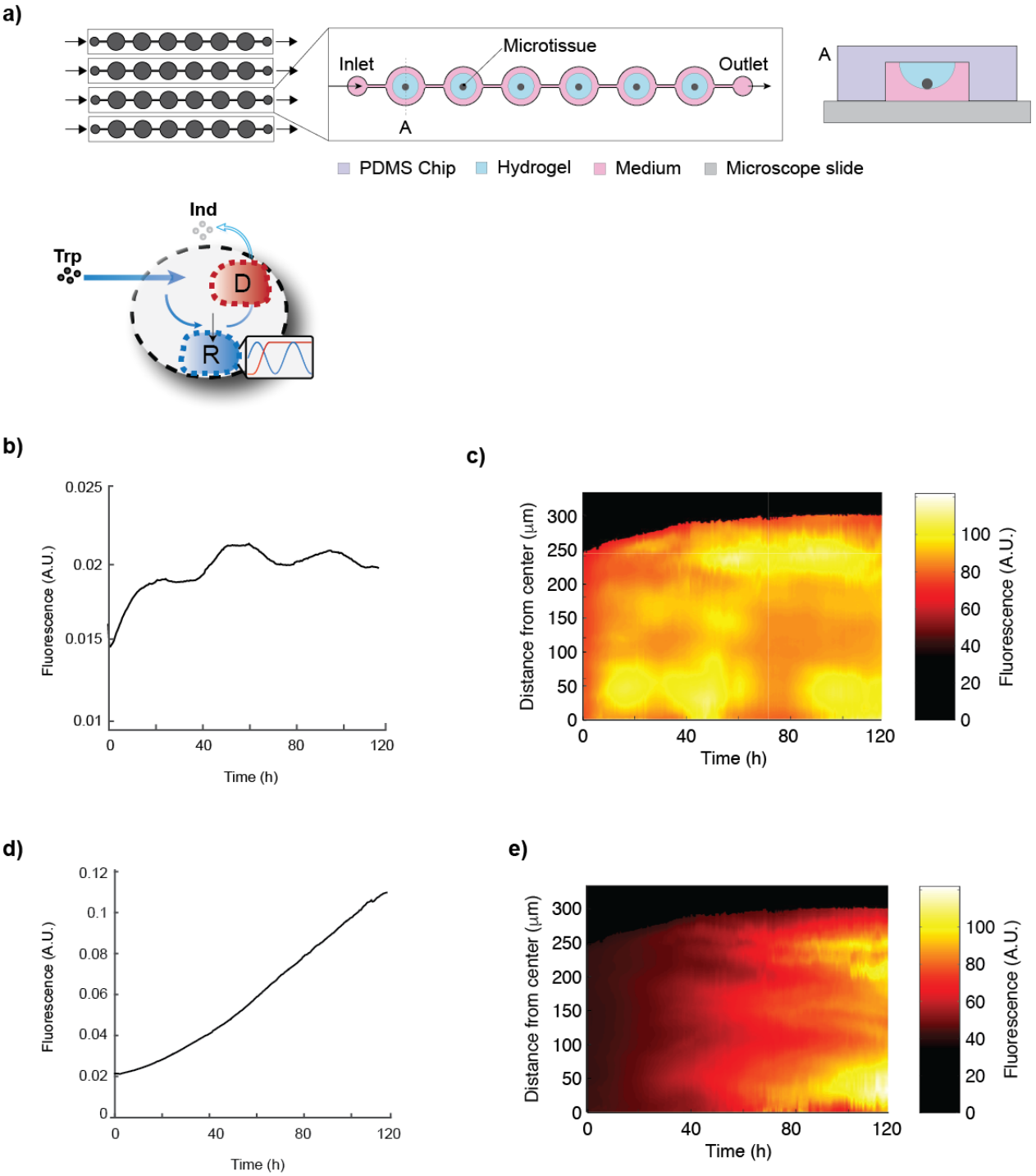

Figure 4. Sustained dynamics in a tissue-perfusion system

a) Layout of the microfluidic device. The tissues (consistent of degrader and reporter cells) are embedded into a hydrogel (0.5% agarose) and constantly perfused by medium. The chip consists of 4x5 chambers.

b),**d)** Quantified fluorescence for the unmaturated (blue) (**b**)/ maturated (red) (**d**) variant as a function of time for the oscillator setup in the spheroid perfusion system in a 3D-microtissue demonstrating dynamic gene expression behaviour. Dashed black lines indicate background fluorescence, black line illustrates mean fluorescence.

c),**e)** Intensity-density diagram showing fluorescence intensity distribution for the unmaturated **(c)** / maturated **(e)** variant over time and cell density.

Discussion and summary

Coupling of clocks is substantial, appearing almost throughout all fields of life: these include computer sciences with synchronization on a common network time protocol (NTP)[31] and cryptography, the global position system (GPS)[32] and laser arrays principle in physics[33] as well as the clock signal for digital circuit synchronization in electronics[34]. Synergistic systems and synthetic biology with its forward-engineering approach can thus help to get insights into these mechanisms by mimicking and recreating these systems using computational modelling and constructed synthetic networks.

Here we showed a synthetic mammalian oscillator in an autonomous multipopulation microtissue uncoupled of the circadian clock and in a spheroid perfusion setup. This could be achieved by the implementation of a fast fluorescent timer, cell-cell communication, artificial 3D-microtissue technologies combined with spheroid microfluidics and a descriptive mathematical model.

We expect that future fine-tuning of the synthetic oscillator and the interplay with the spheroid perfusion setup will increase its amplitude, respectively its synchronicity.

Besides providing a synthetic system with tissue-wide dynamic expression patterns, autonomous of the circadian clock, these findings also provide new insights into rhythmic physiological mammalian functions.

As therapeutic uptake or expression in synchrony with biological clocks has been shown to improve treatments[35], a synthetic tissue oscillator could be used to express these therapeutics or hormones (such as insulin) on a periodic basis.

METHODS SUMMARY

Oscillator components and design

The key oscillator consists of the following plasmids: the producer population consists of **pMM523** (P_{hCMV}-TRT-pA), **pMM161** (P_{hCMV}-C/D_{box}-TrpB-pA), and **pMM162** (P_{TRT}-L7Ae-pA). The degrader population consists of **pWB24** (P_{SV40}-TRT-pA) driving **pMM148** (TrpOP-P_{min}-tTA-pA) and **pMM128** (P_{TRE}-TnaA-pA).

The reporter population consists of **pAK409** (P_{SV40}-TRT-PEST-pA) and **pMM131** (P_{TRT}-Fast-FT-PEST-pA). Construction details for expression vectors are provided Supplementary Table 1. Details on the components and amount transfected for each setup can be found in Supplementary Table 2.

HEK-293T cells (American Type Culture Collection, CRL-11268) were cultivated at 37 °C in DMEM medium (Invitrogen, Basel, Switzerland) supplemented with 10% FCS (lot no. PE01026P; Bioconcept, Allschwil, Switzerland) and 1% penicillin/streptomycin solution (Biowest, Nuaillé, France) in a humidified atmosphere containing 5% CO_2. HEK-293T cells were (co)-transfected using an optimized polyethyleneimine-based protocol. In brief, a transfection solution containing 4 μg of plasmid DNA mixtures (Supplementary Table 2), 600 μl of FCS-free DMEM and 12 μl of polyethyleneimine (1 mg ml^{-1} in water; Polysciences, Eppelheim, Germany) was incubated for 30 min at 22 °C. Prior to dropwise addition to 4×10^5 HEK-293T cells seeded in each well of a six-well plate 16 h before transfection, media was exchanged to minimal Tryptophan-media (low-content (5μM) L–Tryptophan medium (Cell Culture Technologies LLC, Gravesano, Switzerland) which maintains native cell viability while keeping P_{TRT} repressed, without indole).

At 16 h after transfection, the cells were detached using 200 μl of trypsin/EDTA (Biowest, Nuaillé, France), washed once in 1.8 ml of FCS-containing DMEM, resuspended in 0.75 ml of FCS-containing DMEM, re-seeded into 60 wells of a 96-well plate containing various concentrations of Trp and Ind as indicated and cultivated for up to further 72 h before analysis. Gradual Trp-concentrations were achieved by mixing 0μM Trp-DMEM (which was prepared from Tryptophan-free media (Cell Culture Technologies LLC, Gravesano, Switzerland) supplemented with 10% FCS and 300 μM

indole (Sigma Aldrich, Munich, Germany); stock solution: 100 mM in 50% ethanol (Sigma Aldrich, Munich, Germany)) and 100µM-Trp Media (which was prepared from Tryptophan-free media (supplemented with 10% FCS and 100 µM Tryptophan (Sigma Aldrich, Munich, Germany); stock solution: 25mM in water and 100% Ethanol, to compensate for the missing indole)

Microtissue formation

Microtissues were formed using the GravityPlate-System (Insphero AG, Schlieren, Switzerland) according to the manual. In brief, HEK-293T cell populations were mixed (if not stated otherwise 30% reporter cell system, 70% Producer, Degrader, wild type cells) and 15k cells per 40µL drop were applied to a 96-well Gravity-Plate for tissue formation. After 16 h microtissues were transferred to the Gravity-Trapping plate. For further details see the experimental procedure (Fig. 1b).

Fluorescence imaging

Time-lapse fluorescence microscopy was conducted on an inverted fluorescent microscope (Nikon Ti-E; Nikon Europe, Egg, Switzerland) equipped with an incubation chamber; an Orca Flash-4 digital camera (Hamamatsu, Solothurn, Switzerland); a pE-100-LED (CoolLED, Andover, UK) as transmission light source; a Spectra X (Lumencor, Beaverton, OR, USA) as source for fluorescent light and a 10x objective (Plan Apo λ N/A: 0.45; DIC; WD:4). Brightfield (3% intensity -5ms); Maturated variant (RFP) (Ex: 542nm; 15% Intensity -500ms -Cy3HC Filter Dichroic: 562 –Emission: 593/40); YFP (Ex: 475nm; 5% Intensity -70ms –YFP ET Dichroic: 515; Emission: 535/30); unmaturated variant (CFP) (Ex: 390nm; 10% Intensity -500ms –CFP HC Dichroic 458 –Emission: 480/17). A binning of 2x2 was used. Time-lapse videos were recorded and exported using Nikon Analysis software. Images were taken every 30 min. Monolayer fluorescent cells recorded by time-lapse microscopy were tracked and quantified individually and the data summed up for each time frame using Imaris software (Bitplane, Zurich, Switzerland; version 7.5.2).

SEAP assay

In brief, 100 µL cell culture supernatant were heat-inactivated for 30 min at 65°C and centrifuged at 14.000 x g for 15 s. Subsequently, 80 µL of the supernatant were transferred to a well of a 96-well plate containing 100 µL 2x SEAP assay buffer (20 mM homoarginine, 1 mM MgCl2, 21% diethanolamine pH 9.8). After addition of 20 µL 120 mM para-nitrophenylphosphate (pNPP disodium salt, hexahydrate, Acros Organics BVBA, Geel, Belgium) diluted in 1 x SEAP assay buffer, the time-dependent increase in light absorbance was profiled at 405 nm for 30 min using a GeniosPro multi-well reader.

Acknowledgements

I am grateful to Moritz Lang for model data and input and Patrick Misun for the microfluidic realization and input.

Thomas Horn and the Single Cell Unit for assistance with microscopy and advice as well as Marcel Tigges for generous input and Ferdinand Sedlmayer, Luca Siegrist and Andreas Kyburz for experimental support. William Bacchus for providing plasmids pWB48, pWB49, pWB60, pWB69 and pWB70.

References

1 Novák, B. & Tyson, J. J. Design principles of biochemical oscillators. *Nature Reviews Molecular Cell Biology* **9**, 981-991, doi:10.1038/nrm2530 (2008).

2 Purcell, O., Savery, N. J., Grierson, C. S. & di Bernardo, M. A comparative analysis of synthetic genetic oscillators. *Journal of the Royal Society, Interface / the Royal Society* **7**, 1503-1524, doi:10.1098/rsif.2010.0183 (2010).

3 Ukai, H. & Ueda, H. R. Systems biology of mammalian circadian clocks. *Annual review of physiology* **72**, 579-603, doi:10.1146/annurev-physiol-073109-130051 (2010).

4 Zhang, J., Kaasik, K., Blackburn, M. R. & Lee, C. C. Constant darkness is a circadian metabolic signal in mammals. *Nature* **439**, 340-343, doi:10.1038/nature04368 (2006).

5 Bass, J. & Takahashi, J. S. Circadian integration of metabolism and energetics. *Science* **330**, 1349-1354, doi:10.1126/science.1195027 (2010).

6 Takahashi, J. S., Hong, H. K., Ko, C. H. & McDearmon, E. L. The genetics of mammalian circadian order and disorder: implications for physiology and disease. *Nat Rev Genet* **9**, 764-775, doi:10.1038/nrg2430 (2008).

7 Musiek, E. S. Circadian clock disruption in neurodegenerative diseases: cause and effect? *Front Pharmacol* **6**, 29, doi:10.3389/fphar.2015.00029 (2015).

8 Roh, J. H. *et al.* Disruption of the sleep-wake cycle and diurnal fluctuation of beta-amyloid in mice with Alzheimer's disease pathology. *Sci Transl Med* **4**, 150ra122, doi:10.1126/scitranslmed.3004291 (2012).

9 Kudo, T., Loh, D. H., Truong, D., Wu, Y. & Colwell, C. S. Circadian dysfunction in a mouse model of Parkinson's disease. *Exp Neurol* **232**, 66-75, doi:10.1016/j.expneurol.2011.08.003 (2011).

10 Gardner, T. S., Cantor, C. R. & Collins, J. J. Construction of a genetic toggle switch in Escherichia coli. *Nature* **403**, 339-342, doi:10.1038/35002131 (2000).

11 Elowitz, M. B. & Leibler, S. A synthetic oscillatory network of transcriptional regulators. *Nature* **403**, 335-338, doi:10.1038/35002125 (2000).

12 Stricker, J. *et al.* A fast, robust and tunable synthetic gene oscillator. *Nature* **456**, 516-519, doi:10.1038/nature07389 (2008).

13 Tigges, M., Marquez-Lago, T. T., Stelling, J. & Fussenegger, M. A tunable synthetic mammalian oscillator. *Nature* **457**, 309-312, doi:10.1038/nature07616 (2009).

14 Tigges, M., Dénervaud, N., Greber, D., Stelling, J. & Fussenegger, M. A synthetic low-frequency mammalian oscillator. *Nucleic Acids Research* **38**, 2702-2711, doi:10.1093/nar/gkq121 (2010).

15 Mondragón-Palomino, O., Danino, T., Selimkhanov, J., Tsimring, L. & Hasty, J. Entrainment of a population of synthetic genetic oscillators. *Science* **333**, 1315-1319, doi:10.1126/science.1205369 (2011).

16 Fung, E. *et al.* A synthetic gene-metabolic oscillator. *Nature* **435**, 118-122, doi:10.1038/nature03508 (2005).

17 Maharbiz, M. M. Synthetic multicellularity. *Trends in Cell Biology* **22**, 617-623, doi:10.1016/j.tcb.2012.09.002 (2012).

18 Bacchus, W. & Fussenegger, M. Engineering of synthetic intercellular communication systems. *Metabolic engineering* **16C**, 33-41, doi:10.1016/j.ymben.2012.12.001 (2012).

19 Pai, A., Tanouchi, Y., Collins, C. H. & You, L. Engineering multicellular systems by cell–cell communication. *Current Opinion In Biotechnology* **20**, 461-470, doi:10.1016/j.copbio.2009.08.006 (2009).

20 Basu, S., Gerchman, Y., Collins, C. H., Arnold, F. H. & Weiss, R. A synthetic multicellular system for programmed pattern formation. *Nature* **434**, 1130-1134, doi:10.1038/nature03461 (2005).

21 Tabor, J. J. *et al.* A synthetic genetic edge detection program. *Cell* **137**, 1272-1281, doi:10.1016/j.cell.2009.04.048 (2009).

22 Leisner, M., Bleris, L., Lohmueller, J., Xie, Z. & Benenson, Y. Rationally designed logic integration of regulatory signals in mammalian cells. *Nature Nanotechnology* **5**, 666-670, doi:10.1038/nnano.2010.135 (2010).

23 Regot, S. *et al.* Distributed biological computation with multicellular engineered networks. *Nature* **469**, 207-211, doi:10.1038/nature09679 (2011).

24 Weber, W., Daoud-El Baba, M. & Fussenegger, M. Synthetic ecosystems based on airborne inter- and intrakingdom communication. *Proceedings Of The National Academy Of Sciences Of The United States Of America* **104**, 10435-10440, doi:10.1073/pnas.0701382104 (2007).

25 Bacchus, W. *et al.* Synthetic two-way communication between mammalian cells. *Nature Biotechnology* **30**, 991-996, doi:10.1038/nbt.2351 (2012).

26 Saito, H. *et al.* Synthetic translational regulation by an L7Ae-kink-turn RNP switch. *Nature Chemical Biology* **6**, 71-78, doi:10.1038/nchembio.273 (2010).

27 Gossen, M. & Bujard, H. Tight control of gene expression in mammalian cells by tetracycline-responsive promoters. *Proceedings Of The National Academy Of Sciences Of The United States Of America* **89**, 5547-5551 (1992).

28 Subach, F. V. *et al.* Monomeric fluorescent timers that change color from blue to red report on cellular trafficking. *Nature Chemical Biology* **5**, 118-126, doi:10.1038/nchembio.138 (2009).

29 Danino, T., Mondragón-Palomino, O., Tsimring, L. & Hasty, J. A synchronized quorum of genetic clocks. *Nature* **463**, 326-330, doi:10.1038/nature08753 (2010).

30 Kelm, J. M. & Fussenegger, M. Microscale tissue engineering using gravity-enforced cell assembly. *Trends in Biotechnology* **22**, 195-202, doi:10.1016/j.tibtech.2004.02.002 (2004).

31 Mills, D. L. Internet Time Synchronization - the Network Time Protocol. *Ieee T Commun* **39**, 1482-1493, doi:Doi 10.1109/26.103043 (1991).

32 Lewandowski, W., Azoubib, J. & Klepczynski, W. J. GPS: Primary tool for time transfer. *P Ieee* **87**, 163-172, doi:Doi 10.1109/5.736348 (1999).

33 Vladimirov, A. G., Kozyreff, G. & Mandel, P. Synchronization of weakly stable oscillators and semiconductor laser arrays. *Europhys Lett* **61**, 613-619, doi:DOI 10.1209/epl/i2003-00115-8 (2003).

34 Friedman, E. G. Clock distribution networks in synchronous digital integrated circuits. *P Ieee* **89**, 665-692, doi:Doi 10.1109/5.929649 (2001).

35 Grote, L. *et al.* Nocturnal hypertension and cardiovascular risk: consequences for diagnosis and treatment. *J Cardiovasc Pharmacol* **24 Suppl 2**, S26-38 (1994).

Supplementary Information

Table 1. Plasmids used and designed in this study

Plasmid	Description and Cloning Strategy	Reference or
pcDNA3.1(+)	Constitutive mammalian expression vector (P_{hCMV}-MCS-pA).	LifeTechnologies, Carlsbad, CA
pColaDuet^{TM}-1	Prokaryotic expression vector used as filler plasmid for cotransfection of mammalian cells.	Merck, Darmstadt, Germany
pd2EYFP-N1	Constitutive mammalian d2EYFP expression vector (P_{hCMV}-d2EYFP-pA).	Clontech, Mountain View, CA
pDsRed-Express-DR	Constitutive mammalian DsRed-Express-DR-encoding vector (MCS-DsRed-Express-DR-pA).	Clontech, Mountain View, CA
pMT100	Tetracycline-responsive $P_{hCMV*-1}$-driven Ub^{V76}-GFP expression vector ($P_{hCMV*-1}$-Ub^{V76}-GFP).	Tigges et al., 2009
pSA91	Erythromycin-repressible P_{ETR2}-driven L7Ae expression vector (P_{ETR2}-L7Ae-pA).	Ausländer et al., 2012
pSAM200	Constitutive mammalian tTA expression vector (P_{SV40}-tTA-pA).	Fussenegger et al., 1997
pSEAP2-Basic	SEAP-encoding vector (MCS-SEAP-pA).	Clontech, Mountain View, CA
pSEAP2-Control	Constitutive mammalian SEAP expression vector (P_{SV40}-SEAP-pA).	Clontech, Mountain View, CA
pSP16	P_{CREm}-driven SEAP expression vector (P_{CREm}-SEAP-pA).	Saxena et al., unpublished
pTRE-Fast-FT	Tetracycline-responsive P_{tight}-driven Fast-FT expression vector (P_{tight}-Fast-FT-pA).	Addgene plasmid 31913
pTurboGFP-dest1	Constitutive mammalian TurboGFP-dest1 expression vector (P_{hCMV}-TurboGFP-dest1-pA).	Evrogen, Moscow, Russia
pWB22	L-tryptophan-inducible P_{TRT}-driven SEAP expression vector (P_{TRT}-SEAP-pA).	Bacchus et al., 2012
pWB24	Constitutive TRT expression vector (P_{SV40}-TRT-pA).	Bacchus et al., 2012
pWB32	Constitutive TrpB expression vector (P_{hCMV}-TrpB-pA).	Bacchus et al., 2012
pWB35	L-tryptophan-inducible P_{TRT}-driven SEAP expression vector (P_{TRT}-SEAP-pA).	Bacchus et al., 2012
pWW43	Constitutive ET4 expression vector (P_{SV40}-ET4-pA).	Weber et al., 2002
pWW56	Erythromycin-inducible P_{ETR}ON8-driven SEAP expression vector (P_{ETR}ON8-SEAP-pA).	Weber et al., 2002
pZ060	Bidirectional tetracycline-responsive AmCyan and DsRed expression vector (pA-AmCyan←$P_{tight-bi}$→DsRed-pA).	Zhen et al., 2011
pAK409	Constitutive TRT_{PEST} expression vector (P_{SV40}-TRT_{PEST}-pA). TRT_{PEST} was excised	This work

	from pMM523 using *Eco*RI/*Xba*I and ligated into the corresponding sites (*Eco*RI/*Xba*I) of pSEAP2-Control.	
pMM1	pcDNA3.1(+)-derived expression vector containing a modified MCS (P_{hCMV}-MCS-pA; MCS, *Eco*RI-ATG-*Spe*I-*Nhe*I-*Bam*HI-STOP-*Xba*I-*Hind*III-*Fse*I-pA). pcDNA3.1(+) was PCR-amplified using oligonucleotides OMM1 (5'-cggatccaccggtgtctagaaagctttgaggccggcctgcaggGATCAGCCTCGACTGTGCCTTC-3') and OMM2 (5'-ctagcactagtcatggtgaattcgattaatcaattgacgcgtGGAGATCTCCCGATCCGTC-3') and self-ligated.	This work
pMM27	Constitutive SEAP expression vector (P_{hCMV}-SEAP-pA). P_{hCMV} was excised from pcDNA3.1(+) using *Mlu*I/*Eco*RI and ligated into the corresponding sites (*Mlu*I/*Eco*RI) of pSEAP2-Control.	This work
pMM60	Constitutive dsRed-Express-DR expression vector (P_{hCMV}-dsRed-Express-DR-pA).	Ausländer et al., 2012
pMM88	L-tryptophan-inducible P_{TRT}-driven TrpB expression vector (P_{TRT}-TrpB-pA). TrpB was excised from pWB32 using *Eco*RI/*Xba*I and ligated into the corresponding sites (*Eco*RI/*Xba*I) of pWB22.	This work
pMM89	L-tryptophan-inducible P_{TRT}-driven TnaA expression vector (P_{TRT}-TnaA-pA). TnaA was excised from pWB60 using *Eco*RI/*Xba*I and ligated into the corresponding sites (*Eco*RI/*Xba*I) of pWB22.	This work
pMM109	L-tryptophan-inducible P_{TRT}-driven Fast-FT expression vector (P_{TRT}-Fast-FT-pA). Fast-FT was excised from pTRE-Fast-FT using *Eco*RI/*Xba*I and ligated into the corresponding sites (*Eco*RI/*Xba*I) of pWB22.	This work
pMM119	L-tryptophan-repressible P_{TRS}-driven TrpB expression unit (P_{TRS}-TrpB-pA). TrpB was excised from pWB32 using *Eco*RI/*Xba*I and ligated into the corresponding sites (*Eco*RI/*Xba*I) of pWB49.	This work
pMM125	L-tryptophan-repressible P_{TRS2}-driven SEAP expression vector (P_{TRS2}-SEAP-pA). $(O_{Trp})_2$-SEAP was excised from pWB49 using *Hin*dIII/*Xba*I and ligated into the corresponding sites (*Hin*dIII/*Xba*I) of pMM27.	This work
pMM126	L-tryptophan-repressible P_{TRS2}-driven TrpB expression vector (P_{TRS2}-TrpB-pA). TrpB was excised from pWB32 using *Eco*RI/*Xba*I and ligated into the corresponding sites (*Eco*RI/*Xba*I) of pMM125.	This work
pMM127	L-tryptophan-inducible P_{TRT}-driven tTA	This work

	expression vector (P_{TRT}-tTA-pA). tTA was excised from pMM506 using *Eco*RI/*Xba*I and ligated into the corresponding sites (*Eco*RI/*Xba*I) of pWB22.	
pMM128	Tetracycline-responsive P_{tight}-driven TnaA expression vector (P_{tight}-TnaA-pA). TnaA was excised from pWB60 using *Eco*RI/*Xba*I and ligated into the corresponding sites (*Eco*RI/*Xba*I) of pTRE-Fast-FT.	This work
pMM130	Tetracycline-responsive P_{tight}-driven SEAP expression vector (P_{tight}-SEAP-pA). P_{tight} was excised from pTRE-Fast-FT using *Xho*I/*Eco*RI and ligated into the corresponding sites (*Xho*I/*Eco*RI) of pSEAP2-Basic.	This work
pMM131	L-tryptophan-inducible P_{TRT}-driven Fast-FT_{PEST} expression vector (P_{TRT}-Fast-FT_{PEST}-pA). Fast-FT_{PEST} was excised from pMM532 using *Eco*RI/*Xba*I and ligated into the corresponding sites (*Eco*RI/*Xba*I) of pWB22.	This work
pMM142	Constitutive AmCyan expression vector (P_{hCMV}-AmCyan-pA). AmCyan was excised from pZ060 using *Eco*RI/*Xba*I and ligated into the corresponding sites (*Eco*RI/*Xba*I) of pcDNA3.1(+).	This work
pMM146	L-tryptophan-inducible P_{TRT2}-driven SEAP expression vector (P_{TRT2}-SEAP-pA). pWB22 was PCR-amplified using the P_{min}-containing oligonucleotide OMM131 (5'-tagagggtatataatggaagctcgacttccagGAATTCGAGCTCGCCCGGGG-3') and OMM132 (5'Phos-CCTGCAGGATCCTTGTAATG-3') and self-ligated.	This work
pMM147	L-tryptophan-inducible P_{TRT3}-driven SEAP expression vector (P_{TRT3}-SEAP-pA). pSP16 was PCR-amplified using the P_{E1bmin}-containing oligonucleotide OMM134 (5'-ttgtaatgctataatattacaattgtaatgctataatattacaaCACGCGTAAGAGCTCGGTAC-3') and OMM133 (5'Phos-ggtcgacaGCGGAGACTCTAG-3') and and self-ligated.	This work
pMM148	L-tryptophan-inducible P_{TRT2}-driven tTA expression vector (P_{TRT2}-tTA-pA). tTA was excised from pMM506 using *Eco*RI/*Xba*I and ligated into the corresponding sites (*Eco*RI/*Xba*I) of pMM146.	This work
pMM151	L-tryptophan-repressible P_{TRS}-driven L7Ae expression vector (P_{TRS}-L7Ae-pA). L7Ae was excised from pSA91 using *Eco*RI/*Xba*I and ligated into the corresponding (*Eco*RI/*Xba*I) sites of pMM119.	This work
pMM152	L-tryptophan-repressible P_{TRS2}-driven L7Ae	This work

	expression vector (P_{TRS2}-L7Ae-pA). L7Ae was excised from pSA91 using *Eco*RI/*Xba*I and ligated into the corresponding sites (*Eco*RI/*Xba*I) of pMM125.	
pMM153	L-tryptophan-inducible P_{TRT2}-driven L7Ae expression vector (P_{TRT2}-L7Ae-pA). L7Ae was excised from pSA91 using *Eco*RI/*Xba*I and ligated into the corresponding sites (*Eco*RI/*Xba*I) of pMM146.	This work
pMM154	L-tryptophan-inducible P_{TRT3}-driven L7Ae expression vector (P_{TRT3}-L7Ae-pA). L7Ae was excised from pSA91 using *Eco*RI/*Xba*I and ligated into the corresponding sites (*Eco*RI/*Xba*I) of pMM147.	This work
pMM155	Constitutive SEAP expression vector containing a C/D_{box} in the 5'UTR (P_{SV40}-C/D_{box}-SEAP-pA). pSEAP2-Control was PCR-amplified using C/D_{box}-containing oligonucleotide OMM135 (5'-cctagatctgggcgtgatccgaaaggtgacccaccggtcgGAATTCGCCCACCATGCTGC-3') and OMM136 (5'-Phos-GCGATTCGAAGCTTTTTGC-3') and self-ligated.	This work
pMM156	Constitutive SEAP expression vector containing a C/D_{box} in the 5'UTR (P_{hCMV}-C/D_{box}-SEAP-pA). pMM27 was PCR-amplified using C/D_{box}-containing oligonucleotide OMM135 (5'-cctagatctgggcgtgatccgaaaggtgacccaccggtcgGAATTCGCCCACCATGCTGC-3') and OSA159 (5'-Phos-TGGGTCTCCCTATAGTGAGTC-3') and self-ligated.	This work
pMM159	L-tryptophan-inducible P_{TRT}-driven TurboGFP-dest1 expression vector (P_{TRT}-TurboGFP-dest1-pA). TurboGFP-dest1 was PCR-amplified from pTurboGFP-dest1 using oligonucleotides ODA220 (5'-ggccgaattcaagcttCCACCATGGAGAGCGACGAGAG-3') and ODA221 (5'-gctctagaCTACACATTGATCCTAGCAGAAGCACAGGC-3'), restricted with *Eco*RI/*Xba*I and ligated into the corresponding sites (*Eco*RI/*Xba*I) of pWB22.	This work
pMM160	Constitutive TrpB expression vector containing a C/D_{box} in the 5'UTR (P_{SV40}-C/D_{box}-TrpB-pA). TrpB was excised from pWB32 using *Eco*RI/*Xba*I and ligated into the corresponding sites (*Eco*RI/*Xba*I) of pMM155.	This work
pMM161	Constitutive TrpB expression vector containing a C/D_{box} in the 5'UTR (P_{hCMV}-C/D_{box}-TrpB-pA). TrpB was excised from pWB32 using *Eco*RI/*Xba*I and ligated into the corresponding sites (*Eco*RI/*Xba*I) of pMM156.	This work

pMM162	L-tryptophan-inducible P_{TRT}-driven L7Ae expression vector (P_{TRT}-L7Ae-pA). L7Ae was excised from pSA91 using *Eco*RI/*Xba*I and ligated into the corresponding sites (*Eco*RI/*Xba*I) of pWB22.	This work
pMM506	Constitutive tTA expression vector (P_{hCMV}-tTA-pA). tTA was PCR-amplified from pSAM200 using oligonucleotides OMM77 (5'-cggaattcaccatgactagtTCCAGATTAGATAAAAGTAAAG-3') and OMM78 (5'-gctctagacaccggtggatccgctagcCCCACCGTACTCGTCAATTC-3'), restricted with *Eco*RI/*Xba*I and ligated into the corresponding sites (*Eco*RI/*Xba*I) of pMM1.	This work
pMM516	Constitutive TRT expression vector (P_{hCMV}-TRT-pA). TRT was PCR-amplified from pWB24 using oligonucleotides OMM98 (5'-gcgaattcaccatgactagtAAAAATCAAGAGGAGTCTGGC-3') and OMM78 (5'-gctctagacaccggtggatccgctagcCCCACCGTACTCGTCAATTC -3´), restricted with *Eco*RI/*Xba*I and ligated into the corresponding sites (*Eco*RI/*Xba*I) of pMM1.	This work
pMM519	PEST-encoding expression vector (P_{hCMV}-PEST-pA). PEST was PCR-amplified from pd2EYFP-N1 using oligonucleotides OMM109 (5'-cggaattcaccatgactagtAGCCATGGCTTCCCGCCGG-3') and OMM110 (5'-aagcttttctagacaccggtggatccgctagcCACATTGATCCTAGCAGAAGC-3'), restricted with *Eco*RI/*Xba*I and ligated into the corresponding sites (*Eco*RI/*Xba*I) of pMM1.	This work
pMM523	Constitutive TRT_{PEST} expression vector (P_{hCMV}-TRT_{PEST}-pA). PEST was excised from pMM519 using *Spe*I/*Bam*HI and ligated into the compatible sites (*Nhe*I/*Bam*HI) of pMM516.	This work
pMM531	Constitutive Fast-FT expression vector (P_{hCMV}-Fast-FT-pA). Fast-FT was PCR-amplified from pTRE-Fast-FT using oligonucleotides OMM119 (5'-gcgaattcaccatgactagtGTGAGCAAGGGCGAGGAGG-3') and OMM120 (5'-aagcttttctagacaccggtggatccgctagcCTTGTACAGCTCGTCCATG-3''), restricted with *Eco*RI/*Xba*I and ligated into the corresponding sites (*Eco*RI/*Xba*I) of pMM1.	This work
pMM532	Constitutive Fast-FT_{PEST} expression vector (P_{hCMV}-Fast-FT_{PEST}-pA). PEST was excised from pMM519 using *Spe*I/*Bam*HI and ligated into the corresponding sites (*Nhe*I/*Bam*HI) of pMM531.	This work

pWB48	Constitutive TRS expression vector (P_{SV40}-TRS-pA). TrpR was excised from pWB24 using (*Eco*RI/*Bss*HII) and ligated into the corresponding sites of pWW43 (*Eco*RI/*Bss*HII).	This work
pWB49	L-tryptophan-repressible P_{TRS}-driven SEAP expression vector (P_{TRS}-SEAP-pA). P_{SV40} was PCR-amplified from pWW56 using the $(O_{Trp})_2$-containing oligonucleotide OWB68 (5'-gatcaagcttgtttaaacttgtaatattatagcattacaattgtaatatt atagcattacaaGATATCCTGCAGGGAATTCGC C -3') and OWB69 (5'-gatcCAATTGTTGTTGTTAACTTGTTTATTG CAGC-3'), restricted with *Hin*dIII/*Mfe*I and ligated into the corresponding sites (*Hin*dIII/*Mfe*I) of pWW56.	This work
pWB60	Constitutive TnaA expression vector (P_{hCMV}-TnaA-pA). TnaA was PCR-amplified from *Escherichia Coli* chromosomal DNA using oligonucleotides OWB85 (5'-gcataagcttagatctgaattccaccATGGAAAACTTTA AACATCTCCCT GAACCG -3') and OWB86 (5'-gtcgtctagagcggccgcTTAAACTTCTTTCAGTT TTGCGGTGAAGTGAC-3'), restricted with *Eco*RI/*Xba*I and ligated into the corresponding sites (*Eco*RI/*Xba*I) of pcDNA3.1(+).	This work
pWB69	L-tryptophan-inducible P_{TRT}-driven d2EYFP expression vector (P_{TRT}-d2EYFP-pA). d2EYFP was excised from pd2EYFP using *Eco*RI/*Xba*I and ligated into the corresponding sites (*Eco*RI/*Xba*I) of pWB22.	This work
pWB70	L-tryptophan-inducible P_{TRT}-driven Ub^{V76}-GFP expression vector (P_{TRT}-Ub^{V76}-GFP-pA). Ub^{V76}-GFP was excised from pMT100 using *Nhe*I/*Not*I and ligated into the corresponding sites (*Xba*I/*Not*I) of pWB35.	This work

Abbreviations: **AmCyan**, variant of the *Anemonia majano* cyan fluorescent protein; **C/D_{box}**, L7Ae-specific RNA structure; **d2EYFP**, destabilized EYFP variant; **DsRed**, *Discosoma sp.* red fluorescent protein; **DsRed-Express-DR**, destabilized DsRed variant; **ET4**, erythromycin-dependent transsilencer (MphR(A)-KRAB); **ETR**, MphR(A)/ET4-specific operator sequence; **ETR_n**, n-tandem MphR(A)/ET4-specific ETR operator module; **EYFP**, enhanced yellow fluorescent protein; **Fast-FT**; mCherry-derived fluorescent timer with a fast blue-to-red maturation switch; **$Fast\text{-}FT_{PEST}$**, destabilized Fast-FT variant (Fast-FT-PEST); **GFP**, green fluorescent protein; **KRAB**, Krueppel-associated box protein of the human *kox-1* gene; **L7Ae**, C/D_{box}-binding subunit of the archaeal RNAse P; **MCS**, multiple cloning site; **MphR(A)**, *Escherichia coli* macrolide repressor; **$(O_{Trp})_2$**, dimeric TrpR-/TRT-/TRS-specific operator site; **pA**, polyadenylation signal; **P_{CREm}**, synthetic mammalian promoter containing a modified cAMP-response element; **PEST**, mouse ornithine decarboxylase-derived peptide sequence rich in proline (P), glutamic acid (E), serine (S) and threonine (T) acting as protein degradation signal; **P_{E1bmin}**, minimal version of the adenovirus E1b promoter; **P_{ETR2}**,

erythromycin-repressible promoter (ETR-$P_{hCMVmin}$); **P_{ETR}ON8**, erythromycin-inducible promoter (P_{SV40}-ETR_8); **P_{hCMV}**, human cytomegalovirus immediate early promoter; **$P_{hCMVmin}$**, minimal version of P_{hCMV}; **$P_{hCMV*-1}$**, tetracycline-responsive promoter ($tetO_7$-$P_{hCMVmin}$); **P_{min}**, synthetic minimal mammalian promoter; **P_{SV40}**, simian virus 40 promoter; **P_{tight}**, tetracycline-responsive promoter (TRE_{mod}-$P_{hCMVmin}$); **$P_{tight-bi}$**, bidirectional tetracycline-responsive promoter (←$P_{hCMVmin}$–TRE_{mod}–$P_{hCMVmin}$→); **P_{TRS}**, TRS-specific L-tryptophan-repressible promoter (P_{SV40}-$(O_{Trp})_2$); **P_{TRS2}**, TRS-specific L-tryptophan-repressible promoter (P_{hCMV}-$(O_{Trp})_2$); **P_{TRT}**, TRT-specific L-tryptophan-inducible promoter ($(O_{TRP})_2$-$P_{hCMVmin}$); **P_{TRT2}**, TRT-specific L-tryptophan-inducible promoter ($(O_{Trp})_2$-P_{min}); **P_{TRT3}**, TRT-specific L-tryptophan-inducible promoter ($(O_{Trp})_2$-P_{E1bmin}); **SEAP**, human placental secreted alkaline phosphatase; **tetO**; TetR/tTA-specific operator sequence; **$tetO_7$**; TetR/tTA-specific heptameric tetO; **TetR**, *Escherichia coli Tn*10-derived tetracycline-dependent repressor of the tetracycline resistance gene; **TnaA**, *Escherichia coli*-derived tryptophanase; **TRE_{mod}**, modified TetR/tTA-specific Tet response element; **TrpB**, *Escherichia coli*-derived tryptophan synthase *β*-subunit; **TrpR**, *Chlamydia trachomatis*-derived tryptophan repressor; **TRS**, L-tryptophan-dependent transsilencer (TrpR-KRAB); **TRT**, L–tryptophan-dependent transactivator (TrpR-VP16); **TRT_{PEST}**, destabilized TRT variant (TRT-PEST); **tTA**, tetracycline-dependent transactivator (TetR-VP16); **TurboGFP**, improved variant of the copepod *Pontellina plumata* GFP (CopGFP); **TurboGFP-dest1**, destabilized TurboGFP variant; **Ub^{V76}-GFP**, destabilized GFP variant; **VP16**, *Herpes simplex*-derived transactivation domain.

Oligonucleotides: Restriction endonuclease-specific sites are underlined in oligonucleotide sequences. Annealing basepairs contained in oligonucleotide sequences are shown in capital letters.

Table 2. Composition of the oscillator components transfected

Composition Figure 2a) – Reporter cells reversibility

Reporter cells		
Plasmid (ng/ml)	Plasmid name	Description
400	pAK409	P_{SV40} – TRT-PEST
200	pMM131	P_{TRT} – Fast-FT
400	pCola-Duet1	Filler Plasmid

Composition Figure 2b) – Producer-Reporter cells

Producer cells		
Plasmid (ng/ml)	Plasmid name	Description
400	pcDNA3.1	P_{hCMV} – MCS
200	pMM161	P_{hCMV} – C/D_{box} - TrpB
400	pMM162	P_{TRT} – L7Ae
Reporter cells		
Plasmid (ng/ml)	Plasmid name	Description
400	pAK409	P_{SV40} – TRT-PEST
200	pWB22	P_{TRT} – SEAP
400	pCola-Duet1	Filler Plasmid
Filler cells		
Plasmid (ng/ml)	Plasmid name	Description
1000	pCola-Duet1	Filler Plasmid

Composition Figure 2c) – Degrader-Reporter cells

Degrader cells		
Plasmid (ng/ml)	Plasmid name	Description
400	pWB24	P_{SV40} – TRT
400	pBB-tTA	P_{hCMV} – tTA
200	pMM128	P_{TRE} – TnaA
Reporter cells		
Plasmid (ng/ml)	Plasmid name	Description
400	pAK409	P_{SV40} – TRT-PEST
400	pWB22	P_{TRT} – SEAP
200	pCola-Duet1	Filler Plasmid
Filler cells		
Plasmid (ng/ml)	Plasmid name	Description
1000	pCola-Duet1	Filler Plasmid

Composition Figure 2d-f) – Reporter cells in tissue

Reporter cells		
Plasmid (ng/ml)	Plasmid name	Description
400	pAK409	P_{SV40} – TRT-PEST
200	pMM131	P_{TRT} – Fast-FT
400	pCola-Duet1	Filler Plasmid
Filler cells		
Plasmid (ng/ml)	Plasmid name	Description
1000	pCola-Duet1	Filler Plasmid

Composition Figure 2g,h) – Producer-Reporter cells in tissue

Producer cells		
Plasmid (ng/ml)	Plasmid name	Description
400	pBB-TRT	P_{hCMV} – TRT
200	pMM161	P_{hCMV} – C/D_{box} - TrpB
400	pMM162	P_{TRT} – L7Ae
Reporter cells		
Plasmid (ng/ml)	Plasmid name	Description
400	pAK409	P_{SV40} – TRT-PEST
200	pMM131	P_{TRT} – Fast-FT
400	pCola-Duet1	Filler Plasmid
Filler cells		
Plasmid (ng/ml)	Plasmid name	Description
1000	pCola-Duet1	Filler Plasmid

Composition Figure 3 – Closed oscillator composition

Producer cells		
Plasmid (ng/ml)	Plasmid name	Description
400	pBB-TRT	P_{hCMV} – TRT
200	pMM161	P_{hCMV} – C/D_{box} - TrpB
400	pMM162	P_{TRT} – L7Ae
Degrader cells		
Plasmid (ng/ml)	Plasmid name	Description
400	pWB24	P_{SV40} – TRT
400	pMM148	P_{TRTmin} – tTA
200	pMM128	P_{TRE} – TnaA

Reporter cells		
Plasmid (ng/ml)	Plasmid name	Description
400	pAK409	P_{SV40} – TRT-PEST
200	pMM131	P_{TRT} – Fast-FT
400	pCola-Duet1	Filler Plasmid
Filler cells		
Plasmid (ng/ml)	Plasmid name	Description
1000	pCola-Duet1	Filler Plasmid

Composition Figure 4 – Perfusion system composition

Degrader cells		
Plasmid (ng/ml)	Plasmid name	Description
400	pWB24	P_{SV40} – TRT
400	pMM148	P_{TRTmin} – tTA
200	pMM128	P_{TRE} – TnaA
Reporter cells		
Plasmid (ng/ml)	Plasmid name	Description
400	pAK409	P_{SV40} – TRT-PEST
200	pMM131	P_{TRT} – Fast-FT
400	pCola-Duet1	Filler Plasmid
Filler cells		
Plasmid (ng/ml)	Plasmid name	Description
1000	pCola-Duet1	Filler Plasmid

Abbreviations: **C/D_{box}**, RNA motif specifically binding to the L7Ae protein; **Fast-FT**; Fast maturing variant of blue-to-red fluorescent timer; **L7Ae**, archaeal ribosomal protein L7Ae; **MCS**, multiple cloning site; **PEST**, Protein degradation motif of the mouse ornithine decarboxylase; **P_{hCMV},** human cytomegalovirus immediate early promoter; **P_{SV40}**, simian virus 40 promoter; **P_{TRE},** tetracycline-responsive promoter; **P_{TRT}**, L-tryptophan-responsive minimal promoter; **P_{TRTmin}**, L-tryptophan-responsive minimal synthetic promoter; **SEAP**, human placental secreted alkaline phosphatase; **TnaA**, *E.Coli*-derived tryptophanase; **TrpB**, Tryptophan Synthase β-subunit; **TRT**, L-tryptophan-dependent transactivator; **tTA**, tetracycline-dependent transactivator.

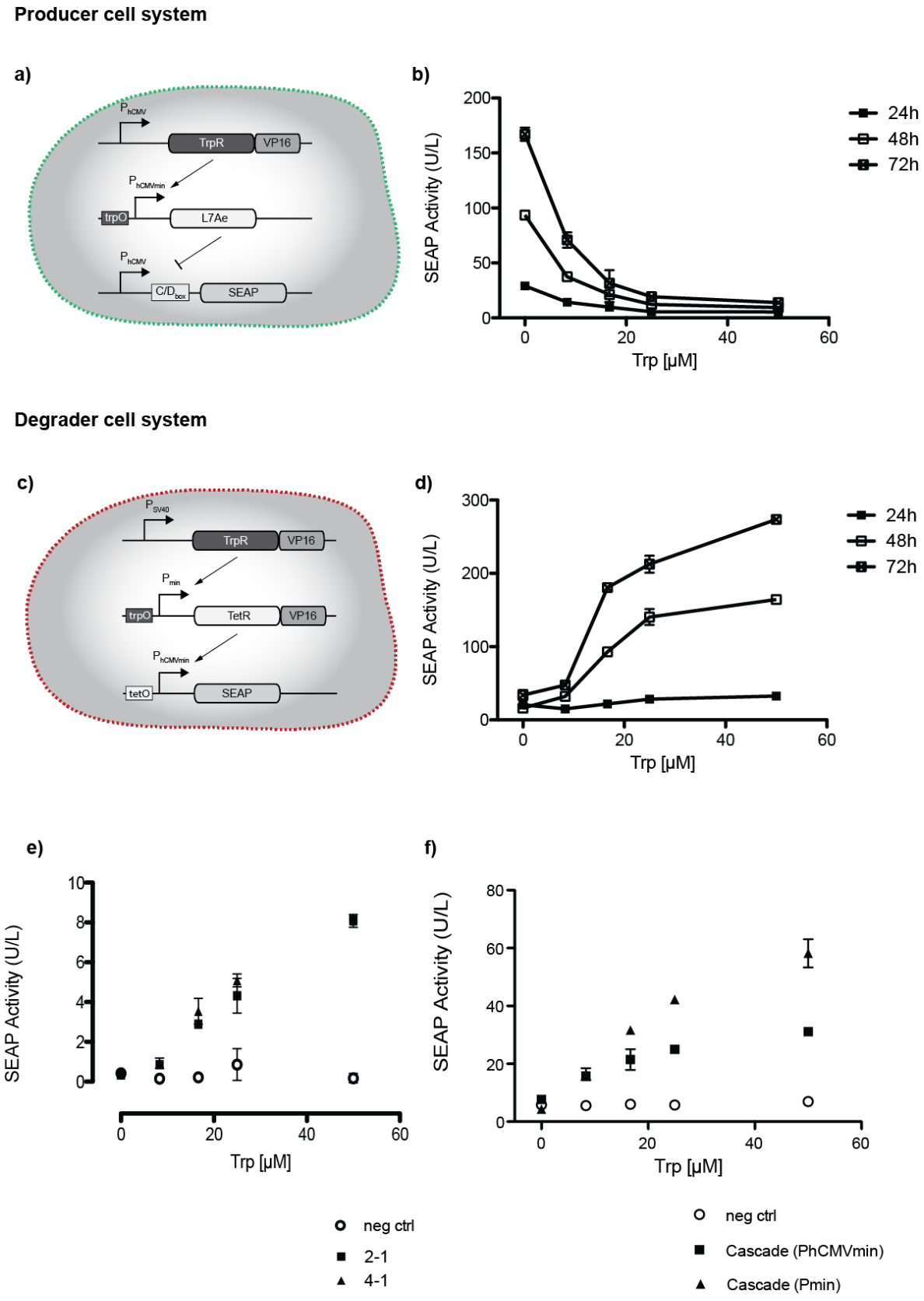

Supplementary Figure 1. Characterisation of the Producer and Degrader cells. a) Diagram of the producer cell population. TrpR-VP16 (TRT) binds to its cognate operator site (trpO) in the presence of L-Tryptophan (Trp) and drives the expression of the RNA-binding protein L7Ae. L7Ae in turn binds to its cognate RNA-binding motif (C/D_{box}) and blocks translation of the constitutive expressed reporter

protein SEAP. **b)** HEK293-T cells were transfected with the producer cell system components and induced with various concentrations of Trp. SEAP expression was quantified in the cell culture supernatant 24,48 and 72hs after induction.
c) Diagram of the degrader cell population. TrpR-VP16 (TRT) binds to its cognate operator site (trpO) in the presence of L-Tryptophan (Trp) and drives the expression of the amplifier component tetR-VP16 (tTA). tTA in turn binds to its cognate operator sequence (tetO) and drives the amplified expression of the reporter protein SEAP. **d)** HEK293-T cells were transfected with the degrader cell components and induced with various concentrations of Trp. SEAP expression was quantified in the cell culture supernatant 24,48 and 72hs after induction. **e)** HEK293-T cells were transfected with different degrader cell components (neg ctrl; pMM146 only, 200ng)(2-1; pWB24, 400ng, pMM146, 200ng)(4-1; pWB24, 800ng, pMM146, 200ng) and induced with various concentrations of Trp. SEAP expression was quantified in the cell culture supernatant 24hs after induction. **f)** HEK293-T cells were transfected with different degrader cell components (neg ctrl; pWB24, 400ng, pWB22, 200ng)(Cascade PhCMVmin; pWB24, 400ng, pMM126, 200ng, pMM130, 200ng)(Pmin; pWB24, 400ng, pMM148, 200ng, pMM130, 200ng) and induced with various concentrations of Trp. SEAP expression was quantified in the cell culture supernatant 24hs after induction.

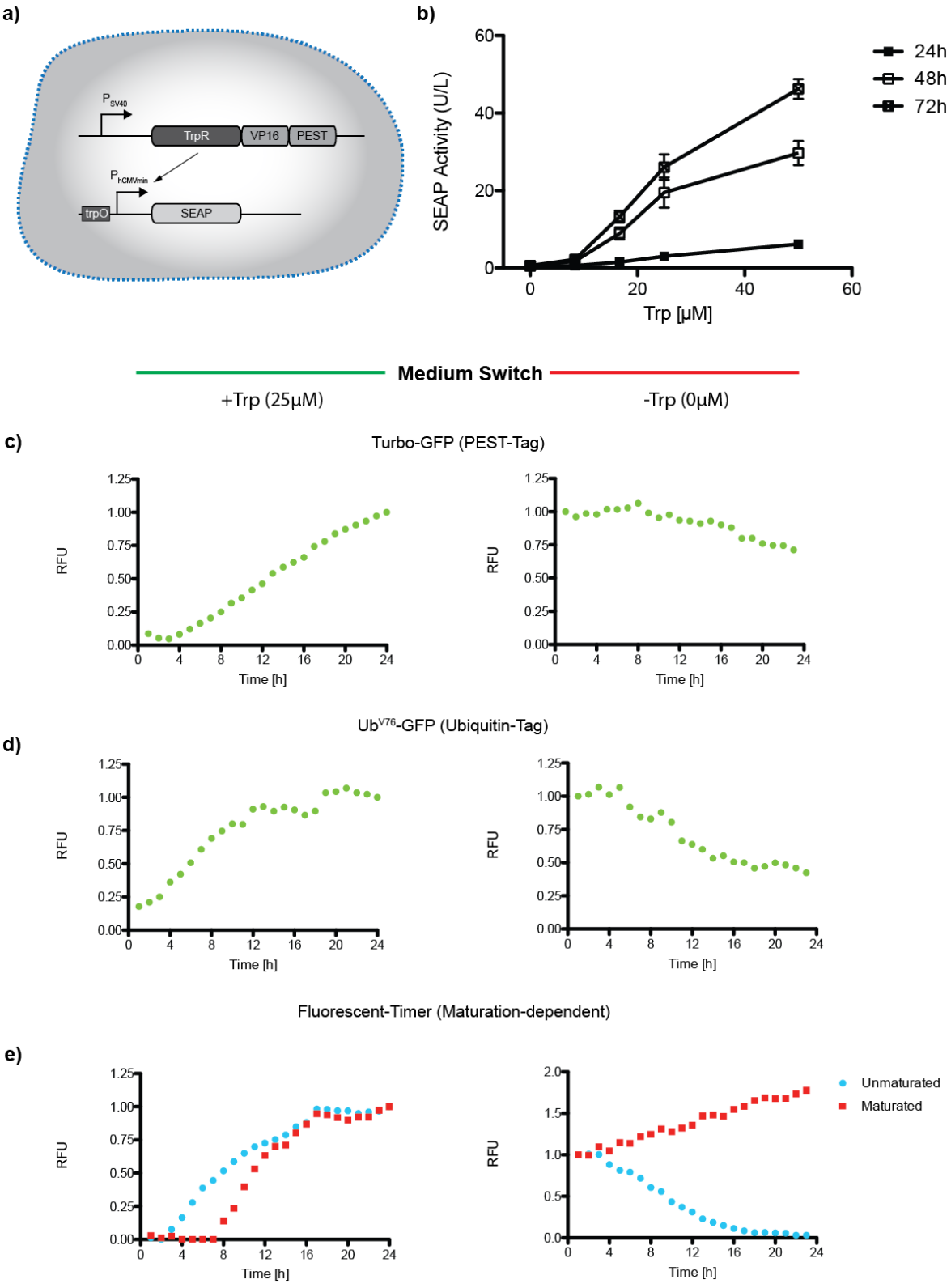

Supplementary Figure 2. Characterisation and comparison of the reporter. a) Diagram of the reporter cell population. The destabilized variant TrpR-VP16-PEST (TRT-PEST) binds to its cognate operator site (trpO) in the presence of L-Tryptophan (Trp) and drives the expression the reporter protein SEAP. **b)** HEK293-T cells were transfected with the reporter cell components and induced with

various concentrations of Trp. SEAP expression was quantified in the cell culture supernatant 24,48 and 72hs after induction. **c-e)** Comparison of system reversibility. HEK293-T cells were transfected with different reporter cell components where the SEAP reporter was replaced by Turbo-GFP (**c**), Ub^{G76V}-GFP (**d**) and the fast Fluorescent-Timer (**e**) and induced with 25μM of Trp for 24hs and then switched to no tryptophan-containing media (0μM). Fluorescence (Citrine for **c)**,**d)**; BFP and RFP for **e)**) was evaluated via time-lapse microscopy.

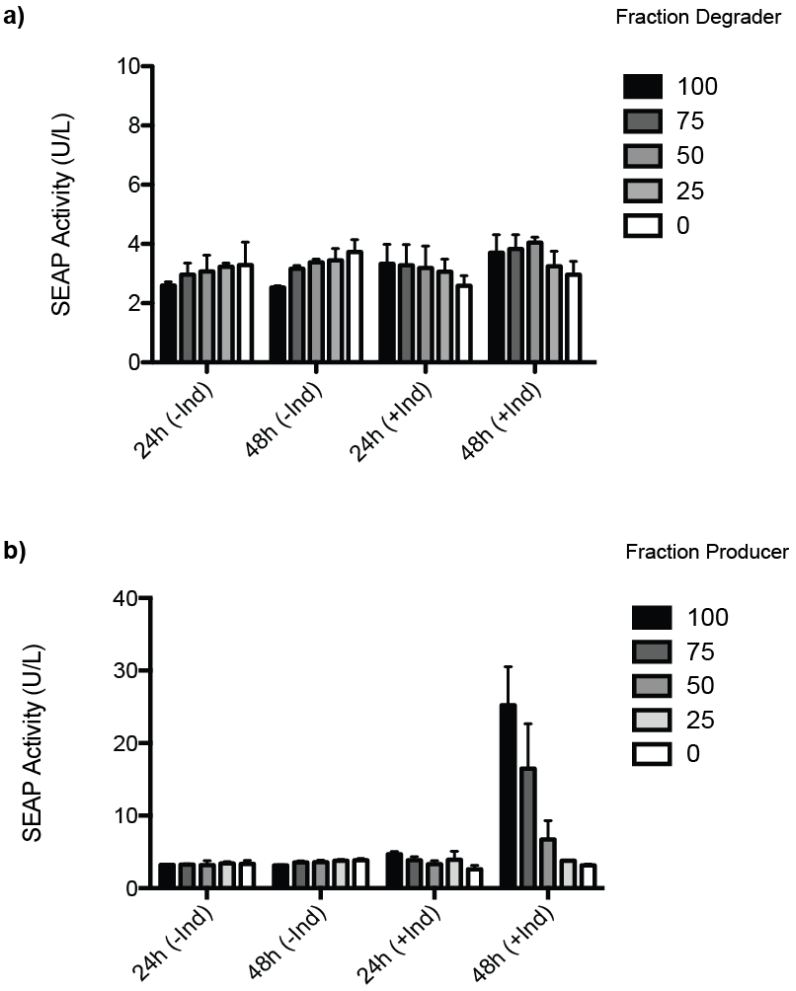

Supplementary Figure 3. Temporal resolution and unidirectional reaction of the Degrader and Producer cell systems.

a) HEK293-T were cotransfected with the degrader cell components and mixed at different indicated fractions with Tryptophan-reporter cells. Cells were induced with 5µM of Tryptophan with (+Ind) and without Indole (-Ind). SEAP levels were scored after 24h and 48h after induction in the cell culture supernatant.

b) HEK293-T were cotransfected with the producer cell components and mixed at different indicated fractions with Tryptophan-reporter cells. Cells were induced with 5µM of Tryptophan with (+Ind) and without Indole (-Ind). SEAP levels were scored after 24h and 48h after induction in the cell culture supernatant.

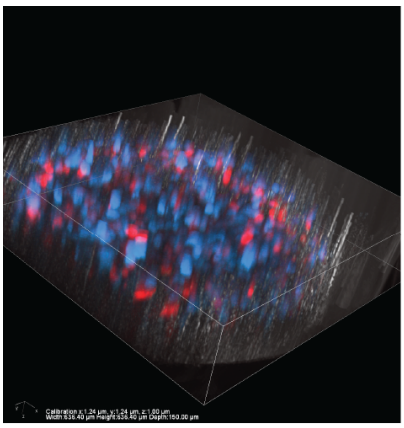

100 Producer - 0 Degrader

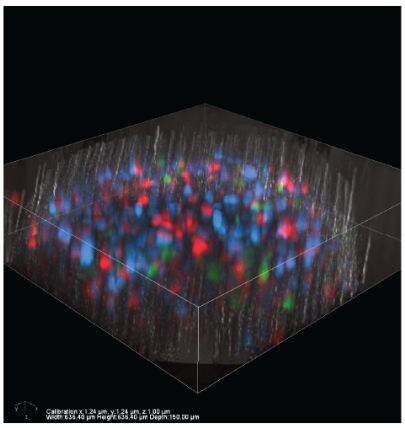

75 Producer - 25 Degrader

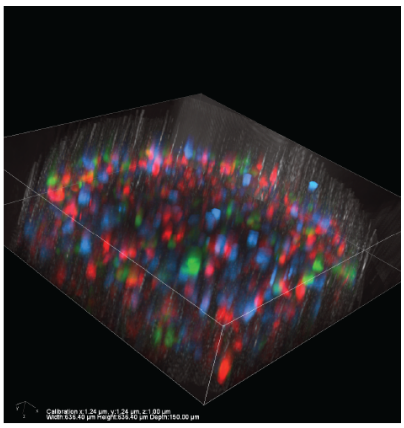

50 Producer - 50 Degrader

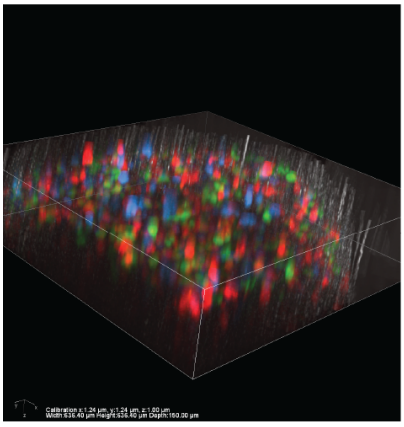

25 Producer - 75 Degrader

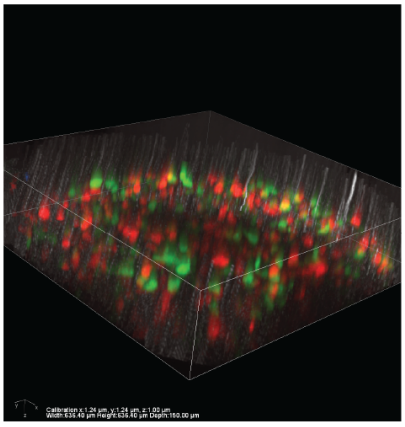

0 Producer - 100 Degrader

Supplementary Figure 4. Cellular distribution within the 3D-tissue. 5000 HEK293-T cells were cotransfected with the reporter cell components, where the fluorescent timer was exchanged with a constitutive expressed RFP and mixed with 10000 HEK293-T cells that were cotransfected with the producer cell components with an additional constitutive BFP and mixed with HEK293-T cells that were cotransfected with the degrader cell components with an additional constitutive Citrine at the indicated ratios. Confocal fluorescence images were taken after 24h.

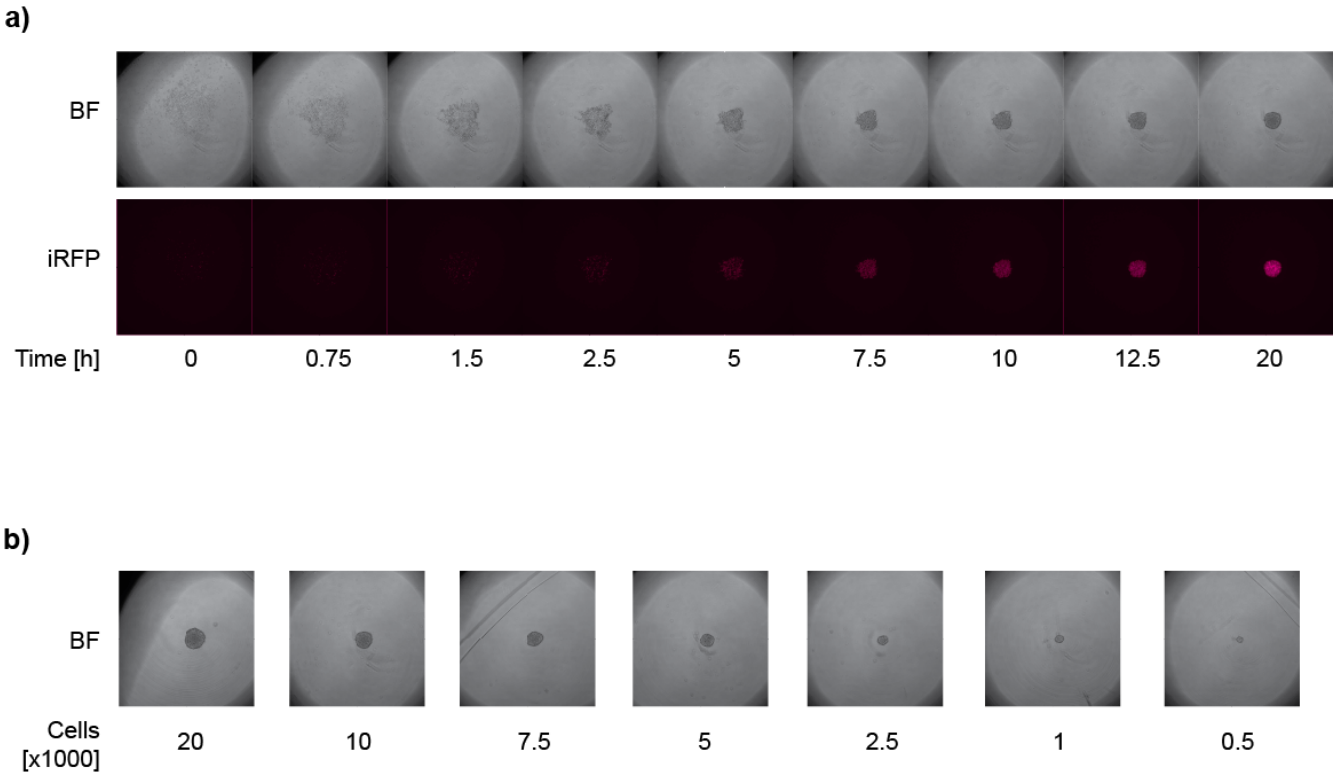

Supplementary Figure 5. Characterisation of the tissue formation process.

a) Tissue formation over time. HEK293-T cells were transfected with the reporter system components. After transfection 10^2 cells were transferred to a U-bottom tissue formation plate and recorded via time lapse microscopy for 20h. Pictures were taken at the indicated time points for the bright field (BF) and infrared fluorescent protein (iRFP) channel. **b)** Tissue formation in correlation to the initial cell number. Microphotographs (BF) were taken after 20hs of the tissue formation process in a U-bottom tissue formation plate.

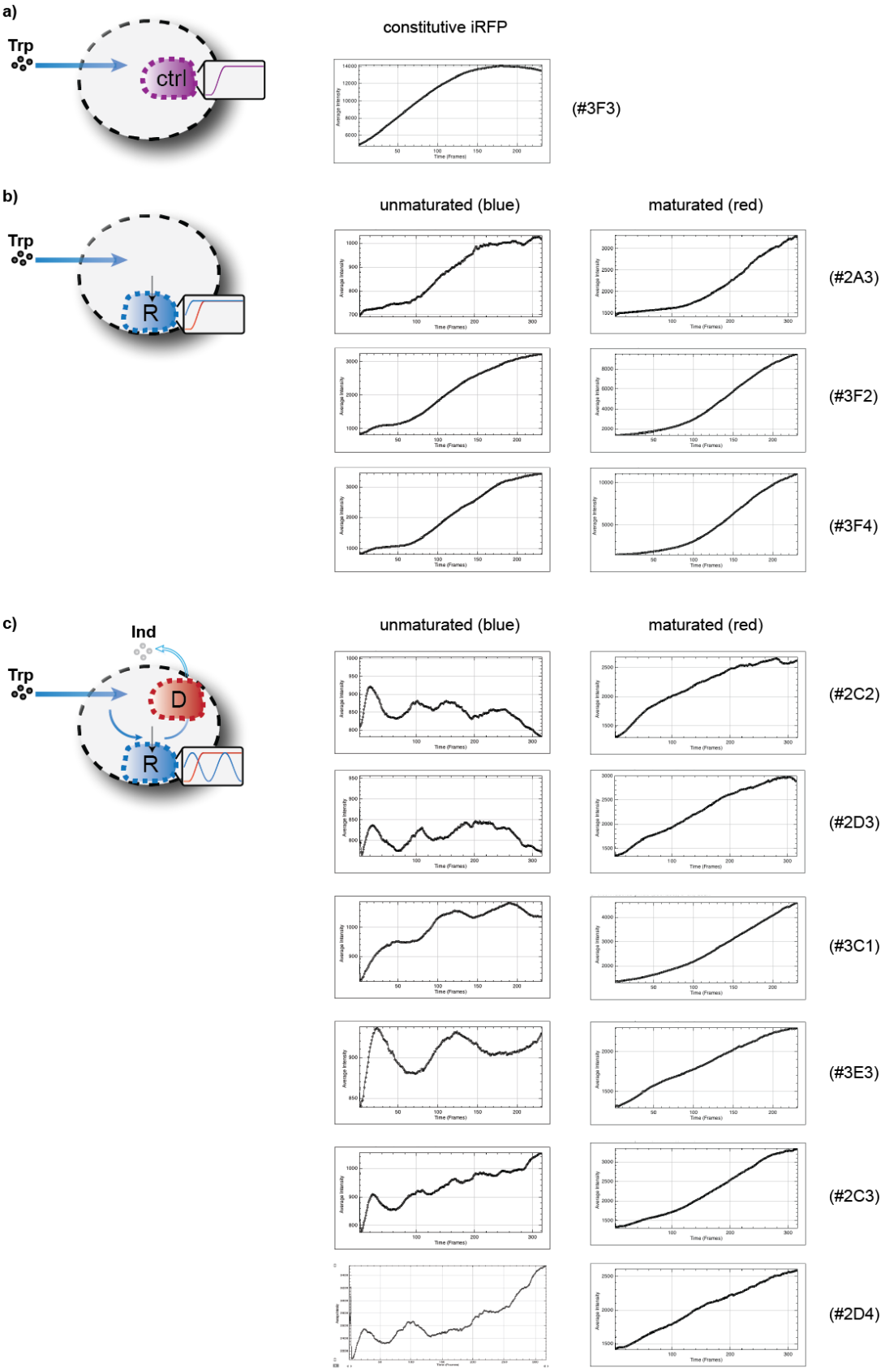

Supplementary Figure 6. Sustained dynamics in a tissue-perfusion setup.

a-c) Quantified fluorescence for constitutive expressed iRFP **(a),** the unmaturated (blue) (**b,c**) and maturated (red) (**b,c**) variant as a function of time for control cells constitutively expressing iRFP **(a)**,

reporter cells only **(b)** and the oscillator setup **(c)** in the spheroid perfusion system in a 3D-microtissue demonstrating dynamic gene expression behaviour. Positions were perfused with flow rates ranging from 0.2µL/min to 0.8µL/min (Positions #3F3, #2A3, #2C2 and #2D3 were perfused with 0.2µL/min, #3F2, #3C1 and #3E3 were perfused with 0.4µL/min and #3F4, #2C3 and #2D4 were perfused with 0.8µL/min).

Conclusion

Conclusion

The term of synthetic biology is nowadays used by multiple "core" disciplines including physics, metabolic engineering and molecular cloning to broadly justify the use of heterologous parts or the creation of non-natural systems. However, the initial intention aimed at the combination of engineering principles with biology in order to describe standardized parts which can rationally be combined and assembled to circuits with predictable functions, analogous to electronic engineering. After first pioneering examples (Elowitz et al. 2000, Gardner et al. 2000), demonstrating synthetic biology's principles (Bhalerao 2009, Purnick et al. 2009, Khalil et al. 2010), these systems were applied to solve real-world problems in diverse fields of natural sciences with strong focus on biomedical relevant topics (Ruder et al. 2011, Weber et al. 2012). Exemplary, several approaches used bacteria, engineered with genetic circuits to respond to metabolites in the patient's gut to produce pharmaceutically relevant drugs (Kotula et al. 2014, Claesen et al. 2015, Woloszynek et al. 2016) or target and invade cancer in patients (Anderson et al. 2006). Human cells bear the potential to respond to a huge range of naturally occurring metabolites –not least due to the ability to signal via GPCRs-, produce disease-relevant compounds with host-specific post-translational modifications and easily adapt to the host's metabolism. Mammalian synthetic biology takes advantage of these features and combines those with the aforementioned engineering principles. Designer cells that respond to disease markers and implanted into a patient's body hold the promise to be the next generation of therapeutics (Fischbach et al. 2013, Rossger et al. 2013, Heng et al. 2015).

This work combines metabolic engineering principles with mammalian synthetic biology for the production of heterologous compounds and incorporation into synthetic systems such as output molecules (indigoidine), cell-cell communication compounds (GLP-1; Tryptophan) or metabolic interconversion (indole to tryptophan) for dynamic output.

Chapter I describes the application of a designer circuit for a novel mammalian synthetic screening platform for sunscreen. Based on CRY2-CIBN, a blue- and UV-light dimerization system from *Arabidopsis thaliana*, components used to control

developmental and circadian signals in the plant, we transferred the UV- and blue-light sensor system to a mammalian background. In order to elicit a gene response upon illumination, we engineered the system to cleave the membrane-bound transcription factor tTA via the site-specific protease TEV to allow translocation to the nucleus and drive corresponding target gene expression (such as the reporter gene SEAP). This network enables intracellular screening of blocking efficacy of commercially available sunscreens for harmful UV-A beams. The system describes the first human cell-based sun cream screening platform and the first UV-A inducible gene-regulation system in mammalian cells.

The current applied screening methods for evaluating sunscreen efficacy are based on physical absorbance screens upon exposure and lack a joint standard and protocol. Application of a synthetic biology screening method based on human cells has several advantages over the common techniques including inherent cytotoxicity evaluation. This work contributes to pioneering cell-based diagnostic approaches. Herein, biomolecular components (Pardee et al. 2016) or bacterial or mammalian designer cells are used for the detection of environmental pollutions as seen for arsenic (Merulla et al. 2013), screening for antibacterial compounds (Weber et al. 2008) or disease states such as allergy profiling (Auslander et al. 2014). In the latter mammalian designer cells, transgenic for the human histamine receptor HRH2 and rewiring of the pathway for the expression of a reporter on receptor activation, enable in-depth profiling of patients' blood for allergic reactions upon exposure to diverse allergens. The advantage of this diagnostic method is its biological nature with inherent cytotoxicity and bioavailability validation, sensitivity in the physiological range and flexibility of the reporter output. Although this method requires cell culture handling and hardware, the compatibility with high-throughput robotics platforms could open this field for broader personalized clinical applications as well as for screening platforms for the identification of new drug targets. Another approach is to reduce the diagnostic systems to cell-free extracts (Pardee et al. 2016). This resolves major practical limitations by using freeze-dried, paper-based diagnosis platforms for the use outside of a research laboratory for the detection of virus from plasma such as Zika for example (Pardee et al. 2016).

In Chapter II we describe a novel reporter system. Thereby, we introduce the pioneering production of a valuable nonribosomal peptide in mammalian cells focusing on the blue-pigment indigoidine as a proof-of-concept nonribosomal peptide. Synthesis requires a two-component system consisting a multi-domain nonribosomal peptide synthase (NRPS) BpsA and a cognate activating enzyme (PPTase) svp. Only in presence of both components cells produce the blue-colored indigoidine, which could be applied as a universal visual and fluorescent reporter system for bacteria and mammalian cells.

This opens the way for the direct production of valuable secondary metabolites in mammalian cells. Encapsulated designer cells could produce a therapeutic output (such as nonribosomal peptides, including anti-cancer, antibacterial and anti-viral compounds) in direct response to disease markers. After the discovery of penicillin in 1928, the screening for polyketide- and nonribosomal peptide-derived active compounds has revealed a large amount (more than 11.000) and diversity of products throughout various kingdoms of life (Dejong et al. 2016), (Wang et al. 2014). However, a great subset of these are only conditionally expressed or are found in strains that are difficult or impossible to cultivate. Genome mining, computational prediction and retro-biosynthesis have advanced the availability of novel valuable compounds (Marahiel 2016).

Transfer of those gene clusters to heterologous production hosts is still limited due to size, strain-specific codon usage and essential co-enzymes. Synthetic biology with its standardization approaches for pathway engineering (Zhao et al. 2016), (Zebec et al. 2016), (Awan et al. 2016) and recent advances in gene synthesis (Kosuri et al. 2014) could provide a way to overcome these hurdles in the near future.

Furthermore, we also capitalized on the production of heterologous compounds in Chapter III for the purpose of cell-cell communication by a gas-to-liquid cell population and an analog-to-digital converter cell population. This consortium enabled the conversion of fragrances to the signaling compounds L-Tryptophan and GLP-1. In a second step, these molecules were integrated and a recombinase-based processing enabled a digital output following AND, OR and NOR logics. The distribution of tasks to single cell populations enabled the high complexity of the system. This framework

could help in future mammalian synthetic biology designs to overcome restrains of single-cell architectures such as metabolic overload compromising the signal processing capacity or potential cross-talk of synthetic components (pathways, binding sites) (Tubio et al. 2010). This setup also provides a higher degree in modularity, complexity and precision.

"Biocomputation" refers to biological systems that perform information processing reminiscent to physical computers. This ranges from first computations with DNA molecules (Adleman 1994), autonomous molecular computers (Benenson et al. 2004) to entire cells (Kramer et al. 2004, Auslander et al. 2012, Tan et al. 2007, Purcell et al. 2014) and state machines (Roquet et al. 2016). They all have in common the processing of a certain input signal (from DNA to small molecules) to a defined output (such as fluorescence). Recent approaches integrate disease related markers within a patient's body such as miRNA (Xie et al. 2011) or cytokines (Schukur et al. 2015), process these signals and resulting in a (visual, fluorescent) reporter output for identification purposes or potentially counteract the disease (by the expression of therapeutics such as cytokines or inducing apoptosis).

The present work taps in this processing step and aims at linking analog nature with digital logic outputs. Likewise, seen for bacterial systems (Siuti et al. 2013),(Rubens et al. 2016) digital logic is used to fix thresholds, increase signal-to-noise ratios and in turn make decisions (Purcell et al. 2014), (Brewster et al. 2014). This work fosters the communication between living and electronic systems. Potential machine-man interfaces as seen for mind-controlled gene expression (Folcher et al. 2014) serve as an example for future treatment strategies. Man-machine interfaces in turn can be used to monitor disease states and transfer the information to an electronic device as a direct readout for patients.

Akin to Chapter III, cell-cell communication-based information processing, resulted in the design of a mammalian consortium for the interconversion of a joint metabolite to achieve a tissue oscillator in Chapter IV. The oscillatory system consists of producer cells that conditionally convert indole to L-tryptophan in absence of Tryptophan. The degrader cells on the contrary convert Tryptophan back to indole in presence of

tryptophan. The final reporter cells show fluorescence dependent on the amount of tryptophan present. Systems biology enabled the rational design through a descriptive model, whereas microfluidic engineering allowed for a tissue perfusion system in order to monitor dynamics over longer periods.

Coupling of synthetic oscillators to external and internal signals has been established in bacteria (Danino et al. 2010) and used for the creation of “biopixels” for sensing arsenic (Prindle et al. 2011), for the study of biofilm formation (Liu et al. 2015) or engineered bacterial lysis *in vivo* for cancer treatment (Din et al. 2016). A mammalian clock in a tissue that is independent of the circadian clock can give insights into its natural pendants or -in combination with cell-based therapies- result in rhythmic therapeutic expression such as insulin or cortisone *in vivo*.

All of these projects underline the principles of synthetic biology with various and broad applications (Figure 4). In common is the standardization of biologic parts, which are assembled in an engineering fashion to sophisticated and trigger-dependent circuits. This is often only possible due to the interdisciplinary of the field, where computational and physical engineering are combined with diverse biological branches, exhausting the potential of each science.

This is in close relation to “soft-robotics”: Park et al. (Park et al. 2016) were inspired by stingrays and combined material science, optical control mechanisms and optogenetically engineered cardiomyocytes to create a soft-robotic ray controllable by optical stimulations.

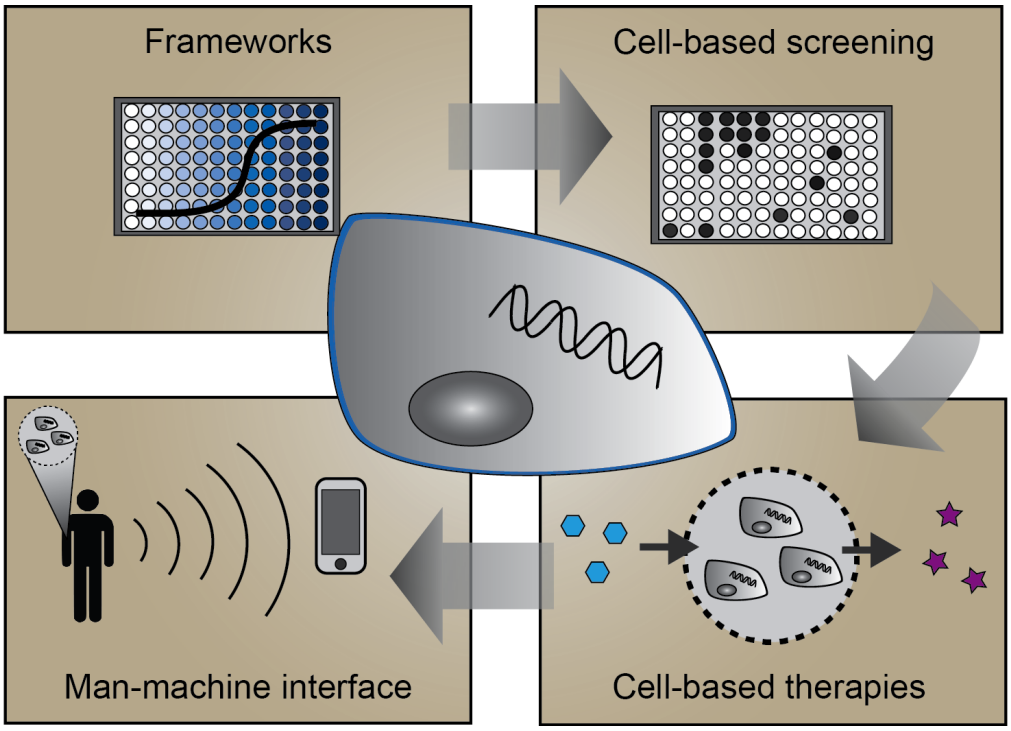

Figure 4. Applications of engineered mammalian cells as outlined in this work.

Mammalian designer cells bear potential in a variety of fields. Frameworks featuring new reporter help in the construction of new gene regulation systems. These frameworks can be applied for cell-based screening platforms, which enable the discovery of new compounds (drugs, creams, etc.). Transfer of pathways to naturally-derived drugs into heterologous hosts can increase the product yield or directly be used in cell-based therapies. Herein, encapsulated designer cells in a patient's body sense disease markers and counteract the disease onset by expression of bioactive drugs (such as nonribosomal peptides or antibodies). Alternatively, these designer cell implants can be used to monitor the current disease state of markers in a patient's body. By man-machine interfaces that combine the cells with electronics, this information is directly transferred to a computer device as real-time readout.

In summary, this work strongly advances the field of mammalian synthetic biology in engineering principles and biotechnological applications by laying the foundation to more sophisticated gene networks by the presented frameworks. Ultimately, this will foster progress in biopharmaceutical production, diagnostics and biomedical approaches.

References

Adleman, L. M. (1994). "Molecular computation of solutions to combinatorial problems." Science 266(5187): 1021-1024.

Anderson, J. C., E. J. Clarke, A. P. Arkin and C. A. Voigt (2006). "Environmentally controlled invasion of cancer cells by engineered bacteria." J Mol Biol 355(4): 619-627.

Auslander, D., et al. (2014). "A designer cell-based histamine-specific human allergy profiler." Nat Commun 5: 4408.

Auslander, S., D. Auslander, M. Muller, M. Wieland and M. Fussenegger (2012). "Programmable single-cell mammalian biocomputers." Nature 487(7405): 123-127.

Awan, A. R., W. M. Shaw and T. Ellis (2016). "Biosynthesis of therapeutic natural products using synthetic biology." Adv Drug Deliv Rev.

Benenson, Y., B. Gil, U. Ben-Dor, R. Adar and E. Shapiro (2004). "An autonomous molecular computer for logical control of gene expression." Nature 429(6990): 423-429.

Bhalerao, K. D. (2009). "Synthetic gene networks: the next wave in biotechnology?" Trends Biotechnol 27(6): 368-374.

Brewster, R. C., et al. (2014). "The transcription factor titration effect dictates level of gene expression." Cell 156(6): 1312-1323.

Claesen, J. and M. A. Fischbach (2015). "Synthetic microbes as drug delivery systems." ACS Synth Biol 4(4): 358-364.

Danino, T., O. Mondragon-Palomino, L. Tsimring and J. Hasty (2010). "A synchronized quorum of genetic clocks." Nature 463(7279): 326-330.

Dejong, C. A., et al. (2016). "Polyketide and nonribosomal peptide retro-biosynthesis and global gene cluster matching." Nat Chem Biol 12(12): 1007-1014.

Din, M. O., et al. (2016). "Synchronized cycles of bacterial lysis for in vivo delivery." Nature 536(7614): 81-85.

Elowitz, M. B. and S. Leibler (2000). "A synthetic oscillatory network of transcriptional regulators." Nature 403(6767): 335-338.

Fischbach, M. A., J. A. Bluestone and W. A. Lim (2013). "Cell-based therapeutics: the next pillar of medicine." Sci Transl Med 5(179): 179ps177.

Folcher, M., et al. (2014). "Mind-controlled transgene expression by a wireless-powered optogenetic designer cell implant." Nat Commun 5: 5392.

Gardner, T. S., C. R. Cantor and J. J. Collins (2000). "Construction of a genetic toggle switch in Escherichia coli." Nature 403(6767): 339-342.

Heng, B. C., D. Aubel and M. Fussenegger (2015). "Prosthetic gene networks as an alternative to standard pharmacotherapies for metabolic disorders." Curr Opin Biotechnol 35: 37-45.

Khalil, A. S. and J. J. Collins (2010). "Synthetic biology: applications come of age." Nat Rev Genet 11(5): 367-379.

Kosuri, S. and G. M. Church (2014). "Large-scale de novo DNA synthesis: technologies and applications." Nat Methods 11(5): 499-507.

Kotula, J. W., et al. (2014). "Programmable bacteria detect and record an environmental signal in the mammalian gut." Proc Natl Acad Sci U S A 111(13): 4838-4843.

Kramer, B. P., C. Fischer and M. Fussenegger (2004). "BioLogic gates enable logical transcription control in mammalian cells." Biotechnol Bioeng 87(4): 478-484.

Liu, J., et al. (2015). "Metabolic co-dependence gives rise to collective oscillations within biofilms." Nature 523(7562): 550-554.

Marahiel, M. A. (2016). "A structural model for multimodular NRPS assembly lines." Nat Prod Rep 33(2): 136-140.

Merulla, D., et al. (2013). "Bioreporters and biosensors for arsenic detection. Biotechnological solutions for a world-wide pollution problem." Curr Opin Biotechnol 24(3): 534-541.

Pardee, K., et al. (2016). "Rapid, Low-Cost Detection of Zika Virus Using Programmable Biomolecular Components." Cell 165(5): 1255-1266.

Park, S. J., et al. (2016). "Phototactic guidance of a tissue-engineered soft-robotic ray." Science 353(6295): 158-162.

Prindle, A., et al. (2011). "A sensing array of radically coupled genetic 'biopixels'." Nature 481(7379): 39-44.

Purcell, O. and T. K. Lu (2014). "Synthetic analog and digital circuits for cellular computation and memory." Curr Opin Biotechnol 29: 146-155.

Purnick, P. E. and R. Weiss (2009). "The second wave of synthetic biology: from modules to systems." Nat Rev Mol Cell Biol 10(6): 410-422.

Roquet, N., A. P. Soleimany, A. C. Ferris, S. Aaronson and T. K. Lu (2016). "Synthetic recombinase-based state machines in living cells." Science 353(6297): aad8559.

Rossger, K., G. Charpin-El-Hamri and M. Fussenegger (2013). "A closed-loop synthetic gene circuit for the treatment of diet-induced obesity in mice." Nat Commun 4: 2825.

Rubens, J. R., G. Selvaggio and T. K. Lu (2016). "Synthetic mixed-signal computation in living cells." Nat Commun 7: 11658.

Ruder, W. C., T. Lu and J. J. Collins (2011). "Synthetic biology moving into the clinic." Science 333(6047): 1248-1252.

Schukur, L., B. Geering, G. Charpin-El Hamri and M. Fussenegger (2015). "Implantable synthetic cytokine converter cells with AND-gate logic treat experimental psoriasis." Sci Transl Med 7(318): 318ra201.

Siuti, P., J. Yazbek and T. K. Lu (2013). "Synthetic circuits integrating logic and memory in living cells." Nature Biotechnology 31(5): 448-452.

Tan, C., H. Song, J. Niemi and L. You (2007). "A synthetic biology challenge: making cells compute." Mol Biosyst 3(5): 343-353.

Tubio, M. R., et al. (2010). "Expression of a G protein-coupled receptor (GPCR) leads to attenuation of signaling by other GPCRs: experimental evidence for a spontaneous GPCR constitutive inactive form." J Biol Chem 285(20): 14990-14998.

Wang, H., D. P. Fewer, L. Holm, L. Rouhiainen and K. Sivonen (2014). "Atlas of nonribosomal peptide and polyketide biosynthetic pathways reveals common occurrence of nonmodular enzymes." Proceedings Of The National Academy Of Sciences Of The United States Of America 111(25): 9259-9264.

Weber, W. and M. Fussenegger (2012). "Emerging biomedical applications of synthetic biology." Nature Reviews Genetics 13(1): 21-35.

Weber, W., et al. (2008). "A synthetic mammalian gene circuit reveals antituberculosis compounds." Proc Natl Acad Sci U S A 105(29): 9994-9998.

Woloszynek, S., et al. (2016). "Engineering Human Microbiota: Influencing Cellular and Community Dynamics for Therapeutic Applications." Int Rev Cell Mol Biol 324: 67-124.

Xie, Z., L. Wroblewska, L. Prochazka, R. Weiss and Y. Benenson (2011). "Multi-input RNAi-based logic circuit for identification of specific cancer cells." Science 333(6047): 1307-1311.

Zebec, Z., et al. (2016). "Towards synthesis of monoterpenes and derivatives using synthetic biology." Current opinion in chemical biology 34: 37-43.

Zhao, H. and M. H. Medema (2016). "Standardization for natural product synthetic biology." Nat Prod Rep 33(8): 920-924.

Acknowledgements

I would like to deeply thank:

…first of all Prof. Martin Fussenegger, for the opportunity to do my research in his laboratory and for support and advice throughout this thesis.

…the Co-examiner Yaakov (Kobi) Beneson for reading my thesis.

…especially Dr. Marcel Tigges, for his patience, mentoring, long-year support and being a great friend.

…also the triplets Simon and David Ausländer, Ferdinand Sedlmayer, Aizhan Tastanova and Hélène Chassin for extensive support, advice and friendship.

…my long year fellows in the lab from the 1st generation: Christian, Marc, William, from the 2nd generation: Marc, Alex, Markus, Michel and from the current generation: Leila, Leon, Xavier, Tobi, Hyojin, David Fuchs, Pascal Schön und nicht, for their support and great atmosphere in and time outside the lab.

…my master-students Luca Siegrist, Andy Kyburz and Joel Busset for their commitment and motivation.

…the fruitful collaborations including Moritz Lang and Prof. Jörg Stelling for the computational model, Patrick Misun, Elise Aeby and Oliver Frey for the microfluidics realization and the members of the SCU including Erica Montani, Verena Jaeggin, Telma Lopes and Thomas Horn for their support for FACS and microscopy and Peter Buchmann for his technical support.

…all the people that helped me throughout all the years but I forgot to mention.

…my dear family Renate, Gerhard and Fabian for their permanent support and love.

THANK YOU!